THE THERMAL CONSTITUTIVE BEHAVIOR OF SUSPENSIONS

by

Thomas Joe McMillen

In Partial Fulfillment of the Requirements

For the Degree of Doctor of Philosophy

California Institute of Technology

Pasadena, California

1977

(Submitted July 15, 1976)

To Nancy

ACKNOWLEDGMENTS

It is with great pleasure that I acknowledge the assistance and patience of my research advisor, Dr. L. G. Leal, who has given considerably of his time and help in making this work possible. My stay at Caltech has been made enjoyable by the academic and social interplay with a number of students too numerous to list. Special thanks, however, must go to Drs. Claude Cohen, Bosco Ho, Grant Robertson, and Erdinc Zana, and to Tom Peterson and Phil Wood for their friendship. George Griffith, Seichi Nakawatase, and John Yehle have offered invaluable support in the laboratory, which I greatly appreciate. I am grateful for financial support from an Atlantic Richfield Fellowship, National Science Foundation Traineeship, ARCS Fellowship, and for Graduate Research and Teaching Assistanceships.

My dear friends Ron Lewis and Toby Wein have enriched my life and introduced me to the myriad pleasures of Southern California. My parents have been a never-ending source of love and inspiration. To all my family, I offer my gratitude for their love and encouragement. Most importantly, I thank my best friend and companion, my wife Nancy, for everything she has meant to me these last six years.

ABSTRACT

The bulk thermal constitutive behavior of flowing, neutrally buoyant suspensions is considered theoretically and experimentally. A general theoretical expression relating the macroscopic heat flux in the suspension to microscale velocity and temperature distributions on the length scale of the particles is derived from statistical considerations of the microstructural configuration of the suspension. Evaluation of the relation for specific conditions is discussed with particular attention given to the role of random Brownian motions of the particles. Constraints imposed by simple shear flow are considered, and it is seen that the flowing suspension may not be described by a complete effective conductivity tensor K_{ij}.

The effective conductivity transverse to the flow of a dilute suspension of slightly deformed droplets is calculated in the limit of small particle Peclet number for the undisturbed bulk shear, $u = \gamma y$, and the linear bulk temperature field, $T = \alpha y$. Two distinct cases of small deformation are considered; deformation dominated by interfacial tension forces, and deformation dominated by viscous forces in the drop. The microscale velocity and temperature fields are obtained as regular, asymptotic expansions in the small

deformation parameter, ϵ, the governing thermal energy equation is then solved for small Peclet number using the methods of matched asymptotic expansions. The results obtained display the possible fundamental change in the dominant flow contribution to the effective conductivity due to the deformation in shape of the particles.

The bulk heat flux of a dilute suspension of rigid prolate spheroids is evaluated in the limit of small particle Peclet number for the undisturbed shear flow, $u_3 = \gamma x_2$, and the linear bulk temperature fields $T = \alpha_1 x_1$ and $T = \alpha_2 x_2$. Microscale velocity fields near the particle are calculated from the Stokes equations for small particle Reynolds number for arbitrary orientation and rotation of the particles, and temperature distributions for the small, but non-negligible Peclet number by the methods of matched asymptotic expansions. The components of the effective conductivity tensor for a stationary suspension is obtained, and the bulk heat flux due to the temperature gradients orthogonal to the flow evaluated for the case of significant rotational Brownian motion of the particles.

A rotating cylinder apparatus designed for the investigation of the bulk heat flux transverse to the flow of a suspension undergoing simple bulk shear flow is described, with special consideration given to describing and minimizing secondary effects such as natural convection, particle

migration, viscous dissipation, and Taylor instability of the flow. Results obtained for the effective conductivity of suspensions of spherical polystyrene particles suspended in a Newtonian fluid are presented and compared to the theoretical prediction of Leal (1973) for the effective conductivity of dilute suspensions of spherical particles at low particle Reynolds and Peclet numbers.

TABLE OF CONTENTS

CHAPTER I

INTRODUCTION

INTRODUCTION

The attempt to understand and predict the behavior of rheologically complex fluids is an old problem which has been the subject of a great deal of theoretical and experimental research activity. One class of such fluids is suspensions, which consist of dispersed 'particles', of either a solid or fluid nature, suspended in a continuous matrix of another material, which, in general may be either solid or liquid. Such fluids occur in various technological applications relating, for example, to polymer processing, pulp and paper making, and processing of paint. Naturally occurring systems include dispersions in the form of aerosols in the atmosphere, biological fluid systems such as blood, and in flows through porous media. In addition, suspensions provide an idealized model for the much wider class of fluids which include solutions of macromolecules.

From an engineering point of view, suspensions frequently appear in a context where it is possible to model their macroscopic behavior in terms of an equivalent homogeneous continuum, using the normal field conservation equations for momentum, thermal energy or mass. In this case, however, one must have available constitutive relations for the diffusive flux of momentum, thermal energy or molecular species concentration. The attempt to deduce such consti-

tutive laws for the mechanical or rheological properties has been the prime focus for much of the research on suspension-like materials. In many applications, however, the constitutive behavior of the material for heat or material transport is of at least equal importance. Nevertheless, comparatively little attention has been given to this topic.

Considering the system as a whole, there are two approaches available for the development of constitutive relations. The first, which we shall refer to as the phenomenological approach, deals with the formulation of general relations describing the behavior of the material based on a 'guess' or hypothesis of the appropriate functional form between dependent and independent variables. The apparent virtue of this classical continuum mechanical method, namely its generality, is in fact its major weakness. Having postulated a constitutive form without reference to any specific material, the theory has no way of predicting the value of the physical parameters of the model, or of even distinguishing a specific material which it describes, from those for which the general form is not applicable.

In the second, or microstructural, approach one attempts to deductively obtain the appropriate transport relations from a detailed study of the system on a smaller scale. The kinetic theory of gases and liquid state theories are concerned with the deduction of material behavior from a know-

ledge of the arrangement and motion of molecules. In the present case, however, the material exhibits a structural scale which is assumed to be large in comparison to molecular dimensions, yet at the same time, small compared to the overall dimensions of the sample of the material, so that it can still be modeled as homogeneous in a macroscopic sense. In general, the microstructural approach thus begins with a description of the 'microstructural state' of the material, then models its microscale behavior in a deductive fashion using the well-known methods of continuum mechanics, and finally passes from this micro-behavior to a prediction of macroscopic of bulk properties by an appropriate statistical averaging process. The phrase 'microstructure state' (or simply microstructure or configuration) is taken to mean the relative positions, orientations, and shapes and sizes of the dispersed particles, along with the relevant parameters describing the material properties of the two phases. The microstructural derivation of macroscopic material properties from a detailed knowledge of the behavior of the particles and suspending media serves as a powerful tool for the engineer or physical scientist. Although one must be content with the study of simple idealized materials in order to obtain a tractable microscale problem, the materials are real (i. e. experimentally realizable) and the theory not only allows prediction of the <u>form</u> of the constitutive relations

describing the material behavior, but also an evaluation of the generated physical coefficients. It is work relating to this second, or microstructural approach that we will be primarily concerned with here. A number of excellent review articles describe much of the work that has been carried on in this field, e. g. Brenner (1970) and Batchelor (1974); only a few specific works shall be referred to below.

The starting point for the study of rheological behavior from this point of view is generally considered to be Einstein's (1906) calculation of the effective viscosity of a dilute suspension of rigid, neutrally buoyant spheres. Later workers have considered a number of different kinds of dispersed particles, higher concentrations, and the complete state of stress of the suspension rather than merely the effective viscosity coefficient.

Detailed considerations of constitutive relations for other transport properties of suspensions are not so numerous, with most studies to date dealing with the diffusive properties (to heat or molecular species for instance) of stationary suspensions. Maxwell (1873) successfully treated the case of a stationary, dilute, dispersion of solid spheres. This work was extended much later to include more concentrated suspensions (Jeffrey, 1973) and inclusions of arbitrary shape (Rocha and Acrivos, 1973). Little attention seems to have been given, however, to the important problem of the thermal properties of

flowing suspensions. The imposed bulk flow can cause considerable changes in the microstructure of the suspension. Further we might expect convective transport of heat on the microscale to provide an additional mechanism for enhanced heat flux. Leal (1973) considered the change in the bulk heat flux of a dilute suspension of spherical drops immersed in a simple bulk shear flow at low microscale Peclet numbers. The resulting flux of heat on the bulk or macroscale was only changed at $O(Pe^{3/2})$ from that for a stationary suspension, despite the fact that the microscale temperature distributions were significantly changed at $O(Pe)$. Nir and Acrivos (1976) considered the corresponding large particle Peclet number problem for a suspension of spheres, obtaining significant enhancement of heat flux transverse to the flow, independent of the thermal properties of the dispersed phase. Analysis of this high Peclet microscale problem, even for the relatively simplified case of spherical inclusions, is complicated by the development of regions of closed streamlines for the flow surrounding the particles. A bounding streamline surface exists, relative to an observer translating with the particle, causing an effectively isothermal region within this boundary to be established. The microscale temperature distribution must then be determined by an appropriate boundary layer analysis on this bounding streamline, introducing considerable complexity to the problem. Consideration of the

thermal properties of flowing suspensions of non-spherical particles, in either low or high Peclet number limits, has not previously appeared in the literature.

The work reported in this thesis deals with the thermal properties of flowing suspensions, both from a theoretical and experimental point of view. The theoretical work will be concerned with the microstructural derivation of constitutive relations describing the flux of heat in a flowing suspension. In Chapter II, we derive and describe the general relations between the bulk heat flux and the microscale distributions of velocity and temperature in a suspension. Included in this discussion will be a model for the inclusion of effects resulting from Brownian motions of the particles. Following this, in Chapters III and IV we present specific predictions for dilute suspensions of neutrally buoyant; (1) slightly deformed droplets and (2) rigid prolate spheroids, for the case of simple bulk shearing motion in the presence of constant bulk temperature gradients orthogonal to the direction of flow. In both cases, the microscale temperature distributions are solved in the asymptotic limit of low, but non-zero Peclet numbers in order to avoid the complications inherent in the high Peclet number problems. Rotational Brownian motion is included in the rigid spheroid analysis. The microscale velocity fields are calculated from the creeping motion Stokes equations, reflecting the

expected low Reynold's number nature of the motions on the (small) particle scale. The restriction to linear variations of the imposed velocity and temperature fields is a reflection of the small length scale of the microstructure when compared to the macroscopic scale of the suspension as a whole. When viewed on this smaller scale, the suspension predominantly reacts to the local value of the gradients of velocity and temperature, so that the results obtained will be a useful first approximation to the behavior in more complicated situations. Finally, the last Chapter V details the design of an apparatus for the experimental investigation of the thermal transport properties of flowing suspensions, and presents some preliminary results for a suspension of rigid spherical particles.

REFERENCES

Batchelor, G.K. 1974 "Transport Properties of Two-Phase Materials with Random Structure" Ann. Rev. Fluid Mech. 6, pp. 227-255.

Brenner, H. 1970 "Rheological Properties of Suspensions" Proceedings of the "Fluid Dynamics Symposium 1970" McMaster University, Hamilton, Ontario, Canada, August 25-27, 1970.

Einstein, A. 1906 "A New Determination of Molecular Dimensions," contained in Investigations on the Theory of Brownian Movement, R. Furth (Ed.) 1956 New York: Dover Publications, Inc., pp. 36-62.

Jeffrey, D.J. 1973 "Conduction Through a Random Suspension of Spheres," Proc. Roy. Soc. Lond. A335, pp. 355-367.

Leal, L.G. 1973 "On the Effective Conductivity of a Dilute Suspension of Spherical Drops in the Limit of Low Particle Peclet Number," Chem. Eng. Comun., 1, pp. 21-31.

Maxwell, J.C. 1873 Electricity and Magnetism, London: Clarendon Press.

Nir, A. and Acrivos,A. 1976 "On the Effective Conductivity of Sheared Suspensions," JFM (to appear)

Rocha and Acrivos, A. 1973 Quart. Journ. Mech. Appl. Math. 26, pp. 217-233.

CHAPTER II

The Relation between Macroscale Heat Flux and the Microstructural State of a Suspension

CHAPTER II

The Relation between Macroscale Heat Flux and the Microstructural State of a Suspension

1) The general relation

We consider a suspension of neutrally buoyant particles in the presence of a bulk shear flow and a bulk temperature field. Our objective is the development of a constitutive equation which describes the effective thermal diffusivity of the suspension considered as an equivalent homogeneous material. The point of view adopted is the conventional one in the field of suspension rheology. We assume that the minimum dimension ℓ of the particles is large compared to the intermolecular length scale α of the suspending medium. The latter may then be treated as a continuum and is modeled for present purposes as an incompressible Newtonian fluid in which a simple scalar Fourier heat conduction law is applicable.

At any arbitrary point in the suspension, when viewed on a length scale of order ℓ, the local variables such as velocity, temperature, enthalpy, or conductive heat flux are random functions of time whose values at any instant depend upon the proximity and motion of suspended particles. The description of bulk or macroscopic quantities for the suspension thus becomes a problem of statistics. At the fundamental level, the most appropriate definition of the bulk variables

is as an ensemble average of the corresponding microscale quantities for a large number of realizations of the system. Instantaneous local values of the velocity, temperature, enthalpy, and conductive heat flux may then be expressed as a sum of the ensemble averaged quantity, and an additional microscale or fluctuating component, i. e.

$$\begin{aligned} u_i &= \langle u_i \rangle + u_i' \\ T &= \langle T \rangle + T' \\ h &= \langle h \rangle + h' \\ q_i &= \langle q_i \rangle + q_i' \quad , \end{aligned} \tag{1}$$

where by definition the averages of the fluctuating components are zero,

$$\langle u' \rangle = \langle T' \rangle = \langle h' \rangle = \langle q_i' \rangle = 0 \quad . \tag{2}$$

As suggested in the introduction, we wish to obtain an operational definition for the bulk conductive heat flux, Q_i, which is consistent with the thermal energy balance for the suspension, viewed as an equivalent homogeneous medium,

$$\frac{\partial \langle h \rangle}{\partial t} + \langle u_i \rangle \frac{\partial \langle h \rangle}{\partial x_i} + \frac{\partial Q_i}{\partial x_i} = 0 \quad . \tag{3}$$

A convenient, if heuristic, method of determining the proper definition of Q_i for this purpose, is to simply apply the same ensemble averaging used in (1) to the exact, instantaneous thermal energy balance which is applicable for each realization of the system,

$$\frac{\partial h}{\partial t} + u_i \frac{\partial h}{\partial x_i} + \frac{\partial q_i}{\partial x_i} = 0 \quad . \tag{4}$$

Taking account of (1) and (2), as well as the continuity relation for an incompressible fluid

$$\frac{\partial u_i}{\partial x_i} = 0 \quad , \tag{5}$$

the result is

$$\frac{\partial \langle h \rangle}{\partial t} + \langle u_i \rangle \frac{\partial \langle h \rangle}{\partial x_i} + \frac{\partial}{\partial x_i} \langle q_i + u_i' h' \rangle = 0 \quad . \tag{6}$$

comparing (6) and (3) it follows that

$$Q_i \quad \langle q_i \rangle + \langle u_i' h' \rangle \quad . \tag{7}$$

It may be seen that the bulk conductive heat flux as defined here, consists of an ensemble average of the instantaneous, microscale conductive heat flux, plus an additional 'convection' term which accounts for the transport of heat by means of the local fluctuating velocity and enthalpy fields.

To proceed further it is necessary to replace the ensemble averages in (7) with the more easily calculable spatial (volume) averages. For this purpose it may be assumed that there exists in the suspension a volume V, containing a statistically significant number of particles, whose linear dimensions of $O(V^{1/3})$ are therefore much larger than the particle length scale ℓ, yet smaller than the length

scale L over which significant variations occur in the bulk velocity or temperature gradients, or in the concentration of particles. The suspension is statistically homogeneous on this scale, and the ergodic hypothesis may be invoked to replace the ensemble averages of (7) by volume averages, i.e.

$$\langle q_i \rangle = \langle\langle q_i \rangle\rangle \equiv \frac{1}{V} \int_V q_i dV$$

These volume averaged quantities clearly vary only on a scale of O(L). They are thus point quantities with respect to the overall macroscopic description of the material, and for this reason we may concern ourselves only with macroscopic velocity and temperature fields which vary linearly in space. The local fluctuating variables, e.g. q_i vary randomly over distances of $o(\ell)$ due to the random nature of the position and motions of the particles in the volume element V.

With the above conditions of statistical homogeneity on the scale of O(V) satisfied, the ensemble averages of (7) may be replaced exactly with volume averages to give

$$Q_i = \langle\langle q_i \rangle\rangle + \langle\langle u_i' h' \rangle\rangle \qquad (8)$$

Expressing the averaging symbols in terms of the appropriate volume integrals, and dividing the averaging volume into its component parts, ΣV_o and $V - \Sigma V_o$, representing the sum of the volumes V_o of the individual particles and the volume of the

surrounding fluid respectively, we obtain

$$Q_i = \frac{1}{V}\int_{V-\Sigma V_o} q_i dV + \frac{1}{V}\int_{\Sigma V_o} q_i dV + \frac{\rho C_p}{V}\int_{V-\Sigma V_o} u_i' T' dV \qquad (9)$$

$$+ \frac{\rho_T C_p}{V}\int_{\Sigma V_o} u_i' T' dV$$

Here, the enthalpy of the fluid and particles have been expressed as

$$h_{fluid} = \rho C_p T \quad ; \quad h_{particles} = \rho_T C_p T \qquad (10)$$

where ρ is the density of the particles and fluid (assumed equal), and $\rho_T C_p$ and C_p are their respective heat capacities. We have assumed these material properties are constant, independent of the temperature, so that they may be taken outside the integral in (9). In the more general case they would be included inside the integral. We assume that the microscale conductive heat fluxes in the fluid and particles satisfy a simple Fourier law for heat conduction, with scalar conductivities k and mk respectively. Then

$$\frac{1}{V}\int_{V-\Sigma V_o} q_i dV + \frac{1}{V}\int_{\Sigma V_o} q_i dV = -\frac{k}{V}\int_{V-\Sigma V_o} \nabla T dV$$

$$- \frac{mk}{V}\int_{\Sigma V_o} \nabla T dV \quad . \qquad (11)$$

Here, again we have assumed the physical properties k and mk are independent of temperature, and may therefore be taken outside the volume integrals as constants. We may

rearrange (11) to the form,

$$- \frac{k}{V} \int_{V-\Sigma V_o} \nabla T dV - \frac{mk}{V} \int_{\Sigma V_o} \nabla T dV = - \frac{k}{V} \int_{V} \nabla T dV + k\frac{(1-m)}{V} \int_{\Sigma V_o} \nabla T dV \quad . \tag{12}$$

Similarly the volume integrals of $u_i'T'$ may be rearranged,

$$\frac{\rho C_p}{V} \int_{V-\Sigma V_o} u_i'T'dV + \frac{\rho \tau C_p}{V} \int_{\Sigma V_o} u_i'T'dV = \frac{\rho C_p}{V} \int_{V} u_i'T'dV + \frac{\rho C_p (\tau-1)}{V} \int_{\Sigma V_o} u_i'T'dV \quad . \tag{13}$$

Thus the expression for the bulk heat flux becomes

$$Q_i = - k \frac{\partial \theta}{\partial x_i} + \frac{k(1-m)}{V} \int_{\Sigma V_o} \nabla T dV + \frac{\rho C_p (\tau-1)}{V} \int_{\Sigma V_o} u_i'T'dV + \frac{\rho C_p}{V} \int_{V} u_i'T'dV \quad , \tag{14}$$

where $\frac{\partial \theta}{\partial x_i} \equiv \langle \nabla T \rangle$, is the bulk average temperature gradient.

Before explicitly discussing the evaluation of the integrals in (14) it is useful to consider the terms in this general expression in some detail. The first term on the right hand side of (14) is just the conductive heat flux which would exist in the absence of the particles if the same average temperature gradient were maintained. The remainder of the terms represent the additional contributions to the bulk heat flux due to the presence of the particles.

The expression (14) for the bulk heat flux may first be considered for a suspension which is completely motionless. In this case, the last two terms are identically zero, and the bulk conductive heat flux differs from that for pure suspending material only when the conductivity of the particles differs from that of the suspending material ($m \neq 1$), and in this case Q_i will depend not only on the conductivity ratio, but also on particle geometry, concentration, relative location, and orientation distribution. For a stationary motionless suspension this microstructural description will be determined by the process of manufacture.

It is generally expected that the flux of heat in the stationary suspension may be related to the gradient of temperature by an 'effective' conductivity tensor K_{ij} defined by

$$Q_i = K_{ij} \frac{\partial T}{\partial x_j} \qquad (15)$$

When the suspension is locally isotropic this tensorial description will reduce to a simple scalar Fourier law for the heat flux $Q_i = -K \frac{\partial \theta}{\partial x_i}$. To show that such a description in terms of an effective conductivity tensor is possible for the general stationary case we merely note that the steady state microstructural behavior of the system is described, in both the continuous and dispersed phases, by the Laplace equation for the microscale temperature distributions:

$$\nabla^2 T_c = 0 \ , \quad \nabla^2 T_d = 0 \ . \tag{16}$$

T_c represents the distribution of temperature in the continuous phase and T_d the distribution in the dispersed particles. Since these governing equations are linear, we may decompose the solution for any arbitrary imposed temperature gradient, $\sum_j \frac{\partial \theta}{\partial x_j} \hat{i}_j = \sum_j \alpha_j \hat{i}_j$,

into three corresponding solutions, called here $T^{(j)}$. $T^{(j)}$ is the solution resulting from the component α_j gradient in the x_j direction. The complete microscale temperature distribution is merely the superposition of the three component solutions. The solutions, $T^{(j)}$, are each linear in the strength of the gradient α_j, and may be written as

$$T^{(j)} = \alpha_j F^{(j)}(x_1, x_2, x_3) \ . \tag{17}$$

The relation (14) for the stationary case is also obviously linear in T, hence the total bulk heat flux Q_i may be expressed as the superposition of the resulting heat fluxes, $Q_i^{(j)}$, for each of the component problems. As a result of this linearity we may evaluate the individual components of the tensor K_{ij} by the formula

$$K_{ij} = -\frac{Q_i}{\alpha_j} = -\frac{Q_i^{(j)}}{\alpha_j} = k\left\{\delta_{ij} + \frac{(m-1)}{V}\int_{\Sigma V_o} VF^{(j)}\,dV\right\} \qquad (18)$$

since only $Q_i^{(j)}$ depends on α_j. For a given microstructural state, the effective thermal conductivity will therefore be a unique, material property of the stationary composite.

In the presence of flow the situation becomes considerably more complicated. Not only are the geometry, location, and orientation of the particles important, but the bulk conductive heat flux, Q_i, depends critically on both the type and strength of the flow. Indeed, even when the thermal properties of the dispersed and continuous phases are identical, the presence of the last term in (14) suggests that the existence of flow may alter the bulk flux Q_i from that of the motionless composite. The bulk conductive flux Qi is a function not only of the material, but also of the flow.

In the general case, the presence of flow has two distinct, though related, effects. First is the flow-induced change in the local temperature distributions for a given

microstructural configuration by the action of local convective heat transfer. As the local temperature distribution is altered, so are the contributions from each of the three volume integrals of (14). For a given microstructure, the local temperature field will respond to any variations in flow or temperature conditions on a time scale which depends on the thermal properties of the two phases and the nature of the flow or bulk temperature profile will generally induce a transient response in the heat flux. At steady state the heat flux will clearly depend directly on the strength and magnitude of the flow, since both the local temperature fields and the volume averaged quantities $\langle\langle u_i' T' \rangle\rangle$ are directly influenced. The flow has a further effect, however, in that the microstructure of the suspension is related to the flow. Changes in the flow will thus produce transients in the response of the system on a second time scale associated with the establishment of the resulting microstructural configuration. As noted previously the bulk heat flux is sensitive to the shape, motion, orientation, and configurational distributions of the suspended particles. For example, rigid nonspherical particles undergo flow-induced rotations, causing changes in the orientation distribution from that for the motionless composite and deformable particles may experience changes in shape due to hydrodynamic interaction with the surrounding fluid. In both examples, the effects depend critically on the type of

bulk flow which is imposed on the material, resulting in a dependence on flow type of the bulk heat flux Q_i. These hydrodynamically induced changes in microstructure are all deterministic (initial-value) processes, thus conferring on the bulk conductive heat flux a perfect 'memory' for past microstructural states of the material. In any real suspension these flow-induced changes in the microstructure are resisted by one or more 'restoring' mechanisms, such as rotational Brownian motion or particle elasticity, which would maintain the equilibrium or rest configuration in the absence of the flow. The existence of a mechanism which acts to restore the rest state of the material on a finite time scale insures that this memory is 'fading' in the sense that the dependence of Q_i on the recent microstructural states is stronger than its dependence on earlier states. The steady state microstructural configuration will represent a balance between the hydrodynamic and restoring mechanism forces. The dependence of this microstructural state on the type of flow, and the relative strengths of the flow and restoring mechanism will result in bulk heat flux dependence on the type and strength of the flow, the thermal properties of the particles and fluid, as well as those geometrical and mechanical properties of the particles and fluid which play a role in the restoring mechanism.

We shall only be concerned with steady state situations

in what follows, for even in this simplified situation there will be considerable complexities in the constitutive behavior of the flowing suspension. The results obtained for a specific type of flow, consequently the thermal transport properties of a flowing composite will therefore no longer be a unique property of the material.

2) Evaluation of the general relation in the case of dilute concentrations

Having made these general statements regarding the interpretation of the various terms in (14) we may now consider its evaluation for certain cases. It is convenient to seperately consider the particle contribution to the flux, denoted by Q_i, defined by

$$Q_i^* = \frac{k(1-m)}{V} \int_{\Sigma V_o} VT dV + \frac{\rho C_p(\tau-1)}{V} \int_{\Sigma V_o} u_i' T' dV + \frac{\rho C_p}{V} \int_V u_i' T' dV \quad . \tag{19}$$

We may further define the average contribution per particle $\bar{Q}_i^*$ by simply dividing the contribution Q_i^* by the number n of particles in the averaging volume V

$$\bar{Q}_i^* \equiv Q_i^*/n \quad . \tag{20}$$

Although in the general case, the contribution Q_i^* depends on the configuration and orientation distributions of all the n particles in the volume V of the suspension, it has been the assumption in much of the previous work on suspension problems of this general type, that for small concentrations, the flux could be expressed as a series in integral powers of the volume fraction $\emptyset$. The first, $O(\emptyset)$, term was calculated by assuming the particles were non-interacting. Single particle problems for the microscale fields near a represen-

tative particle could then be solved and the bulk properties related to this single particle solution. Higher order (ϕ^m) corrections were then calculated by considering successively, m-particle interactions. In order to establish the exact circumstances under which this method of evaluation of the bulk properties was valid, as well as to clear up certain ambiguities arising in the evaluation of each of the m-particle interactions, Jeffrey (1974) rigorously developed an expansion technique for the evaluation of the succesive ϕ^m corrections. We shall only be concerned, here with the result obtained for the non-interacting particle case. As long as the configuration and orientation distributions are established by hydrodynamic interactions, with or without the additional effects of Brownian motion, Jeffrey demonstrates that the $O(\phi)$ correction to the heat flux may be calculated by considering an isolated particle immersed in a flow and temperature field corresponding to the bulk average values. If the particles are all identical, and have exactly the same deterministic orientation and motion, then values obtained for the integrals is (19) upon substitution of the single particle, deterministic, fields may simply be multiplied by the number of particles in the volume V to obtain the contribution Q_i^* to the flux. Often it will be the case that the particles are small enough to be subjected to the influences of random Brownian motions. The motions and orientations of the individual particles will therefore be

of a random nature, about which we will only have statistical knowledge. In this case the individual single particle contributions are not equal and $\overline{Q_i^*}$ must still be regarded as the average contribution per particle. Because of the assumption that the volume V contains a statistically large sample n of particles, the average contribution per particle can be calculated either as the ensemble average over all possible realizations of the single particle problem or as a long time average for the single particle problem; both averages being identical to the value obtained by dividing the total contribution Q_i^* by the number of particles, according to the ergodic hypothesis. We may therefore express the bulk heat flux Q_i for the dilute case as

$$Q_i = -k \frac{\partial \theta}{\partial x_i} + Q_i' \tag{21}$$

where, using the relation $n = \frac{\phi V}{V_o}$, V_o being the volume of each identical particle,

$$Q_i' = \frac{k(1-m)\phi}{V_o} \int_{V_o} \overline{\nabla T} dV + \frac{\rho C_p (\tau-1)\phi}{V_o} \int_{V_o} \overline{u_i' T'} dV$$

$$+ \frac{\rho C_p \phi}{V_o} \int_V u_i' T' dV \quad . \tag{22}$$

The final volume integral is evaluated in the limit $V \to \infty$, and the overbar over the integrands indicates that the quantity must be considered as an appropriate statis-

tical average of the quantity. A more detailed discussion of the treatment of (22) in the presence of Brownian motions of the particles will be delayed until a little later. Application of the Gauss-divergence theorem to (22) allows us to write

$$Q_i' = \frac{k(1-m)\phi}{V_o}\int_{A_o}\overline{n_i T}\,dA + \frac{\rho C_p(\tau-1)}{V_o}\int_{V_o}u_i'T'\,dV + \frac{\rho C_p\phi}{V_o}\int_{V\to\infty}\overline{u_i'T'}\,dV \quad . \tag{23}$$

Here, A_o is the surface of the particle and n_i the i-component of the unit-vector normal to the surface directed outward. We shall drop the overbar in the following, understanding the integrals to be averaged, and nondimensionalize the quantities in (23). We nondimensionalize lengths with respect to the characteristic length scale of the particle, ℓ. Areas and volumes are therefore nondimensionalized with respect to a velocity scale V_c characteristic of the bulk motion. As we are primarily concerned here with simple shearing motions with shear rate γ, the characteristic velocity scale is $u_c = \gamma\ell$. The governing differential equations for the microscale temperature distributions in the particle and the suspending fluid are linear in T, as is the bulk heat flux relation (23), so that we may separately consider gradients in each of the principal direc-

tions, i.e. $T^{(j)} = \alpha_j x_j$ (no summation implied). A characteristic temperature scale is therefore $\alpha_j \ell$. In terms of nondimensional velocities, temperatures, areas, and volumes, (23) is then

$$\frac{Q_i^{(j)'}}{\alpha_{jk}} = \frac{(1-m)\phi}{V_o} \int_{A_o} n_i T^{(j)} dA + \frac{(\tau-1)Pe_f\phi}{V_o} \int_{V_o} u_i' T^{(j)'} dV + \frac{Pe_f\phi}{V_o} \int_{V\to\infty} u_i' T^{(j)'} dV \qquad (24)$$

where the Peclet number for the microscale advective-diffusion heat problem, based on fluid properties, is

$$Pe_f = \frac{\rho C_p \gamma \ell^2}{k} .$$

For the stationary case we found that the bulk heat flux could be expressed in terms of an effective conductivity tensor that was a unique material property of the specific composite. The existence of a bulk flow has not only added the complexity that the bulk heat flux is no longer a unique material property, but has apparently precluded the existence of an effective conductivity tensor for the specific flow being considered. The differential equation describing the local distribution of temperature cannot be satisfied for a linear bulk temperature distribution having any component gradient in the direction of flow, since the far field boundary conditions do not satisfy the advective-diffusion equation for any non-zero Peclet number.

The requirement that the final volume integral in (24) be taken over a volume tending to infinity requires, therefore, the consideration of the exact bulk flow and temperature distributions, not just their linear (first derivative) parts, so that the governing differential equation may be satisfied. In the case of simple shearing flow, we are limited to the consideration of temperature gradients orthogonal to the flow. The resulting heat fluxes are linearly related to the gradients of temperature in the two principal directions orthogonal to the flow direction, and the general case of an arbitrarily oriented temperature gradient in the plane orthogonal to the flow may be considered by superposition of the flux resulting from the two component gradients. It will therefore be convenient to express a particular component of the bulk heat flux in terms of the proportionality constants between the flux and the particular temperature gradients, which will be referred to as particular effective conductivities. To emphasize the critical distinction between the flowing and stationary cases we summarize the differences caused by the motion of the suspension:

1) The motion of the suspension introduces the additional mechanism of convective transport of heat on the microscale.
2) The microscale structure of the suspension will be influenced by the nature and strength of the flow,

as well as any mechanisms tending to restore the structure to an equilibrium state.

3) The bulk heat flux cannot be expressed in terms of an effective conductivity tensor since the existence of locally non-orthogonal, linear, velocity and temperature fields on the bulk scale, violates the governing differential equation on the microscale.

3) The effects of Brownian motion

We have seen that evaluation of the particle contribution to the bulk heat flux, Q_i, reduces to evaluation of the average value, for an isolated non-interacting particle, of the integrals

$$Q_i' = \frac{k(1-m)\phi}{V_o} \int_{V_o} \overline{\nabla T}\, dV + \frac{\rho C_p(\tau-1)\phi}{V_o} \int_{V_o} \overline{u_i' T'}\, dV$$

$$+ \frac{\rho C_p \phi}{V_o} \int_{V\to\infty} u_i' T'\, dV \quad , \qquad (22)$$

where the overbar indicates averaging of the integrand over an ensemble of possible realizations of the isolated particle problem. If the single particle problem is completely deterministic and all the particles have identical size, shape, and orientation, then evaluation of the average is equivalent to determining the values of the integrals for the deterministic one particle problem. If on the other hand, the particles are small enough to exhibit significant Brownian motions, then the single particle problem will no longer be deterministic in nature. In particular, the orientation and motions of the particle will exhibit a random component, and the effects of these random motions on the bulk heat flux must be accounted for in some rational manner. Fortunately, this can still be done within the general framework of equation (22).

Brownian motion is a reflection of the essentially molecular nature of the suspending fluid at the scale of the sufficiently small particles. Nevertheless, it is not necessary to completely surrender the benefits of a continuum model for the suspending fluid in order to model the Brownian motions of the particle. In the present context, our concern is not merely with the random motions of the particles, but the resulting fluid motions and temperature variations as well. Thus, the usual treatment of Brownian motion by the addition of random or fluctuating forces to the systematic hydrodynamic forces in the equation of motion for the particle (i.e. the Langevin equation) is unsuitable for our present purposes. An alternative which does satisfy our objectives, and still retains a continuum view of the suspending fluid, is the theory of hydrodynamic fluctuations, described by Landau and Lifshitz (1959) and recently extended to include Brownian motions of a particle by several investigators, i.e. Fox and Uhlenbeck (1970), Chow and Hermans (1972), Hauge and Martin-Löf (1972), and Hinch (1975). For convenience, we shall refer to these works as FU, CH, HML, and H respectively.

The main assumption of the theory of fluctuating hydrodynamics is that the governing continuum equations of motion and thermal energy are valid for the complete problem, including fluctuations in all the independent variables.

Fluctuations in the stress tensor and heat flux vector occur not only due to the fluctuations in the velocity and temperature gradients, but also as a result of spontaneous local stresses and heat fluxes, denoted by $\underline{S}$ and $\vec{g}$, which are independent of each other, and of the local velocity and temperature gradients (c.f. Hinch 1975). The quantities $\nabla\cdot\underline{s}$ and $\nabla\cdot\vec{g}$ drive fluctuations in the other hydrodynamical and thermal variables, and these fluctuations in the fluid, away from any macroscopic boundaries, are responsible for its dissipative transport properties. Relations between the statistical properties of $\underline{s}$ and $\vec{g}$ and the continuum transport parameters such as μ or k, are contained in so-called fluctuation-dissipation theorems which may be derived from certain postulates of non-equilibrium thermodynamics, (c.f. Hinch (1975)).

The introduction of colloidal particles into the fluctuating fluid introduces a possible source of random motions on a much longer time scale than that characterizing $\nabla\cdot s$. The key property of particles (whether solid, elastic, drops etc.) which is responsible for these longer time scale random motions is that they resist deformation of shape so that at least part of the fluctuating force in the suspending fluid can be sustained with no local deformation. In these circumstances, the random fluctuating forces can contribute to random translational and rotational motions of the par-

ticles, but only on a relatively slow continuum time-scale. For translational motion this time scale is a measure of the time required for a particle to slow down following an initial impulse, and is given by m/γ where m is the mass of the particle, and γ the fluid mechanical drag which acts on it. These random motions of the particle will also induce random motions in the suspending fluid with the same relatively slow time-scale, which are superposed on any deterministic local motions which may be present due to the bulk flow of the suspension. We shall refer to the random motions of particles and suspending fluid on the time scale m/γ (or its equivalent for rotational motion) as 'Brownian', in order to distinguish them from the much more rapid fluctuations which occur at the molecular scale.

It is thus convenient, for discussion purposes, to split the <u>fluid</u> velocity and stress fields for the single-particle microscale problem into three parts: deterministic contributions $\vec{U}$ and $\underline{\underline{\Sigma}}$, associated with the motion of the suspension as a whole; Brownian contributions, $\vec{v}$ and $\underline{\underline{\tilde{\sigma}}}$, associated with the random continuum level motions of particles and fluid; and fluctuating parts $\vec{U}^{\dagger}$, $\underline{\underline{\sigma}}^{\dagger}$ and $\underline{\underline{s}}$ due directly to molecular fluctuations, i.e.

$$\vec{u} = \vec{U} + \vec{v} + \vec{u}^{\dagger}$$

and $$\underline{\underline{\sigma}} = \underline{\underline{\Sigma}} + \underline{\underline{\tilde{\sigma}}} + \underline{\underline{\sigma}}^{\dagger} + \underline{\underline{s}} \qquad (25)$$

The equations governing these distributions will be characterized by small Reynolds numbers for the velocities $\vec{U}$ and $\vec{v}$, and small amplitude for the fluctuation $\vec{u}^{\dagger}$, so that the linear Stokes equations are applicable. As a result of the linearization we may pose the single particle microscale problem in a coordinate frame of reference that instantaneously is centered in the particle with axes concident to the particle axes. The velocities in the governing equations are still the velocities measured relative to a fixed coordinate frame (c.f. HML).

We shall be primarily concerned here with suspended particles which are rigid but not necessarily spherical. We consider first the governing equations of motion for the rigid particle of mass m, volume V_o, surface area S_o, moment of inertia tensor $\underline{J}_p$, and density ρ, in an incompressible fluid of equal density ρ and of viscosity μ. The linearized equations for the complete velocity and pressure fields in the fluid are

$$\left.\begin{aligned} \rho \frac{\partial \vec{u}}{\partial t} &= \nabla \cdot \underline{\underline{\sigma}} \\ \nabla \cdot \vec{u} &= 0 \\ \underline{\underline{\Sigma}} &= -P\underline{\underline{I}} + \mu(\nabla\vec{u} + \nabla\vec{u}^{T}) \\ \underline{\underline{\sigma}} &= -p\underline{\underline{I}} + \mu(\nabla\vec{v} + \nabla\vec{v}^{T}) \\ \underline{\underline{\sigma}}^{\dagger} &= -p^{\dagger}\underline{\underline{I}} + \mu(\nabla\vec{u}^{\dagger} + \nabla\vec{u}^{\dagger T}) \end{aligned}\right\} \quad \bar{x}_{\varepsilon V - V_o} \qquad (26), (27), (28)$$

Here $\nabla\vec{u}^T$ is the transpose of the tensor $\nabla\vec{u}$, and $\underline{\underline{\Sigma}}$, $\underline{\underline{\tilde{\sigma}}}$, and $\underline{\underline{\sigma}}^{\ddagger}$ are the Newtonian stress tensors related to the deterministic, Brownian, and fluctuating fluid velocities respectively. As a result of the linearization of the problem, we may for convenience consider the Brownian and fluctuating velocity problems separately from the deterministic motions, the complete velocity fields being merely the super-position of the separate parts. Considering just the $\vec{v}$ and $\vec{u}^{\ddagger}$ fields, and averaging the governing equations (26) - (29) over the time scale $\delta t \sim m/\gamma$ characteristic of the relatively slow Brownian motions of the particle, we obtain:

$$\left.\begin{aligned} \rho\,\frac{\partial\vec{v}}{\partial t} &= -\nabla p + \mu\nabla^2\vec{v} \\ \nabla\cdot\vec{v} &= 0 \end{aligned}\right\} \quad \vec{x}\in V-V_o \qquad (31),\ (32)$$

Comparison of (31) and (32) with (26), (27) and (28) shows that the fluctuations satisfy the equations

$$\left.\begin{aligned} \rho\,\frac{\partial\bar{u}^{\ddagger}}{\partial t} &= -\nabla p^{\ddagger} + \mu\nabla^2\bar{u}^{\ddagger} + \nabla\cdot\underline{\underline{s}} \\ \nabla\cdot\bar{u}^{\ddagger} &= \end{aligned}\right\} \quad \bar{x}\in V-V_o \qquad (33),\ (34)$$

We note that the time derivative must be included in the averaged equation (31), as was first pointed out by Lorentz in 1911, and recently restated by Zwanzig (1970), CH, HML, and Hinch. Substitution of a typical Stokes law drag formula $\gamma \sim \Lambda\mu\ell$ for steady motion, into the expression m/ℓ for the characteristic decay time δt shows that the latter is precisely equal to the time for vorticity to diffuse over the length of the particle, ℓ^2/ν_f, where ν_f is the kinematic viscosity of the fluid. The flow, $\vec{v}$, induced by the Brownian motion of the particle can therefore not possibly be steady when viewed on this time scale, and unsteady contributions to the particle drag must be as important as the steady viscous forces.

Boundary conditions for the Brownian field $\vec{v}$, are that it vanish far from the particle

$$\vec{v} \to 0 \quad , \quad |\vec{x}| \to \infty \quad . \tag{35}$$

so that the total velocity field $\vec{u}$ simply reduces to the deterministic macroscopic undisturbed velocity at infinity. At the particle surface, the Brownian velocity additionally satisfies the no-slip condition,

$$\vec{v} = \vec{v}_p \equiv V_p + \vec{\omega}_p \Lambda \vec{x} \quad , \quad \vec{x} \varepsilon S_o \quad . \tag{36}$$

Here, the motion $\vec{v}_p$ of any point inside the particle has been split into a translational motion V_p of the center of mass, and a solid body rotation of the particle given by its angular rotation $\vec{\omega}_p$. (Similar to the fluid velocity $\vec{u}$ we have considered the particle velocity distribution $\vec{u}_p$ to be composed of a deterministic, $\vec{U}_p$, and Brownian part. The deterministic motion $\vec{U}_p$ may also be split into a translational and rotational motion, defined as $\vec{U}_p = \vec{U}_p + \vec{\Omega}_p \Lambda \vec{x}$.)

The fluctuations are required to be bounded everywhere, and to vanish on the particle surface.

$$\vec{u}^{\ddagger} = 0 \qquad \vec{x} \epsilon S_o \tag{37}$$

This last condition is a result of the fact that the particle cannot itself move on the short time scale of fluctuations in the fluid, coupled with the no slip condition at the particle surface. The fluctuating motion of the fluid is thus seen to derive from the divergence of the fluctuating stress tensor $\underline{\underline{s}}$. The particle moves on the longer continuum time scale, and its motion results in random motions of the surrounding fluid due to the condition (36). A direct result of the splitting of the governing equations into the 'Brownian' and fluctuating parts is that the quantities in (31), (32), (35) and (36) are <u>independent</u> of those in (33), (34) and (37), (HML). The formulation of the problem is completed by specifying equations for the

particle velocities, $\bar{V}_p$ and $\bar{\omega}_p$. These are simply the equations of motion for the particle

$$m \frac{d\vec{V}_p}{dt} = \vec{F}_p(t) = \int_{S_o} \vec{n} \cdot (\tilde{\underline{\underline{\sigma}}} + \underline{\underline{\sigma}}^{\dagger} + \underline{\underline{s}}) dS \quad . \tag{38}$$

$$\underline{\underline{J_p}} \frac{d\vec{\omega}_p}{dt} = \vec{M}_p(t) = \int_{S_o} \vec{x} \Lambda (\vec{n} \cdot (\tilde{\underline{\underline{\sigma}}} + \underline{\underline{\sigma}}^{\dagger} + \underline{\underline{s}}) dS \quad . \tag{39}$$

Here, in the absence of externally applied forces and couples, the force $\vec{F}_p(t)$ and torque $\vec{M}_p(t)$ on the particle are equivalent to integration of the stress over the surface of the particle. Hinch (1975) has clearly demonstrated that the spontaneous fluctuating stress $\underline{\underline{s}}$ must be allowed to act on the boundary of the particle, as well as in the fluid. Equations (38) and (39) can be written in the form of generalized (Non-Markovian) Langevin equations, (HML,H). The friction tensor of the equation is found from the solution of the average problem (31), (32), (35), and (36), and is known for simple particle shapes such as spheres. A fluctuation - dissipation theorem may be constructed relating this friction to the spectrum of the fluctuating force on the particles, from which the statistical properties of the motions $\vec{V}_p$ and $\vec{\omega}_p$ may be calculated. Finally,

for a time scale very long compared to the Brownian time scale δt, the description of the motion of a particle reduces to the traditional Einstein-Smoluchowski theory of Brownian motion, with the only parameter describing the evolution of the particles position or orientation distribution being the diffusion tensor, $\underline{\underline{D}}_{Br}$, defined over the same space. As we have previously seen, this long time average is precisely the average denoted in (22) by the overbar. Even on the shorter time scale, the average of the fluctuations $\vec{u}'$ is zero, so that averaging of the total distributions $\vec{u}$, $\vec{u}_p$ over the longer time-scale results in

$$\bar{\vec{u}} = \bar{\vec{U}} + \bar{\vec{v}} \quad ; \qquad \bar{\vec{u}}_p = \bar{\vec{U}}_p + \bar{\vec{v}}_p \quad . \tag{40}$$

The most important implication of these relationships is that the random Brownian velocities $\vec{v}$ and $\vec{v}_p$ will have a non-zero mean on this long-time-scale, whenever there exist gradients in the statistical distribution of particle concentration or orientation. Having made the assumption of local homogeneity of the concentration $\emptyset$ in the present work, only longer-time-scale or 'mean' values of $\vec{v}$ and $\vec{v}_p$ resulting from gradients in the orientation distribution will be of concern here. For example, if we consider axisymmetric particles which are characterized by a rotational diffusion coefficient, D_r, the mean velocity fields $\bar{\vec{v}}$ and $\bar{\vec{v}}_p$ are those associated with a rotation of the particle in the orientation space $\vec{\emptyset}$, at a rate

$$\bar{\vec{\omega}}_{p_{Br}} = -D_r \nabla_{\vec{\phi}} \ln F(\vec{\phi}) \qquad (41)$$

in a quiescent fluid. Here $F(\vec{\phi})$ is the probability density function for particle orientation, which may be obtained by solution of a Fokker-Plank equation representing the competition between purely hydrodynamic and Brownian rotation, (see, for example, Hinch and Leal (1972) who have considered the orientation distribution function $F(\theta,\phi,)$ for rigid spheroids in a simple linear shear flow). For future reference, we denote the parts of $\vec{v}$ and $\vec{v}_p$ which have zero mean relative to the long time average as $\vec{v}^*$ and $\vec{v}_p^*$, i.e.

$$\vec{v} = \bar{\vec{v}} + \vec{v}^* \; ; \quad \vec{v}_p = \bar{\vec{v}}_p + \vec{v}_p^* \qquad (42a)$$

A second implication of (40) which may appear surprising at first is that the average $\bar{\vec{U}}$ is <u>not</u> simply $\bar{U}$. Instead, in the presence of Brownian rotation, the velocity field $\bar{\vec{U}}$ is the fluid motion induced by the deterministic rotation of the particle and the imposed bulk motion of the suspension, calculated as a function of the <u>instantaneous</u> particle orientation, and then averaged with the probability density function for orientation as a weighting factor. The difference between these mean velocity distributions $\bar{\vec{U}}$ and $\bar{\vec{U}}_p$ and the instantaneous fields $\vec{U}$ and $\vec{U}_p$ will similarly be denoted by $\vec{U}^*$ and $\vec{U}_p^*$, i.e.

$$\vec{u} = \bar{\vec{u}} + \vec{u}^* \quad ; \qquad \vec{U}_p = \bar{\vec{u}}_p + \vec{u}^*_p \quad . \tag{42b}$$

Having formulated the description for the velocity distributions we now consider the effects of fluctuations and Brownian motions on the temperature distributions in the suspension, and on the heat flux Q_i. We begin with the governing equations for the temperature distributions in the suspending fluid and particle. The basic equations, including the fluctuating nature of the velocities in the fluid and the fluctuations of temperature and heat flux in both the fluid and particle, are

$$\rho C_p\left\{\frac{\partial T}{\partial t} + \vec{u}\cdot\nabla T\right\} = k\nabla^2 T - \nabla\cdot\vec{g} \qquad \vec{x}\varepsilon V-V_o \tag{43}$$

$$\rho_T C_p\left\{\frac{\partial T_p}{\partial t} + \vec{u}_p\cdot\nabla T_p\right\} = mk\nabla^2 T_p - \nabla\cdot\vec{g}_p \qquad \vec{x}\varepsilon V_o \tag{44}$$

in which T and T_p denote the temperature in the fluid and particle respectively, and $\vec{g}$ and $\vec{g}_p$ the corresponding fluctuating heat flux vectors (c.f. FU). We restrict ourselves to temperature fields that are everywhere bounded and continuous, so that the boundary conditions at the particle surface are

$$\left.\begin{aligned} T_p &= T && (45)\\ \vec{n}\cdot(mk\nabla T_p - \vec{g}_p) &= \vec{n}\cdot(k\nabla T - \vec{g}) && (46)\end{aligned}\right\} \quad x\varepsilon S_o$$

Analogously to the temperature problem, we have allowed the fluctuating heat fluxes $\vec{g}$ and $\vec{g}_p$ to act not only in the fluid and particle, but also across the boundary.

The most convenient procedure at this point, is to simply expand the temperature distributions as a sum of three parts, analogous to the expansions for the velocity fields,

$$\begin{aligned} T &= \bar{T} + \tilde{T} + T^{\ddagger} \quad , \\ T_p &= \bar{T}_p + \tilde{T}_p + T_p^{\ddagger} \quad . \end{aligned} \qquad (47)$$

The last terms in these expressions are the temperature fluctuations arising from $\vec{g}$ and $\vec{g}_p$, which vanish identically when averaged over the Brownian motion time scale. The remaining two terms in each expansion, $\tilde{T}$ and $\tilde{T}_p$ are Brownian motion contributions defined in such a fashion that

$$\bar{\tilde{T}} = \bar{\tilde{T}}_p = 0 \quad . \qquad (48)$$

The physical significance of the 'mean' temperatures T and T_p will become evident shortly. To proceed further it is necessary to substitute the expansions (47) into the governing equations (43) and (44) and the boundary conditions (45) and (46), linearized for the small amplitude fluctuations, and average over the Brownian time scale. This results in the equations

$$\rho C_p\left\{\frac{\partial (T+\tilde{T})}{\partial t} + (\vec{U} + \vec{v})\cdot\nabla(T + \tilde{T})\right\} = k\nabla^2(T + \tilde{T}) \qquad (49)$$

$$x\varepsilon V-V_o$$

$$\rho\tau C_p\left\{\frac{\partial}{\partial t}(T_p + \tilde{T}_p) + (\vec{U}_p + \vec{v}_p)\cdot\nabla(T_p + T_p)\right\} =$$

$$mk\nabla^2(T_p + T_p) \qquad \vec{x}\varepsilon V_o \qquad (50)$$

with the matching conditions at the surface,

$$\left.\begin{aligned} T_p + \tilde{T}_p &= T + T \qquad (51)\\ m\vec{n}\cdot\nabla(T_p + \tilde{T}_p) &= \vec{n}\cdot\nabla(T + T) \qquad (52)\end{aligned}\right\} \quad \vec{x}\varepsilon S_o \quad .$$

and the condition that the temperature distribution becomes merely the macroscopically imposed distribution far from the particle. In terms of a coordinate frame that is at any instant centered in the particle and aligned with its axes, we will find that the outer boundary condition is in

general a function of time (due to the changing position and orientation of the particle) so that this condition becomes,

$$T + \tilde{T}_p \Rightarrow T_{bulk}(\vec{x},t) \qquad \text{as } |\vec{x}| \to \infty \quad . \tag{53}$$

Comparison of equations (49) - (53) with (43) - (46) shows that the fluctuations satisfy separately,

$$\rho\tau C_p\left\{\frac{\partial T_p^{\ddagger}}{\partial t}\right\} = mk\nabla^2 T_p^{\ddagger} - \nabla\vec{g}_p \tag{54}$$

$$\rho C_p\left\{\frac{\partial T^{\ddagger}}{\partial t}\right\} = k\nabla^2 T^{\ddagger} - \nabla\vec{g} \tag{55}$$

subject to the conditions that $T^{\ddagger}$, $T^{\ddagger}_p$, $\vec{g}$ and $\vec{g}_p$ are everywhere bounded and that at the surface

$$\left.\begin{aligned} T^{\ddagger} &= T_p^{\ddagger} && (56)\\ \vec{n}\cdot(mk\nabla T_p^{\ddagger} - \vec{g}_p) &= \vec{n}\cdot(k\nabla T^{\ddagger} - \vec{g}) && (57)\end{aligned}\right\} \vec{x}\varepsilon S_o$$

We note that the separation, like that for the velocity problem, means that the quantities in (49) - (53) are independent of those in (54) - (57). Further we note there is no systematic temperature distribution induced by the purely random fluctuating heat fluxes $\vec{g}$ and $\vec{g}_p$. Those

heat fluxes merely drive fluctuations in the temperature distributions both inside and outside of the particle, which produce no measurable effect on the bulk heat flux. The temperature distribution inside the particle, unlike the corresponding velocity of the particle, can react on the much shorter time-scale of the fluctuations, resulting in a coupling between the fluctuations in the fluid and particle, but no systematic heating or cooling of the particle on the time scale δt. The random portions of the more slowly varying composite temperature fields, $T + \tilde{T}$ and $T_p + \tilde{T}_p$ thus exist solely as a result of the Brownian motions of the particle in a non-uniform ambient temperature distribution (i.e. from the condition (53)).

To perform the final averaging over the longer-time scale denoted by the overbar it is first necessary to substitute the expansions for the mean and 'random' velocity fields (42) into (49) and (50) and formally expand the operators. We then obtain

$$\rho C_p \Big\{ \frac{\partial T}{\partial t} + \frac{\partial \tilde{T}}{\partial t} + \bar{\vec{U}}\cdot\nabla T + \bar{\vec{v}}\cdot\nabla T + \vec{U}^*\cdot\nabla T + \vec{v}^*\cdot\nabla T + \bar{\vec{U}}\cdot\nabla\tilde{T}$$

$$+ \bar{\vec{v}}\cdot\nabla\tilde{T} + \vec{U}^*\cdot\nabla\tilde{T} + \vec{v}^*\cdot\nabla\tilde{T} \Big\} = k\nabla^2 T + k\nabla^2\tilde{T} \qquad (58a)$$

$$\vec{x}\varepsilon V - V_o$$

$$\rho_T C_p \Big\{ \frac{\partial T_p}{\partial t} + \frac{\partial \tilde{T}_p}{\partial t} + \bar{\vec{U}}_p \cdot \nabla T + \bar{\vec{v}}_p \cdot \nabla T + \vec{U}_p^* \cdot \nabla T + \vec{v}_p \cdot \nabla T$$

$$+ \bar{\vec{U}}_p \cdot \nabla T + \bar{\vec{v}} \cdot \nabla T + \vec{U}^* \cdot \nabla \tilde{T} + \vec{v}^* \cdot \nabla \tilde{T} \Big\}$$

$$= mk\nabla^2 T_p + mk\nabla^2 \tilde{T}_p \qquad (59a)$$

$$\vec{x} \epsilon V_0$$

We may now perform the long time scale averaging, remembering that T, T_p, $\bar{\vec{U}}$, $\bar{\vec{v}}$, $\bar{\vec{U}}_p$ and $\bar{\vec{v}}_p$ are already averaged quantities, and that the fluid and particle are incompressible. The resulting equations for the mean temperature fields are then,

$$\rho C_p\left\{ \frac{\partial T}{\partial t} + (\bar{\vec{U}} + \bar{\vec{V}})\cdot\nabla T \right\} = k\nabla^2 T - \rho C_p \nabla\cdot(\vec{U}^*\tilde{T} + \vec{V}^*\tilde{T})$$

$$\vec{x}\notin V-V_o \qquad (60a)$$

$$\rho_T C_p\left\{ \frac{\partial T_p}{\partial t} + (\bar{\vec{U}}_p + \bar{\vec{V}}_p)\cdot\nabla T_p \right\} = k\nabla^2 T_p$$

$$- \rho_T C_p \nabla\cdot(\vec{U}^*_p\tilde{T}_p + \vec{V}^*_p\tilde{T}_p) \qquad \vec{x}\in V_o \qquad (61a)$$

Before explicitly discussing the interpretation of the various terms in equations (60) and (61) it is useful to nondimensionalize the equations (58) and (59) and the 'mean' equations (60) and (61) in order to characterize the magnitudes of the various terms. For this purpose we nondimensionalize all lengths with respect to the characteristic particle length scale. There are two characteristic velocity scales of interest in the problem; the first being a scale characteristic of the bulk imposed deterministic motions V_{Bulk}, which for simple shearing motion of shear rate γ would be $V_{Bulk} \sim \gamma\ell$. It is convenient to not only scale the deterministic motions $\vec{U}$ and $\vec{U}_p$ with this scale, but the effective Brownian velocities $\bar{\vec{V}}$ and $\bar{\vec{V}}_p$ as well. The exact magnitude of these effective velocities will be determined by equation (41) and the probability density function $F(\vec{\phi})$ resulting from the Fokker-Plank equation, which similarly is nondimensionalized with the velocity scale characteristic of the hydrodynamic motions, (c.f. Hinch & Leal 1972). The

Purely random velocity fields $\bar{V}^*$ and $\bar{V}_p^*$ are characterized by the second velocity scale, $V_{Brownian} \sim (KT/m)^{\frac{1}{2}}$ of the short-time scale Brownian motions. These two velocity scales will in turn yield two characteristic Peclet numbers for each of the equations (58) - (61). It is convenient to define a single Peclet number for the fluid and particle based on the characteristic velocity scale V_{Bulk},

$$Pe_f \equiv \frac{\rho C_p V_{Bulk} \ell}{k} \quad ; \quad Pe_p \equiv \frac{\rho \tau C_p V_{Bulk} \ell}{mk} = \frac{\tau}{m} Pe_p$$

and further define the nondimensional ratio of the velocity scales by the parameter $\varepsilon \equiv \frac{V_{Brownian}}{V_{Bulk}}$. For the simple shear flows of interest here $\varepsilon = (KT/\rho \ell^5 \gamma^2)^{\frac{1}{2}}$. The time dependence of the Brownian and mean temperature distributions are due merely to the Brownian movement of the particle in the non-uniform temperature distribution, so that the times are sealed by the characteristic times ℓ/V_{Bulk} for the mean temperature distributions T, and $\ell/V_{Brownian}$ for the Brownian temperature distributions $\tilde{T}$. In nondimensional terms, the equations are

$$Pe_f\Big\{ \frac{\partial T}{\partial t} + \bar{\vec{U}}\cdot\nabla T + \bar{\vec{v}}\cdot\nabla T + \vec{U}^*\cdot\nabla T + \bar{\vec{u}}\cdot\nabla T + \bar{\vec{v}}\cdot\nabla T + \vec{U}^*\cdot\nabla\tilde{T}$$

$$+ \varepsilon\Big(\frac{\partial\tilde{T}}{\partial t} + \vec{v}^*\cdot\nabla T + \vec{v}^*\cdot\nabla T\Big)\Big\} = \nabla^2 T + \nabla^2 T \qquad (58b)$$

$$\vec{x}\varepsilon V - V_o$$

$$Pe_p\Big\{ \frac{\partial T_p}{\partial t} + \bar{\vec{U}}_p\cdot\nabla T_p + \bar{\vec{v}}_p\nabla\cdot T_p + \vec{U}_p^*\cdot\nabla T_p + \bar{\vec{U}}_p\cdot\nabla\tilde{T} + \bar{\vec{v}}_p\cdot\nabla\tilde{T}_p$$

$$+ \vec{U}^*\cdot\nabla\tilde{T}_p + \varepsilon\Big(\frac{\partial\tilde{T}_p}{\partial t} + \vec{v}_p^*\cdot\nabla T + \vec{v}_p^*\cdot\nabla\tilde{T}_p\Big)\Big\} = \nabla^2 T_p + \nabla^2\tilde{T}_p$$

$$x\varepsilon V_o \qquad (59b)$$

and the mean equations,

$$Pe_f\Big\{ \frac{\partial T}{\partial t} + (\bar{\vec{U}} + \bar{\vec{v}})\cdot\nabla T\Big\} = \nabla^2 T - Pe_f\Big\{\nabla\cdot(\overline{\vec{u}^*\tilde{T}}) + \varepsilon\nabla\cdot(\overline{\vec{v}^*\tilde{T}})\Big\}$$

$$\vec{x}\varepsilon V - V_o \qquad (60b)$$

$$Pe_p\Big\{ \frac{\partial T_p}{\partial t} + (\bar{\vec{U}}_p + \bar{\vec{v}}_p)\cdot\nabla T_p\Big\} = \nabla^2 T_p - Pe_p\Big\{\cdot\nabla(\overline{\vec{U}_p^*\tilde{T}_p}) + \varepsilon\nabla\cdot(\overline{\vec{v}^*\tilde{T}})$$

$$\vec{x}\varepsilon V_o - V_o \qquad (61b)$$

The long-time mean temperature fields T and T_p, defined by (60) and (61), would reduce in the absence of Brownian motion ($\varepsilon \to 0$, $D_r \to 0$), to the local deterministic temperature field near a single particle. This mean temperature distribution is affected by Brownian motion in three distinct ways: first, the deterministic fluid motions in the mean convection term is weighted with respect to the orientation distribution for particle orientation, which is itself affected by the Brownian motion; second, there is an additional mean convection velocity which corresponds to the effective particle rotation due to Brownian motions in the presence of gradients in the orientation distribution; and third, there are additional convective fluxes of heat associated with the long-time correlations of the (zero-mean) velocity and temperature fields; $\overline{\vec{U}^*\tilde{T}}$, $\overline{\vec{v}^*\tilde{T}}$, $\overline{\vec{U}^*_p\tilde{T}_p}$, and $\overline{\vec{v}^*_p\tilde{T}_p}$. We may note that in the absence of bulk flow both $\vec{U} = 0$, and the mean field $\vec{\vec{V}} = 0$, the latter because the orientation distribution will then be uniform at steady state. However, the added flux terms $\overline{\vec{v}^*\tilde{T}}$ and $\overline{\vec{v}^*_p\tilde{T}_p}$ will persist even if the suspension is macroscopically stationary, provided the particles are free to move about in the suspending matrix.

These Brownian motion effects on the microscale temperature distribution will similarly be reflected on the bulkscale through equation (22). Substituting the expan-

sions for the velocity and temperature distributions inside and outside of the particle and performing the averages, we obtain

$$\overline{\nabla T} = \nabla T_p \qquad \text{for } \vec{x} \varepsilon V_o \tag{62}$$

$$\overline{U_i' T'} = (\bar{\vec{U}}_p + \bar{\vec{v}}_p - \vec{U}_{bulk})(T_p - T_{bulk}) + \overline{\vec{U}^* \tilde{T}_p} + \overline{\vec{v}_p^* \tilde{T}_p}$$

$$\vec{x} \varepsilon V_o \tag{63}$$

$$\overline{U_i' T'} = (\bar{\vec{U}} + \bar{\vec{v}} - \vec{U}_{bulk})(T - T_{bulk}) + \overline{\vec{U}^* \tilde{T}} + \overline{\vec{v} \tilde{T}}$$

$$\vec{x} \varepsilon V - V_o \tag{64}$$

With these expressions, the calculation of the particle associated bulk heat flux Q_i may now proceed in principle. From equations (38) and (39) the statistical properties of the particle Brownian motions may be calculated. The orientation distribution is calculated from the Fokker-Plank equation, and the mean Brownian motions from (41). The fluid Brownian velocity fields for arbitrary orientation and motion may be calculated from (31) and (32) along with the boundary conditions (35) and (36). From equations (58) - (61) one may then in principle obtain the temperature distributions resulting from any arbitrary orientation and motion of the particle, which may then be statistically averaged with the known probability density functions for

orientation and velocity of the particle, to obtain the mean temperature and micro-convective contributions (62)-(64). The spatial volume averages of (22) may then be evaluated to obtain the thermal constitutive behavior of the suspension.

REFERENCES

Chow, T.S. and Hermans, J.J. 1972 "Effect of Inertia on the Brownian Motion of Rigid Particles in a Viscous Fluid," The Journal of Chemical Physics 56, pp. 3150-3154.

Fox, R.F. and Uhlenbeck, G.E. 1970 "Contributions to Non-Equilibrium Thermodynamics. I. Theory of Hydrodynamic Fluctuations," Physics of Fluids 13, pp. 1893-1902.

Hauge, E.H. and Martin-Löf, A. 1972 "Fluctuating Hydrodynamics and Brownian Motion," Journal of Statistical Physics 7 pp. 259-281.

Hinch, E.J. 1975 "Application of the Langevin Equation to Fluid Suspensions," JFM 72, pp. 499-511.

Jeffrey, D.J. 1974 "Group Expansions for the Bulk Properties of a Statistically Homogeneous, Random Suspension." Proc. Roy. Soc. Lond. A338, pp. 503-516.

Landau, L.D. and Lifshitz, E.M. 1959 "Fluctuations in Fluid Dynamics," Chapter 17 of Fluid Mechanics, Reading, Massachusetts: Addison-Wesley Publishing Company, Inc.

Hinch, E. J. and Leal, L. G. 1972 "The Effect of Brownian Motion on the Rheological Properties of a Suspension of Non-spherical Particles," JFM 52 pp. 683-712.

Zwanzig, R. 1970 Phy. Rev. A2, p. 2005.

CHAPTER III

The Effect of Deformation on the Effective Conductivity of a Dilute Suspension of Drops in the Limit of Low Particle Peclet Number

The following paper, co-author Dr. L. G. Leal, was submitted to the *International Journal of Multiphase Flow*, and appeared in slightly shortened form in volume 2, 1975.

The Effect of Deformation on the Effective Conductivity of a Dilute Suspension of Drops in the Limit of Low Particle Peclet Number

T. J. McMillen and L. G. Leal
Chemical Engineering
California Institute of Technology
Pasadena, California

Abstract

The effective thermal conductivity of a dilute suspension of slightly deformed droplets is calculated in the limit of small particle Peclet number for the undisturbed bulk shear, $u = \gamma y$, and the linear bulk temperature gradient, $T = \alpha y$. The theory is based upon the general relationship, derived by Leal (1973), between the bulk heat flux of a dilute suspension of particles and the microscale temperature and velocity fields. Two distinct cases of small deformation are considered; deformation dominated by interfacial tension forces, and deformation dominated by viscous forces in the drop. The microscale velocity and temperature fields are obtained as regular, asymptotic expansions in the small deformation parameter, ϵ. At each order in the deformation parameter, ϵ, the governing thermal energy equation is then solved for small Peclet using the methods of matched asymptotic expansions.

INTRODUCTION

Leal (1973) has considered the effective conductivity of a dilute suspension of neutrally buoyant spherical drops in the limit of low particle Peclet number for the case of a simple bulk shear flow ($u = \gamma y$, $v = w = 0$) and a linear bulk temperature distribution ($T = \bar{\alpha} y$). A general expressions was presented relating the effective (bulk) conductivity of the suspension to the microscale velocity and temperature fields associated with each individual particle. Using this relationship, the effective conductivity was evaluated for $Re << Pe << 1$, with the velocity fields obtained from the classical creeping flow solution of Taylor (1932) for a spherical drop in shear flow, and the microscale temperature field calculated using the method of matched asymptotic expansions.

Provided that either the surface tension or the droplet fluid viscosity is sufficiently large, the solution of Leal will provide an adequate first estimate of the modification of the effective conductivity due to the presence of fluid droplets in a flowing suspension. Of course, the droplet shape will never be exactly spherical in any real system, and in some instances the deviations from a spherical shape may become quite large, so that one may logically ask whether the assumption of a spherical shape has any major influence on the results for the effective conductivity. In particular, it was found in the earlier study that the first order modification in the local temperature field due to the fluid motion actually makes no contribution to the bulk conductivity, which is only finally influenced at $O(Pe^{3/2})$. Since this result is essentially caused by the symmetry of the problem, it might be expected that the dependence of the conductivity on Peclet number would be altered fundamentally when the shape is allowed to deviate from spherical. In the present communication we consider only the

case of small deformations of the shape due to the action of the imposed shear field. The effects of the deformation on the microscale velocity and temperature fields are obtained as a perturbation expansion in terms of a small parameter ε, following the basic method of Cox (1969). The perturbed temperature and velocity fields are then used to calculate the effective conductivity of a dilute suspension of such slightly deformed droplets. There are two separate physical cases of small deformation; one in which the interfacial tension forces overwhelm viscous forces ($\varepsilon \sim a\gamma\mu/\sigma \ll 1$), and the other where viscous effects inside the drop predominate ($\varepsilon \sim 1/\lambda \ll 1$). Here μ is the viscosity of the suspending fluid, λ the ratio of internal to external viscosities, a the undeformed radius of the drop, and σ the interfacial tension. The case when both effects are the same order of magnitude will not be considered. In the following analysis all lengths have been nondimensionalized by the undeformed radius of the particle a, all velocities by the characteristic velocity γa, and all temperatures by $\bar{\alpha}a$.

THE PARTICLE SHAPE, LOCAL VELOCITY FIELD, AND TEMPERATURE DISTRIBUTION

Following Taylor (1932), the nondimensional equation for the surface of the nearly spherical drop may be expressed in the form

$$r_s = 1 + \varepsilon f(\theta,\phi) + O(\varepsilon^2) \tag{1}$$

with respect to a spherical coordinate axis system (r, θ, ϕ) which has its origin at the geometric center of the drop. The precise nature of the deformation parameter ε and the shape function $f(\theta,\phi)$ depends on the physical limit which is considered. For the case of dominant surface tension forces, Taylor has shown

$$\varepsilon = \frac{a\gamma\mu}{\sigma}\left[\frac{19\lambda + 16}{16\lambda + 16}\right] \quad ; \quad f(\theta,\phi) = \sin^2\theta \sin 2\phi \tag{2}$$

On the other hand, for dominant internal viscosity the corresponding results are (Taylor, 1932),

$$\varepsilon = \frac{5}{4\lambda} \quad ; \quad f(\theta,\phi) = \sin^2\theta \cos 2\phi \tag{3}$$

The creeping flow velocity fields outside and inside the drop may be represented, in either case, by the asymptotic expansions

$$\begin{aligned} \vec{u} &= \vec{u}^{o} + \varepsilon\vec{u}^{1} + O(\varepsilon^2) \\ \hat{u} &= \hat{u}^{o} + \varepsilon\hat{u}^{1} + O(\varepsilon^2) \end{aligned} \tag{4}$$

The functions $\vec{u}^{o}$ and $\hat{u}^{o}$ are the solutions for a spherical drop as given by Taylor (1932)--see also Batchelor (1967). The $O(\varepsilon)$ solutions for the surface tension dominant case were given by Chaffey, Brenner, and Mason (1965). The $O(\varepsilon)$ velocity fields in the dominant internal viscosity limit can be calculated using Lamb's general solution of the creeping motion equations

$$\vec{u} = \sum_n \left\{ \nabla\times(\vec{r}\chi_n) + \nabla\phi_n + \frac{r^2(n+3)\nabla P_n}{2(n+1)(2n+3)\mu} - \frac{n\vec{r}P_n}{(n+1)(2n+3)\mu} \right\} \tag{5}$$

where χ_n, ϕ_n, and P_n are spherical harmonics of order n. The velocity fields $\vec{u}^{>1}$ and $\vec{u}^{\geq 1}$ require only harmonics of order 4 and 2, and these are given in Table 1 for the nondimensional velocity fields.

Proceeding from the velocity fields (4), we now turn to the calculation of the deformation-induced modifications of the temperature fields inside and outside of the drop. The governing equations, nondimensionalized, are

$$\nabla^2 \bar{T} = Pe_2(\vec{u} \cdot \nabla \vec{T}) \qquad \text{(inside)} \tag{6}$$

$$\nabla^2 T = Pe_1(\vec{u} \cdot \nabla T) \qquad \text{(outside)} \tag{7}$$

where

$$Pe_1 \equiv \frac{a^2 \gamma \rho C p_1}{k_1} \quad ; \quad Pe_2 \equiv \frac{a^2 \gamma \rho C p_2}{k_2}$$

and the subscripts 1 and 2 refer to the suspending fluid and the fluid in the drop, respectively. As noted previously, we shall assume that both Pe_1 and Pe_2 are small. Thus, the temperature distributions are calculated as perturbation expansions for the double limit $\epsilon << 1$ and Pe_1, $Pe_2 << 1$. The expansion in the deformation parameter ϵ is regular. However, at each order in ϵ, the expansion in Pe is singular, and most conveniently obtained by the well-known method of matched asymptotic expansions, with the equations in the region far from the body re-scaled in a manner consistent with the fact that convective terms must be retained at large distances, even in the limit as $Pe \to 0$.

In the inner region, which includes the drop, the temperature distribution is expressed in the asymptotic form

$$\begin{aligned} T = {} & f_0^0(Pe_1)T_0^0 + f_1^0(Pe_1)T_1^0 + f_2^0(Pe_1)T_2^0 + \ldots \\ & + \epsilon\left[f_0^1(Pe_1)T_0^1 + f_1^1(Pe_1)T_1^1 + f_2^1(Pe_1)T_2^1 + \ldots\right] + O(\epsilon^2) \end{aligned} \tag{8a}$$

$$\bar{T} = f_0^0(Pe_2)\bar{T}_0^0 + f_1^0(Pe_2)\bar{T}_1^0 + f_2^0(Pe_2)\bar{T}_2^0 + \ldots$$
$$+ \varepsilon\left[f_0^1(Pe_2)\bar{T}_0^1 + f_1^1(Pe_2)\bar{T}_1^1 + f_2^1(Pe_2)\bar{T}_2^1 + \ldots\right] + O(\varepsilon^2) \tag{8b}$$

where as usual,

$$\lim_{Pe_1 \to 0} \frac{f_{n+1}^m}{f_n^m} \to 0$$

The precise form of the gauge functions $f_i^j(Pe_1)$ is found as part of the solution. Substituting (8a) and (8b) into (6) and (7), it may be easily shown that the governing equations at the first two orders in ε are

$$\nabla^2\bar{T}_i^0 = Pe_2\left(\vec{\bar{u}}^0 \cdot \nabla\bar{T}_i^0\right)$$
$$\nabla^2 T_i^0 = Pe_1\left(\vec{\bar{u}}^0 \cdot \nabla T_i^0\right) \qquad (i = 0, 1, 2, \ldots) \tag{9a}$$

$$\nabla^2\bar{T}_i^1 = Pe_2\left(\vec{\bar{u}}^1 \cdot \nabla\bar{T}_i^0 + \vec{\bar{u}}^0 \cdot \nabla\bar{T}_i^1\right)$$
$$\nabla^2 T_i^1 = Pe_1\left(\vec{\bar{u}}^1 \cdot \nabla T_i^0 + \vec{\bar{u}}^0 \cdot \nabla T_i^1\right) \qquad (i = 0, 1, 2, \ldots) \tag{9b}$$

which are to be solved subject to the conditions of temperature and heat flux continuity at the drop surface,

$$\bar{T}\Big|_{r=r_s} = T\Big|_{r=r_s} \tag{10}$$

$$k_1(\vec{n} \cdot \nabla T)\Big|_{r=r_s} = k_2(\vec{n} \cdot \nabla\bar{T})\Big|_{r=r_s} \tag{11}$$

plus boundedness at r = 0 and matching for large r with the solution in the outer region.

In the outer region, the radial coordinate r is rescaled according to

$$\rho = rPe_1^{1/2}$$

and, for convenience, T* is used to denote the temperature. The exact form

of the convective-diffusion equation in this outer region depends on the physical limit which is considered. For the case of deformation dominated by surface tension forces:

$$\nabla_\rho^2 T^* - \hat{y}\,\frac{\partial T^*}{\partial \hat{x}} = Pe_1^{3/2}\left\{ \frac{C}{4\rho^2}\sin^2\theta\,\sin 2\phi + \varepsilon\left[\frac{3A_{-3}^2}{2\rho^2}\sin^2\theta\,\cos 2\phi + \frac{5A_{-3}}{14\rho^2}(2 - 3\sin^2\theta)\right]\right\}\frac{\partial T^*}{\partial \rho} + O\left(Pe_1^{5/2}\right) \tag{12}$$

where $(\hat{x},\hat{y}) = \left(Pe_1^{1/2}x,\ Pe_1^{1/2}y\right)$, ∇^2 represents the usual Laplacian operator with ρ replacing r, and A_{-3}^2 and A_{-3} are coefficients given by Chaffey, Brenner and Mason as:

$$A_{-3}^2 = \frac{19\lambda + 16}{15(\lambda + 1)} \qquad A_{-3} = \frac{25\lambda^2 + 41\lambda + 4}{25(\lambda + 1)^2} \qquad C = -\frac{(2 + 5\lambda)}{(\lambda + 1)}$$

For the case of deformation dominated by internal viscous forces, we obtain

$$\nabla_\rho^2 T^* - \hat{y}\,\frac{\partial T^*}{\partial x} = Pe_1^{3/2}\left\{ \frac{C}{4\rho^2}\sin^2\theta\,\sin 2\phi \cdot \frac{\partial T^*}{\partial \rho}\right\} + O\left(Pe_1^{5/2}\right) \tag{13}$$

As in the inner region, the temperature distribution is expressed in the asymptotic form:

$$T^* = F_0^0(Pe_1)T_0^{*0} + F_1^0(Pe_1)T_1^{*0} + F_2^0(Pe_1)T_2^{*0} + \ldots + \varepsilon\left\{F_0^1(Pe_1)T_0^{*1} + F_1^1(Pe_1)T_1^{*1} + F_2^1(Pe_1)T_2^{*1} + \ldots\right\} + O(\varepsilon^2) \tag{14}$$

with

$$\lim_{Pe_1 \to 0} \frac{F_{n+1}^m}{F_n^m} \to 0$$

In this outer region, the solutions must satisfy the condition

$$T^* \to \frac{\alpha\rho\sin\theta\,\sin\phi}{Pe_1^{1/2}} \qquad \text{as } \rho \to \infty \tag{15}$$

and the matching condition

$$\lim_{\rho \to 0} T^*(\rho,\theta,\phi) = \lim_{r \to \infty} T(r,\theta,\phi) \quad \text{as } Pe_1 \to 0 \tag{16}$$

At first order in ϵ, the solutions T_i^0, $\bar{T}_i^0$ and T_i^{*0} are simply the solutions for a perfectly spherical drop which were evaluated previously by Leal (1973) up to T_2^0, $\bar{T}_2^0$, and T_2^{*0}. However, the two solutions T_1^0 and $\bar{T}_1^0$ were slightly in error in the earlier work, and have thus been given in corrected form in Table 2 of the present paper.

The task here is to obtain solutions for the $O(\epsilon)$ distributions of temperature in the expansions (8) and (14), in order to evaluate the role of shape deformation in contributing to the effective conductivity of a dilute emulsion of drops in simple shear flow. In the outer region, the first nonzero $O(\epsilon)$ term will be either $O(Pe_1)$, arising from the non-homogeneous right hand side of (12) (or (13)) with T^* replaced by $F_0^0(Pe_1)T_0^{*0}$, or perhaps a larger term arising from the matching condition with the inner solution, equation (16). Hence, before investigating the solution in the outer region in any detail, it is convenient to consider the first terms in the inner region, which satisfy

$$T_0^1 \to 0 \quad \text{as } r \to \infty \tag{17}$$

In the inner region, the solution is generated at $O(\epsilon)$ by any mismatch in the temperature or heat flux which occurs in the $O(1)$ solutions (i.e. T_0^0, $\bar{T}_0^0$, T_1^0, $\bar{T}_1^0$, etc.) when they are evaluated at the deformed surface $r = r_s = 1 + \epsilon f(\theta,\phi)$ according to the conditions (10) and (11). At $O(\epsilon)$, these conditions become simply

$$\epsilon \sum_i f_i^1(Pe_1)\left(T_i^1 - \tau_i^1 \bar{T}_i^1\right)\Big|_{r=1} = -\sum_i f_i^0(Pe_1)\left(T_i^0 - \tau_i^0 \bar{T}_i^1\right)\Big|_{r=1+\epsilon f} \tag{18}$$

$$\varepsilon \sum_i f_i^1(Pe_1) \left[\frac{\partial T_i^1}{\partial r} - m\tau_i^1 \frac{\partial \bar{T}_i^1}{\partial r} \right]_{r=1} = \sum_i f_i^0(Pe_1) \left\{ - \left[\frac{\partial T_i^0}{\partial r} - m\tau_i^1 \frac{\partial \bar{T}_i^0}{\partial r} \right]_{r=1+\varepsilon f} \right.$$

$$\left. + \varepsilon \frac{\partial f}{\partial \theta} \left[\frac{\partial T_i^0}{\partial \theta} - m\tau_i^0 \frac{\partial T_i^0}{\partial \theta} \right]_{r=1} + \frac{\varepsilon}{\sin^2\theta} \frac{\partial f}{\partial \phi} \left[\frac{\partial T_i^0}{\partial \phi} - m\tau_i^0 \frac{\partial T_i^0}{\partial \phi} \right]_{r=1} \right\} \tag{19}$$

where $m \equiv k_2/k_1$ and $\tau_i^j \equiv f_i^j(Pe_2)/f_i^j(Pe_1)$. Evaluating the right hand side of these equations using the sphere solutions of Leal (1973), it can be shown that nonhomogeneous terms arise at each order in Peclet number, i.e. at $O(f_0^0(Pe_1))$, $O(f_1^0(Pe_1))$ etc. Thus the first order solution at $O(\varepsilon)$ in the inner region is generated by the mismatch of temperature and heat flux represented by the right hand sides of (18) and (19) with $i = 0$. The gauge function $f_0^0(Pe_1) \equiv 1$, thus clearly $f_0^1(Pe_1) \equiv 1$ also and the governing equations at the first approximation are the pure conduction equations

$$\nabla^2 T_0^1 = 0 \; ; \quad \nabla^2 \bar{T}_0^1 = 0 \; . \tag{20}$$

The solutions satisfying these equations, with the conditions (17), (18) and (19) are listed in Table 3. Examining these solutions, it is clear that the mismatch with $T^* = 0$ in the outer region is $O(Pe_1)$, and this mismatch will generate $O(Pe_1)$ terms in the outer solution. However, before investigating the solution in the outer region it is most convenient to obtain one further term in the inner region since it too produces $O(Pe_1)$ terms in the matching condition at the region of overlap.

Thus, again examining equations (18) and (19), the next nonzero term on the right hand side is $f_1^0(Pe_1)$ which Leal (1973) has shown to be $O(Pe_1)$. It follows that $f_1^1(Pe_1) = Pe_1$, so that the governing equations for T_1^1 and $\bar{T}_1^1$ are

$$\nabla^2 T_1^1 = \underline{u}^1 \cdot \nabla T_0^0 + \underline{u}^0 \cdot \nabla T_0^1$$
$$\nabla^2 \bar{T}_1^1 = \bar{\underline{u}}^1 \cdot \nabla \bar{T}_0^0 + \bar{\underline{u}}^0 \cdot \nabla \bar{T}_0^1 \qquad (21)$$

The solutions of (21), satisfying (18) and (19) are quite long, and, in the interest of brevity, will not be given here explicitly.

Of prime importance for present purposes is the form of the first two inner solutions in the region of overlap, since it is the largest term of these solutions, together with the nonhomogeneous term of the equation (12) (or (13)), which is responsible for the largest nonzero term in the outer solution. Expressing the inner solution in terms of the outer variables, and putting the coefficients of all terms of $O(Pe^{-n})$ equal to zero in anticipation of the obvious implications of the matching condition, equation (16), we obtain for the case of dominant surface tension forces

$$\lim_{r \to \infty} \left(T_0^1 + Pe_1 T_1^1\right) \sim Pe_1 \left\{ \frac{D_{11}}{\rho^2} P_1^1 \cos\phi + \left[\frac{21\alpha A_{-3}^2 + 5\alpha A_{-3} - 14 D_{11}}{70} \right] P_1^1 \sin\phi \right. \qquad (22)$$
$$\left. - \left[\frac{7\alpha A_{-3}^2 + 10\alpha A_{-3} + 7 D_{11}}{840} \right] P_3^1 \sin\phi - \left[\frac{\alpha A_{-3}^2 - D_{11}}{240} \right] P_3^3 \sin 3\phi \right\} + O\left(\frac{Pe_1^2}{\ell n Pe_1} \right)$$

while for the case of dominant viscous forces

$$\lim_{r \to \infty} \left[T_0^1 + Pe T_1^1 \right] \sim Pe_1 \left\{ \frac{D_{11}^*}{\rho^2} P_1^1 \sin\phi + \frac{3 D_{11}^*}{10} P_1^1 \cos\phi - \frac{D_{11}^*}{120} P_3^1 \cos\phi \right. \qquad (23)$$
$$\left. - \frac{D_{11}^*}{240} P_3^3 \cos 3\phi \right\} + O\left(\frac{Pe_1^2}{\ell n Pe_1} \right) .$$

We now turn to the $O(\epsilon)$ solution in the outer region. In view of the fact that the largest nonhomogeneous term in the governing equation (12) (or (13)), and the largest term generated by the inner solution in the overlap

region are both $O(Pe_1)$, it is clear that the first nonzero term in the outer region is also of that magnitude. For convenience in comparing with Leal (1973), and in maintaining symmetry between the subscript/superscript notation in the inner and outer regions, we arbitrarily set $F_0^1(Pe_1)$ and $F_1^1(Pe_1)$ equal to zero, and begin the outer expansion with T_2^{*0} and

$$F_2^1(Pe_1) = Pe_1 .$$

The governing equation for the case of deformation dominated by surface tension is

$$\nabla\rho^2 T_2^{*1} - \hat{y}\frac{\partial T_2^{*1}}{\partial x} = \left[\frac{A^2}{2\rho^2}\frac{-3}{}P_2^2\cos 2\phi + \frac{5A}{7\rho^2}\frac{-3}{}P_2\right]\frac{\partial T_0^{*0}}{\partial\rho} \qquad (24)$$

and for the case of internal viscosity dominating

$$\nabla\rho^2 T_2^{*1} - \hat{y}\frac{\partial T_2^{*1}}{\partial\hat{x}} = 0 . \qquad (25)$$

The required boundary conditions are $T_2^{*1} \to 0$ as $\rho \to \infty$ (from equation 15), plus matching with the expression (22) or (23). The relevant homogeneous and particular solutions of the equations (24) and (25), which go to zero at infinity have been discussed, in effect, by Leal (1973) in solving for T_2^{*0} in the spherical drop problem. It is sufficient here to note that the particle acts as a heat dipole, both at $O(1)$ and at $O(\varepsilon)$. We denote the present $O(\varepsilon)$ dipole strength, which must be obtained by matching with the inner solution, as $2A$. The dipole lies in the xy plane, with an arbitrary orientation which must also be determined from the matching condition. We denote by ϕ_0 the angle between the dipole axis and the x-axis of the coordinate system.

Comparing the solution of equation (24) with the matching requirement (22), it may be shown for the surface tension dominated case, that

$$A = -8D_{11}$$

and

$$\phi_0 = \pi/2$$

That is, the $O(\varepsilon)$ heat dipole is oriented along the y-axis. With this choice, the outer solution becomes, for $\rho \to 0$,

$$T_2^{*1} = \frac{D_{11}}{\rho^2} P_1^1 \cos\phi + \left[\frac{21\alpha A_{-3} + 5\alpha A_{-3} - 14D_{11}}{70}\right] P_1^1 \sin\phi$$
$$- \left[\frac{7\alpha A_{-3}^2 + 10\alpha A_{-3} + 7D_{11}}{840}\right] P_3^1 \sin\phi - \left[\frac{\alpha A_{-3}^2 - D_{11}}{240}\right] P_3^3 \sin 3\phi \quad (26)$$
$$- .0676D_{11}\rho P_1^1 \cos\phi + .0963D_{11}\rho P_1^1 \sin\phi + O(\rho^2) + \ldots$$

For the case of deformation dominated by viscosity forces, it may similarly be shown that $A = -D_{11}^*/2$ and $\phi_0 = 0$, so that the dipole is oriented along the x-axis. In this case, as $\rho \to 0$

$$T_2^{*1} = \frac{D_{11}^*}{\rho^2} P_1^1 \sin\phi + \frac{3D_{11}^*}{10} P_1^1 \cos\phi - \frac{D_{11}^*}{120} P_3^1 \cos\phi - \frac{D_{11}^*}{240} P_3^3 \cos 3\phi \quad (27)$$
$$+ .392D_{11}^*\rho P_1^1 \sin \; + .0963D_{11}^*\rho P_1^1 \cos\phi + O(\rho^2)$$

In both cases the first four terms match exactly with the $O(Pe_1)$ contributions from the inner solution. The remaining two terms (of order (ρPe_1)) give rise to an $O(rPe_1^{3/2})$ mismatch which is resolved at the next order in the inner expansion. As we shall see in the next section, the first deformation-induced flow contribution to the effective conductivity in the surface tension dominant case arises from the solutions which we have already obtained. However, in the case of dominant internal viscosity, it is necessary to obtain one further term in the inner expansion in order to obtain a nonzero flow contribution to the effective conductivity at $O(\varepsilon)$.

Clearly, the next inner solution can be easily generated in both cases, however we shall limit ourselves here to the dominant viscosity case where it is critical in determining the influence of drop deformation on the effective viscosity.

From (27), we see that the next inner solution in the dominant viscous case must have $f_2^1(Pe_1) = Pe_1^{3/2}$, so that

$$\nabla^2 T_2^1 = 0 \; ; \quad \nabla^2 \bar{T}_2^1 = 0 \tag{28}$$

which are to be solved subject to the matching condition

$$T_2^1 \to 0.392 D_{11} r P_1^1 \sin\phi + .0963 D_{11} \rho P_1^1 \cos\phi, \text{ as } r \to \infty$$

and the interface conditions (18) and (19) with i = 2. The solutions are

$$\begin{aligned} T_2^1 = {} & .392 D_{11} r P_1^1 \sin\phi + .0963 D_{11} r P_1^1 \cos\phi + \frac{H_{11}}{r^2} P_1^1 \sin\phi \\ & + \frac{I_{11}}{r^2} P_1^1 \cos\phi + \frac{H_{31}}{r^4} P_3^1 \sin\phi + \frac{I_{31}}{r^4} P_3^1 \cos\phi + \frac{H_{33}}{r^4} P_3^3 \sin 3\phi \\ & + \frac{I_{33}}{r^4} P_3^3 \cos 3\phi \end{aligned} \tag{29}$$

and

$$\begin{aligned} \bar{T}_2^1 = {} & J_{11} r P_1^1 \sin\phi + K_{11} r P_1^1 \cos\phi + J_{31} r^3 P_3^1 \sin\phi + K_{31} r^3 P_3^1 \cos\phi \\ & + J_{33} r^3 P_3^3 \sin 3\phi + K_{33} r^3 P_3^3 \cos 3\phi \; . \end{aligned} \tag{30}$$

The constants H_{11}, I_{11}, J_{11}, K_{11} etc. are quite long, and hence again will not be presented here in order to preserve reasonable brevity.

We now turn to our main objective, namely, the calculation of the first deformation-induced flow contributions to the effective conductivity of a dilute suspension of slightly deformed drops.

CALCULATION OF EFFECTIVE CONDUCTIVITY FROM MICROSCALE FIELDS

A general expression for the effective conductivity of a dilute suspension of identical particles was obtained by Leal (1973) for heat transfer across a linear bulk shear flow. For the case of slightly deformed particles this expression is:

$$k_{eff} = k_1 - \frac{Q_i'}{\alpha} \tag{31}$$

where in terms of nondimensional quantities

$$\begin{aligned} Q_i' = {} & \frac{3(k_1 - k_2)\phi}{4\pi} \int_0^{2\pi}\int_0^{\pi} (n_y T)_{r=r_s} r_s^2 \sin\theta \, \partial\theta\partial\phi \\ & + \frac{3k_1}{4\pi} Pe_1 \phi \int_0^{2\pi}\int_0^{\pi}\int_{r_s}^{\infty} u_y' T' r^2 \sin\theta \, \partial r\partial\theta\partial\phi \\ & + \frac{3k_2}{4\pi} Pe_2 \phi \int_0^{2\pi}\int_0^{\pi}\int_0^{r_s} \bar{u}_y' \bar{T}' r^2 \sin\theta \, \partial r\partial\theta\partial\phi \end{aligned} \tag{32}$$

Here, ϕ is the volume fraction of suspended particles, u_y' and T' are the disturbance velocity and temperature fields, $u_y' = u_y$, $T' = T - \alpha y$, and n_y is the $\hat{j}$ component of unit outer normal to the particle surface. In the present work, the asymptotic expressions for T, $\bar{T}$, T^*, u, $\bar{u}$ and n_y in terms of ε and Pe are used to evaluate this general expression for the effective conductivity. For the case of surface tension controlling deformation, we obtain

$$\begin{aligned} \frac{k_{eff}}{k_1} \equiv k_{eff}^* = 1 + \phi\Bigg\{ & \frac{3(m-1)}{(m+2)} + \Bigg[\frac{1.176(m-1)^2}{(m+2)^2} + \frac{5\lambda+2}{\lambda+1} \Bigg(.12\left|\frac{5\lambda+2}{\lambda+1}\right| \\ & - .028\left|\frac{m-1}{m+2}\right| \Bigg) \Bigg] Pe_1^{3/2} + I(m,\lambda,\tau)\varepsilon Pe_1 + O(\varepsilon^2) + O(Pe_1^2) + O\left(\varepsilon Pe_1^{3/2}\right) + \ldots \Bigg\} \end{aligned} \tag{33}$$

where $I(m,\lambda,\tau)$ is a rather complex function of the ratios m, λ, and τ

which is given explicitly in Table 4.

For the case of internal viscous forces controlling deformation, we find

$$k^*_{eff} = 1 + \phi\left\{\frac{3(m-1)}{(m+2)} + \left[3.00 - \frac{.14(m-1)}{(m+2)} + \frac{1.176(m-1)^2}{(m+2)^2}\right] Pe_1^{3/2}\right.$$

$$- \left[\frac{3.6(m-1)^2}{(m+2)^2}\right]\varepsilon + \left[\frac{1.411m(m-1)^2}{(m+2)^3}\left[\left[\frac{\tau}{m}\right]^{3/2} - 1\right] - \frac{.168(m-1)^2}{(m+2)^2}\right]\varepsilon Pe_1^{3/2}$$

$$\left. + O(\varepsilon^2) + O\left(Pe_1^2\right) + O\left(\varepsilon Pe_1^2\right) + \ldots \right\} \qquad (34)$$

In each case, the $O(1)$ and $O(Pe_1)^{3/2}$ terms are from the calculation of Leal (1973 for a spherical drop. The new terms arising due to drop deformation are seen to be of order (εPe_1) for the case of deformation dominated by surface tension forces, and of orders (ε) and $\left(\varepsilon Pe_1^{3/2}\right)$ for the case of viscous forces dominating. The fact that these corrections occur at different levels of approximation is apparently due to the differences in the nature of the particle deformation in the two cases. In the first case the drop deforms along the principal axis of strain of the flow in the xy plane, hence elongating along an axis 45 degrees away from the positive x-axis and contracting along an axis 45 degrees away from the positive y-axis. In the second case, however, the axis of elongation lies along the x-axis while the axis of contraction is coincident with the y-axis.

For the case of deformation controlled by surface tension forces, the dominant deformation induced correction, $O(\varepsilon Pe_1)$, can be either positive or negative depending on the values of the ratio of internal to external conductivity, m, the ratio of heat capacities, τ, and the ratio of viscosities, λ. The general characteristics of the function $I(m,\lambda,\tau)$ are

demonstrated graphically in Figure 1 where we have plotted $I(m,\lambda,\tau)$ as a function of m and λ for several values of τ. (Note that $\lambda \leq O(1)$ is required for validity of the expressions (2) and (4) which we have used for the fluid velocity and drop deformation.) For moderate to large values of the internal to external conductivity ratio, the deformation-induced correction to the effective conductivity can be either positive or negative but is small in magnitude.

Indeed, in the limit as $m \to \infty$, the correction term is easily shown to have the asymptotic form

$$I\varepsilon Pe_1 \sim \frac{1}{(\lambda+1)^2}\left\{\tau(.12\lambda^3 - .22\lambda^2 - .884\lambda - 0.534) + .663\lambda^2 + .351\lambda - 1.644\right\}\varepsilon Pe_1 \quad \text{as} \quad m \to \infty \tag{35}$$

with a corresponding expression for k^*_{eff}

$$k^*_{eff} \sim 1 + \phi\left\{3 + \left[1.176 + \frac{5\lambda+2}{\lambda+1}\left(.12\left(\frac{5\lambda+2}{\lambda+1}\right) - .028\right)\right] Pe_1^{3/2} + \varepsilon Pe_1 \frac{1}{(\lambda+1)^2}\left\{(.12\lambda^3 - .22\lambda^2 - .884\lambda - .534)\tau + .663\lambda^2 + .351\lambda - 1.644\right\} + \ldots\right\} \tag{36}$$

There are two points worth noting in these limiting results. First, both of the corrections of $O(Pe_1^{3/2})$ and $O(\varepsilon Pe_1)$ remain small for $\lambda \leq O(1)$, so that the relative importance of each depends upon the magnitudes of ε and Pe_1. Second, it is important to remember that some care must be taken in considering limits such as $m \to \infty$ in order to assure that the basic theory remains relevant. Hence, for example, the limit $m \to \infty$ must be applied for small, fixed values of Pe_1 in order that both Pe_1, Pe_2 remain small. This

latter point is more graphically illustrated by considering the limit of small m. As evident in Figure 1, $I(m,\lambda,\tau)$ is very strongly negative in this case, apparently approaching negative infinity as m goes to zero. Indeed, for $m \to 0$,

$$I(m,\lambda,\tau) \sim \frac{1}{32m}\frac{1}{(\lambda+1)^2}\left\{(-9.382\,\lambda^2 - 17.640\,\lambda - 24.543)\tau + 1.341\lambda^2 + 7.096\lambda + 2.940\right\} \quad ; \quad m \to 0 \tag{37}$$

In this case, the limit $m \to 0$ must be taken with $Pe_2 \ll 1$ and fixed, in order that both Pe_1, Pe_2 remain small. Thus, while I becomes very large (positive or negative depending on the magnitude of τ) as $m \to 0$, the effective conductivity approaches a constant value for λ, τ and Pe_2 held fixed (the latter small),

$$k^*_{eff} \sim 1 + \phi\left\{-\frac{3}{2} + \left[-0.294 + \frac{5\lambda+2}{\lambda+1}\left(.12\,\frac{5\lambda+2}{\lambda+1} + .028\right)\right]\frac{m^{3/2}}{\tau^{3/2}}\,Pe_2^{3/2} + \frac{\varepsilon Pe_2}{32(\lambda+1)^2\tau}\left\{(-9.382\lambda^2 - 17.640\lambda - 24.543)\tau + 1.341\lambda^2 + 7.096\lambda + 2.940\right\}\right\} \sim 1 + \phi\left\{-\frac{3}{2} + \left[(-9.382\lambda^2 - 17.640\lambda - 24.543) + \frac{1}{\tau}(1.341\lambda^2 + 7.096\lambda + 2.940)\right]\frac{\varepsilon Pe_2}{32(\lambda+1)^2} + \ldots\right\} \quad ; \quad m \to 0. \tag{38}$$

It is particularly noteworthy that in this surface-tension dominant case, the deformation-induced flow contribution to k^*_{eff} may dominate the largest flow contribution which occurs for a spherical drop. Hence, as we suggested in the introduction, the presence of the shape deformation in this case causes a fundamental change in the nature of the dominant flow contribution to the effective thermal conductivity.

One further limit of special interest is the case when the conductivities of the two fluids are equal so that the particle contribution to the effective conductivity is produced entirely by the convective action of the fluid. For this case

$$k^*_{eff} = 1 + \phi\left[.12\left(\frac{(5\lambda + 2)^2}{(\lambda + 1)^2}\right) Pe_1^{3/2} + \cdots\cdots\right] \tag{39}$$

Here, the $0(Pe_1)$ term identically vanishes for the equal conductivity, i.e. m=1, case, so that to order $Pe_1^{3/2}$, the only contribution arises from the convective contribution for a perfect sphere.

When all physical properties for the two fluids are equal, $m = 1$, $\lambda = 1$, and $\tau = 1$, we have simply

$$k^*_{eff} = 1 + \phi\left\{1.48Pe_1^{3/2} + \cdots\cdots\right\} \tag{40}$$

Finally, for the case of deformation dominated by internal viscous effects, we have plotted in Figure 2 the magnitude of the deformation-induced convective contribution to the effective conductivity as a function of the conductivity ratio m for several values of the heat capacity ratio τ, i.e. the last term in equation (34). Although behavior of this term may seem to depend strongly on the value of the heat capacity ratio τ, in all cases it is positive for m sufficiently small, negative when m is large, and zero at $m = 1$. Between these limiting cases, $\tau = 1$ is the critical value of the heat capacity ratio which separates two distinct regimes. In particular, for $\tau < 1$, the contribution to the effective conductivity is <u>negative</u> for all $m \gtrsim .176\tau^3$, except for $m = 1$ where it is <u>zero</u>. For $\tau > 1$ on the other hand, the behavior is more complicated. In this case, the contribution is positive for $m \leq 1$, goes through zero at $m = 1$ and subsequently increases again to a positive maximum before ultimately decreasing

to negative values for large m. It thus follows that for $m \to \infty$, with τ, ε and Pe_1 fixed (ε and Pe_1 being small), the deformation-induced convection contribution to k^*_{eff} is always negative and asymptotically approaches the value

$$k^*_{eff} \sim 1 + \phi\left\{3 + 4.13Pe_1^{3/2} - 3.6\varepsilon - 1.579\varepsilon Pe_1^{3/2}\right\} \quad (m \to \infty) \qquad (41)$$

for arbitrary τ. In this limit, both deformation-induced terms are small corrections to the dominant terms which correspond to a strictly spherical drop. For the limit $m \to 0$,

$$k^*_{eff} \sim 1 + \phi\left\{ -\frac{3}{2} + 3.36\,\frac{m^{3/2}}{\tau^{3/2}}\,Pe_2^{3/2} - 0.9\varepsilon + .176m\varepsilon Pe_2^{3/2}\right\} \quad (m \to 0) \qquad (42)$$

and both of the convective corrections are positive and vanishingly small. However, the deformation-induced convective correction vanishes more slowly, $O(m\varepsilon Pe_2^{3/2})$, than the convective correction for a spherical drop, $O(m^{3/2}Pe_2^{3/2})$, for ε and Pe_2 both small but of fixed value. Finally, when $m = 1$

$$k^*_{eff} = 1 + \phi\left\{3Pe_1^{3/2} + O(\varepsilon^2) + 0\ Pe_1^2 + O\left(\varepsilon Pe_1^2\right) + \ldots\right\} \quad (m = 1) \qquad (43)$$

Thus, not only do the pure conduction contributions to k^*_{eff} vanish, as expected, when the thermal conductivities are equal, but, surprisingly, the $O\left(\varepsilon Pe_1^{3/2}\right)$ deformation-induced convective term also vanishes. The results (41), (42), (43) and Figure 3, would seem to imply that, unlike the surface-tension dominated case where the deformation-induced flow correction can be of the same magnitude or even larger than the corresponding contributions for a spherical drop, the deformation contributions in the present case are small compared to the contributions of a spherical drop, except for the case when $m \to 0$ when both are very small. This is especially true when the internal and external conductivities are of similar magnitude, as indicated by the expression (43).

LITERATURE CITED

Batchelor, G. K., An Introduction to Fluid Dynamics, Cambridge University Press, (1967)

Chaffey, C. F., H. Brenner and S. G. Mason, "Particle motions in sheared suspensions XVII: Deformation and migration of liquid drops," Rheol. Acta, 4, 56 (1965)

Cox, R. G., "The deformation of a drop in a general time-dependent fluid flow," J. Fluid Mech., 37, 601 (1969)

Leal, L. G., "On the effective conductivity of a dilute suspension of spherical drops in the limit of low particle Peclet number," Chem. Eng. Communications, 1, 21 (1973)

McMillen, T. J., Ph.D. Thesis, California Institute of Technology, 1975.

Taylor, G. I., "The viscosity of a fluid containing small drops of another fluid," Proc. Roy. Soc. (London), A138, 41 (1932)

ACKNOWLEDGEMENT

This work was supported by grants from the Research Corporation and from the Petroleum Research Fund of the American Chemical Society.

Table 1: Required Harmonic Functions for the

$O(\varepsilon)$ Velocity Fields

in the Case of Deformation Controlled by Internal Viscosity

outer field $\tilde{u}^{1}$ (nondimensional)	inner field $\tilde{u}^{1}$ (nondimensional)
$P_{-5} = \frac{u}{6r^5} P_4^4(\cos\theta)\sin 4\phi$	$\chi_1 = rP_1(\cos\theta)$
$\phi_{-5} = \frac{1}{336r^5} P_4^4(\cos\theta)\sin 4\phi$	P_4, ϕ_4, and χ_3 all of order (λ^{-1})
$\chi_{-4} = \frac{1}{6r^4} P_3(\cos\theta)$	
$\chi_{-2} = 0$	

Table 2: Corrected O(Pe) Temperature Distributions

for a Spherical Drop Outside the Particle (Nondimensional)

$$T_1^0 = \left\{ \frac{C_{11}}{r^2} - \frac{\alpha C}{20} - \frac{3\alpha\kappa}{10} + \frac{\alpha\kappa C}{20r^3} - \frac{\alpha\kappa D}{20r^5} \right\} P_1^1(\cos\theta)\cos\phi$$

$$+ \left\{ \frac{C_{31}}{r^4} + \frac{\alpha C}{720} - \frac{\alpha\kappa}{120} - \frac{\alpha D}{120r^2} - \frac{\alpha\kappa C}{180r^3} - \frac{\alpha\kappa D}{120r^5} \right\} P_3^1(\cos\theta)\cos\phi$$

$$+ \left\{ \frac{C_{33}}{r^4} + \frac{\alpha C}{1440} - \frac{\alpha\kappa}{240} - \frac{\alpha D}{240r^2} - \frac{\alpha\kappa C}{360r^3} - \frac{\alpha\kappa D}{240r^5} \right\} P_3^3(\cos\theta)\cos\phi$$

inside the particle:

$$\bar{T}_1^0 = \left\{ A_{11} r + \frac{K(\bar{D} - 1)}{20} r^3 + \frac{\bar{C}K}{280} r^5 \right\} P_1^1(\cos\theta)\cos\phi$$

$$+ \left\{ A_{31} r^3 + \frac{\bar{C}K}{5670} r^5 \right\} P_3^1(\cos\theta)\cos\phi$$

$$+ \left\{ A_{33} r^3 + \frac{\bar{C}K}{11340} r^5 \right\} P_3^3(\cos\theta)\cos 3\phi$$

where $\kappa = \dfrac{k_1 - k_2}{k_2 + 2k_1}$ $\qquad K = \dfrac{3\alpha k_1}{k_2 + 2k_1}$

$D = \dfrac{\lambda}{\lambda + 1}$ $\qquad C = \dfrac{5\lambda + 1}{\lambda + 1}$ $\qquad \bar{D} = \dfrac{3}{2(\lambda + 1)}$ $\qquad \bar{C} = \dfrac{21}{2(\lambda + 1)}$

$$C_{11} = \left(\frac{k_1}{k_2 + 2k_1} \right) \left\{ \frac{3\alpha\kappa C}{20} - \frac{\alpha\kappa D}{4} + \frac{k_2}{k_1} \left[\frac{\alpha C}{20} - \frac{3\alpha\kappa}{10} + \frac{\alpha\kappa C}{20} - \frac{\alpha\kappa D}{20} \right] + \frac{Cp_2}{Cp_1} \left[\frac{\kappa(1 - \bar{D})}{10} - \frac{\kappa\bar{C}}{70} \right] \right\}$$

$$C_{31} = \left(\frac{k_1}{3k_2 + 4k_1}\right)\left\{\frac{\alpha D}{60} + \frac{\alpha\kappa C}{60} + \frac{\alpha\kappa D}{24} - \frac{k_2}{k_1}\left[\frac{\alpha C}{240} - \frac{\alpha\kappa}{40} - \frac{\alpha D}{40} - \frac{\alpha\kappa C}{60} - \frac{\alpha\kappa D}{40}\right]\right.$$

$$\left. - \frac{Cp_2}{Cp_1}\frac{\bar{\alpha}\kappa}{2835}\right\}$$

$$A_{11} = \left(\frac{Cp_1 k_2}{Cp_2 k_1}\right)\left\{C_{11} - \frac{\alpha C}{20} + \frac{3\alpha\kappa}{10} - \frac{\alpha\kappa C}{20} + \frac{\alpha\kappa D}{20}\right\} - \frac{\kappa}{20}\left\{\frac{\bar{C}}{14} + \frac{\bar{D} - 1}{1}\right\}$$

$$A_{31} = \left(\frac{Cp_1 k_2}{Cp_2 k_1}\right)\left\{C_{31} + \frac{\alpha C}{720} - \frac{\alpha\kappa}{120} - \frac{\alpha D}{120} - \frac{\alpha\kappa C}{180} - \frac{\alpha\kappa D}{120}\right\} - \frac{\bar{C}\kappa}{5670}$$

$$C_{33} = C_{31}/2 \qquad A_{33} = A_{31}/2$$

Table 3: The Temperature Fields T_0^1, $\bar{T}_0^1$

For Deformation Dominated by Surface Tension Forces

$$T_0^1 = \frac{D_{11}}{r^2} P_1^1 \cos\phi + \frac{D_{31}}{r^4} P_3^1 \cos\phi + \frac{D_{33}}{r^4} P_3^3 \cos 3\phi$$

$$\bar{T}_0^1 = B_{11} r P_1^1 \cos\phi + B_{31} r^3 P_3^1 \cos\phi + B_{33} r^3 P_3^3 \cos 3\phi$$

where

$$D_{11} = \frac{3\alpha(1 + m - 2m^2)}{5(m + 2)^2} \qquad B_{11} = \frac{9\alpha(m - 1)}{5(m + 2)^2}$$

$$D_{31} = \frac{\alpha(9m^2 - 5m - 4)}{15(3m + 4)(m + 2)} \qquad B_{31} = \frac{-8\alpha(m - 1)}{15(3m + 4)(m + 2)}$$

$$D_{33} = \frac{\alpha(9m^2 - 5m - 4)}{30(3m + 4)(m + 2)} \qquad B_{33} = \frac{-4\alpha(m - 1)}{15(3m + 4)(m + 2)}$$

For Deformation Dominated by Internal Viscous Forces

$$T_0^1 = \frac{D_{11}^*}{r^2} P_1^1 \sin\phi + \frac{D_{31}^*}{r^4} P_3^1 \sin\phi + \frac{D_{33}^*}{r^4} P_3^3 \sin 3\phi$$

$$\bar{T}_0^1 = B_{11}^* r P_1^1 \sin\phi + B_{31}^* r^3 P_3^1 \sin\phi + B_{33}^* r^3 P_3^3 \sin 3\phi$$

$$D_{11}^* = \frac{6\alpha(m - 1)^2}{5(m + 2)^2} \qquad B_{11}^* = \frac{-18\alpha(m - 1)}{5(m + 2)^2}$$

$$D_{31}^* = \frac{-\alpha(3m^2 + m - 4)}{5(3m + 4)(m + 2)} \qquad B_{31}^* = 0$$

$$D_{33}^* = \frac{-\alpha(3m^2 + m - 4)}{10(3m + 4)(m + 2)} \qquad B_{33}^* = 0$$

Table 4: $0(Pe_1)$ Contribution to the Effective Conductivity for Deformation Controlled by Surface Tension Forces

$$I(m, \lambda, \tau) = \frac{(m-1)}{(3m+4)(m+2)^3 m(\lambda+1)^2} \times \Big\{ \tau \Big([\, .36m^4 + .84m^3 - .24m^2 - .96m]\lambda^3 + [-.66m^4 - 1.607m^3 + .807m^2 + 8.714m + 9.382]\lambda^2 + [-2.652m^4 - 9.430m^3 - 1.108m^2 + 22.769m + 17.640]\lambda - 1.604m^4 + 12.473m^3 + 61.970m^2 + 83.779m + 24.543 \Big) + [\, 1.990m^4 - .659m^3 - 48.344m^2 - 21.753m - 1.341]\lambda^2 + [\, 1.053m^4 - 3.786m^3 - 39.684m^2 - 27.892m - 7.096]\lambda - 4.931m^4 + 18.011m^3 + 32.118m^2 - 6.830m - 2.940 \Big\}$$

where $m = k_2/k_1$, $\lambda = \mu_2/\mu_1$, $\tau = Cp_2/Cp_1$

FIGURE CAPTIONS

Figure 1: The $O(\varepsilon Pe_1)$ term, $I(m,\lambda,\tau)$, in the effective conductivity when interfacial tension forces control, as a function of the conductivity ratio, $m = k_2/k_1$, and the viscosity ratio, $\lambda = \mu_2/\mu_1$, for several values of the heat capacity ratio, $\tau = Cp_2/Cp_1$.
Detail A: $\tau = .5$ Detail B: $\tau = 1$ Detail C: $\tau = 2.$

Figure 2: The $O\left(\varepsilon Pe_1^{3/2}\right)$ term in the effective conductivity when viscous forces control, as a function of the conductivity ratio, $m = k_2/k_1$, for several values of the heat capacity ratio, $\tau = Cp_2/Cp_1$.
a: $\tau = 3$, b: $\tau = 2$, c: $\tau = 1$, d: $\tau = .5$, e: $\tau = 0.$

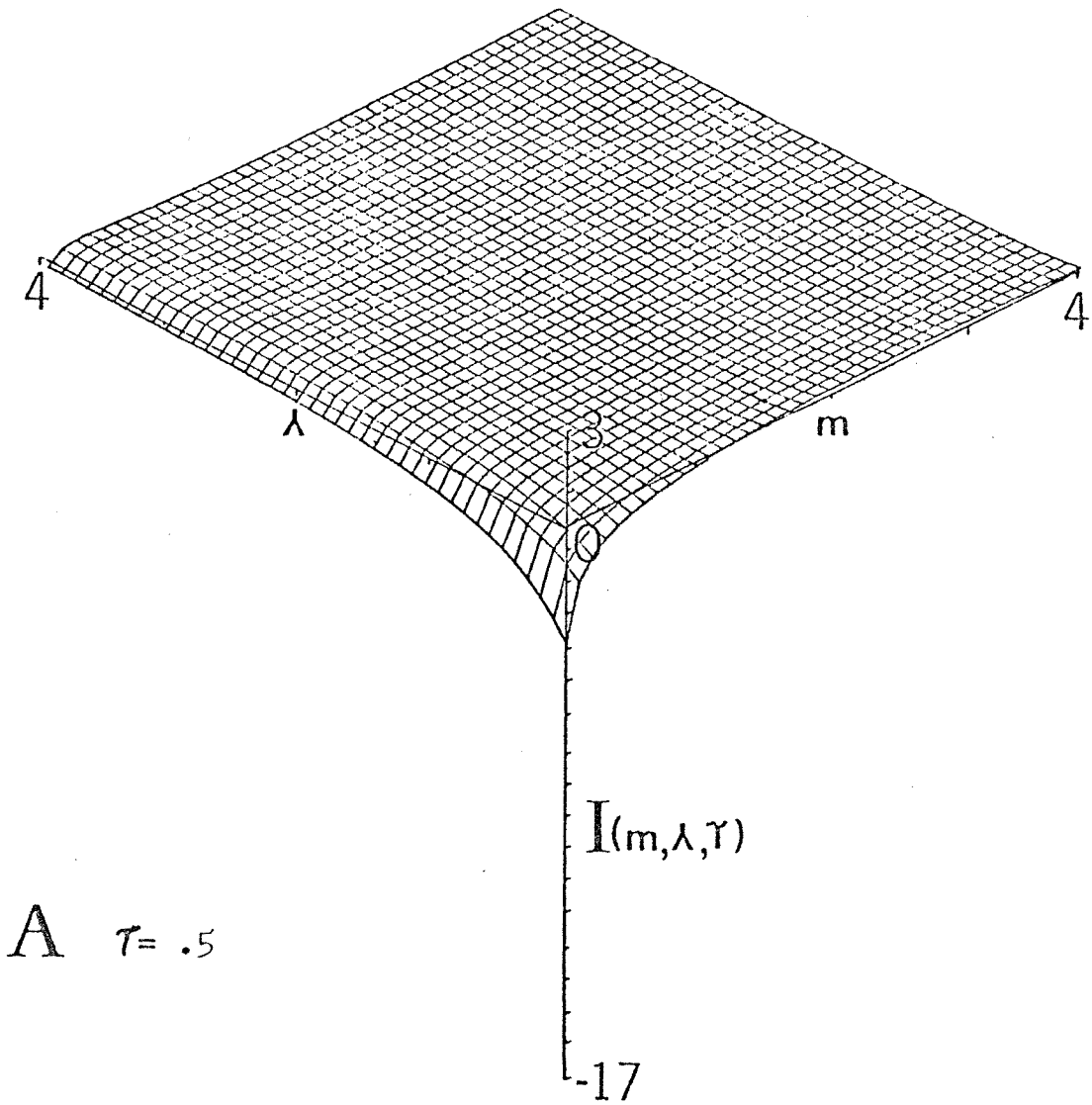

Figure 1

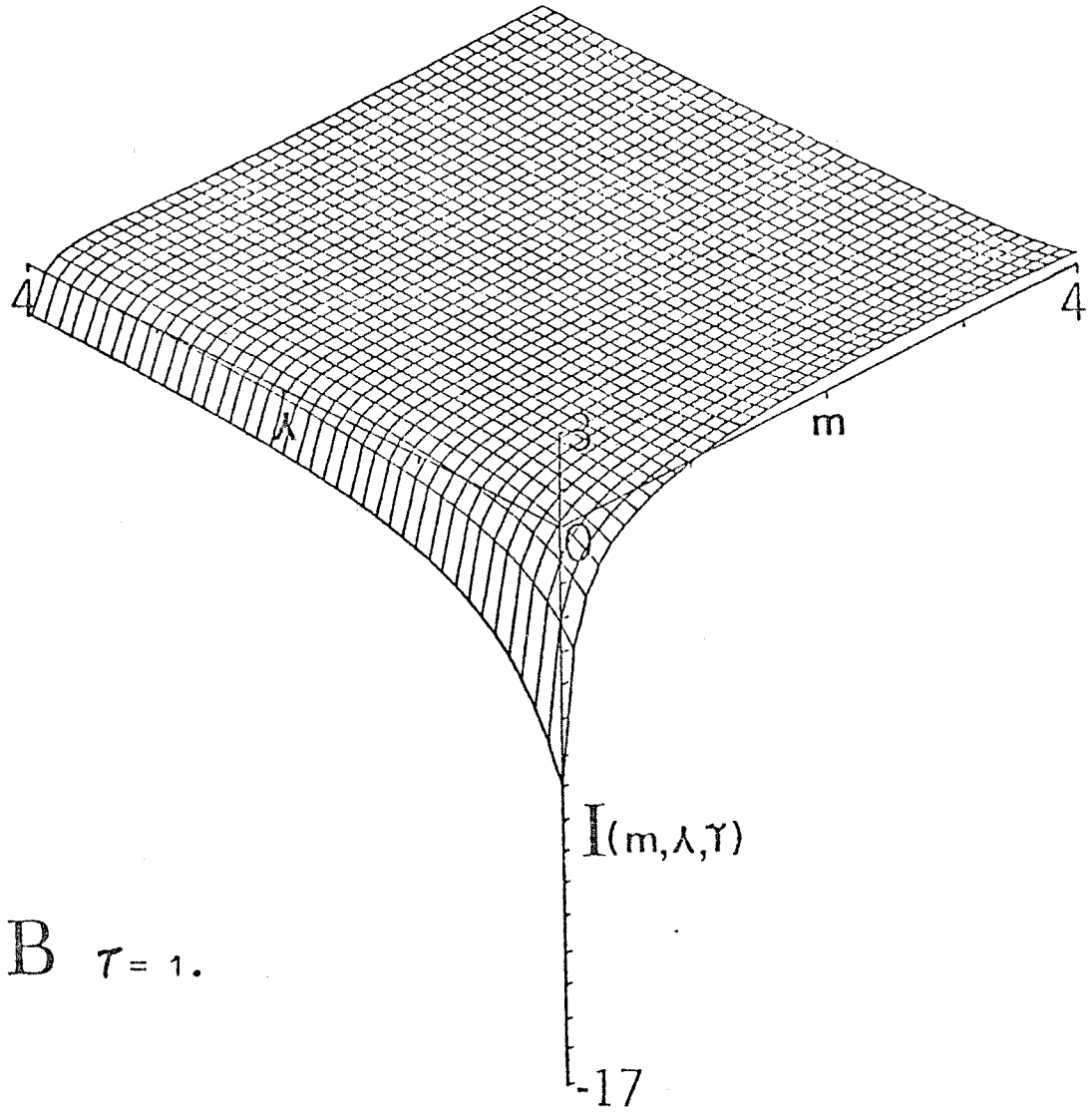

B $\tau = 1.$

Figure 1

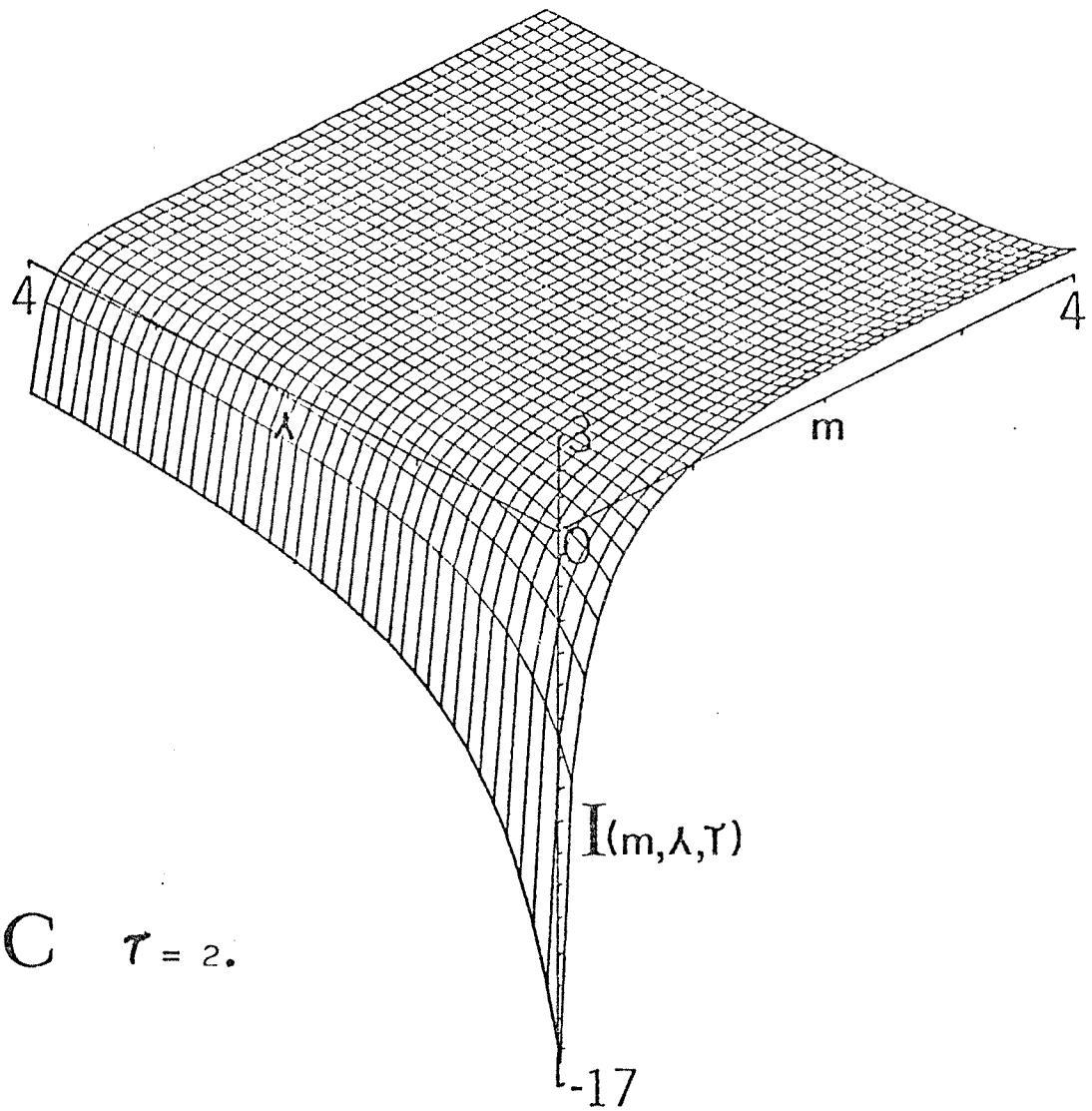

Figure 1

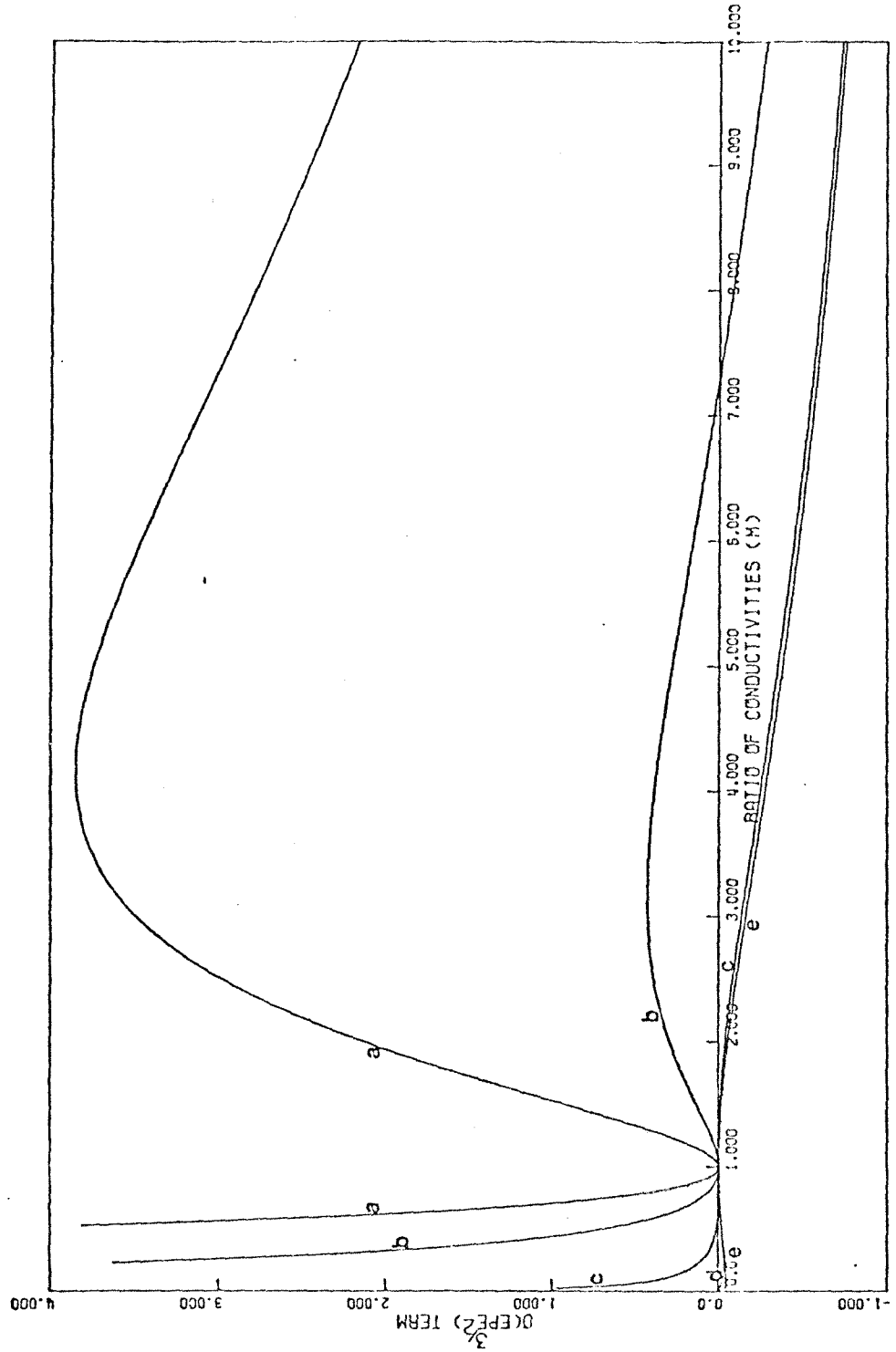
RATIO OF CONDUCTIVITIES (M)
1.000
2.000
3.000
4.000
5.000
6.000
7.000
8.000
9.000
10.000
a
b
c
d
e
-1.000
0.0
1.000
2.000
3.000
4.000
∂(EPE2) TERM

Figure 2

CHAPTER IV

THE BULK HEAT FLUX FOR A SHEARED SUSPENSION OF RIGID SPHEROIDS AT LOW PARTICLE PECLET NUMBER

by

T. J. McMillen and L. G. Leal
Chemical Engineering Department
California Institute of Technology
Pasadena, California

I. INTRODUCTION

There have been many theoretical studies in recent years concerned with the rheological properties of dilute suspensions. Such investigations play a dual role: on the one hand, providing definite predictions of the macroscopic behavior of specific, realizable materials, and, on the other, serving as idealized model studies from which one can gain insight into the qualitative relationships between microstructure and macroproperties for a more general class of 'suspension-like' fluids.

Recently, work has also begun to appear which is concerned with the equally important constitutive behavior of flow suspensions for conductive heat transfer, diffusive mass transfer, and other related transport processes. Of course, investigations of these properties for stationary suspensions have a long history, extending back at least to Maxwell (1873), who obtained a correct prediction of the effective thermal conductivity for a dilute dispersion of solid spheres. Our concern here is the effect of motion, specifically of shearing motions, on the macroscopic thermal properties of a suspension. Three papers exist, so far as we are aware, which address this question for dilute systems; the work of Leal (1973) for a suspension of spherical drops in simple shear flow, under the assumption of small particle Peclet number; of McMillen and Leal (1975-1976) for slightly deformed drops in simple shear flow, again with small Peclet

number, and of Nir and Acrivos (1976) for a suspension of rigid spheres in simple shear flow, but with large particle Peclet number. In all of these studies, the particles were either spherical or at least near-spheres, and, in addition, assumed implicitly to be sufficiently large (or massive) that Brownian motion could be completely neglected. Even with these simplifications, however, the thermal properties of the suspension were found to depend not only on the thermal and mechanical properties of its constituents, but also critically on the strength and type of any bulk flow which is present (cf. McMillen and Leal, 1976).

The present paper is concerned with the transport of heat in a sheared suspension of rigid, prolate spheroids. The particle Peclet number will be assumed small, as in our previous studies. However, no restriction is placed on the axis ratio for the particles, which may thus range from perfect spheres to highly elongated slender bodies. Furthermore, we explicitly include contributions of Brownian rotation in the analysis. The limit of small Peclet number (Pe) is, of course, the limit of weak local convection heat transfer relative to conduction, and the bulk heat flux is dominated by the stationary suspension results. In spite of the relatively weak effects of motion, however, this limit is of considerable qualitative interest since calculations can actually be completed for a variety of particle shapes and flow types including time dependent problems.

The other limit of large Peclet number is potentially of greater practical interest since the effect of convection is dominant at the particle scale, and the magnitude of flow effects on the bulk heat flux therefore potentially large. The disadvantage for analytical investigation is that very few problems appear to be tractable. For example, in shear flow, even the problem of steady flow with spherical particles has not yet been completely resolved (cf. Nir and Acrivos, 1976).

II. BACKGROUND

We consider a suspension of neutrally buoyant prolate spheroids in the presence of a general bulk shear flow and a bulk temperature field. Our objective is the development of a constitutive equation which describes the effective thermal diffusivity of the suspension considered as an equivalent homogeneous material. The point of view adopted is the conventional one in the field of suspension rheology. We assume that the minimum dimension ℓ of the particles is large compared to the intermolecular length scale α of the suspending medium. The latter may then be treated as a continuum and is modelled for present purposes as an incompressible Newtonian fluid in which a simple scalar Fourier heat conduction law is applicable.

At any arbitrary point in the suspension, when viewed on a length scale of order ℓ, the local variables such as velocity, temperature, enthalpy, or conductive heat flux are random functions of time whose values at any instant depend upon the proximity and motion of suspended particles. The description of bulk or macroscopic quantities for the suspension thus becomes a problem of statistics. At the fundamental level, the most appropriate definition of bulk variables is as an ensemble average of the corresponding microscale quantities for a large number of realizations of the system. Instantaneous local values of the velocity, temperature, enthalpy, and conductive heat flux may then be

expressed as a sum of the ensemble averaged quantity, and an additional microscale or fluctuating component, i.e.,

$$\begin{aligned} u_i &= \langle u_i \rangle + u_i' \\ T &= \langle T \rangle + T' \\ h &= \langle h \rangle + h' \\ q_i &= \langle q_i \rangle + q_i' \quad , \end{aligned} \tag{1}$$

where by definition the averages of the fluctuating components are zero,

$$\langle u' \rangle = \langle T' \rangle = \langle h' \rangle = \langle q_i' \rangle = 0 \tag{2}$$

An operational definition for the bulk conductive heat flux Q_i may now be derived, from the requirement that the thermal energy balance for the suspension, viewed as an equivalent homogeneous material, take its usual form

$$\frac{\partial \langle h \rangle}{\partial t} + \langle u_i \rangle \frac{\partial \langle h \rangle}{\partial x_i} + \frac{\partial Q_i}{\partial x_i} = 0 \quad . \tag{3}$$

As shown by Leal and McMillen (1976), the appropriate form for Q_i is

$$Q_i \equiv \langle q_i \rangle + \langle u_i' h' \rangle \tag{4}$$

Thus, the bulk 'conductive' heat flux consists of the ensemble averaged local values, plus an additional contribution due to the local, instantaneous convective heat flux as measured in a frame of reference which is translating with the ensemble average velocity, $\langle \vec{u} \rangle$. For present

purposes, it is convenient to assume that the suspension is statistically homogeneous on a scale of $0(V^{1/3})$, which is much larger than the microscale, ℓ, yet still much smaller than the macroscale, L, over which significant variations occur in the bulk velocity or temperature gradients, or in the concentration of particles. In these circumstances, the ergodic hypothesis may be invoked to replace the ensemble averages of (1) or (4) with volume averages, e.g.

$$\langle q_i \rangle = \frac{1}{V} \int_V q_i dV \quad .$$

Starting with volume averages in (4), the volume integrals may be split into two parts, ΣV_o and $V - \Sigma V_o$, representing the sum of the volumes V_o of the individual particles in V and the volume of the surrounding fluid, respectively, and re-expressed using the Fourier heat conduction law in each phase to give

$$Q_i = -k \frac{\partial \theta}{\partial x_i} + \frac{k(1-m)}{V} \int_{\Sigma V_o} \nabla T dV + \frac{\rho C_p (\tau-1)}{V} \int_{\Sigma V_o} u_i' T' dV + \frac{\rho C_p}{V} \int_V u_i' T' dV \qquad (5)$$

Here, $\partial\theta/\partial x_i$ is the macroscale temperature gradient, k and mk the thermal conductivities of the fluid and particles, C_p and τC_p the respective heat capacities and ρ the density (assumed equal for fluid and particles). Temperature variations of the physical properties have been neglected in writing equation (5).

The expression (5) for the bulk conductive heat flux, Q_i, is not restricted to any particular range of particle concentrations. However, its evaluation in the general case would require the existence of a solution to the many-body microscale problem for all of the n particles in a typical averaging volume V. Here, we restrict our attention to dilute suspensions (i.e., small volume fraction, $\phi << 1$), where the first $0(\phi)$ correction to Q_i may be determined by considering the average contribution for a single, isolated particle, subject to the macroscopic or bulk average temperature and velocity fields as boundary conditions at infinity (Jeffrey, 1974). It should be noted, that the motions and orientations of the particles will exhibit a random nature in the presence of significant Brownian motion. In these circumstances, the (instantaneous) individual particle contributions to Q_i will be different for each particle and the average contribution per particle can then only be determined in a statistical sense. In view of the assumed steadiness of the macroscale velocity and temperature fields, one approach is to simply average the contribution from a single particle over a period which is long compared to that characteristic of Brownian motion. An equivalent approach, more convenient for calculation, is to first determine the instantaneous, orientation-dependent contribution and then average over all possible orientations with the probability density function for orientation as a weighting factor. In

either case, we shall denote the averaging process by the use of an overbar, and with this understanding, the particle contribution to the bulk heat flux may be expressed in the form

$$Q_i^* = \frac{k(1-m)}{V_o}\,\phi\int_{V_o}\overline{\nabla T}\,dV + \frac{\rho C_p(\tau-1)\phi}{V_o}\int_{V_o}\overline{u_i'T'}\,dV$$

$$+ \frac{\rho C_p\phi}{V_o}\int_{V}\overline{u_i'T'}\,dV \quad . \tag{16}$$

Here, V_o is the volume of a particle (assumed equal for all particles), while V is the fluid volume which is assumed to extend to infinity in the single particle microscale problem.

It should not be supposed, however, that the only influence of Brownian motion is a thermally passive randomization of particle orientation or motion. In general, when averaged on the long time scale (compared with a Brownian motion time scale), any random rotation which occurs in the presence of a nonuniform orientation distribution will produce a mean rotation of the particle at a rate

$$\omega_{Br} = -D_R\nabla_{\vec{\phi}}(\ell n P(\vec{\phi})) \tag{7}$$

where D_R is the Stokes-Einstein rotational diffusion coefficient and $P(\vec{\phi})$ is the probability density function for particle orientation. Thus, in the presence of Brownian rotation, the convection velocity at the microscale which is relevant to the determination of Q_i is not simply the deterministic field associated with the presence of motion for the suspension as a whole, but also includes the fluid

motions corresponding to the effective rotational motion (6). In addition, the particle and fluid motions which are purely random on the long-time scale will generally be correlated with random fluctuations in the temperature and this constitutes a direct mechanism for heat transfer, which must be 'added' to the local conductive transfer in each phase, and the local convective transfer in the fluid associated with the overall bulk motions of the suspension. Further details for the general Brownian motion problem may be found in McMillen (1976), or in a slightly abbreviated form in Leal (1976).

Here, we consider only the case of small local (particle Peclet numbers, and specifically only the first, $0(Pe)$, convective contributions to the bulk 'conductive' heat flux, Q_i. At first order in Pe, the microscale thermal energy problem is pure conduction. At second order, the first convection effects come into the analysis, including all Brownian motion effects, since these are due to fluid motion at the microscale of single particles. At each order, the governing equations and boundary conditions are linear. The most important consequence of restricting ourselves to the low Pe limit is that the random temperature field, relative to the long-time average, is completely independent of the velocity fields so that the direct flux of heat due to Brownian motion is negligible through $0(Pe)$. Thus, to $0(Pe)$, the only effects of Brownian motion on Q_i are due to the

influence of the orientation distribution on the bulk motion of the suspension, (called the "indirect" Brownian effect in suspension rheology), and to the microconvective effects of the mean Brownian rotation, (6), resulting from inhomogeneities in the orientation distribution of the particles (called the "direct" Brownian effect). Since the governing equations and boundary conditions, plus the expression (6) for Q_i, are all linear in the temperature at O(Pe), the deterministic and mean Brownian convection contributions may be calculated independently of one another at the same level of approximation. Our approach in the present work is to first calculate the microscale temperature fields associated with the deterministic velocity field and a specific (but arbitrary) particle orientation, from this solution to determine the instantaneous and orientation dependent contributions to the integrals in (6); and then finally, to average these orientation dependent quantities by integrating over the complete orientation space with the probability density function for orientation as a weighting factor. The additional convection contribution due to the long-time averaged Brownian rotation, is similarly determined by first considering the temperature field associated with steady rotation of the particle in a quiescent fluid; from this and (6) to determine the instantaneous and orientation dependent contributions to Q_i; and finally again average the results using the orientation distribution function.

The probability distribution function for particle orientation is governed by a modified Fokker-Plank equation, and can be solved analytically for either strong or weak Brownian motion (cf. Leal and Hinch (1971) and Hinch and Leal (1972) where references to earlier work are also given). The present calculation is restricted to the limit of strong Brownian motion, $D_R/\gamma >> 1$, where γ is the bulk shear rate for the suspension.

III. THE MICROSCALE PROBLEM

In order to evaluate the volume integrals in the expression (6) for the $0(\phi)$ particle contributions to the bulk conductive heat flux, we have seen that it is necessary to calculate the microscale velocity and temperature field near a particle, with the bulk velocity and temperature distributions as boundary conditions at 'infinity.' Since hydrodynamic interactions are completely neglected at this $0(\phi)$ level of approximation, and the flow is creeping, the center of mass of a typical particle will translate with the macroscale mean velocity, $\langle u_i \rangle = \frac{1}{V}\int_V u_i dV$. In view of the assumed homogeneity of the suspension on the scale $0(V^{1/3})$, it is thus convenient to formulate the single particle problem in a frame of reference fixed to the particle, i.e., also translating with velocity $\langle u_i \rangle$. This shift of reference frame requires no modification of (6) since the simple translational motion of the particles makes no contribution to the bulk conductive heat flux.

We are interested here in the influence of a general shearing motion on the conductive transport of heat. However, the small scale of the averaging volume V relative to spatial variations in the macroscale velocity or temperature gradients suggests that it is appropriate to consider <u>locally</u> linear temperature and velocity fields, e.g.,

$$T_\infty = \alpha_i x_i \quad \text{and} \quad (\vec{u}_\infty)_i = \gamma_{ij} x_j \qquad (8a)$$

as boundary values for the single particle microscale calculations. It is important to note, however, that some further restriction on the possible values α_j is required in order that this far-field behavior for the microscale temperature field be compatible with the general advection-diffusion equation. In particular, as $|x| \to \infty$, it is required that

$$u_i \alpha_i \equiv 0 \tag{9}$$

where u_i represents the macroscale velocity vector. In the case of simple linear shear flow, we are thus restricted to temperature gradients which are orthogonal to the undisturbed flow. To calculate the bulk heat flux due to temperature gradients in the flow direction, it would be necessary to consider the exact macroscale velocity and temperature distributions locally, not just their linear approximations. This fact apparently precludes the existence of an effective conductivity tensor since the resulting bulk heat flux could not possibly be linearly related to ∇T. We shall be concerned here with the bulk heat flux due to gradients of the bulk temperature field which satisfy (9).

We consider a prolate spheroid of major axis 2a and minor axis 2b, whose axis of revolution is at polar and azimuthal angles θ_1 and ϕ_1 relative to a non-rotating Cartesian coordinate system (x_1, x_2, x_3) which has its origin fixed in the center of the particle. The geometric relationship between θ_1, ϕ_1 and the undisturbed shear flow, which is

$$u_3 = \gamma x_2 \tag{8b}$$

relative to this coordinate system, is shown in Figure 1. The orientation of the particle will, in general, be a function of time. In the absence of all external forces and couples and Brownian motion, Jeffery (1922) has shown that a particle in creeping flow will rotate in closed orbits, given by the equations

$$\phi_1 = \tan^{-1}\left\{\Gamma_p \tan\left(\frac{\Gamma_p \gamma t}{\Gamma_p^2 + 1}\right)\right\}$$

$$\theta_1 = \tan^{-1}\left\{\frac{\Gamma_p}{C\left[\Gamma_p^2 \cos^2\phi_1 + \sin^2\phi_1\right]^{1/2}}\right\} . \tag{10}$$

Here Γ_p is the particle axis ratio, $\Gamma_p \equiv a/b$, and C is an undetermined constant of integration, having possible values $0 \leq C \leq \infty$. The orbit for a particle is determined by the constant C.

For purposes of the microscale analysis, it is convenient to utilize a coordinate system which is coincident, at any instant, with the principle (major and minor) axes of the particle. We may transform from the system (x_1, x_2, x_3) to this new system $(x_1^\ddagger, x_2^\ddagger, x_3^\ddagger)$ by means of the orthogonal transformation given by the direction cosines of the orientation angles;

$$x_i^\ddagger = \ell_{ij} x_j \tag{11}$$

where

$$\ell_{ij} \equiv \begin{bmatrix} \cos\theta_1 & \sin\theta_1\cos\phi_1 & \sin\theta_1\sin\phi_1 \\ -\sin\theta_1 & \cos\theta_1\cos\phi_1 & \cos\theta_1\sin\phi_1 \\ 0 & -\sin\phi_1 & \cos\phi_1 \end{bmatrix} .$$

A further convenience is to use prolate spheroidal coordinates (ξ, η, ϕ) defined by the equations

$$\begin{aligned} x_1^{\ddagger} &= c\ \cosh\xi\ \cos\eta \\ x_2^{\ddagger} &= c\ \sinh\xi\ \sin\eta\ \cos\phi \\ x_3^{\ddagger} &= c\ \sinh\xi\ \sin\eta\ \sin\phi \end{aligned} \qquad (12)$$

where

$$c \equiv \frac{(a^2 - b^2)^{1/2}}{\ell} \equiv \frac{(\Gamma_p^2 - 1)^{1/2}}{\Gamma_p^{1/3}}$$

and the surface of the particle is given by $\xi = \xi_o = \mathrm{ctnh}^{-1}\Gamma$. Typical coordinate lines for this system are illustrated in Figure 3.

a) The microscale velocity field

The motion of the fluid, as well as the particle (equation 10), for a general ellipsoidal particle in a general linear flow was obtained by Jeffery (1922), under the assumption of small Reynolds number. Unfortunately, the solution is expressed in terms of a Cartesian coordinate system instantaneously aligned with the particle major and minor axes, and thus involves complicated integral functions of a parameter λ which is the positive root of the equation

$$\frac{x_1^{\ddagger 2}}{a^2 + \lambda} + \frac{x_2^{\ddagger 2}}{b^2 + \lambda} + \frac{x_3^{\ddagger 2}}{c^2 + \lambda} = 1 \quad .$$

Transformation of this solution to prolate spheroidal coordinates which are suitable for the thermal problem, is therefore extremely difficult, and we have adopted the alternative of simply rederiving the solution directly in spheroidal coordinates.

The problem which we consider is the motion of a prolate spheroidal particle, together with surrounding fluid, which is subjected to the linear shear flow given by equation (8b). A convenient approach to this calculation, which we follow, is to first solve for the case in which the particle is rotating at some instantaneous rate (ω_1, ω_2, ω_3) relative to the axes ($x_1^{\ddagger}$, $x_2^{\ddagger}$, $x_3^{\ddagger}$). An appropriate characteristic length scale is $\ell = [ab^2]^{1/3}$, and the relevant velocity scale is $\gamma\ell$. Because the particles are assumed to be very small, the Reynolds number at the microscale is also very small

$$\mathrm{Re} \equiv \frac{\rho\gamma\ell^2}{\mu} << 1 \quad .$$

Finally, we assume that there are no imposed changes of particle orientation which occur faster than those arising naturally from the shear field, equation (10). In these circumstances, the microscale velocity field in the fluid is governed by the creeping motion equations

$$\nabla^2\vec{u} = \nabla p \quad , \quad \nabla\cdot\vec{u} = 0 \qquad (13)$$

The velocity field in the particle is simply the solid body rotation described by the rotation vector $\vec{\omega}$, referred to as the instantaneously aligned Cartesian coordinate system $(x_i^{\ddagger})$. The microscale velocity field in the fluid must match the particle velocity at the surface of the spheroid, $\xi = \xi_o$, and reduce to the non-dimensional simple shear field $u_3 = x_2$ (referred to the non-rotating Cartesian coordinate system x_i) far from the spheroid. For convenience, we actually solve for the <u>disturbance</u> velocity field

$$\vec{u}^* = \vec{u} - \vec{u}_\infty \quad ,$$

which satisfies the same equations (13), but vanishes at infinity.

The velocity field in the particle, $\vec{\bar{u}}$, will simply be that given by the solid body rotation,

$$\begin{aligned} \bar{u}_1^{\ddagger} &= \omega_2 x_3^{\ddagger} - \omega_3 x_2^{\ddagger} \\ \bar{u}_2^{\ddagger} &= \omega_3 x_1^{\ddagger} - \omega_1 x_3^{\ddagger} \\ \bar{u}_3^{\ddagger} &= \omega_1 x_2^{\ddagger} - \omega_2 x_1^{\ddagger} \end{aligned} \qquad (14)$$

and at the particle surface, $\xi = \xi_o$, must equal the velocity in the fluid, $\vec{u}^* + \vec{u}_\infty$.

We therefore have the following governing equation for the disturbance flow field;

$$\begin{aligned} \nabla \cdot \vec{u}^* &= 0 \\ \nabla^2 \vec{u}^* &= \nabla p^* \end{aligned} \qquad (15a)$$

subject to the boundary conditions

$$\vec{u}^* \to 0 \quad \text{as } \xi \to \infty; \qquad \vec{u}^* = \vec{u} - \vec{u}_\infty \quad \text{at } \xi = \xi_o \tag{15b}$$

Following Lamb (1932) or Jeffrey, the general solution to (15a) can be written in terms of four harmonic functions, χ_n, ϕ_n, R_n and S_n in the form

$$\vec{u}^* = \sum_n \left\{ \nabla \times (\vec{r}\chi_n) + \nabla\phi_n + r^2 \nabla R_n - \vec{r} S_n \right\} \tag{16}$$

where $\vec{r}$ is the normal position vector associated with a point in space,

$$\vec{r} = \frac{c\mu(\mu^2 - 1)^{1/2}}{(\mu^2 - \ )^{1/2}} \vec{e}_\xi - \frac{c\ (1 - \ )^{1/2}}{(\mu^2 - \ )^{1/2}} \vec{e}_\eta \ , \tag{17}$$

in which

$$\mu = \cosh\xi$$

$$\nu = \cos\eta \quad .$$

and $\vec{e}_\xi$, $\vec{e}_\eta$, and $\vec{e}_\phi$ are unit vectors in the ξ, η, and ϕ directions. The distance of a point in space from the origin of our coordinate reference frame is simply

$$r = c[\mu^2 + \nu^2 - 1]^{1/2} \tag{18}$$

The harmonic functions R_n and S_n are related through the continuity equation

$$\sum_{n=0}^{\infty} \left\{ \nabla r^2 \cdot \nabla R_n - \vec{r} \cdot \nabla S_n - 3S_n \right\} = 0 \tag{19}$$

In prolate spheroidal coordinates, the general harmonic function which is continuous in η is given by

$$F = \sum_{n=o}^{\infty} F_n = \sum_{m=o}^{\infty} \sum_{n=m}^{\infty} \left[\left\{ A_{nm} Q_n^m(\mu) + B_{nm} P_n^m(\mu) \right\} P_n^m(\nu) \cos m\phi \right.$$

$$\left. + \left\{ C_{nm} Q_n^m(\mu) + D_{nm} P_n^m(\mu) \right\} P_n^m(\nu) \sin m\phi \right] \qquad (20)$$

where $P_n^m(\mu)$ and $Q_n^m(\mu)$ are the associated Legendre functions of the first and second kind, of degree n and order m. However, since the disturbance vanishes at infinity in the present problem, the harmonic functions χ_n, ϕ_n, R_n and S_n must not contain terms involving the associated Legendre functions of the first kind. To further restrict the general form (20), it is necessary to consider the boundary conditions at the particle surface, including the simple shear field as a result of (15b). For this purpose, we first transform these conditions to the (ξ, η, ϕ) prolate spheroidal coordinate system. For the solid body rotation given by (14), this results in

$$\bar{u}_\xi = \frac{C}{(\mu^2 - \nu^2)^{1/2} (\mu^2 - 1)^{1/2}} \left\{ - \frac{i\omega_3}{3} P_1^1(\mu) P_2^1(\nu) \cos\phi \right.$$

$$\left. + \frac{i\omega_2}{3} P_1^1(\mu) P_2^1(\nu) \sin\phi \right\}$$

$$\bar{u}_m = \frac{C}{(\mu^2 - \nu^2)^{1/2} (1 - \nu^2)^{1/2}} \left\{ - \frac{i\omega_3}{3} P_2^1(\mu) P_1^1(\nu) \cos\phi \right.$$

$$\left. + \frac{i\omega_2}{3} P_2^1(\mu) P_1^1(\nu) \sin\phi \right\}$$

$$\bar{u}_\phi = \frac{c(\mu^2-1)^{1/2}(1-\nu)^{1/2}}{(\mu^2-\nu^2)} \left\{ \frac{2}{3}\omega_1 P_2(\mu)P_o(\nu) - \frac{2}{3}\omega_1 P_o(\mu)P_2(\nu) + \left[-\frac{i\omega_2}{9} \frac{P_2^1(\mu)P_2^1(\nu)}{(1-\mu^2)} + \frac{i\omega_2}{9} \frac{P_2^1(\mu)P_2^1(\nu)}{(1-\nu^2)} \right] \cos\phi + \left[-\frac{i\omega_3}{9} \frac{P_2^1(\mu)P_2^1(\nu)}{(1-\mu^2)} + \frac{i\omega_3}{9} \frac{P_2^1(\mu)P_2^1(\nu)}{(1-\nu^2)} \right] \sin\phi \right\} \tag{21}$$

The imaginary number i arises in the coefficients of the terms involving Legendre functions of odd order because we have chosen to define these functions by

$$P_n^m(z) = (1 - z^2)^{m/2} \frac{d^m P_n}{dz^m} \tag{22}$$

Since the variable μ assumes values from one to infinity along the real axis, the odd order functions $P_n^1(\mu)$ are purely imaginary.

The flow field far from the particle is re-expressed in the prolate spheroidal system by first transforming from the fixed Cartesian coordinate system, $u_3 = x_2$, into the system $(x_i^\ddagger)$ aligned with the particle, using

$$u_j^\ddagger = \sum_i \ell_{i2}\ell_{j3}x_i^\ddagger = \sum_i d_{ij}x_i^\ddagger \tag{23}$$

The matrix d_{ij} is a function of the orientation θ_1, ϕ_1 of the particle,

$$d_{ij} = \begin{bmatrix} a_o & ia_4 & -ia_3 \\ ia_4 & a_1-a_o & -a_6 \\ i(a_2-a_3) & a_5-a_6 & -a_1 \end{bmatrix} \tag{24}$$

with

$$\begin{aligned} a_o &= \sin^2\theta_1 \sin\phi_1 \cos\phi_1 \\ a_1 &= \sin\phi_1 \cos\phi_1 \\ a_2 &= -i\sin\theta_1 \\ a_3 &= -i\sin\theta_1 \sin^2\phi_1 \\ a_4 &= -i\sin\theta_1 \cos\theta_1 \sin\phi_1 \cos\phi_1 \\ a_5 &= \cos\theta_1 \\ a_6 &= \cos\theta_1 \sin^2\phi_1 \end{aligned} \tag{25}$$

Using (23), the far-field condition, $u_3 = x_2$, may be expressed in terms of the prolate spheroidal coordinate system as

$$\begin{aligned} u_{\xi_\infty} = \frac{C}{(\mu^2-\nu^2)^{1/2}(\mu^2-1)^{1/2}} \Bigg\{ & \frac{2}{5} a_o P_3(\mu)P_2(\nu) - \frac{2}{5} a_o P_1(\mu)P_2(\nu) \\ & + \left[\frac{4a_4}{45} P_3^1(\mu)P_2^1(\nu) - \frac{a_4}{5} P_1^1(\mu)P_2^1(\nu) \right] \cos\phi \\ & + \left[\frac{2}{45}(a_2-2a_3) P_3^1(\mu)P_2^1(\nu) + \frac{(a_2+3a_3)}{15} P_1^1(\mu)P_2^1(\nu) \right] \sin\phi \\ & + \frac{a_o}{90} P_3^2(\mu)P_2^2(\nu) \cos 2\phi + \frac{(2a_6-a_5)}{90} P_3^2(\mu)P_2^2(\nu) \sin 2\phi \Bigg\} \end{aligned}$$

$$U_{\mu_\infty} = \frac{C}{(\mu^2-\nu^2)^{1/2}(1-\nu^2)^{1/2}} \left\{ \frac{2}{5} a_o P_2(\mu)P_3(\nu) - \frac{2}{5} a_o P_2(\mu)P_1(\nu) \right.$$

$$+\left[\frac{4a_4}{45}P_2^1(\mu)P_3^1(\nu) - \frac{a_4}{5}P_2^1(\mu)P_1^1(\nu)\right]\cos\phi \qquad (26)$$

$$+\left[\frac{2}{45}(a_2-2a_3)P_2^1(\mu)P_3^1(\nu) + \frac{(a_2+3a_3)}{15}P_2^1(\mu)P_1^1(\nu)\right]\sin\phi$$

$$+\frac{a_o}{90}P_2^2(\mu)P_3^2(\nu)\cos2\phi + \frac{(2a_6-a_5)}{90}P_2^2(\mu)P_3^2(\nu)\sin2\phi\Bigg\}$$

$$u_{\phi_\infty} = \frac{c(\mu^2-1)^{1/2}(1-\nu^2)^{1/2}}{(\mu^2-\nu^2)}\Bigg\{\frac{a_5}{3}P_2(\mu)P_o(\nu) - \frac{a_5}{3}P_o(\mu)P_2(\nu)$$

$$+\left[\frac{(a_3-a_2)}{9}\frac{P_2^1(\mu)P_2^1(\nu)}{(1-\mu^2)} - \frac{(a_3-a_2)P_2^1(\mu)P_2^1(\nu)}{9\quad(1-\nu^2)}\right]\cos\phi$$

$$+\left[\frac{a_4}{9}\frac{P_2^1(\mu)P_2^1(\nu)}{(1-\mu^2)} - \frac{a_4}{9}\frac{P_2^1(\mu)P_2^1(\nu)}{(1-\nu^2)}\right]\sin\phi$$

$$+\left[\frac{(a_5-2a_6)}{18}\frac{P_2^2(\mu)P_2^2(\nu)}{(1-\mu^2)} - \frac{(a_5-2a_6)}{18}\frac{P_2^2(\mu)P_2^2(\nu)}{(1-\nu^2)}\right]\cos2\phi$$

$$+\left[\frac{(a_o-2a_1)}{18}\frac{P_2^2(\mu)P_2^2(\nu)}{(1-\mu^2)} - \frac{(a_o-2a_1)}{18}\frac{P_2^2(\mu)P_2^2(\nu)}{(1-\nu^2)}\right]\sin2\phi\Bigg\} \quad .$$

From the expressions (21) and (26), plus the general solution forms (16) and (19), it follows that

$$\Sigma\phi_n = c^2\sum_{n=2}^{\infty}G_{no}Q_n(\mu)P_n(\nu) + c^2\sum_{n=2}^{\infty}G_{n1}Q_n^1(\mu)P_n^1(\nu)\cos\phi$$

$$+ c^2\sum_{n=2}^{\infty}H_{n1}Q_n^1(\mu)P_n^1(\nu)\sin\phi + c^2\sum_{n=2}^{\infty}G_{n2}Q_n^2(\mu)P_n^2(\nu)\cos2\phi$$

$$+ c^2 \sum_{n=2}^{\infty} H_{n2} Q_n^2(\mu) P_n^2(\nu) \sin 2\phi$$

$$\Sigma\chi_n = c \sum_{n=3}^{\infty} C_{no} Q_n(\mu) P_n(\nu) + c \sum_{n=1}^{\infty} C_{n1} Q_n^1(\mu) P_n^1(\nu) \cos\phi$$

$$+ c \sum_{n=1}^{\infty} D_{n1} A_n^1(\mu) P_n^1(\nu) \sin\phi + c \sum_{n=3}^{\infty} C_{n2} Q_n^2(\mu) P_n^2(\nu) \cos 2\phi$$

$$+ c \sum_{n=3}^{\infty} D_{n2} Q_n^2(\mu) P_n^2(\nu) \sin 2\phi \qquad (27)$$

$$\Sigma R_n = \sum_{n=4}^{\infty} K_{no} Q_n(\mu) P_n(\nu) + \sum_{n=4}^{\infty} K_{n1} Q_n^1(\mu) P_n^1(\nu) \cos\phi$$

$$+ \sum_{n=4}^{\infty} L_{n1} Q_n^1(\mu) P_n^1(\nu) \sin\phi + \sum_{n=4}^{\infty} K_{n1} Q_n^1(\mu) P_n^1(\nu) \cos\phi$$

$$+ \sum_{n=4}^{\infty} L_{n2} Q_n^2(\mu) P_n^2(\nu) \sin 2\phi$$

$$\Sigma S_n = \sum_{n=4}^{\infty} M_{no} Q_n(\mu) P_n(\nu) + \sum_{n=4}^{\infty} M_{n1} Q_n^1(\mu) P_n^1(\nu) \cos\phi$$

$$+ \sum_{n=4}^{\infty} N_{n1} Q_n^1(\mu) P_n^1(\nu) \sin\phi + \sum_{n=4}^{\infty} M_{n2} Q_n^2(\mu) P_n^2(\nu) \cos 2\phi$$

$$+ \sum_{n=4}^{\infty} N_{n2} Q_n^2(\mu) P_n^2(\nu) \sin 2\phi$$

It can be seen that when a particular summation begins with an even or odd number, such as n = 1 or n = 4, only even or odd degree functions are required in that expression. However, an infinite number of terms is still required in each summation to exactly describe the velocity fields for a general rotation $\vec{\omega}$ of the particle. Fortunately, as we shall

see, not all of the terms needed for the velocity field are required in the computation of the bulk heat flux via equation (6). The unknown constants, G_{no}, G_{n1} etc. are related via algebraic equations expressing the no slip condition on the boundary of the particle of which the following are typical;

$$\frac{6}{5} G_{20}\left[Q_3(\psi) - Q_1(\psi)\right] + \frac{80}{189} K_{40}\left[Q_5(\psi) - Q_3(\psi)\right] =$$

$$- \frac{2}{5} a_o\left[P_3(\psi) - P_1(\psi)\right] \frac{6}{5} G_{20}Q_2(\psi) + \frac{16}{21} K_{40}Q_4(\psi) =$$

$$- \frac{2}{5} a_o P_2(\psi) \qquad (28)$$

where

$$\psi \equiv \cosh\{\xi_o\} = \cosh\{\text{ctnh}^{-1}\Gamma_p\} = \Gamma_p/(\Gamma_p^2-1)^{1/2} \qquad (29)$$

is the value of μ at the surface of the particle. We therefore obtain values of the "constants" G_{20}, K_{40}, . . ., which may be expressed as a function of orientation, say a_o or rotation vector $\vec{\omega}$, multiplied by a function of shape of the particle only, for instance

$$K_{40} = a_o S_1 \qquad (30)$$

where a_o is defined by (25) and

$$S_1 = \frac{-5/6}{\left\{\frac{200}{189}Q_5(\psi)Q_2(\psi) - \frac{200}{189}Q_3(\psi)Q_2(\psi) - \frac{40}{21}Q_4(\psi)Q_3(\psi) + \frac{40}{21}Q_4(\psi)Q_1(\psi)\right\}}$$

We may, with increasing complexity, evaluate as many of the coefficients as are necessary. It will turn out, however,

that to evaluate the O(Pe) correction to the bulk heat flux we will require only

$$G_{20} = a_o S_1$$
$$K_{40} = a_o S_2$$
$$C_{30} = (a_3 - 2\omega_1) S_3$$
$$C_{11} = a_3 S_7 S_9 - i\omega_2 S_8 S_9 + a_2 S_{17} S_9$$
$$C_{31} = a_3 S_7 - i\omega_2 S_8 + a_2 S_{17}$$
$$D_{11} = a_4 S_7 S_9 - i\omega_3 S_8 S_9$$
$$D_{31} = a_4 S_7 - i\omega_3 S_8$$
$$G_{21} = a_4 S_{11} + i\omega_3 S_{12}$$
$$H_{21} = -a_3 S_{11} - i\omega_2 S_{12} + a_2 S_{18}$$
$$K_{41} = a_4 S_{14} + i\omega_3 S_{15}$$
$$L_{41} = -a_3 S_{14} - i\omega_3 S_{15}$$
$$G_{22} = a_o S_{24}$$
$$H_{22} = (2a_6 - a_5) S_{24}$$
$$K_{42} = a_o S_{23}$$
$$L_{42} = (2a_6 - a_5) S_{23}$$
$$C_{32} = 0$$
$$D_{32} = 0$$

The shape functions $S_1 - S_{24}$ were evaluated numerically. Exact expressions for these functions are available in McMillen (1976).

b) The microscale temperature field

Having calculated the components of the velocity field for an individual particle, we may now turn to the task of

calculating the corresponding temperature distributions for the particle immersed in simple shear flow, and subjected to a nondimensional linear temperature field $T^{(j)} = X_j$ $(j = 1,2)$, where we have nondimensionalized the temperature with respect to the characteristic temperature $\alpha_j \ell$. The disturbance temperature field will be a function of both position and time, resulting from the fact that the particle changes its orientation with time, and therefore "sees" a different boundary condition at infinity at different times. The microscale temperature problem is governed by the usual (non-dimensional) convective-diffusion equation of thermal energy both outside and inside the particle,

$$Pe_1\left(\frac{\partial T}{\partial t} + \vec{u}\cdot\nabla T\right) = \nabla^2 T \tag{31a}$$

$$Pe_2\left(\frac{\partial \bar{T}}{\partial t} + \vec{\bar{u}}\cdot\nabla \bar{T}\right) = \nabla^2 \bar{T} \tag{31b}$$

where the Peclet numbers, Pe_1 and Pe_2, for the suspending fluid and the suspended particle respectively, are defined by

$$Pe_1 \equiv \frac{\rho C_p \ell^2 \gamma}{k} \quad ; \qquad Pe_2 \equiv \frac{\rho \tau C_p \ell^2 \gamma}{mk} = \frac{\tau}{m} Pe_2$$

and are assumed small, but non-negligible.

The equations (31) describing the temperature field outside and inside the particle are solved subject to the boundary conditions

$$T = \bar{T} \quad \text{and} \quad \frac{\partial T}{\partial \xi} = m \frac{\partial \bar{T}}{\partial \xi} \quad \text{at} \quad \xi = \xi_o \tag{32}$$

and

$$T \Rightarrow T^j = x_j \quad \text{as} \quad \xi \to \infty \quad . \tag{33}$$

As usual in problems of this type, a uniformly valid solution for Pe << 1 can only be constructed via the technique of matched asymptotic expansions, with the equations in the fluid region far from the particle expressed in terms suitable to the fact that convective terms must be retained at large distances even in the limit Pe → 0. Since the techniques involved in the expansion procedure are standard, we shall concentrate primarily on those portions of the analysis and results that are pertinent to evaluating the bulk heat flux.

In the inner region, the temperature distributions are governed by (31a) and (31b) subject to the conditions (32), plus an appropriate matching condition at large μ with the solution in the outer region. We assume that in this inner region, the temperature field can be expanded in asymptotic expansions of the form

$$\begin{aligned} T &= f_o(Pe_1)T_o + f_1(Pe_1)T_1 + f_2(Pe_1)T_2 + \ldots \\ \bar{T} &= f_o(Pe_2)\bar{T}_o + f_1(Pe_2)\bar{T}_1 + f_2(Pe_2)\bar{T}_2 + \ldots \end{aligned} \tag{34}$$

where

$$\lim_{Pe_1 \to 0} \frac{f_{n+1}}{f_n} \to 0 \quad .$$

As usual, the precise form of the asymptotic gage functions

$f_n(Pe_1)$ is to be found in the course of the analysis.

In the outer region, the "radial" coordinate $\mu = \cosh\xi$, is re-scaled according to

$$\rho = \mu Pe^{1/2} = Pe^{1/2} \cosh\xi \tag{35a}$$

and the convective-diffusion equation is expressed as

$$\nabla_\rho^2 \hat{T} - \hat{X}_2 \frac{\partial \hat{T}}{\partial \hat{X}_3} - \frac{\partial \hat{T}}{t} \equiv 0(Pe_1) \tag{35b}$$

where $\hat{T}$ is utilized to denote the temperature function in this region. The symbol ∇_ρ^2 represents the usual Laplacian operator with ρ replacing μ. The Cartesian coordinates X_i are similarly stretched according to $\hat{X}_i = Pe_1^{1/2} X_i$. In terms of the (ρ, ν, ϕ) coordinates (35b) is written as

$$\nabla_\rho^2 \hat{T} - \Big\{a_o\nu^2 + 2ia_4\nu(1-\nu^2)^{1/2}\cos\phi + i(a_2 - 2a_3)\nu(1-\nu^2)^{1/2}\sin\phi$$

$$+ (a_5 - 2a_6)(1-\nu^2)\sin\phi\cos\phi + (a_1 - a_o)(1-\nu^2)\cos^2\phi$$

$$- a_1(1-\nu^2)\sin^2\phi\Big\}\rho\frac{\partial \hat{T}}{\partial \rho} + \Big\{a_o(\nu-\nu^3)$$

$$+ \Big[ia_4(1-\nu^2)^{3/2} - ia_4\nu^2(1-\nu^2)^{1/2}\Big]\cos\phi + \Big[-ia_3(1-\nu^2)^{3/2}$$

$$- i(a_2 - a_3)\nu^2(1-\nu^2)^{1/2}\Big]\sin\phi - (a_1 - a_o)(\nu-\nu^3)\cos^2\phi$$

$$+ a_1(\nu-\nu^3)\sin^2\phi - (a_5 - 2a_6)(\nu-\nu^3)\sin\phi\cos\phi\Big\}\frac{\partial \hat{T}}{\partial \nu}$$

$$+\left\{ia_4\frac{\nu}{(1-\nu^2)^{1/2}}\sin\phi + i(a_2-a_3)\frac{\nu}{(1-\nu^2)^{1/2}}\cos\phi + (a_o-2a_1)\sin\phi\cos\phi + a_6\sin^2\phi + (a_5-a_6)\cos^2\phi\right\}\frac{\partial\hat{T}}{\partial\phi} \tag{36}$$

$$+\frac{\partial\hat{T}}{\partial t} = O(Pe_1)\cdot\frac{\partial\hat{T}}{\partial\rho} + O(Pe_1)\cdot\frac{\partial\hat{T}}{\partial\nu} + O(Pe_1)\frac{\partial\hat{T}}{\partial\phi} + O(Pe_1^{3/2})$$

It may be noted, that to first order in Pe_1, the stretched μ coordinate appears to play the role of a radial coordinate in a spherical coordinate system ($\rho = r$, $\eta = \theta,\phi$). This is merely a reflection of the fact that in the outer region the particular geometry of the particle is lost, and the particle is merely viewed as a point singularity. The time derivative must be retained, however, since the outer boundary condition is a function of time when expressed in the instantaneous coordinate axes (ρ, η, ϕ).

As in the inner region, we assume an asymptotic expansion for $\hat{T}$ of the form

$$\hat{T} = F_o(Pe_1)\hat{T}_o + F_1(Pe_1)\hat{T}_1 + F_2(Pe_1)\hat{T}_2 + \ldots$$

with

$$\lim_{Pe_1 \to 0}\left\{\frac{F_{n+1}(Pe_1)}{F_n(Pe_1)}\right\} \to 0 \quad .$$

In this outer region, the solutions are to satisfy the condition that

$$\hat{T} \to Pe^{-1/2}\hat{X}_j \quad \text{as} \quad \rho \to \infty \tag{37a}$$

which may be expressed as

$$\hat{T} \to Pe^{-1/2} c\left\{ \ell_{1j}\rho\nu + \ell_{2j}\rho(1-\nu^2)^{1/2}\cos\phi + \ell_{3j}\rho(1-\nu^2)^{1/2}\sin\phi \right\}$$

$$+ O\left(\frac{Pe^{1/2}}{\rho}\right) \qquad \text{as} \quad \rho \to \infty \quad j = 1,2 \qquad (37b)$$

plus the matching condition,

$$\lim_{\rho \to o} \hat{T}(\rho,\nu,\phi,t) = \lim_{\mu \to \infty} T(\mu,\nu,\phi,t) \quad . \qquad (38)$$

As usual, the solution sequence alternates between approximations in the inner and outer regions, and begins with the observation that the condition (37) provides a uniformly valid first approximation to the temperature distribution throughout the outer region. Therefore

$$\hat{T}_o = \hat{X}_j \quad ; \quad F_o(Pe_1) = Pe_1^{-1/2} \qquad (39)$$

The first approximation in the inner region satisfies the pure conduction equations

$$\nabla^2 T_o = 0 \quad ; \quad \nabla^2 \bar{T}_o = 0 \quad . \qquad (40)$$

Obviously T_o and $\bar{T}_o$ are harmonic, and may be represented by expressions of the form of (20). The solution which satisfies the zero-order matching condition and the conditions (30) at the particle surface ($\mu_{surface} \equiv \psi = \cosh\xi_o$), is simply

$$T_o = A^T_{01}P_1(\mu)P_1(\nu) + A^T_{11}P^1_1(\mu)P^1_1(\nu)\cos + B^T_{11}P^1_1(\mu)P^1_1(\nu)\sin$$

(41a)

$$+ C^T_{01}Q_1(\mu)P_1(\nu) + C^T_{11}Q^1_1(\mu)P^1_1(\nu)\cos + D^T_{11}Q^1_1(\mu)P^1_1(\nu)\sin$$

$$\bar{T}_o = E^T_{01}P_1(\mu)P_1(\nu) + E^T_{11}P^1_1(\mu)P^1_1(\nu)\cos\phi + F^T_{11}P^1_1(\mu)P^1_1(\nu)\sin\phi$$

(41b)

where

$$C^T_{01} = \ell_{1j}\bar{C}^T_{01} = c\ell_{1j}\,\frac{(1-m)}{(m-A_1)}\,\frac{1}{(Q_o(\psi) - 1/\psi)}$$

$$C^T_{11} = -i\ell_{2j}\bar{C}^T_{11} = -ic\ell_{2j}\,\frac{(1-m)}{(m-A_2)}\,\frac{1}{(Q_o(\psi) - 1/\psi)}$$

$$D^T_{11} = -i\ell_{3j}\bar{C}^T_{11}$$

(41c)

$$A^T_{01} = c\ell_{1j}\,,\quad A^T_{11} = -ic\ell_{2j}\,,\quad B^T_{11} = -ic\ell_{3j}$$

$$E^T_{01} = \ell_{1j}\bar{E}^T_{01} = c\ell_{1j}\,\frac{(1-A_1)}{(m-A_1)}$$

$$E^T_{11} = -i\ell_{2j}\bar{E}^T_{11} = -ic\ell_{2j}\,\frac{(1-A_2)}{(m-A_2)}$$

$$F^T_{11} = -i\ell_{3j}\bar{E}^T_{11}$$

$$A_1 = \frac{\left\{Q_o(\psi) - \dfrac{\psi}{\psi^2-1}\right\}}{\left\{Q_o(\psi) - \dfrac{1}{\psi}\right\}};\quad \left\{|A_1| < 0\ ;\quad \lim_{\Gamma_p\to 1} A_1 \Rightarrow -2\ ;\right.$$

$$\left.\lim_{\Gamma_p\to\infty} A_1 \Rightarrow -\infty\right\}$$

$$A_2 = \frac{\left\{Q_o(\psi) - \frac{\psi^2-2}{\psi^3-4}\right\}}{\left\{Q_o(\psi) - \frac{\psi}{\psi^2-1}\right\}} \; ; \; \left\{|A_2| < 0 \; ; \quad \lim_{\Gamma_p \to 1} A_2 \Rightarrow -2; \right.$$

$$\left. \lim_{\Gamma_p \to 1} A_2 \Rightarrow -1 \right\}$$

The $Q_1(\mu)$ and $Q_1^1(\mu)$ terms in the solution (41), which occur solely due to the difference in the internal and external conductivities, give rise to terms that behave as $\frac{1}{\mu^2}$ as $\mu \to \infty$. They consequently give rise to a mismatch of $O(Pe_1)^{3/2}$ in the overlap region between the inner and outer solutions.

Before turning to the next outer solution we therefore consider the $O(Pe)$ inner solutions. Here $f_1(Pe_1) = Pe_1$, $f_1(Pe_2) = Pe_2$, and equations (31a) and (31b) become

$$\nabla^2 T_1 = \vec{u} \cdot \nabla T_o + \frac{\partial T_o}{\partial t} \tag{42}$$

$$\nabla^2 \bar{T}_1 = \vec{u} \cdot \nabla \bar{T}_o + \frac{\partial \bar{T}_o}{\partial t} \tag{43}$$

with boundary conditions at the particle surface,

$$T_1 = \frac{\tau}{m} \bar{T}_1 \; ; \quad \frac{\partial T_1}{\partial \xi} = \tau \frac{\partial \bar{T}_1}{\partial \xi} \qquad \text{at } \xi = \xi_o \; .$$

and the matching condition (38).

After considerable algebra, both equations (42) and (43) may be written in the form

$$\nabla^2 T_1 = \frac{1}{(\mu^2-\nu^2)} \left\{ \sum_{n=o}^{\infty} F_n^o(\mu) P_n(\nu) + \sum_{n=1}^{\infty} F_n^1(\mu) P_n^1(\nu) \cos\phi \right.$$

$$+ \sum_{n=1}^{\infty} G_n^1(\mu) P_n^1(\nu) \sin\phi + \sum_{n=2}^{\infty} F_n^2(\mu) P_n^2(\nu) \cos 2\phi$$

$$+ \sum_{n=2}^{\infty} G_n^2(\mu) P_n^2(\nu) \sin 2\phi + \sum_{n=3}^{\infty} F_n^3(\mu) P_n^3(\nu) \cos 3\phi$$

$$+ \sum_{n=3}^{\infty} G_n^3(\mu) P_n^3(\nu) \sin 3\phi \Bigg\} \qquad (44)$$

where $F_n^m(\mu)$ and $G_n^m(\mu)$ are known functions of μ, not necessarily associated Legendre function of degree n. The solution to these equations may then be represented as a combination of the general, homogeneous solution of the form of (20), plus a particular solution of (44) of the form

$$T_{particular} = \sum_{n=o}^{\infty} f_n^o(\mu) P_n(\nu) + \sum_{n=1}^{\infty} f_n^1(\mu) P_n^1(\nu) \cos\phi$$

$$+ \sum_{n=1}^{\infty} g_n^1(\mu) P_n^1(\nu) \sin\phi + \sum_{n=2}^{\infty} f_n^2(\mu) P_n^2(\nu) \cos 2\phi$$

$$+ \sum_{n=2}^{\infty} g_n^2(\mu) P_n^2(\nu) \sin 2\phi + \sum_{n=2}^{\infty} f_n^2(\mu) P_n^2(\nu) \cos 2\phi$$

$$+ \sum_{n=3}^{\infty} g_n^3(\mu) P_n^3(\nu) \sin 3\phi \quad . \qquad (45)$$

Here, the functions $f_n^m(\mu)$ and $g_n^m(\mu)$ are particular solutions of the inhomogeneous Legendre equation

$$\frac{d^2 f_n^m(\mu)}{d\mu^2} - \frac{2\mu}{(1-\mu^2)} \frac{df_n^m(\mu)}{d\mu} + \left\{ \frac{(n)(n+1)}{(1-\mu^2)} - \frac{m^2}{(1-\mu^2)^2} \right\} f_n^m(\mu)$$

$$= \frac{c^2 F_n^m(\mu)}{(1-\mu^2)} \qquad (46)$$

If the function $F_n^m(\mu)$ is an associated Legendre function $W_q^m(\mu)$ of either the first or second kind, where the degree q is <u>not</u> equal to the degree n of the term $P_n^m(\nu)$ for the (ν) dependence of the inhomogeneous term in the equation (44), then the particular solution to (39) is simply

$$f_n^m(\mu) = \frac{c^2 W_q^m(\mu)}{q(q+1) - n(n+1)} \qquad (q \neq n) \qquad (47)$$

If, however, the degrees are equal (q = n), or the function F_n^m is not expressable as an associated Legendre function of order m, then the solution must be constructed by the method of variation of parameters,

$$f_n^m(\mu) = c^2 P_n^m(\mu) \int^{\mu} \frac{Q_n^m(z) F_n^m(\mu)\, dz}{(1-z^2)\left[Q_n^m(z) \frac{dP_n^m(z)}{dz} - P_n^m(z) \frac{dQ_n^m(z)}{dz}\right]} \qquad (48)$$

$$+ c^2 Q_n^m(\mu) \int^{\mu} \frac{P_n^m(z) F_n^m(z)\, dz}{(1-z^2)\left[P_n^m(z) \frac{dQ_n^m(z)}{dz} - Q_n^m(z) \frac{dP_n^m(z)}{dz}\right]}$$

In either case, we may obtain explicit representations for the particular solutions $f_n^m(\mu)$ and $g_n^m(\mu)$. The appropriate solutions, taking into account the inner region-outer region matching, are

$$\bar{T}_1 = \sum_{n=o}^{\infty} \left[I_{0n}^T P_n(\mu) + \bar{f}_n(\mu)\right] P_n(\nu) + \sum_{n=1}^{\infty} \left[I_{1n}^T P_n^1(\mu)\right.$$

$$+ \bar{f}_n^1(\mu)\Big] P_n^1(\nu)\cos\phi + \sum_{n=1}^{\infty}\Big[J_{1n}^T P_n^1(\mu) + \bar{g}_n^1(\mu)\Big]P_n^1(\nu)\sin\phi$$

$$+ \sum_{n=2}^{\infty}\Big[I_{2n}^T P_n^2(\mu) + \bar{f}_n^2(\mu)\Big]P_n^2(\nu)\cos 2\phi + \sum_{n=2}^{\infty}\Big[J_{2n}^T P_n^2(\mu)$$

$$+ \bar{g}_n^2(\mu)\Big]P_n^2(\nu)\sin 2\phi + \sum_{n=3}^{\infty}\Big[I_{3n}^T P_n^3(\mu) + \bar{f}_n^3(\mu)\Big]P_n^3(\nu)\cos 3\phi$$

$$+ \sum_{n=3}^{\infty}\Big[J_{3n}^T P_n^3(\mu) + \bar{g}_n^3(\mu)\Big]P_n^3(\nu)\sin 3\phi \quad . \tag{49}$$

$$T_1 = \sum_{n=o}^{\infty}\Big[G_{0n}^T Q_n(\mu) + f_n(\mu)\ P_n(\nu) + \sum_{n=1}^{\infty}\Big[G_{1n}^T Q_n^1(\mu)$$

$$+ f_n^1(\mu)\Big]P_n^1(\nu)\cos\phi + \sum_{n=1}^{\infty}\Big[H_{1n}^T Q_n^1(\mu) + g_n^1(\mu)\Big]P_n^1(\nu)\sin\phi$$

$$+ \sum_{n=2}^{\infty} G_{2n}^T Q_n^2(\mu) + f_n^2(\mu)\Big]P_n^2(\nu)\cos 2\phi + \sum_{n=2}^{\infty}\Big[H_{2n}^T Q_n^2(\mu)$$

$$+ g_n^2(\mu)\Big]P_n^2(\nu)\sin 2\phi + \sum_{n=3}^{\infty}\Big[G_{3n}^T Q_n^3(\mu) + f_n^3(\mu)\Big]P_n^3(\nu)\cos 3\phi$$

$$+ \sum_{n=3}^{\infty}\Big[H_{3n}^T Q_n^3(\mu) + g_n^3(\mu)\Big]P_n^3(\nu)\sin 3\phi$$

The boundary conditions at the particle surface (32) are then satisfied if

$$G_{nm}^T = \Bigg\{\frac{\tau}{m}\bar{f}_n^m(\psi)\left[\frac{dP_n^m(\mu)}{d\mu}\right]_{\mu=\psi} - f_n^m(\psi)\left[\frac{dP_n^m(\mu)}{d\mu}\right]_{\mu=\psi} - \frac{\tau}{m}P_n^m(\psi)$$

$$\left[\frac{d\bar{f}_n^m(\mu)}{d\mu}\right]_{\mu=\psi} + \frac{1}{m}P_n^m(\psi)\left[\frac{df_n^m(\mu)}{d\mu}\right]_{\mu=\psi}\Bigg\} \Bigg/ \Bigg\{Q_n^m(\psi)\left[\frac{dP_n^m(\mu)}{d\mu}\right]_{\mu=\psi}$$

$$- \frac{1}{m} P_n^m(\psi) \left[\frac{dQ_n^m(\mu)}{d\mu}\right]_{\mu=\psi}$$

and

$$I_{mn}^T = \left\{ \frac{\tau}{m} \bar{f}_n^m(\psi) \left[\frac{dQ_n^m(\mu)}{d\mu}\right]_{\mu=\psi} - f_n^m(\psi) \left[\frac{dQ_n^m(\mu)}{d\mu}\right]_{\mu=\psi} - Q_n^m(\psi) \left[\frac{df_n^m(\mu)}{d\mu}\right]_{\mu=\psi} + Q_n^m(\psi) \left[\frac{df_n^m(\mu)}{d\mu}\right]_{\mu=\psi} \right\} \left\{ \tau \left\{ Q_n^m(\psi) \left[\frac{dP_n^m(\mu)}{d\mu}\right]_{\mu=\psi} - \frac{1}{m} P_n^m(\psi) \left[\frac{dQ_n^m(\mu)}{d\mu}\right]_{\mu=\psi} \right\} \right\}$$

with similar relations involving H_{mn}^T, J_{mn}^T, $g_n^m(\psi)$, and $\bar{g}_n^m(\psi)$.

The solution (49) in the fluid gives rise to terms that behave like a constant as $\mu \to \infty$. These terms arise from the particular solutions $f_n^m(\mu)$ and $g_n^m(\mu)$, (for example, $\lim_{\mu\to\infty} f_1^o(\mu) \to c^2/30 \left\{a_o C_{01}^T + 2a_4 C_{11}^T - 4a_2 D_{11}^T - 2a_3 D_{11}^T\right\} - 1/3\ A_{11}^T D_{11} + 1/3\ B_{11}^T C_{11}$) which give rise to a mismatch of $0(Pe_1^{3/2})$ in the overlap with the outer solution region. The mismatch with the zero order (T_o) solution was of this order also, causing $F_1(Pe_1) = Pe_1$. Contributions to the effective bulk heat flux from this outer solution will be of $0(Pe_1^{3/2})$ however, whereas the two inner solutions so far generated give rise to contributions of $0(Pe_1)$. Thus, we will not consider the next outer solution here. As in the case of the velocity description, it is evident that we again

require an infinite number of coefficients for an exact solution for T_1 and $\bar{T}_1$. However, only a finite number of the constants G^T_{nm}, H^T_{nm}, I^T_{nm}, and J^T_{nm}, and only a finite number of the particular functions $f^m_n(\mu)$, $g^m_n(\mu)$, $\bar{f}^m_n(\mu)$, and $\bar{g}^m_n(\mu)$, will be needed to obtain the bulk heat flux to $0(Pe_1)$.

IV. EVALUATION OF THE BULK HEAT FLUX

a) General considerations

The microscale velocity distributions and temperature distributions obtained in sections IIIa and IIIb are valid for any arbitrary orientation and rotation of the particle and may now be utilized in expression (6) to evaluate the bulk heat flux of the suspension, given the orientation distribution and rotation of the particles. Leal and Hinch (1971, 1972) have studied the steady state orientation distribution $P(\theta_1, \phi_1)$ in a suspension of spheroidal particles. As we have previously pointed out, in the absence of all but viscous forces the rotation of particles is periodic and described by the orbit equations of Jeffrey, equations (10). The action of rotary Brownian motion is a randomizing influence on the particle orientation, and the steady state distribution of orientation in the suspension represents a compromise between the hydrodynamic-induced distribution resulting from unopposed Jeffrey orbits and the uniform distribution resulting from unopposed Brownian rotation. The probability distribution function $P(\vec{\phi},t)$ is governed by a modified Fokker-Plank equation, and at steady state simply expresses the conservation of probability in the orientation space,

$$\nabla \cdot (\gamma \vec{\omega}_H F) = D_r \nabla^2 F \quad . \tag{50}$$

Here, D_r is the rotational Brownian diffusion coefficient

$$D_r = \frac{KT}{\frac{16}{3}\pi\mu a^* b^{*2}} \frac{(K_3\Gamma_p^2 + K_1)}{(\Gamma_p^2 + 1)} \quad , \tag{51}$$

K is Boltzmann's constant, K_3 and K_1 are shape functions defined by

$$K_3 = \int_o^\infty \frac{\Gamma_p d\lambda}{(\Gamma_p^2+\lambda)^{3/2}(1+\lambda)}$$

$$K_1 = \int_o^\infty \frac{\Gamma_p d\lambda}{(\Gamma_p^2+\lambda)^{3/2}(1+\lambda)}$$

and the rotation vector $\gamma\vec{\omega}_H$ describes the time rate of change of orientation due to the purely hydrodynamic motion about Jeffrey orbits. The vector operator ∇ is defined on the unit sphere-orientation space (θ_1, ϕ_1), and $P(\theta_1, \phi_1)$ is normalized by

$$\int_o^{2\pi}\int_o^{\pi} P(\theta_1,\phi_1)\sin\theta_1 \, d\theta_1 d\phi_1 = 1 \quad . \tag{52}$$

As Leal and Hinch show, the resulting probability function P depends essentially on two parameters--the particle aspect ratio Γ_p and the non-dimensional measure of shear strength γ/D_r. The results for the distribution function $P(\theta_1, \phi_1)$ may be obtained analytically in several limiting cases and are briefly reviewed here. In the limiting case of weak Brownian motion, $\gamma/D_r >> 1$, the particles are found to proceed nearly undisturbed around closed Jeffrey orbits. The first effect of the small Brownian rotations is to eliminate the

dependence of the relative population of different orbits on the initial orientation state of the suspension. A careful examination of the conditions under which the resulting expansion for the probability distribution function P is valid suggests the existence of an additional regime corresponding to intermediate shear rates for particles of extremely large aspect ratios, $\Gamma_p \to \infty$ (rod-like particles). This additional complexity will not be described here, the interested reader is referred to the original paper, Leal and Hinch (1972). For the case of strong rotational Brownian motion, $\gamma/D_r << 1$, the function P may be represented by a regular expansion in the small parameter γ/D_r, the first few terms of which are:

$$P(\theta_1,\phi_1) = \frac{1}{4\pi} + \left(\frac{\gamma}{D_r}\right)\frac{1}{16\pi}\left(\frac{\Gamma_p^2-1}{\Gamma_p^2+1}\right)\sin^2\theta\,\sin 2\phi$$

$$+ \left(\frac{\gamma}{D_r}\right)^2\left\{\left(\frac{\Gamma_p^2-1}{\Gamma_p^2+1}\right)^2\left[\frac{1}{256\pi}\cos^4\theta_1 - \frac{1}{128\pi}\cos^2\theta_1\right.\right.$$

$$\left. + \frac{7}{6720\pi} - \frac{1}{256\pi}\sin^4\theta_1\cos 4\phi_1\right]$$

$$\left. - \left(\frac{\Gamma_p^2-1}{\Gamma_p^2+1}\right)\frac{1}{96\pi}\sin^2\theta_1\cos 2\phi_1\right\} + O\left(\frac{\gamma}{D_r}\right)^3 \qquad (53)$$

For this limiting case, the distribution of orientation is significantly different from the purely hydrodynamic Jeffrey orbits, at first order being merely the purely random

orientation distribution resulting from unopposed rotary Brownian diffusion. The effective Brownian mean rotation $\vec{\omega}_{Br}$ resulting from this distribution, from which the mean velocities $\bar{\vec{v}}$ and $\bar{\vec{v}}_p$ will result, is therefore of comparable order of magnitude to the hydrodynamically induced rotations, and is found from (7) to be

$$\omega_{2Br} = \frac{(\Gamma_p^2-1)}{(\Gamma_p^2+1)} \frac{\sin\theta_1}{2} \cos 2\phi_1 + 0\left(\frac{\gamma}{D}\right)$$
$$\omega_{3Br} = -\frac{(\Gamma_p^2-1)}{(\Gamma_p^2+1)} \frac{\sin\theta_1\cos\theta_1}{2} \sin 2\phi_1 + 0\left(\frac{\gamma}{D}\right) \quad . \tag{54}$$

The mean velocity fields, $\overline{\vec{U} + \vec{v}}$ and $\overline{\vec{U}_p + \vec{v}_p}$, are linear in the particle rotation rate, $\vec{\omega} \equiv \vec{\omega}_{Br} + \vec{\omega}_H$, as is evident from the governing equations and boundary conditions (13) and (14). Furthermore, the temperature field is also linear in $\vec{\omega}$ to 0(Pe), since T_o and T_{p_o} are independent of $\vec{\omega}$, and T_1 and T_{p_1} depend linearly on $\vec{\omega}$ through the differential equations (42) and (43). Finally, the bulk heat flux expression (6) is linear in $\vec{\omega}$ to 0(Pe), since it depends linearly on T_{p_1} and $(\bar{\vec{u}} + \bar{\vec{v}} - \vec{u}_\infty)(T - T_\infty)$, $(\bar{\vec{U}}_p + \bar{\vec{v}}_p - \vec{u}_\infty)$ $(T_p - T_\infty)$. It therefore follows that we may either substitute the total expression for $\vec{\omega}$

$$\vec{\omega} = \vec{\omega}_{Br} + \vec{\omega}_H$$

into the boundary condition (14) at the particle surface, and calculate the microscale temperature distributions and

the bulk heat flux directly for the full velocity fields $\bar{\vec{U}} + \vec{v}$, $\bar{\vec{U}} + \vec{v}_p$, or conversely, obtain separately the contributions to the bulk heat flux arising from the purely hydrodynamic motions and the contributions arising from the Brownian induced motions; with the total bulk heat flux being merely the sum. For present purposes we follow the latter course, since the separation more clearly identifies the role of the two types of motion in the final result.

We proceed then as follows. Having obtained the microscale velocity fields $\vec{u}$ and $\bar{\vec{u}}$ outside and inside the particle for arbitrary orientation and rotation of the particle, we formally split the velocity distributions into two parts,

$$\vec{u}(\vec{\omega},\theta_1,\phi_1) = \vec{u}_H(\vec{\omega}_H,\theta_1,\phi_1) + \vec{u}_{Br}(\vec{\omega}_{Br},\theta_1,\phi_1)$$

$$\bar{\vec{u}}_p(\vec{\omega},\theta_1,\phi_1) = \bar{\vec{u}}_{H_p}(\vec{\omega}_H,\theta_1,\phi_1) + \bar{\vec{u}}_{Br_p}(\vec{\omega}_{Br},\theta_1,\phi_1)$$

The microscale temperature fields to 0(Pe), may then also be written as a sum of the form

$$T = T_o(\theta_1,\phi_1) + Pe_f T_{1,H}(\vec{\omega}_H,\theta_1,\phi_1) + Pe_f T_{1,Br}(\vec{\omega}_{Br},\theta_1,\phi_1)$$

$$\bar{T} = \bar{T}_o(\theta_1,\phi_1) + Pe_p \bar{T}_{1,H}(\vec{\omega}_H,\theta_1,\phi_1) + Pe_p \bar{T}_{1,Br}(\vec{\omega}_{Br},\theta_1,\phi_1) \quad .$$

Since the order one temperature distributions, T_o and $\bar{T}_o$, are independent of $\vec{\omega}$, splitting only occurs at 0(Pe). The individual fields $T_{1,H}$, $\bar{T}_{1,H}$, $T_{1,Br}$, $\bar{T}_{1,Br}$ may be evaluated directly from the general solutions (49), by specifying $\vec{\omega}$ as either $\vec{\omega}_{Br}$ or $\vec{\omega}_H$. Since $\vec{\omega}_{Br}$ and $\vec{\omega}_H$ are known to depend on

orientation (cf. equations (10) and (54)), the individual temperature and velocity fields can be completely expressed as functions of spatial position, with the instantaneous orientation (θ_1,ϕ_1) as a parameter. The long-time or ensemble average result for the bulk heat flux may thus be calculated in two steps. First, the orientation dependent temperature and velocity fields are used to calculate the necessary volume integrals of (5), thus producing an instantaneous expression for Q_i as a function of the instantaneous particle orientation, plus the physical properties of the two phases, and the axis ratio Γ_p of the particles. Second, the relevant macroscopic heat flux is determined by averaging the orientation dependent result, $Q_i(\theta_1,\phi_1)$, over all possible orientations with the steady-state orientation distribution function as a weighting factor.

Following this plan, the orientation dependent results for an undisturbed temperature field, $T_\infty^{(j)} = \alpha_j x_j$, satisfying (9) with $(u_i)_\infty = \gamma x_2 \delta_{i3}$ may be expressed in the form

$$Q_{i,hyd}^{(j)*}(\theta_1,\phi_1) = -\alpha_j k\phi \left\{ \frac{(m-1)}{\frac{4}{3}\pi} \int_o^{2\pi}\int_o^{\pi} \left[\frac{\bar{n}_i \bar{T}_o^{(j)}}{h_\mu h_\phi} \right]_{\xi=\xi_o} d\eta d\phi \right.$$

$$+ Pe_f \left[\frac{(m-1)\tau}{\frac{4}{3}\pi m} \int_o^{2\pi}\int_o^{\pi} \left[\frac{\bar{n}_i \bar{T}_{1,hyd}^{(j)}}{h_\mu h_\phi} \right]_{\xi=\xi_o} d\eta d\phi \right.$$

$$\left. - \frac{1}{\frac{4}{3}\pi} \int_o^{2\pi}\int_o^{\pi}\int_{\xi_o}^{\infty} \frac{u'_{i,hyd} T_o^{(j)'}}{h_\xi h_\mu h_\phi} d\xi d\eta d\phi \right.$$

$$- \frac{\tau}{\frac{4}{3}\pi}\int_o^{2\pi}\int_o^{\pi}\int_o^{\xi_o} \frac{\bar{u}'_{i,hyd}\bar{T}_o^{(j)'}}{h_\xi h_\mu h_\phi} d\xi d_\mu d\phi \Bigg\} + O(Pe_f^{3/2}) \Bigg\}$$

$$+ O(\phi^2) + \ldots \qquad (55)$$

$$Q_{i,Br}^{(j)*}(\theta_1,\phi_1) = -\alpha_j k\phi Pe_f \left\{ \frac{(m-1)\tau}{\frac{4}{3}\pi m} \int_o^{2\pi}\int_o^{\pi} \left| \frac{n_i \bar{T}_{1,Br}^{(j)}}{h_\mu h_\phi} \right|_{\xi=\xi_o} d\eta d\phi \right.$$

$$- \frac{1}{\frac{4}{3}\pi} \int_o^{2\pi}\int_o^{\pi}\int_{\xi_o}^{\infty} \frac{u_{i,Br}T_o^{(j)'}}{h_\xi h_\mu h_\phi} d\xi d\eta d\phi - \frac{\tau}{\frac{4}{3}\pi} \int_o^{2\pi}\int_o^{\pi}\int_o^{\xi_o}$$

$$\left. \frac{\bar{u}_{iBr}\bar{T}_o^{(j)'}}{h_\xi h_\mu h_\phi} d\xi d\eta d\phi \right\} + O(Pe_f^{3/2}) + O(\phi^2) + \ldots \qquad (56)$$

The particle contribution to the bulk conductive heat flux at any arbitrary orientation is then $Q_{itotal}^{(j)*}(\theta_1,\phi_1) = Q_{ihyd}^{(j)*}(\theta_1,\phi_1) + Q_{iBr}^{(j)*}(\theta_1,\phi_1)$ and the total orientation-dependent bulk conductive flux corresponding to this is simply

$$Q_i^{(j)}(\theta_1,\phi_1) = -k\alpha_j + \phi\left\{Q_i^{(j)o}(\theta_1,\phi_1) + PeQ_i^{(j)1}(\theta_1,\phi_1) \right.$$

$$\left. + O(Pe_f^{3/2}) \right\} + O(\phi^2) \quad . \qquad (57)$$

Here, the superscript o, 1, etc., identifies the order of Peclet number multiplying the specific term in the expansion For example, $Q_i^{(j)o}(\theta_1,\phi_1)$ is the purely conductive contribution to the orientation-dependent bulk heat flux Q_i resulting from a constant temperature gradient in the j

direction. The macroscopically significant bulk conductive heat flux for the suspension is then calculated by integrating (57) over the probability distribution function for orientation, $P(\theta_1,\phi_1)$,

$$Q_i^{(j)} \equiv \int_o^{2\pi}\int_o^{\pi} Q_i^{(j)}(\theta_1,\phi_1)P(\theta_1,\phi_1)\sin\theta_1\partial\theta_1\partial\phi_1 \qquad (58)$$

As noted earlier, we restrict our attention to the limit of strong rotational Brownian motion where the distribution function takes the form (53). A convenient form for the resulting bulk heat flux expression is thus

$$\langle Q_i^{(j)}\rangle = -k\alpha_j\delta_{ij} + \Phi\Big\{\langle Q_i^{(j)o}\rangle_o + \left[\frac{\gamma}{D_r}\right]\langle Q_i^{(j)o}\rangle_1 + \left[\frac{\gamma}{D_r}\right]^2\langle Q_i^{(j)o}\rangle_2$$

$$+ \ldots + \mathrm{Pe}\langle Q_i^{(j)1}\rangle_o + \mathrm{Pe}\left[\frac{\gamma}{D_r}\right]\langle Q_i^{(j)1}\rangle_1 + \ldots\Big\}$$

$$+ O(\Phi^2) + \ldots \qquad (59)$$

The brackets are used to indicate that the result has been averaged with respect to the orientation distribution of the suspension, and the subscripts 0,1,2,... identify the particular order of the parameter (γ/D_r) multiplying each term.

Although a sheared suspension does not have a complete effective conductivity tensor K_{ij} describing its constitutive behavior, as we have already noted, the restriction to temperature gradients α_1 and α_2, orthogonal to the bulk flow direction assures that the resulting fluxes $Q_i^{(j)}$ will be

linearly related to the strength of the gradient. Thus, for this limited set of problems, it is convenient to represent the results in terms of the specific effective thermal conductivity components (non-dimensionalized with respect to the fluid conductivity)

$$K_{ij} \equiv - \frac{Q_i^{(j)*}}{k\alpha_j} \quad . \tag{60}$$

These effective conductivities will be expressed in the same notation used for the general expansion of $Q_i^{(j)}$. Having explained the notation utilized to express the results, we may now proceed to the calculation.

b) The pure conduction contribution to the bulk conductivity.

We turn first to the pure conduction contribution $Q_i^{(j)o}$. This term has considerable significance in its own right, since it is the bulk heat flux of a stationary suspension of the particles. For the case of a stationary suspension we may exactly relate the proportionality relation (60) with the complete effective thermal conductivity tensor for the suspension expressed as

$$K_{ij} = k(\delta_{ij} + \phi K_{ij}^{o}) \quad .$$

The orientation specific results in this case are calculated from

$$K_{ij}^{o}(\theta_1, \phi_1) = \frac{(m-1)}{\frac{4}{3}\pi} \int_o^{2\pi} \int_o^{\pi} \left[\frac{n_i T_o^{(j)}}{h_\mu h_\phi} \right]_{\xi=\xi_o} d\eta d\phi \quad .$$

We express the variables (ξ,μ) in terms of (μ,ν) and utilize the results

$$\left[\frac{n_i}{h_\mu h_\phi}\right]_{\mu=\psi} = c^2(1-\nu^2)^{1/2}\left\{\ell_{1i}(\psi^2-1)P_1(\nu) + \ell_{2i}\psi(\psi^2-1)^{1/2}\right.$$

$$\left. P_1'(\nu)\cos\phi + \ell_{3i}\psi(\psi^2-1)^{1/2} P_1'(\nu)\sin\phi\right\} \qquad (61)$$

and

$$\left[T_o^{(j)}\right]_{\mu=\psi} = c\left\{\ell_{1j}\frac{(1-A_1)}{(m-A_1)}\psi P_1(\nu) + \ell_{2j}\frac{(1-A_2)}{(m-A_2)}(\psi^2-1)^{1/2}\right.$$

$$\left. P_1'(\nu)\cos\phi + \ell_{3j}\frac{(1-A_2)}{(m-A_2)}(\psi^2-1)^{1/2} P_1'(\nu)\sin\phi\right\} \qquad (62)$$

plus the identity

$$c^3(\psi^3 - \psi) \equiv 1$$

to obtain

$$K_{ij}^o(\theta_1,\phi_1) = (m-1)\left\{\ell_{1i}\ell_{1j}\frac{(1-A_1)}{(m-A_1)} + [\ell_{2i}\ell_{2j} + \ell_{3i}\ell_{3j}]\frac{(1-A_2)}{(m-A_2)}\right\} \qquad (63)$$

The matrix ℓ_{ij} was defined previously (equation 11), and the products $\ell_{ni}\ell_{nj}$ contain all the orientation dependence of K_{ij}. The expressions $(1-A_1)/(m-A_1)$ and $(1-A_2)/(m-A_2)$ arise from the equivalence of microscale temperature and normal heat flux at the particle surface and contain only information regarding the shape of the particle and its conductivity, these being the only relevant physical properties in the pure conduction limit. Formulae for the

specific components of K^{o}_{ij} may be obtained from (63) by simply substituting from (11) for the orientation tensor ℓ_{ij}, and the results are listed in Table 1.

Examination of these results shows that the orientation-dependent effective conductivity tensor in a stationary suspension is symmetric, but that the particle contribution can be anisotropic. We may also note that the formula (63) properly reduces, in the degenerate case of a spherical particle, to the scalar effective conductivity given by Maxwell. This is easily seen, since $\Gamma_p = 1$ for a sphere, and

$$\lim_{\Gamma_p \to 1} A_1 = \lim_{\Gamma_p \to 1} A_2 = -2 \; ; \quad \frac{1-A_1}{m-A_1} = \frac{1-A_2}{m-A_2} = \frac{3}{m+2} \quad ,$$

so that the off-diagonal and anisotropic terms identically vanish, leaving

$$K_{ii} = K = k\left[1 + \frac{3(m-1)}{(m+2)}\,\Phi + O(\Phi^2)\right] \quad ; \quad \forall\,(\theta_1, \phi_1) \qquad (64)$$

It is clear from this, that the anisotropy and the existence of the off-diagonal terms in the orientation-dependent effective conductivity for arbitrary particles, $\Gamma_p > 1$, is a reflection of their non-spherical geometry. Particles with a higher thermal conductivity than that of the suspending fluid ($m > 1$) will enhance the conductive transport of heat on the microscale, the enhancement being greatest parallel to the (longer) major axis of the particle. Suspensions of particles which have the elongated axis preferentially

aligned in one direction will therefore show a larger enhancement of the conductivity in that preferential direction, than in orthogonal directions corresponding to the minor axes. For particles with a smaller thermal conductivity than that of the suspending fluid, the converse will obviously be true. The off-diagonal terms exist when a particle has its principal axes aligned in some direction other than strictly perpendicular or parallel to the undisturbed temperature gradient. In that case, conduction of heat along the particle's major axis, due to the temperature difference of the two ends, will produce an effective flux of heat in the direction orthogonal to the gradient.

In order to transform the orientation-dependent effective conductivities to averaged values relevant to the suspension as a whole, we must integrate the formulae of Table 1 over all possible orientations, using the orientation distribution (53) as a weighting factor. Since $\alpha_3 = 0$ in general with flow (cf. equation (9)), we restrict our attention here to the orientation averaged bulk conductive heat flux corresponding to gradients α_1 and α_2. The results of this averaging process are most conveniently presented in the form

$$\langle K^o_{11} \rangle = \langle K^o_{11} \rangle_o + \left(\frac{\gamma}{D}\right)^2 \langle K^o_{11} \rangle_2 + 0\left(\frac{\gamma}{D}\right)^4$$

$$\langle K^o_{22} \rangle = \langle K^o_{22} \rangle_o + \left(\frac{\gamma}{D}\right)^2 \langle K^o_{22} \rangle_2 + 0\left(\frac{\gamma}{D}\right)^4$$

$$\langle K^o_{21}\rangle = \langle K^o_{12}\rangle = 0\left(\frac{\gamma}{D}\right)^3 \quad ; \quad \langle K^o_{31}\rangle = 0\left(\frac{\gamma}{D}\right)^3$$

$$\langle K^o_{32}\rangle = \left(\frac{\gamma}{D}\right)\langle K^o_{32}\rangle_1 + 0\left(\frac{\gamma}{D}\right)^3$$

We note, that the only contributions at $0(1)$ in γ/D are the diagonal components $\langle K^o_{11}\rangle_o$ and $\langle K^o_{22}\rangle_o$. These are altered at $0(\gamma/D)^2$ by the nonuniform orientation distribution which exists in the presence of flow. In addition, there is a flow-induced contribution to K^o_{32} at $0(\gamma/D)$. The remaining terms and corrections are $0(\gamma/D)^3$ or smaller.

The terms $\langle K^o_{11}\rangle_o$ and $\langle K^o_{22}\rangle_o$ represent the scalar contribution to the effective conductivity of a stationary suspension of randomly oriented particles, and are equal

$$\langle K^o_{11}\rangle_o = \langle K^o_{22}\rangle_o = \frac{(m-1)}{3}\left[\frac{(1-A_1)}{(m-A_1)} + \frac{2(1-A_2)}{(m-A_2)}\right] \qquad (65)$$

The right hand side of (65) is plotted in Figure 4 as a function of the particle axis ratio for various values of the conductivity ratio m. When the conductivity of the particle is much smaller than that of the suspending fluid, the particle contribution to the thermal conductivity of the suspension is seen to be slightly negative (i.e., the overall conductivity is decreased by the presence of the particles) and relatively insensitive to the axis ratio. On the other hand, as the particle conductivity is sufficiently increased, the particle contribution is positive and strongly dependent on the axis ratio, though still

approaching a bounded asymptotic limit as $\Gamma_p \to \infty$ for any fixed $m < \infty$, namely

$$\lim_{\Gamma_p \to \infty} \langle K_{11}^o \rangle_o = \frac{(m-1)(m+5)}{3(m+1)} \quad ; \forall\ m < \infty \quad .$$

When the conductivity ratio m is allowed to increase without bound, for any finite axis ratio, $\Gamma_p < \infty$, an asymptotic limit is reached, denoted by curve (g), which is the line

$$\lim_{m \to \infty} \langle K_{11}^o \rangle_o = \frac{3-A_1-2A_2}{3} \quad ; \quad \forall\ \Gamma_p < \infty \quad .$$

Finally, we may note that $\langle K_{11}^o \rangle_o$ increases without bound when both m and Γ_p are allowed to increase indefinitely, reflecting the unphysical situation of infinitely long, perfectly conductive rods which would transfer an infinite amount of heat for any nonzero gradient. The general result of increasing effective conductivity, with increasing length to width ratio and conductivity of the particles is essentially a reflection of the tendency to this limit.

Let us now turn to a consideration of the simplest effect of flow on the thermal conductivity of a dilute suspension; namely, the changes induced in the pure conduction results due to the presence of a nonuniform distribution of orientations for particles of arbitrary axis ratio, $\Gamma_p > 1$. First, we consider the $0(\gamma/D)^2$ corrections to $\langle K_{11}^o \rangle$ and $\langle K_{22}^o \rangle$ which are given by

$$\langle K^{o}_{11}\rangle_2 = \left(\frac{\Gamma_p^2-1}{\Gamma_p^2+1}\right)^2 \frac{(m-1)}{630}\left[\frac{(1-A_2)}{(m-A_2)} - \frac{(1-A_1)}{(m-A_1)}\right] \tag{66}$$

$$\langle K^{o}_{22}\rangle_2 = \left\{\left(\frac{\Gamma_p^2-1}{\Gamma_p^2+1}\right)\frac{(m-1)}{180} - \left(\frac{\Gamma_p^2-1}{\Gamma_p^2+1}\right)^2 \frac{(m-1)}{1260}\right\}\left[\frac{(1-A_2)}{(m-A_2)} - \frac{(1-A_1)}{(m-A_1)}\right] \tag{67}$$

The expressions are plotted in Figures (5) and (6), again as a function of Γ_p for several values of m. The main features of interest are: first, that the $0(\gamma/D)^2$ corrections are strictly negative, and second, that the decrease in heat transfer across the plane of the bulk flow (i.e., the x_2 direction) is always larger than that in the direction of the undisturbed vorticity (x_1). The first of these facts is easily explained, once it is realized that the effect of flow is to change the random orientation distribution, which results in isotropic behavior of the suspension, to one exhibiting a slight preferential alignment of the major axis of the particle in the direction of the undisturbed bulk flow. The second, simply reflects the nonuniformity, with respect to the 1 and 2 directions, of this alignment process.

Finally, we consider the orientation-induced, off-diagonal contribution, $\langle K^{o}_{32}\rangle$, which reflects heat transfer in the flow direction due to a temperature gradient across

the flow in the presence of a particle alignment of the particles with long axis parallel to the undisturbed flow. This contribution is found to be

$$\langle K_{32}^{o} \rangle_1 = \frac{(\Gamma_p^2-1)}{(\Gamma_p^2+1)} \frac{(m-1)}{30} \left[\frac{1-A_1}{m-A_1} - \frac{1-A_2}{m-A_2} \right] \tag{68}$$

and is presented in Figure (7). The contribution is seen to always be positive, and of increasing dependence on the axis ratio for increasing particle conductivity, as expected on qualitative grounds.

c) The direct flow contribution to the bulk conductivity

Finally, we may now turn to the main results of the present investigation, namely the $0(Pe)$ flow contributions to the bulk conductive heat flux Q_i. We begin with the effective conductivity for arbitrary orientation (θ_1,ϕ_1) and arbitrary rotation $\vec{\omega}$ of the particle. The general result

$$K_{ij}^1 = F_{ij}(\vec{\omega},\theta_1,\phi_1,\tau,m,\Gamma_p)$$

is of the form

$$K_{ij}^1 = \sum_{n=1}^{15} C_n(\tau,m,\Gamma_p)\psi_n^{ij}(\Gamma_p,\vec{\omega},\theta_1,\phi_1)$$

$$= \frac{\tau}{m}\left\{ \frac{(m-1)}{(m-A_1)}\psi_1^{ij} + \frac{(m-1)}{(m-A_2)}\psi_2^{ij} + \frac{(m-1)}{(m-A_1)^2}\psi_3^{ij} \right.$$

$$\left. + \frac{(m-1)}{(m-A_1)(m-A_2)}\psi_4^{ij} + \frac{(m-1)}{(m-A_2)^2}\psi_5^{ij} \right\} + \tau\left\{ \frac{(m-1)}{(m-A_1)}\psi_6^{ij} \right.$$

$$+ \frac{(m-1)}{(m-A_2)} \psi_7^{ij} + \frac{(m-1)}{(m-A_1)^2} \psi_8^{ij} + \frac{(m-1)}{(m-A_1)(m-A_2)} \psi_9^{ij}$$

$$+ \frac{(m-1)}{(m-A_2)^2} \psi_{10}^{ij} \Bigg\} + \Bigg\{ \frac{(m-1)}{(m-A_1)} \psi_{11}^{ij} + \frac{(m-1)}{(m-A_2)} \psi_{12}^{ij}$$

$$+ \frac{(m-1)^2}{(m-A_1)^2} \psi_{13}^{ij} + \frac{(m-1)^2}{(m-A_1)(m-A_2)} \psi_{14}^{ij} + \frac{(m-1)^2}{(m-A_2)^2} \psi_{15}^{ij} \Bigg\} \qquad (69)$$

The fifteen material coefficients, $C_n = \frac{\tau}{m} \frac{(m-1)}{(m-A_1)}$, ..., $\frac{(m-1)^2}{(m-A_2)^2}$, depend on the thermal properties of the particles, and also on the particle shape through the two shape functions A_1 and A_2, which were defined in (41c). We note that the 0(Pe) contribution identically vanishes whenever the particle conductivity is equal to the conductivity of the suspending fluid. The 0(Pe) contribution is hence dependent on the difference in thermal properties of the continuous and dispersed phases, in conjunction with the local convective action of the fluid motion. The remaining fifteen functions ψ_n^{ij} $(\Gamma_p, \vec{\omega}, \theta_1, \phi_1)$ depend on particle shape, instantaneous orientation, and linearly on the instantaneous rate of rotation, $\vec{\omega}$.

We may first consider the case of a suspension of spheroids with no Brownian motion, by substituting the Jeffrey expressions for the particle rotation $\vec{\omega}_H(\theta_1, \phi_1)$ into (69). The result is orientation specific expressions for the components K_{ij}. In this case, each of the functions

ψ_n^{ij} $(\Gamma_p, \vec{\omega}, \theta_1, \phi_1)$ may be resolved into expressions of the form

$$\psi_n^{ij} = \sum_m f_{nm}^{ij} (\Gamma_p) \chi_{nm}^{ij} (\theta_1, \phi_1) \qquad (70)$$

in which all of the dependence on particle shape is continned in the functions f_{nm}^{ij} (Γ_p), and all of the orientation dependence in χ_{nm}^{ij} (θ_1, ϕ_1). The functions f_{nm}^{ij} are complicated, and will not be presented here in explicit form. The interested reader may refer to McMillen (1976) for details. The orientation functions are of direct interest and are reasonably simple. They are listed in Table 2 for K_{11}, K_{22}, $K_{12} = K_{21}$, K_{31} and K_{32}. Significantly, the number which are nonzero for each K_{ij} is small, reaching a maximum of seven for K_{32}. In the absence of Brownian rotation, the orientation distribution is simply the distribution around each Jeffrey orbit as determined by the rate of rotation at each point on the orbit, coupled with the distribution of various orbits as determined by the initial orientations of the particles. It is therefore of considerable interest to note that all of the 0(Pe) contributions to K_{ij} vanish identically when averaged around any orbit $(0 \leq \rho \leq \infty)$, except K_{32}^1. Thus, with this one exception, contributions to the bulk conductive heat flux (and particularly all components orthogonal to the flow) will only be nonzero in the presence of Brownian rotation, or deterministic couples which act to move the orientation distribution away from that due

to hydrodynamic rotation.

One case which can be examined readily (and which may also be of practical interest in the context of ferro-fluid technology) is that in which an external couple is applied to the particle, causing it to remain permanently aligned in some specified direction. In this case $(\omega_H)_2 = (\omega_H)_3 = 0$, and the general expression (69) simplifies both because ψ_1^{ij}, $\psi_3{}^{ij}$, ψ_4^{ij}, ψ_8^{ij} and ψ_9^{ij} are identically zero, and because the remaining ψ_n^{ij} are reduced somewhat in complexity. This is reflected in simpler forms for the shape functions $f_{nm}^{ij}(\Gamma_p)$ in (70). The orientation functions χ_{nm}^{ij} are the same as those listed in Table 2. From the forms of these orientation functions, we may immediately note certain specific orientations of the particles for which the 0(Pe) contributions to K_{ij} vanish identically. Thus for example, it may be seen from the forms of χ_{nm}^{11} that K_{11}^1 is zero if $\theta_1 = 0$ or $\phi_1 = 0, \frac{\pi}{2}$. This corresponds to situations in which the particle major axis lies completely in the (x_1x_3) plane or the (x_1x_2) plane. Similarly the 0(Pe) contribution to K_{22} identically vanishes when $\phi = 0, \frac{\pi}{2}$, corresponding also to alignment in the (x_1x_2) and (x_1x_3) planes. The K_{21}^1 and K_{12}^1 0(Pe) contributions are found to vanish when $\phi = 0$, $\theta = 0, \pm \frac{\pi}{2}$, corresponding to alignment in any of the planes (x_1x_2), (x_1x_3) and (x_2x_3). Similarly the K_{31}^1 0(Pe) contribution vanishes when $\phi = \frac{\pi}{2}$; $\theta = 0, \pm \frac{\pi}{2}$, corresponding to alignment in the planes (x_1x_3) and (x_2x_3). The K_{32}^1

contribution at this order does not vanish in general for any arbitrary orientations.

Finally, we may now turn to the evaluation of the 0(Pe) contribution to the bulk conductive heat flux (or K^1_{ij}) in the presence of simple shear and Brownian rotation. As noted earlier, the calculation of K^1_{ij} proceeds in two stages from the general result (69). First, the deterministic hydrodynamic contribution is calculated by substituting $\vec{\omega}_H(\theta_1,\phi_1)$ from Jeffrey (1923) into (69) to give (70), and then averaging (70) with the orientation distribution function (62) as weighting factor. Second, the contribution due to <u>mean</u> Brownian rotation is calculated using the same procedure but with $\vec{\omega}_{Br}(\theta_1,\phi_1)$ from (7) replacing $\vec{\omega}_H$. For strong Brownian motion ($D/\gamma >> 1$), the effective or mean Brownian rotation of the particle is of the same order of magnitude as the hydrodynamic rotations. Furthermore, the rotations give rise to the same orientation functions χ^{ij}_{nm} as were found previously (Table 2) for purely hydrodynamic rotation, this fortunate coincidence being due to the exact nature of the Brownian rotations. The composite expression for $\langle K^1_{ij}\rangle$, including both the deterministic and mean Brownian rotation contributions may then be written in the form

$$\langle K^1_{11}\rangle = \left(\frac{\gamma}{D}\right)\langle K^1_{11}\rangle_1 + 0\left(\frac{\gamma}{D}\right)^3$$

$$\langle K^1_{22}\rangle = \left(\frac{\gamma}{D}\right)\langle K^1_{22}\rangle_1 + 0\left(\frac{\gamma}{D}\right)^3$$

$$\langle K_{21}^1 \rangle \; ; \quad \langle K_{12}^1 \rangle = 0\left(\frac{\gamma}{D}\right)^3$$

$$\langle K_{31}^1 \rangle = 0\left(\frac{\gamma}{D}\right)^3$$

$$\langle K_{32}^1 \rangle = \langle K_{32}^1 \rangle_o + 0\left(\frac{\gamma}{D}\right)^2$$

Corresponding to (59), the full expression for those components of the particle contribution to the bulk effective conductivity which exist (i.e., excludes $\langle K_{33} \rangle$, $\langle K_{23} \rangle$ and $\langle K_{13} \rangle$) is then

$$\langle K_{ij} \rangle = \langle K_{ij}^o \rangle_o + \left(\frac{\gamma}{D}\right) \langle K_{ij}^o \rangle_1 + \left(\frac{\gamma}{D}\right)^2 \langle K_{ij}^o \rangle_2 + \ldots$$
$$+ Pe \langle K_{ij}^1 \rangle_o + Pe\left(\frac{\gamma}{D}\right) \langle K_{ij}^1 \rangle_1 + \ldots \qquad (71)$$

For a purely random distribution of orientations the 0(Pe) contributions to the bulk heat flux vanish, just as they did upon integration around any arbitrary Jeffrey orbit, except for the contribution $\langle K_{32}^1 \rangle$. Upon allowing for inhomogeneities in the orientation distribution due to the alignment of particles due to the flow, contributions to the bulk heat flux in directions orthogonal to the flow direction also arise. Each of the three nonzero contributions up to $0\left(\frac{\gamma}{D}\right)$, i.e. $\langle K_{11}^1 \rangle_1$, $\langle K_{22}^1 \rangle_1$, and $\langle K_{32}^1 \rangle_o$ are of the form

$$\langle K_{ij}^1 \rangle_q \quad \sum_{n=1}^{15} C_n(\tau, m, \Gamma_p) \langle \psi_n^{ij} \rangle_q$$

The $\langle \psi_n^{ij} \rangle_q$ functions are now strictly functions of particle shape only, having been integrated over the distribution

function, and shall be designated by α_{nm}^{ij} for the purely hydrodynamic contributions and β_{nm}^{ij} for the contributions arising from the effective Brownian rotations. To evaluate the contributions for specific particle axis ratio requires numerical evaluation of the various shape factors α_{nm}^{ij} and β_{nm}^{ij}, which are quite complicated functions of the particle axis ratio, Γ_p. The functional dependence on shape is contained in the expressions by means of the shape factors $S_o - S_{24}$ arising from the velocity fields, similar shape factors $B_o - B_{24}$ arising from the solution of the $0(Pe)$ temperature fields, plus additional shape factors coming from the volume integration inside and outside of the particle. In each of these functions, the Γ_p dependence is contained in terms of associated Legendre functions of both kinds evaluated at $\mu = \psi$ (c.f. Eq. (30)). As can readily be seen from (29), $\psi \to \infty$ as $\Gamma_p \to 1$. Since the associated Legendre functions of the first kind have the property $\lim_{\psi \to \infty} P_n^m(\psi) \sim \psi^m$, this causes considerable numerical problems in the evaluation of the various shape functions α_{nm}^{ij} and β_{nm}^{ij} for particles which are nearly spherical. It was, in fact necessary to evaluate a number of the functions by means of series representations in $1/\psi$ to obtain values near the spherical case. The numerical programs used to evaluate the shape factors are presented in McMillen's (1976) thesis from which the complicated expressions for the individual factors may be extracted. Let us now consider

the qualitative behavior of the 0(Pe) contributions to $\langle K_{ij} \rangle$.

Turning first to the component of the bulk heat flux orthogonal to the plane of the shear flow, the total $0\left(\frac{\gamma}{D} \text{Pe}\right)$ contribution $\langle K^1_{11} \rangle_1$ is presented in Figure (8) as a function of the particle axis aspect ratio Γ_p, for several values of the conductivity ratio m, when $\tau = 1$. The contribution is practically independent of τ, as long as τ is 0(1), as can be seen from Figure (9), so that the values plotted are essentially valid for any heat capacity ratio of 0(1). Further, as long as the ratio of conductivities m, is not very small compared to 1, the purely hydrodynamic contribution dominates the effective Brownian rotation contribution in all cases so that the total contribution is effectively equivalent to the hydrodynamic contribution. We see that the contribution vanishes for a sphere, and is small when the particle is nearly spherical either positive or negative depending on the exact value of Γ_p and m. As the particles become more elongated, the magnitude of the contribution increases, being negative for particles whose conductivity than the fluid. In the asymptotic limit $m \to \infty$ in which the particles are "perfect" conductors compared to the fluid, the 0(Pe) resulting contribution to $\langle K_{11} \rangle$ is finite for particles of finite aspect ratio, but increases rapidly as the particles become more highly elongated. This contribution for "perfect" conductors eventually becomes infinitely huge in the limit of infinitely long, slender

particles ($\Gamma_p \to \infty$) in a manner reminiscent of the purely conductive contributions. In the case where the conductivity of the particle is infinitesimally small compared to that of the fluid, (i.e., $m \to 0$, 'perfectly insulating particles'), some care must be taken in interpreting the results. In particular, the form of the first five material coefficients, $C_n^{ij} \sim \frac{\tau}{m}$, would seem to imply that the contribution becomes of infinite magnitude as $m \to 0$. In this case, the limit $m \to 0$ must be taken with $Pe_p << 1$ and <u>fixed</u>, in order that both Pe_f and Pe_p remain small since $Pe_p = \frac{\tau}{m} Pe_p$. Thus while the contribution $\langle K_{11}^1 \rangle_1$ becomes infinitely negative as $m \to 0$, the actual effective conductivity contribution is finite when expressed in terms of Pe_p, and in fact is a function only of particle shape

$$\langle K_{11}' \rangle_1 \to f(\Gamma_p) \quad , \quad \text{as } m \to 0.$$

This result is plotted in Figure (10) for the separate contributions resulting from the purely hydrodynamic contribution, the Brownian contribution, and the resulting total contribution. We see in this case that the Brownian and hydrodynamic contributions are of the same order of magnitude, and that the total result is actually more strongly influenced by the Brownian contribution. The contribution further changes rapidly for nearly spherical particles, approaching the asymptotic result for very elongated particles by $\Gamma_p \sim 5$.

The behavior of the contribution $\langle K_{22}^1 \rangle_1$ to the effective bulk conductivity, for heat flux to the transverse to the flow in the direction of the velocity gradient is seen in Figure (11) to be somewhat more complex. Here again the contribution is only weakly dependent on τ for $\tau \sim 0(1)$ so that only representative values for $\tau = 1$ have been presented. In this case the contribution again vanishes for spheres, and is always small for nearly spherical particles. However, as the particles become increasingly elongated, the contribution is dominated by the Brownian contribution, the purely hydrodynamic contribution being negligible in comparison, and the contribution is seen to be mainly positive for any conductivity ratio $m > 0$, approaching the asymptotic limit plotted for $m \to \infty$. The magnitude of this contribution is always larger than the corresponding $\langle K_{11}^1 \rangle_1$ term, indicating preferential enhancement of heat flux in this direction. Figure (12) shows the effective independence of the contribution on the value of τ. As the conductivity ratio becomes sufficiently small, the $0(Pe)$ contribution to $\langle K_{22} \rangle$ eventually becomes negative and in the limit $m \to 0$ must also be expressed in terms of Pe_p. Figure (13) presents the limiting behavior in this case. We note that the contribution is of smaller magnitude than that found for $\langle K_{11}^1 \rangle_1$, and that in this case the dominant term is due to the purely hydrodynamic contributions, in opposition to the previous results for $\langle K_{11}^1 \rangle_1$.

We finally consider the $\langle K_{32}^1 \rangle_o$ contributions which are presented in Figure (14), for $\tau = 1$. We first note that the contribution is always dominated by the pure hydrodynamic contribution and, becomes small for spherical particles, but non-zero. Although Leal did not explicitly consider this contribution to the bulk heat flux in his work on spherical drops, the result is easily extracted from his results for the velocity and temperature fields, and is found to be

$$\langle K_{32}^1 \rangle_{o(\text{sphere})} = -.1 \frac{\tau}{m} \frac{(m-1)}{(m+2)} + .3\tau \frac{(m-1)}{(m+2)^2} - .5 \frac{(m-1)^2}{(m+2)^2} .$$

The behavior of this contribution, even in the spherical limit, is fairly complicated. The contribution vanishes when $m = 1$, and $m = (.5 + .2\tau) \pm (.25 + .2\tau - .36\tau^2)^{1/2}$. As long as $\tau < 1.16$, these zeros will be real and the contribution will change sign three times. Allowing for elongation of the spheroid further complicates the result, as is seen in the Figure (14). For $m < 1$, the contribution is always positive, and increases in magnitude with increasing Γ_p. For $m > 1$ the contribution is negative, and similarly of increasing magnitude with increasing Γ_p. As m increases, however, the contribution for nearly spherical particles first is negative of increasing magnitude, but as the particle becomes longer the contribution becomes smaller than that for smaller m, Γ_p being fixed. For $m >> 1$, and fixed, the contribution initially is negative, but rapidly goes through a local minimum and becomes positive for $\Gamma_p > 15$,

then increasing in magnitude rapidly with increasing Γ_p. The asymptotic limit as $m \to \infty$ is plotted in Figure (15) for three different values of τ, showing the fairly weak dependence of the result on the exact value of the heat capacity ratio. Finally Figure (16) illustrates the purely-hydrodynamic contribution as $m \to 0$, when expressed in terms of Pe_p. The <u>total</u> contribution in this case is completely dominated by the purely hydrodynamic contribution which we have plotted, and is independent of the ratio τ. The contribution is initially positive for spheres, but rapidly decreases in magnitude as the particle becomes elongated, and is negative for $\Gamma_p > 4$ and rapidly approaching the asymptotic value of $-.008$ for $\Gamma_p >> 1$.

The results obtained here clearly indicate the complex nature of the thermal constitutive behavior of the flowing suspension. The heat transfer behavior is seen to not only depend critically on the thermal properties of the continuous and dispersed phases, but on the flow strength and type as well as the magnitude of other forces involved in the microstructural configuration of the suspension. Although the mathematical difficulties of the analysis have restricted us to the cases of small effects, the complexity of the results in even these limiting situations should serve as an indication of the wide variety of thermal constitutive behavior that real fluids might be expected to exhibit.

TABLE 1

The orientation specific effective conductivity for a dilute stationary suspension.

$$K_{11} = k\left\{1 + (m-1)\Phi\left[\frac{(1-A_1)}{(m-A_1)} + \left\{\frac{(1-A_2)}{(m-A_2)} - \frac{(1-A_1)}{(m-A_1)}\right\}\sin^2\right]1\right\}$$

$$K_{22} = k\ 1 + (m-1)\Phi\left[\frac{(1-A_2)}{(m-A_2)} + \left\{\frac{(1-A_1)}{(m-A_1)} - \frac{(1-A_2)}{(m-A_2)}\right\}\frac{\sin^2\theta_1}{2}\right.$$

$$\left.\left\{\frac{(1-A_1)}{(m-A_1)} - \frac{(1-A_2)}{(m-A_2)}\right\}\frac{\sin^2\theta}{2}\cos 2\phi_1\right]\Bigg\}$$

$$K_{33} = k\left\{1 + (m-1)\Phi\left[\frac{(1-A_2)}{(m-A_2)} + \left\{\frac{(1-A_1)}{(m-A_1)} - \frac{(1-A_2)}{(m-A_2)}\right\}\frac{\sin^2\theta_1}{2}\right.\right.$$

$$\left.\left.- \left\{\frac{(1-A_1)}{(m-A_1)} - \frac{(1-A_2)}{(m-A_2)}\right\}\frac{\sin^2\theta}{2}\cos 2\phi_1\right]\right\}$$

$$K_{12} = K_{21} = k(m-1)\Phi\left\{\frac{(1-A_1)}{(m-A_1)} - \frac{(1-A_2)}{(m-A_2)}\right\}\sin\theta_1\cos\theta_1\cos\phi_1$$

$$K_{13} = K_{31} = k(m-1)\Phi\left\{\frac{(1-A_1)}{(m-A_1)} - \frac{(1-A_2)}{(m-A_2)}\right\}\sin\theta_1\cos\theta_1\sin\phi_1$$

$$K_{23} = K_{32} = k(m-1)\Phi\left\{\frac{(1-A_1)}{(m-A_1)} - \frac{(1-A_2)}{(m-A_2)}\right\}\frac{\sin^2\theta_1}{2}\sin 2\phi_1$$

TABLE 2

The orientation functions $\chi_{nm}^{ij}(\theta_1,\phi_1)$ for purely hydrodynamic rotation of the particles

	K_{11}	K_{22}	K_{21} & K_{12}	K_{31}	K_{32}
χ_{n1}^{ij}	$\sin^4\theta_1\sin2\phi_1$	$\sin^4\theta_1\sin4\phi_1$	$\sin^3\theta_1\cos\theta_1\sin3\phi_1$	$\sin^3\theta_1\cos\theta_1\cos3\phi_1$	$\sin^4\theta_1\cos4\phi_1$
χ_{n2}^{ij}	$\sin^2\theta_1\sin2\phi_1$	$\sin^2\theta_1\sin4\phi_1$	$\sin\theta_1\cos\theta_1\sin3\phi_1$	$\sin\theta_1\cos\theta_1\cos3\phi_1$	$\sin^2\theta_1\cos4\phi_1$
χ_{n3}^{ij}		$\sin4\phi_1$	$\sin^3\theta_1\cos\theta_1\sin\phi_1$	$\sin^3\theta_1\cos\theta_1\cos\phi_1$	$\cos^4\phi$;
χ_{n4}^{ij}		$\sin^4\theta_1\sin2\phi_1$	$\sin\theta_1\cos\theta_1\sin\phi_1$	$\sin\theta_1\cos\theta_1\cos\phi_1$	$\sin^2\theta_1\cos2\phi_1$
χ_{n5}^{ij}		$\sin^2\theta_1\sin2\phi_1$			$\sin^4\theta_1$
χ_{n6}^{ij}		$\sin2\phi_1$			$\sin^2\theta_1$
χ_{n7}^{ij}					1

REFERENCES

Abramowitz, M. and Segon, I. 1968. Handbook of Mathematical Functions, 5th ed. New York: Dover Publications.

Happel, J. and Brenner, H. 1965. Low Reynolds Number Hydrodynamics. Englewood Cliffs: Prentice-Hall, Inc.

Hinch, E. J. and Leal, L. G. 1972. Journal of Fluid Mech. 52, pp. 683-712.

Jeffrey, D. J. 1974. Proc. Roy. Soc. Lond. A338, pp. 503-516.

Jeffery, G. B. 1922, Proc. Roy. Soc. Lond. A102, pp. 161-179.

Lamb, H. 1932. Hydrodynamics, 6th ed. Cambridge: Cambridge Univ. Press.

Leal, L. G. 1973. Chemical Engineering Communications 1, pp. 21-31.

Leal, L. G. 1976. Journal Colloid Interface Sci. (to appear); also, Proc. of the International Conference on Colloids and Surfaces, San Jaun, Puerto Rico, June 1976.

Leal, L. G. and Hinch, E. J. 1971. Journal of Fluid Mech. 46, pp. 685-703.

Maxwell, J. C. 1873. Electricity and Magnetism, 1st ed., p. 365. Oxford: Clarendon Press.

McMillen, T. J. 1976 Ph.D. Thesis, California Institute of Technology, Pasadena, California.

McMillen, T. J. and Leal, L. G. 1975. Int. Journal of Multiphase Flow 2, pp. 105-112.

McMillen, T. J. and Leal, 1976. Archives of Mechanics/ Archiwum Mechaniki Stosowenej, No. 3.

Nir, A. and Acrivos, A. 1976. Journal Of Fluid Mech. (to appear).

FIGURE CAPTIONS

Figure 1: The Orientation Angles θ_1 and ϕ_1 for the Rigid Prolate Spheroid.

Figure 2: The Jeffery Orbits Corresponding to Different Values of the Orbit Constant, C.

Figure 3: The Prolate Spheroidal Coordinate System.

Figure 4: The Purely Conductive, Random Orientation Contributions $(K_{11}^0)_0$ and $(K_{22}^0)_0$ as a Function of the Particle Aspect Ratio for Various Values of the Conductivity Ratio, $m = k_2/k_1$. a) $m = 0$; b) $m = .5$; c) $m = 1$; d) $m = 2$; e) $m = 10$; f) $m = 100$; g) $m \to \infty$.

Figure 5: The Purely Conductive, Flow-Induced Orientation Contribution $(K_{11}^0)_2$ as a Function of the Particle Aspect Ratio for Various Values of the Conductivity Ratio, $m = k_2/k_1$. a) $m = 0$; b) $m = .5$; c) $m = 1$; d) $m = 2$; e) $m = 10$; f) $m = 100$; g) $m \to \infty$.

Figure 6: The Purely Conductive, Flow-Induced Orientation Contribution $(K_{22}^0)_2$ as a Function of the Particle

Aspect Ratio for Various Values of the Conductivity Ratio, $m = k_2/k_1$. a) $m = 0$; b) $m = .5$; c) $m = 1$; d) $m = 2$; e) $m = 10$; f) $m = 100$; g) $m \Rightarrow \infty$.

Figure 7: The Purely Conductive, Flow-Induced Orientation Contribution $(K_{32}^{0})_1$ as a Function of the Particle Aspect Ratio for Various Values of the Conductivity Ratio, $m = k_2/k_1$. a) $m = 0$; b) $m = .5$; c) $m = 1$; d) $m = 2$; e) $m = 10$; f) $m = 100$; g) $m \Rightarrow \infty$.

Figure 8: The Total O(Pe) Convective Contribution $(K_{11}^{1})_1$ as a Function of the Particle Aspect Ratio for Various Values of the Conductivity Ratio, $m = k_2/k_1$, when $\mathcal{T} = 1$. a) $m = .1$; b) $m = .5$; c) $m = 1$; d) $m = 2$; e) $m = 10$; f) $m = 100$; g) $m \Rightarrow \infty$.

Figure 9: The Total O(Pe) Convective Contribution $(K_{11}^{1})_1$ as a Function of the Particle Aspect Ratio for Various Values of the Heat Capacity Ratio, $\mathcal{T} = .5, 1, 2$, when $m = 2$.

Figure 10: The $O(Pe_p)$ Convective Contribution $(K_{11}^{1})_1$ as a Function of the Particle Aspect Ratio when $m = 0$, $\mathcal{T} = O(1)$. a) Purely Hydrodynamic Contribution

b) "Direct" Brownian Motion Contribution; c) Total Contribution.

Figure 11: The Total O(Pe) Convective Contribution $(K_{22}^{1})_1$ as a Function of the Particle Aspect Ratio for Various Values of the Conductivity Ratio, $m = k_2/k_1$, when $\tau = 1$. a) $m = .1$; b) $m = .5$; c) $m = 1$; d) $m = 2$; e) $m = 10$; f) $m = 100$; g) $m \Rightarrow \infty$.

Figure 12: The Total O(Pe) Convective Contribution $(K_{22}^{1})_1$ as a Function of the Particle Aspect Ratio for Various Values of the Heat Capacity Ratio, $\tau = .5, 1, 2$, when $m = 2$.

Figure 13: The $O(Pe_p)$ Convective Contribution $(K_{22}^{1})_1$ as a Function of the Particle Aspect Ratio when $m = 0$, $\tau = O(1)$. a) Purely Hydrodynamic Contribution; b) "Direct" Brownian Motion Contribution; c) Total Contribution.

Figure 14: The Total O(Pe) Convective Contribution $(K_{32}^{1})_0$ as a Function of the Particle Aspect Ratio for Various Values of the Conductivity Ratio, $m = k_2/k_1$, when $\tau = 1$. a) $m = .1$; b) $m = .5$; c) $m = 1$; d) $m = 2$; e) $m = 10$; f) $m = 100$; g) $m \Rightarrow \infty$.

Figure 15: The Total O(Pe) Convective Contribution $(K_{32}^{1})_0$ as a Function of the Particle Aspect Ratio for Various Values of the Heat Capacity Ratio, γ= .5, 1, 2, when m = 2.

Figure 16: The Total $O(Pe_p)$ Convective Contribution $(K_{32}^{1})_0$ as a Function of tht Particle Aspect Ratio when m = 0.

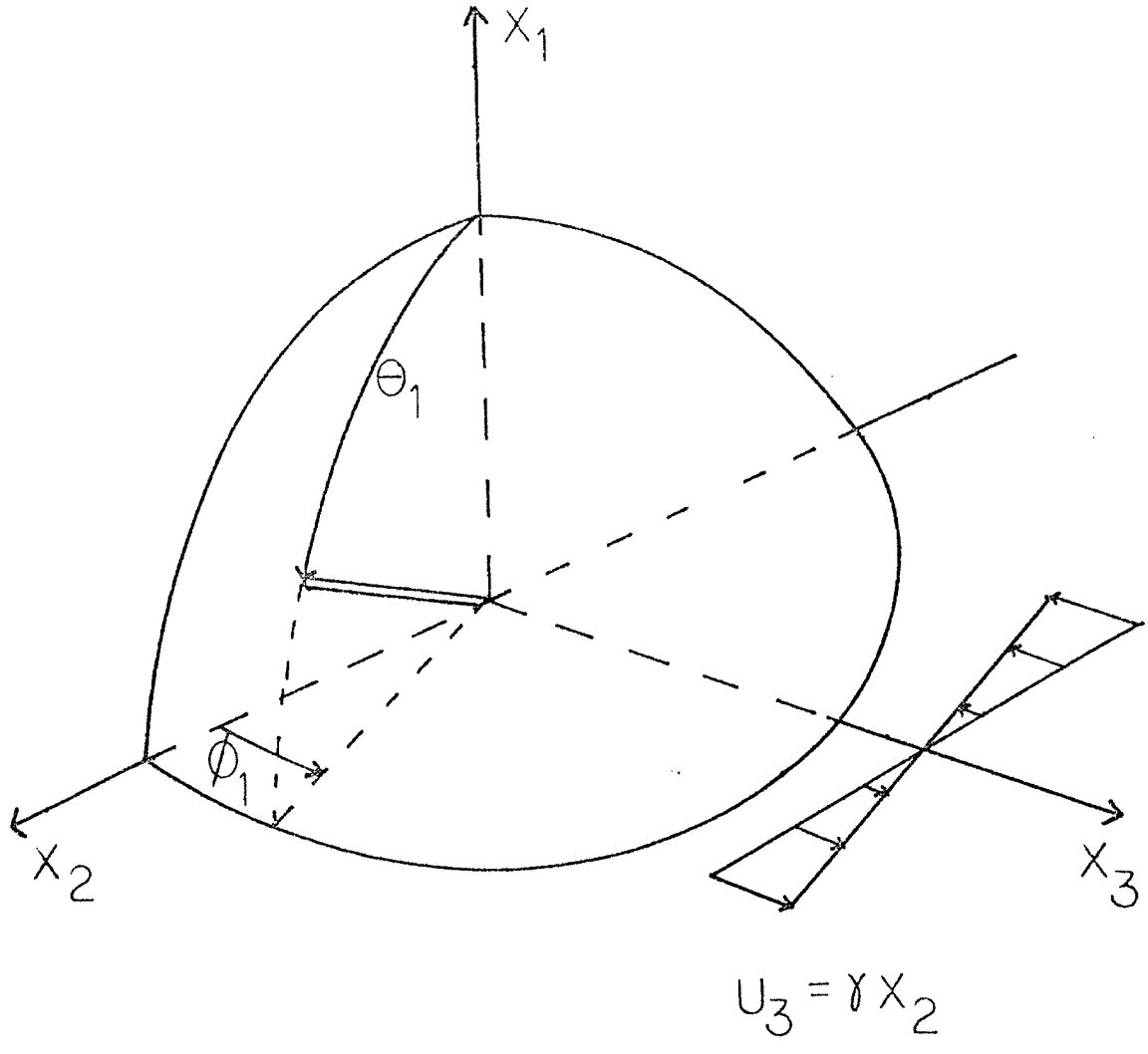

Figure 1: The Orientation Angles θ_1 and ϕ_1

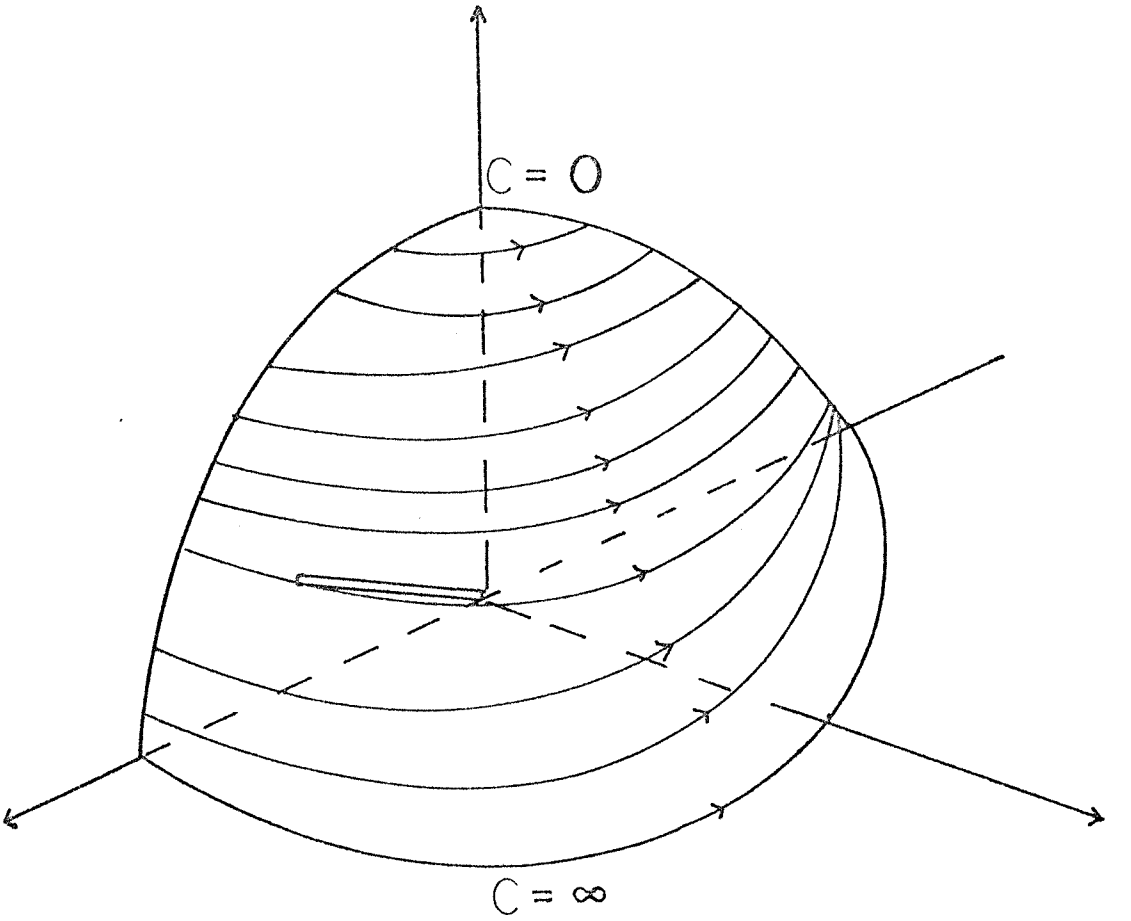

Figure 2: The Jeffery Orbits Corresponding to Different Values of the Orbit Constant

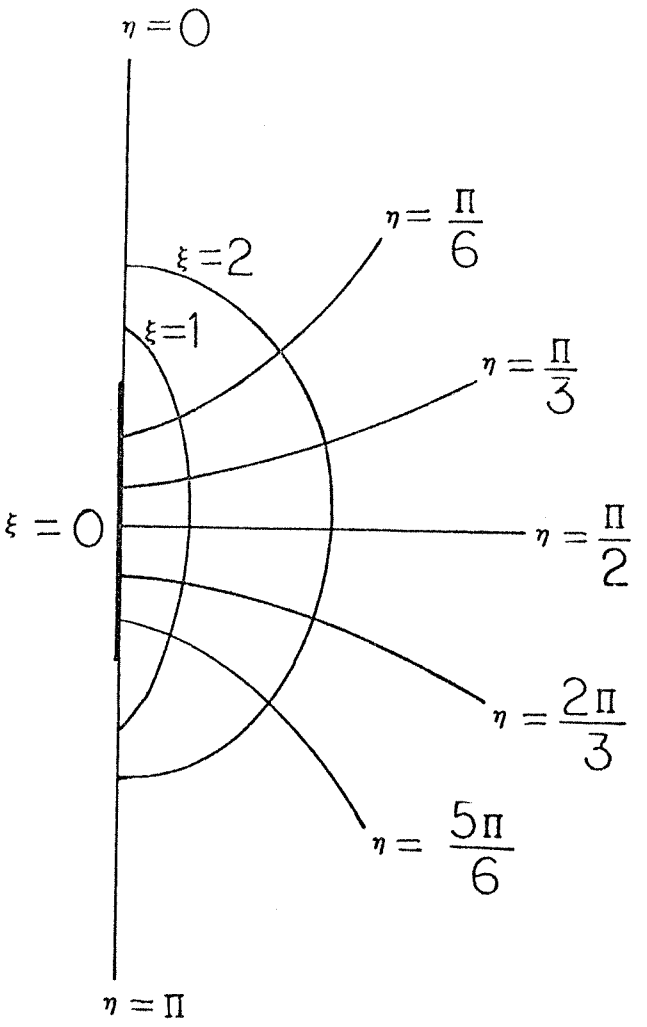

Figure 3: The Prolate Spheroidal Coordinate System

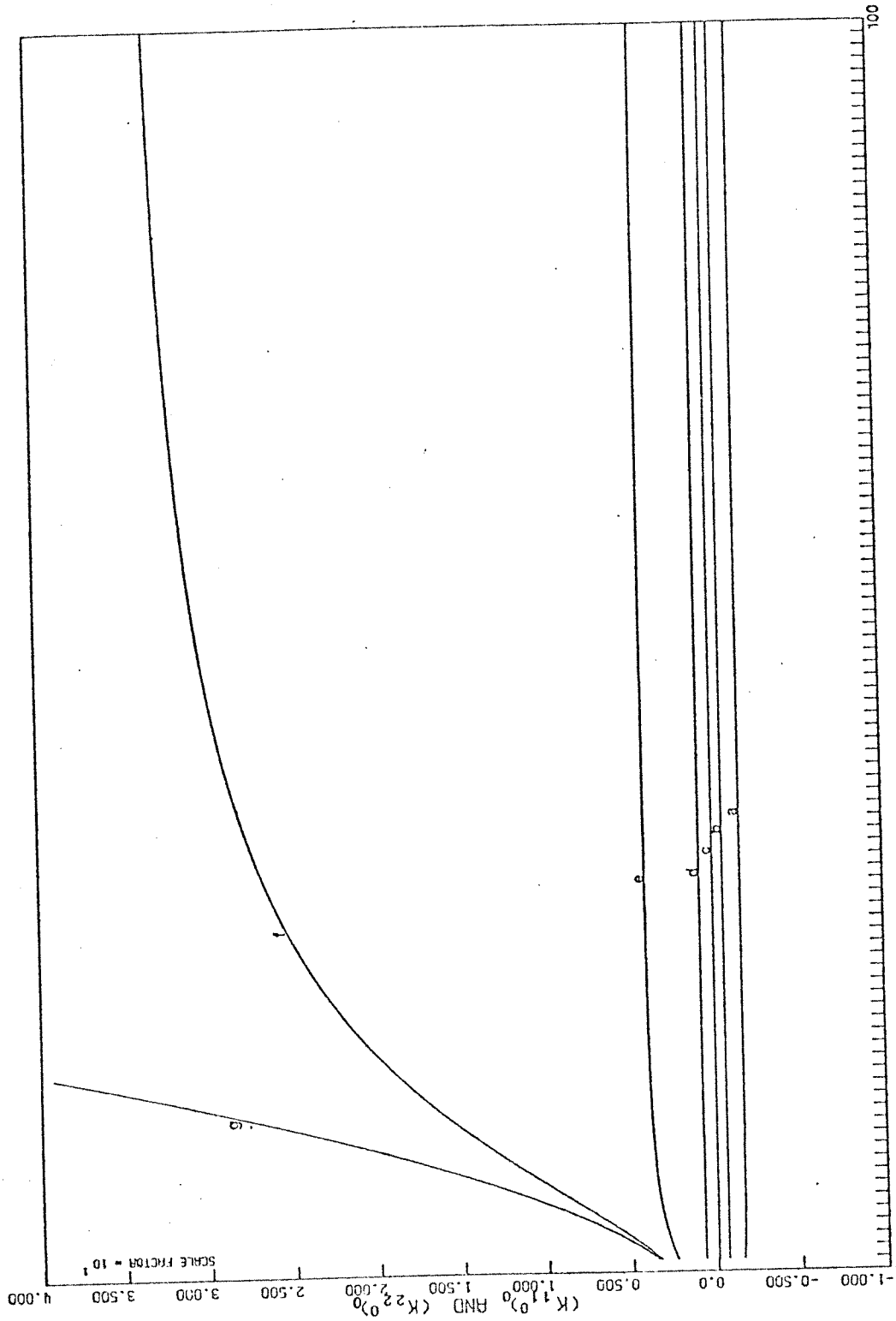

Figure 4: The Purely Conductive, Random Orientation Contributions

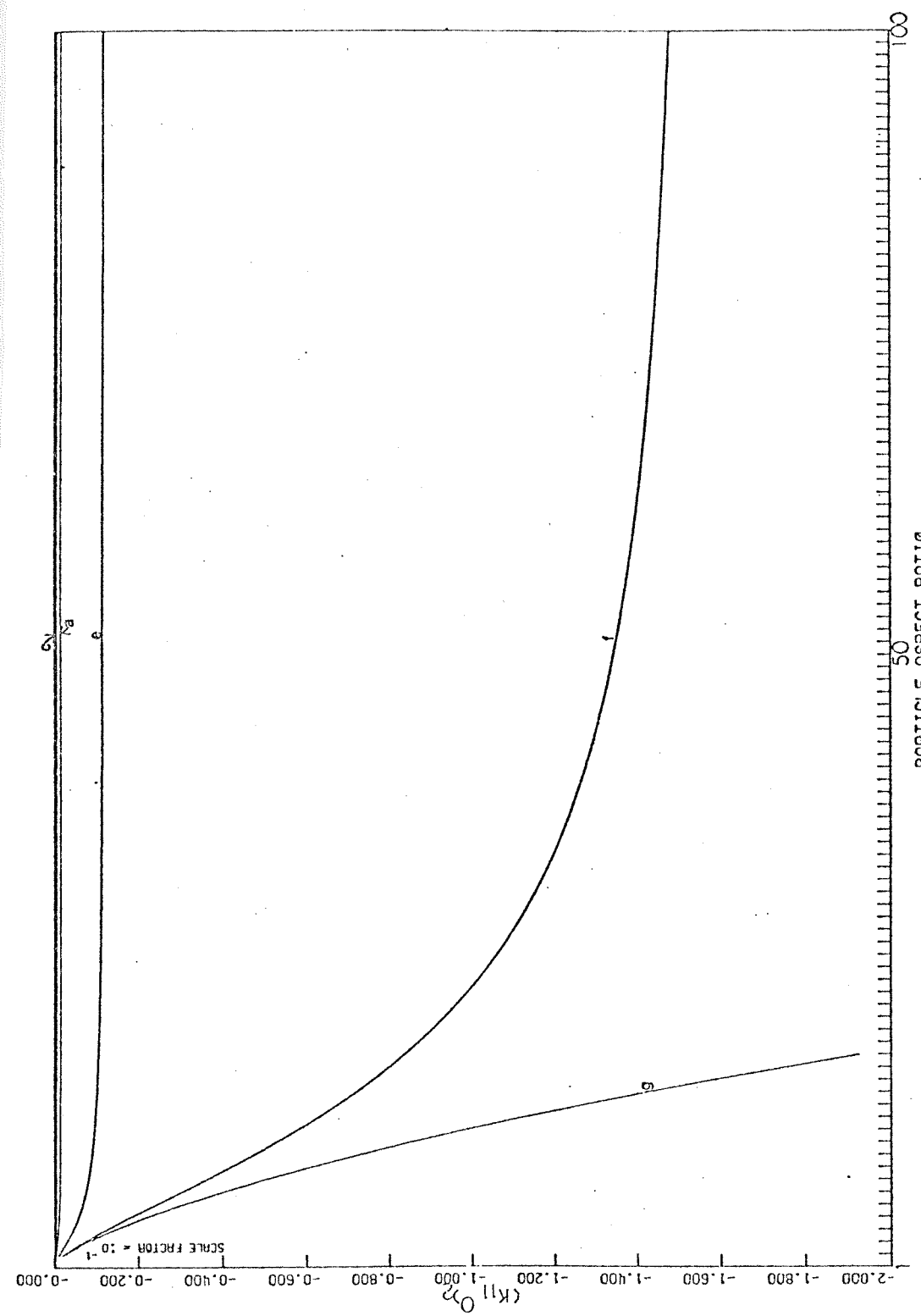

Figure 5: The Purely Conductive, Flow-Induced Orientation Contribution $(K_{11}^{0})_2$

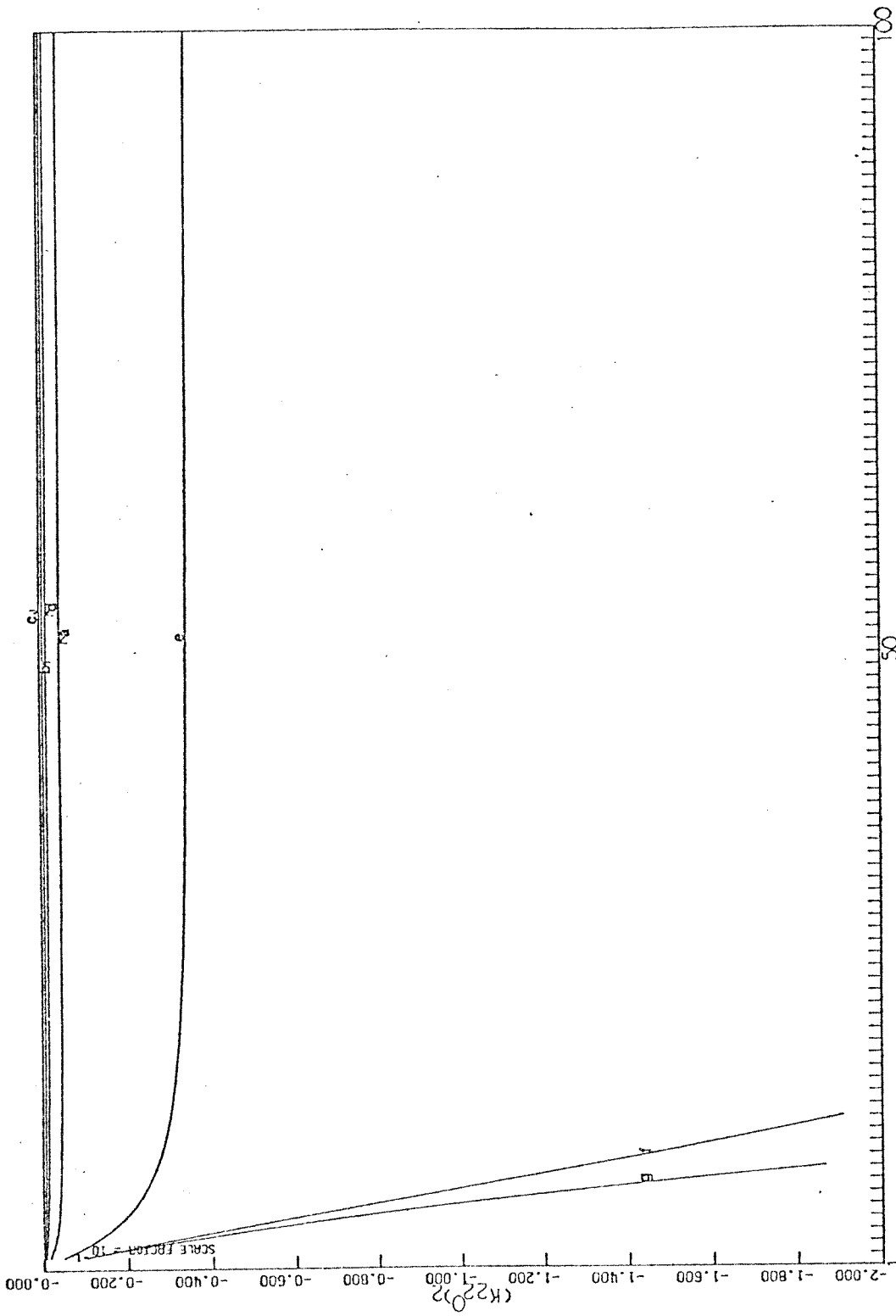

Figure 6: The Purely Conductive, Flow-Induced Orientation Contribution $(K_{22}^{0})_2$

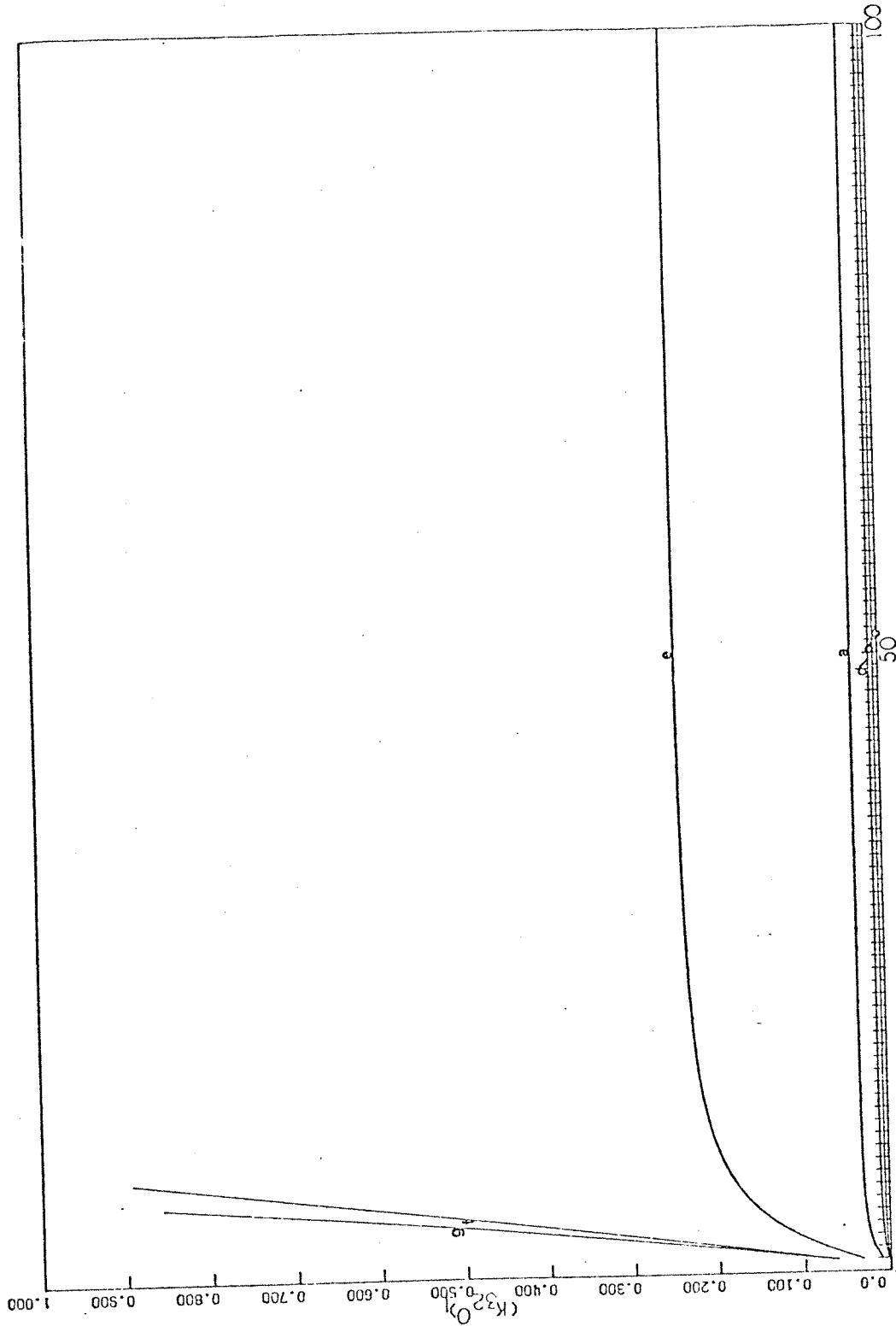

Figure 7: The Purely Conductive, Flow-Induced Orientation Contribution $(K_{32}^{0})_1$

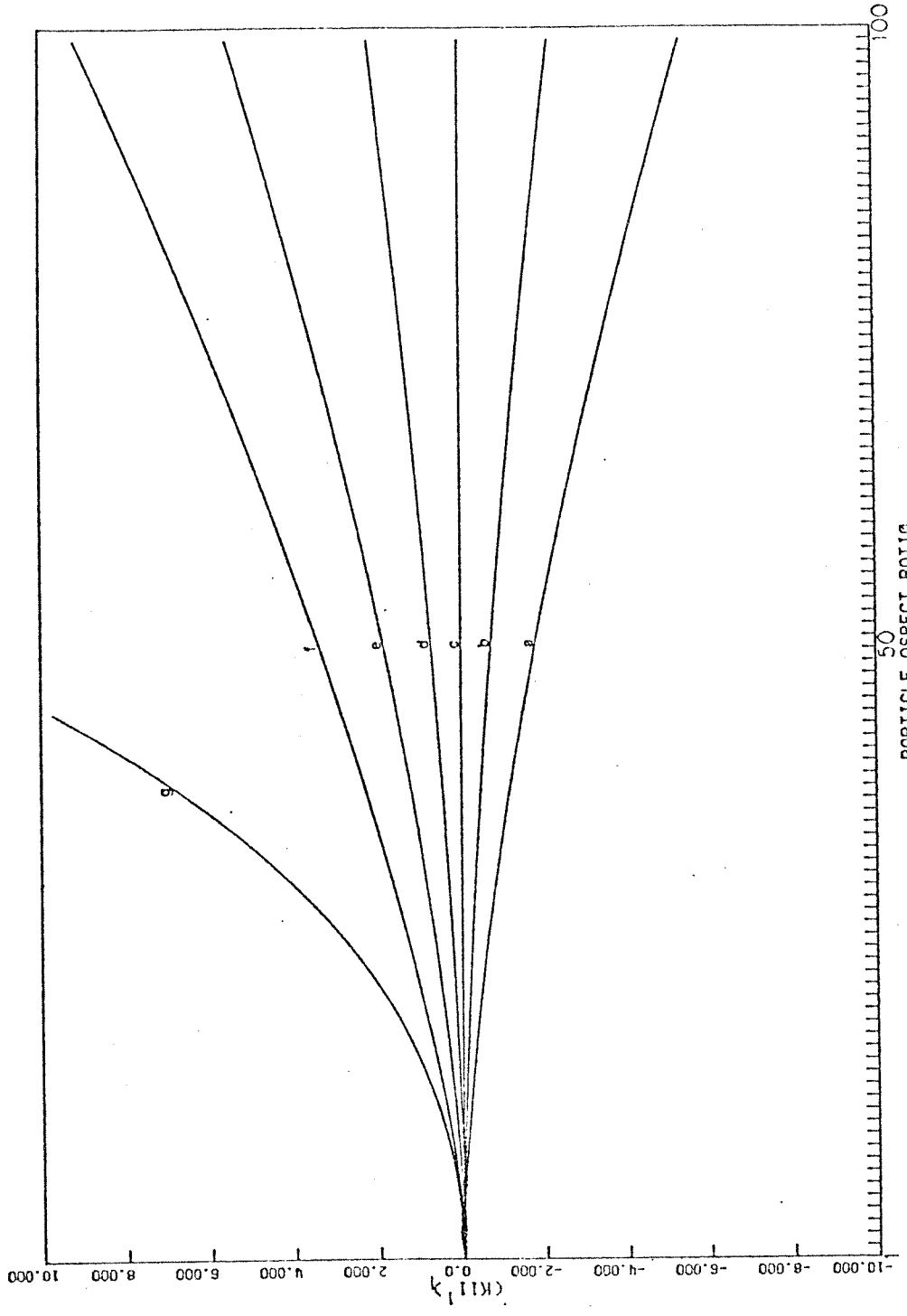

Figure 8: The Total O(Pe) Convective Contribution $(K_{11}^1)_1$

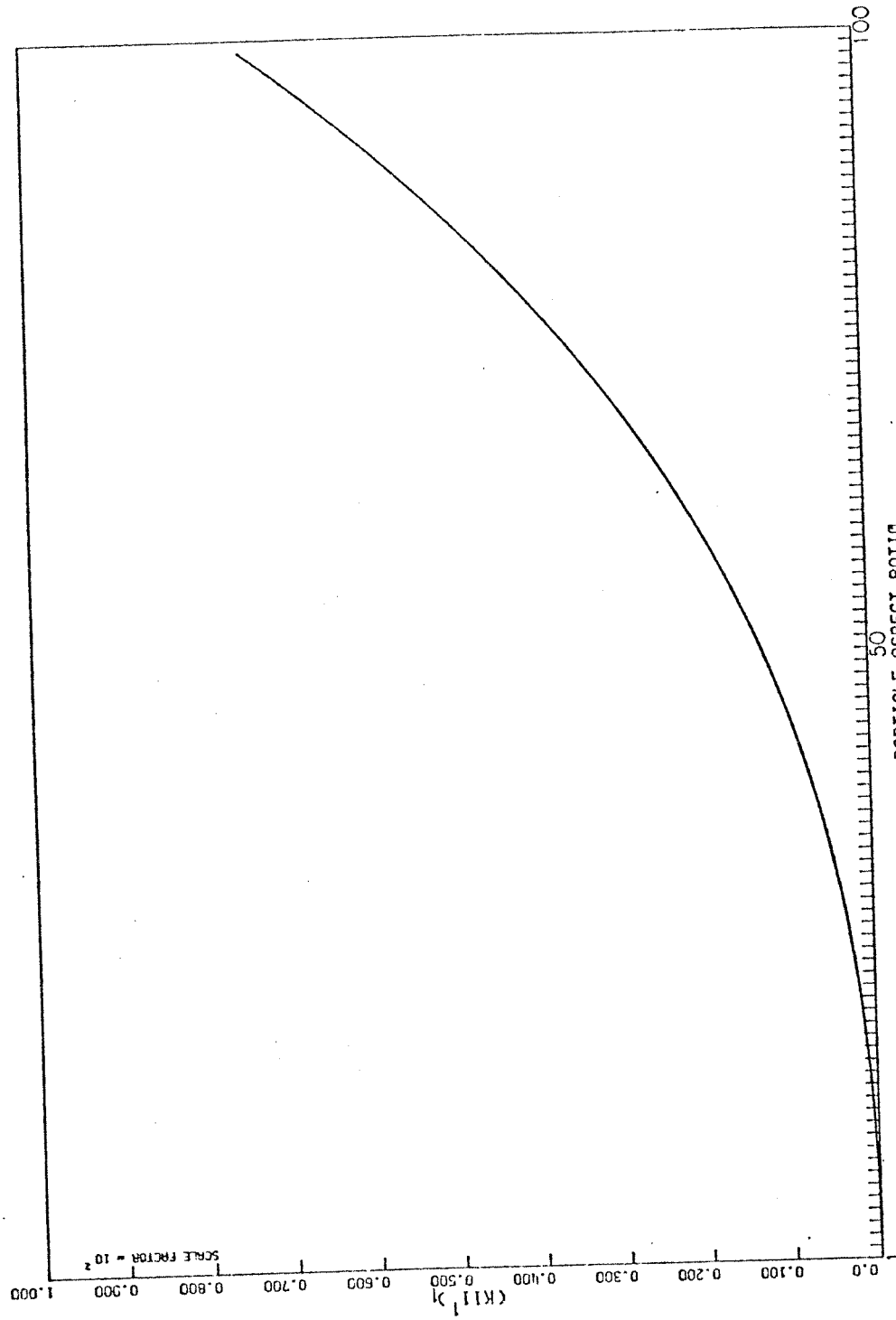

Figure 9: The Total O(Pe) Convective Contribution $(K_{11}^1)_1$

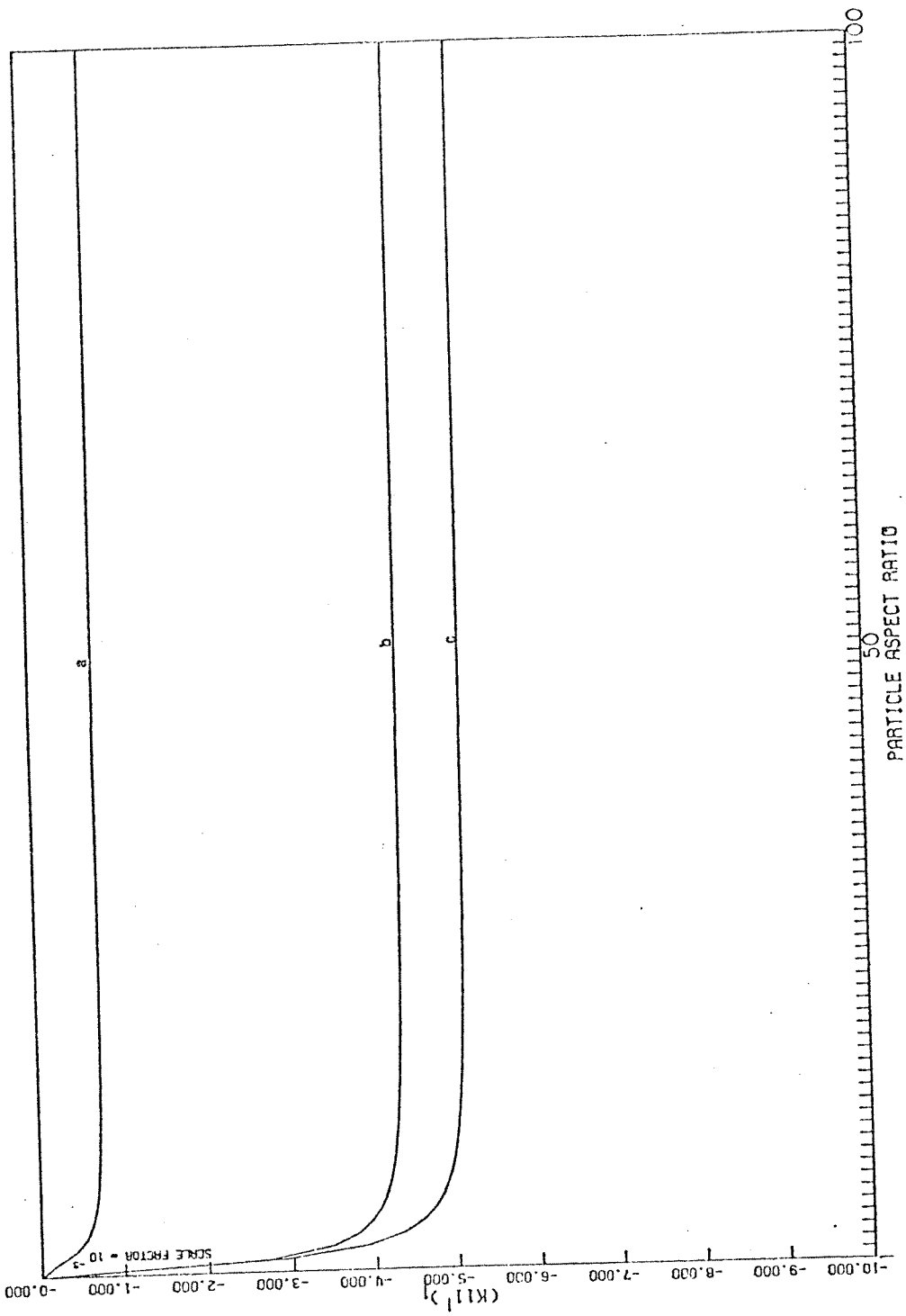

Figure 10: The $O(Pe_p)$ Convective Contribution $(K_{11}^1)_1$ for m = 0.

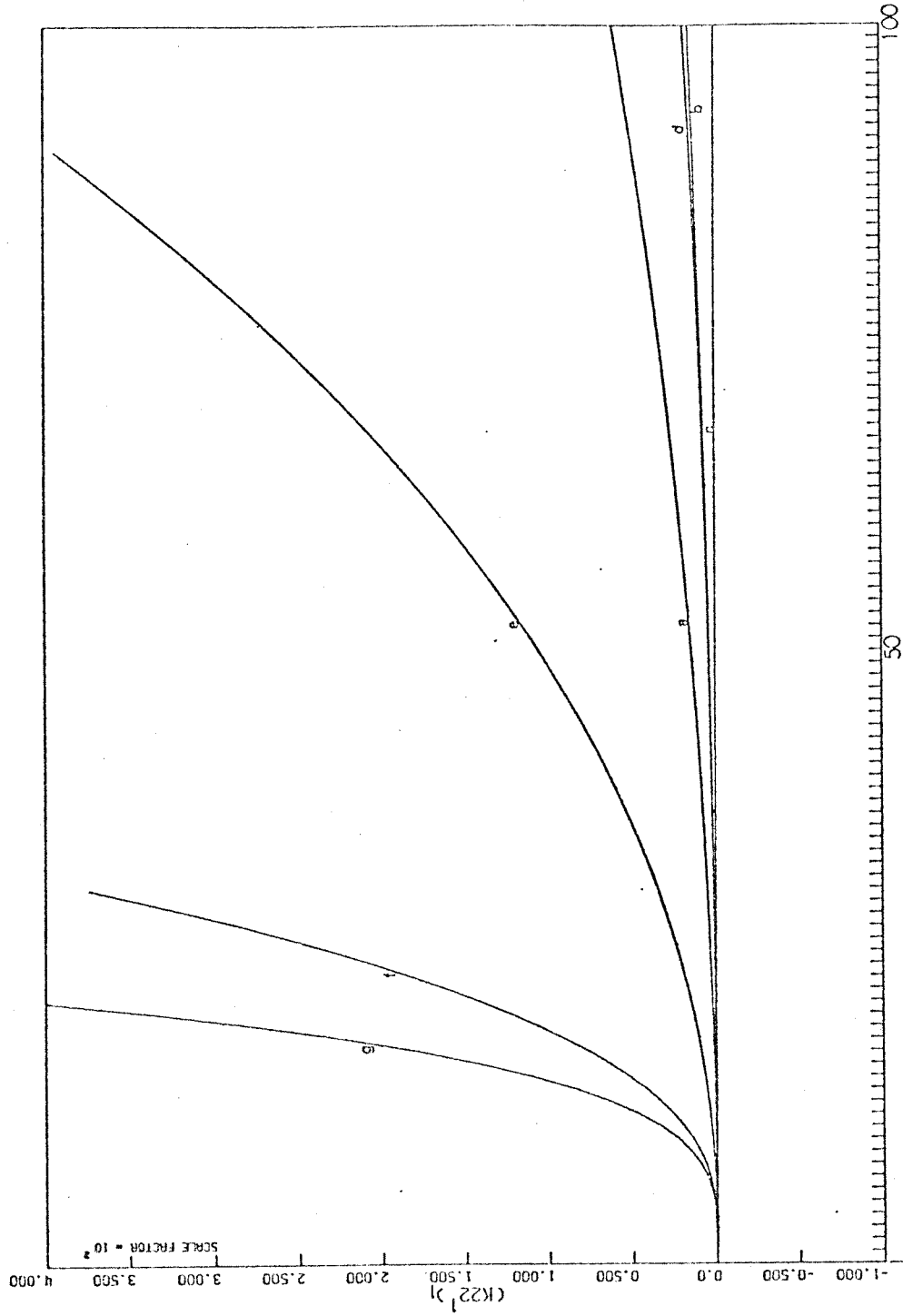

Figure 11: The Total O(Pe) Convective Contribution $(K_{22}^{1})_1$

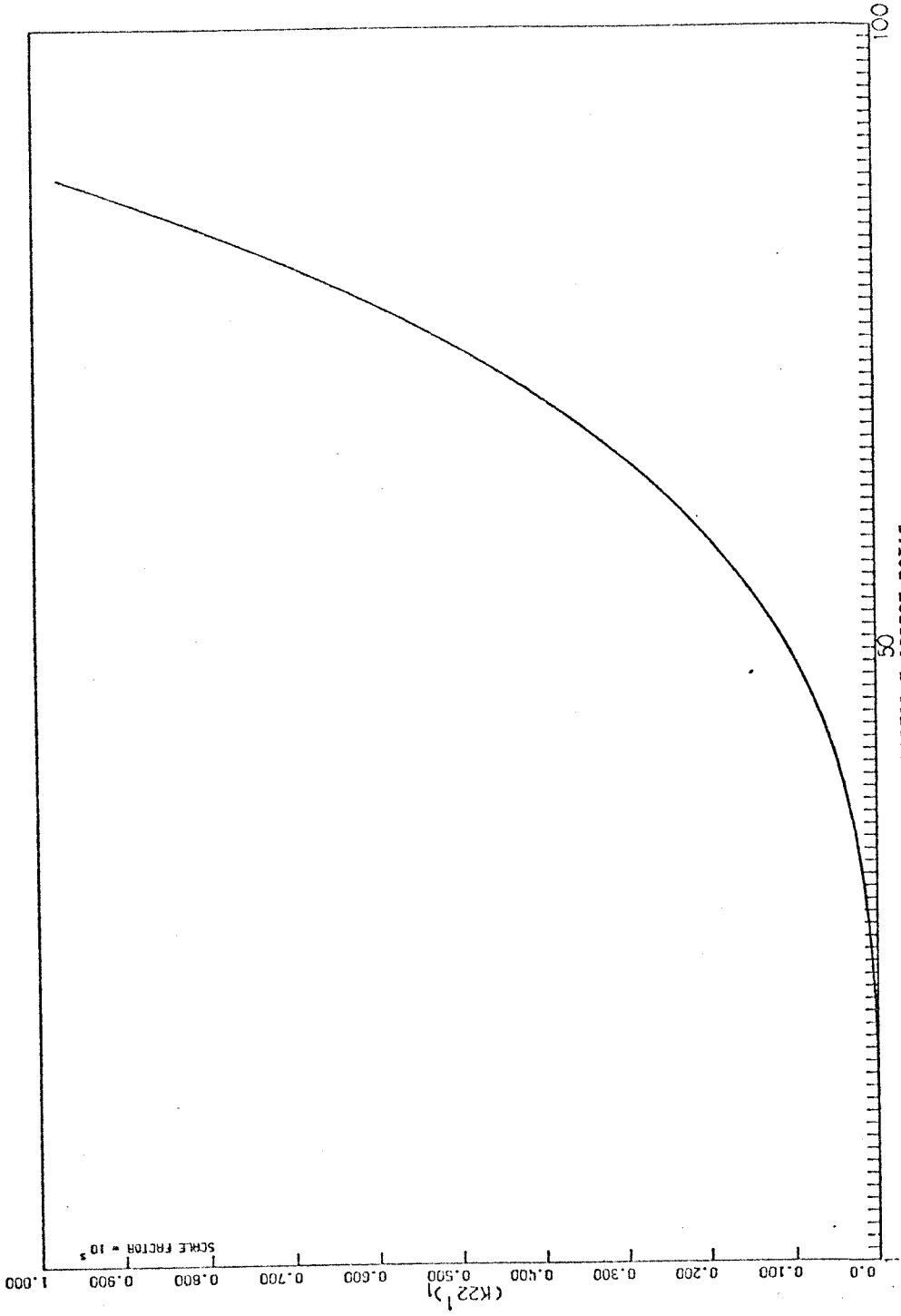

Figure 12: The Total O(Pe) Convective Contribution $(K_{22}^1)_1$

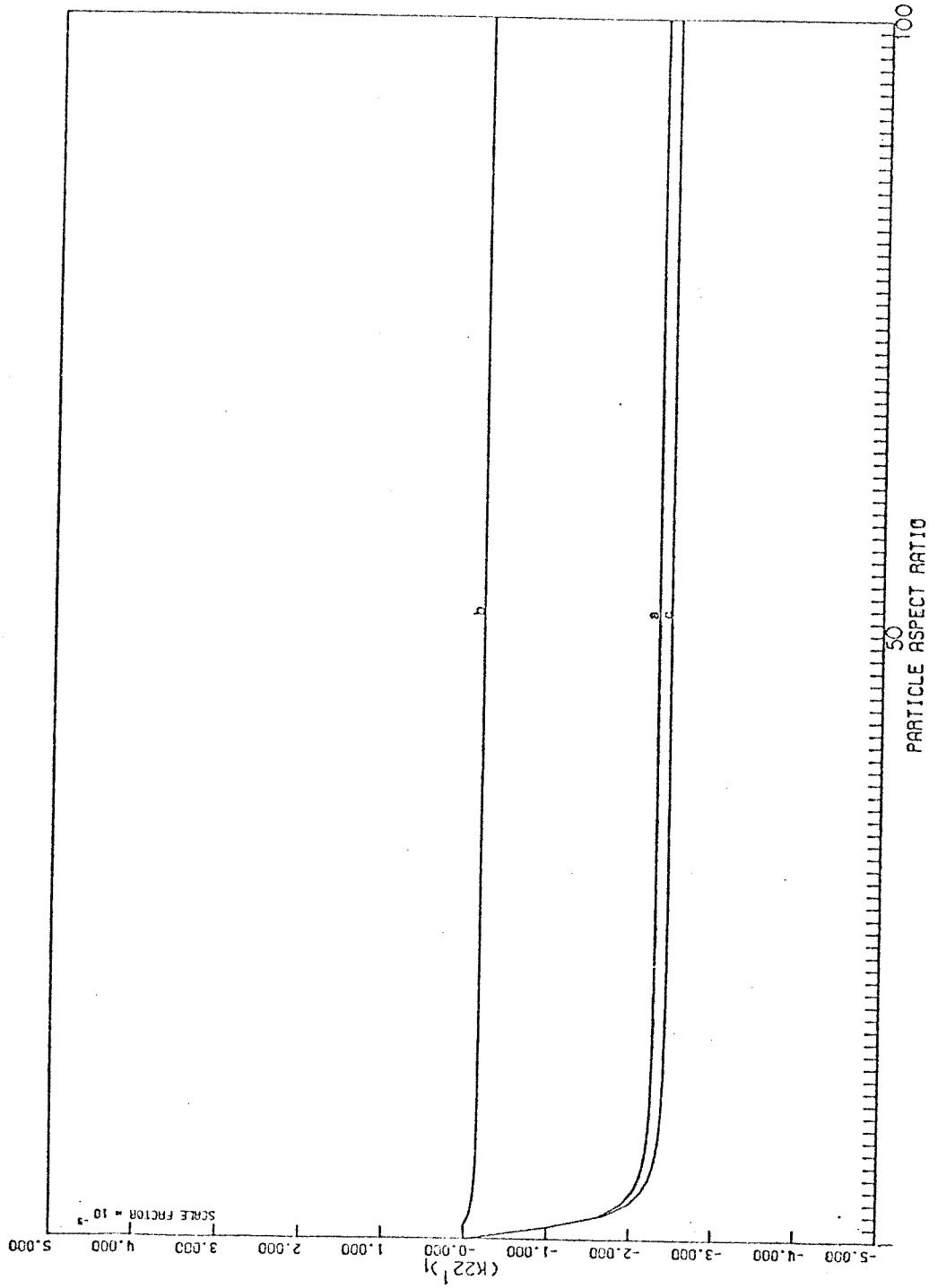

Figure 13: The $O(Pe_p)$ Convective Contribution $(K_{22}^1)_1$ for m = 0.

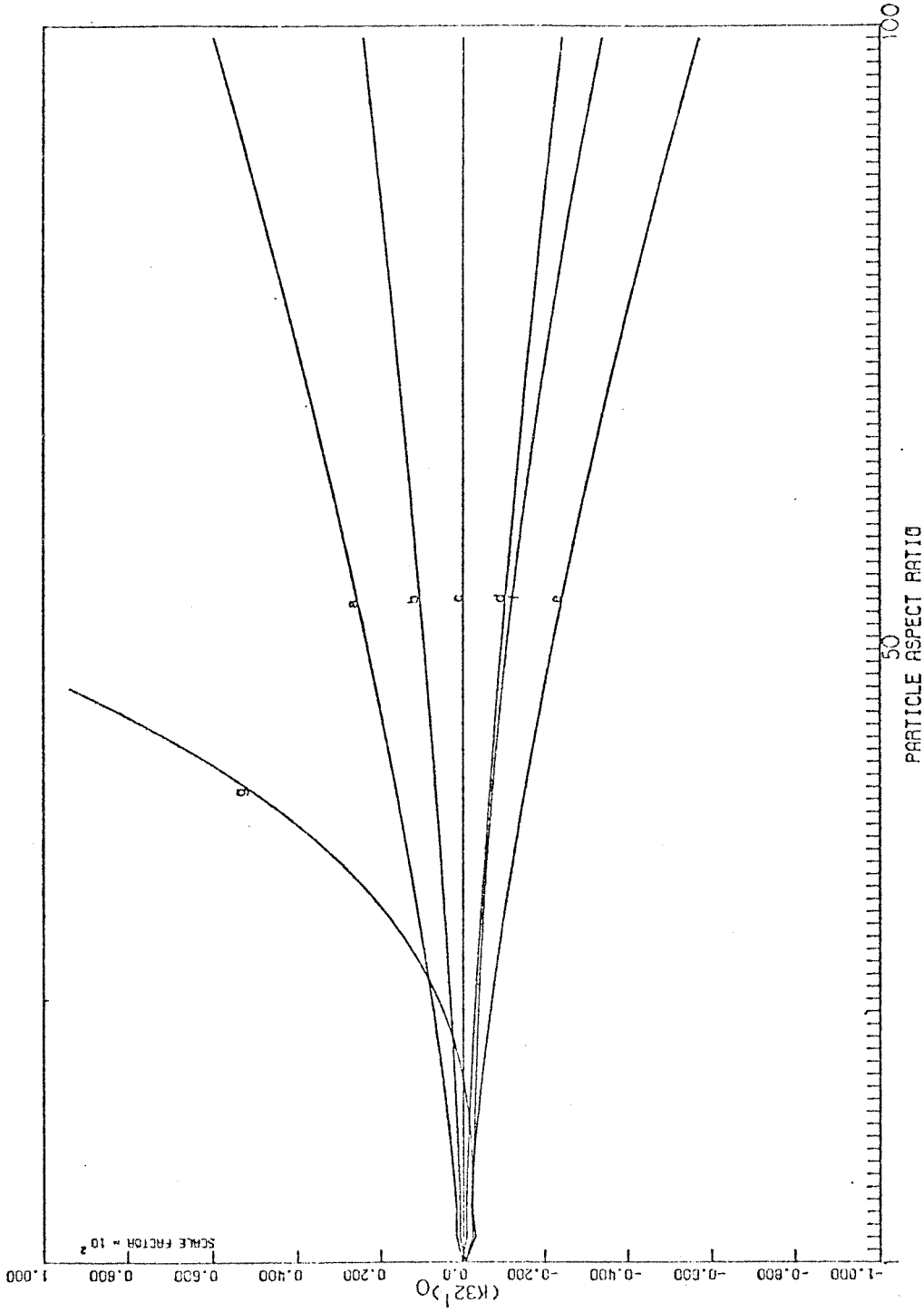

Figure 14: The Total O(Pe) Convective Contribution $(K_{32}^1)_0$

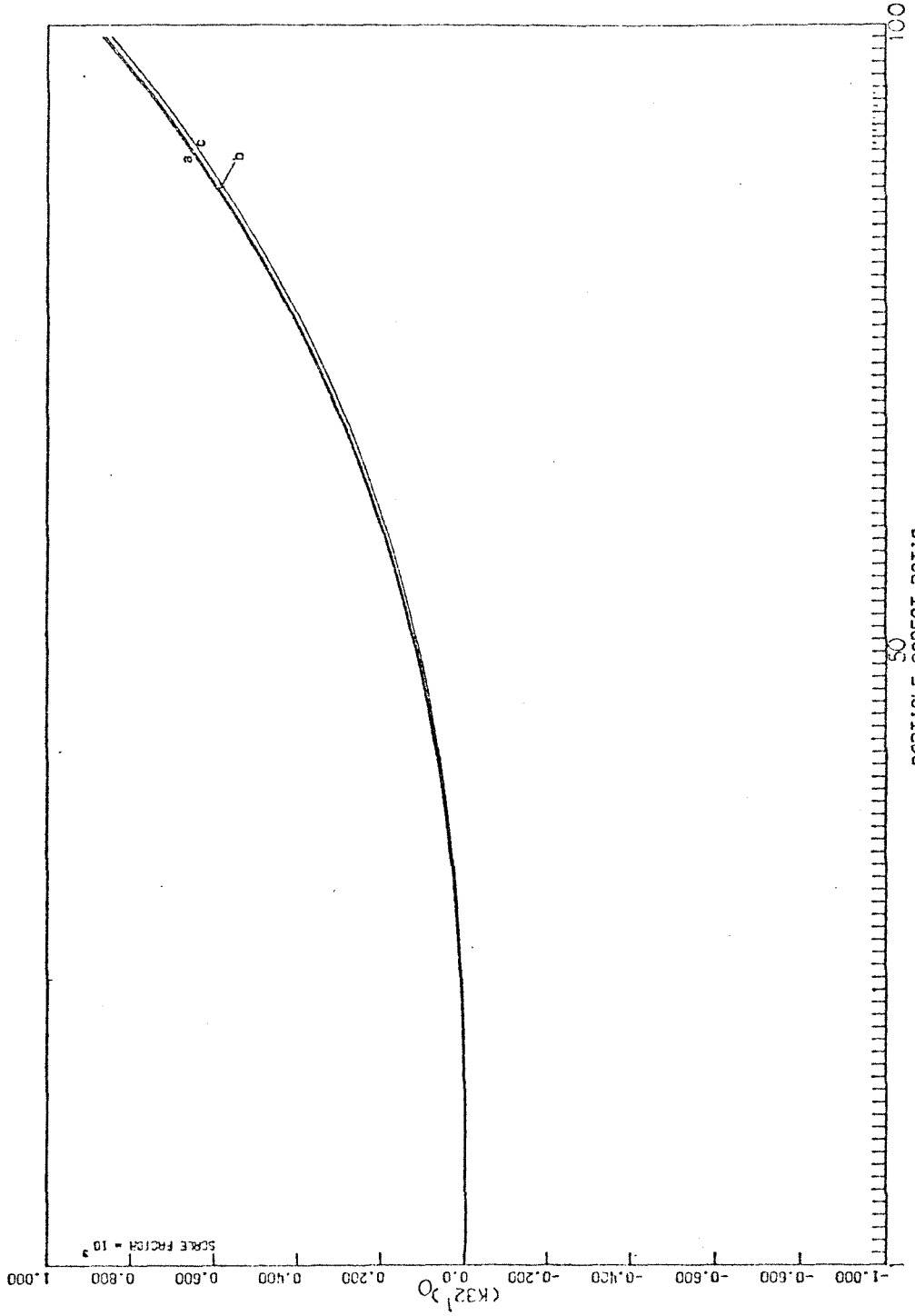

Figure 15: The Total O(Pe) Convective Contribution $(K_{32}^1)_O$

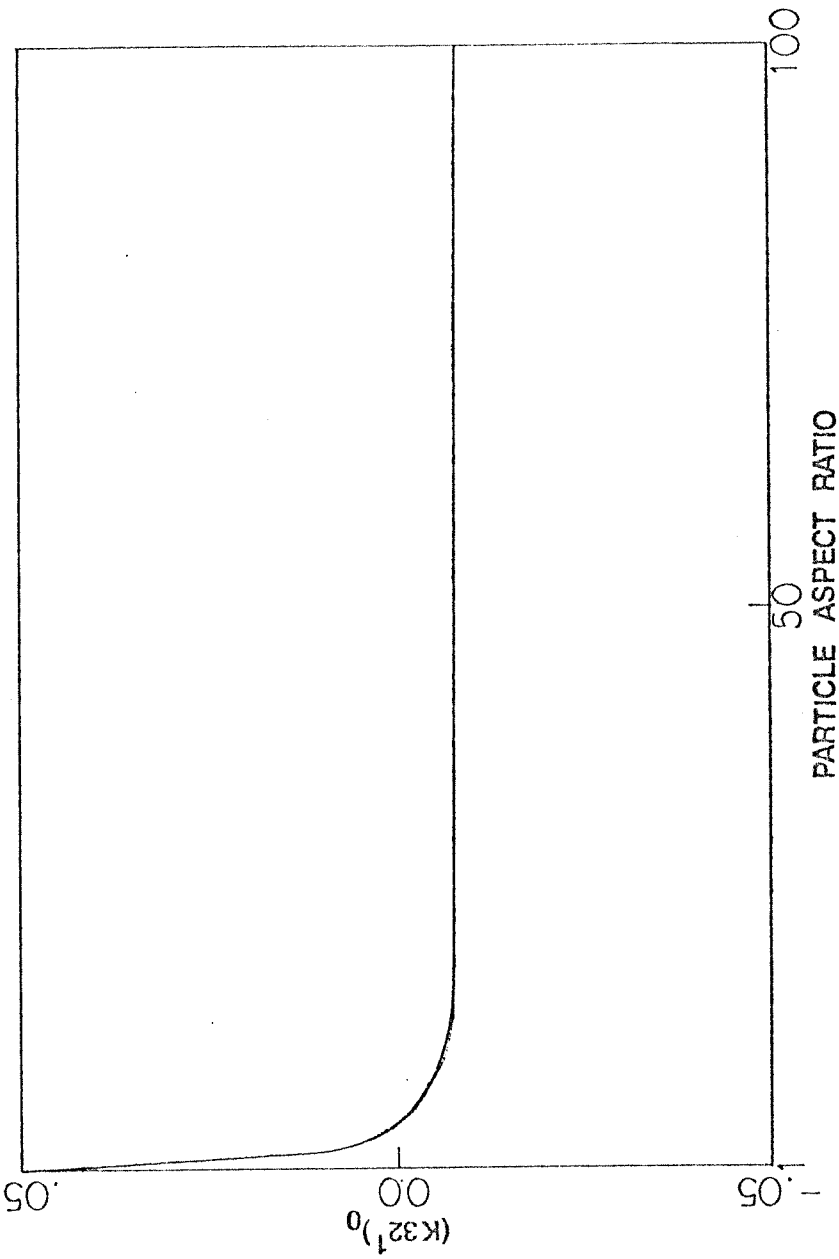

Figure 16: The $O(Pe_p)$ Total Convective Contribution $(K_{32}^1)_0$ for m = 0

APPENDIX

1) The General Solution to the Creeping Motion Equations

We shall demonstrate, in the following, that the general solution to the creeping motion equations:

$$\nabla^2\vec{U} = \nabla p \tag{A1}$$

$$\nabla\cdot\vec{U} = 0 \tag{A2}$$

may be expressed as a combination of four general harmonic functions, χ, ϕ, R, and S in the following manner,

$$\vec{U} = \nabla\times(\vec{r}\chi) + \nabla\phi + r^2\nabla R - \vec{r}S \tag{A3}$$

where $\vec{r}$ is the usual position vector with magnitude r, and the functions R and S satisfy the relation,

$$2\vec{r}\cdot\nabla R - \vec{r}\cdot\nabla S - 3S = 0. \tag{A4}$$

We begin by recognizing that we may express the solution to these linear, inhomogeneous partial differential equations as the sum of a homogeneous solution $\vec{U}_h$, (that is

the solution in a constant pressure field) and a particular solution $\vec{U}_p$ satisfying (A1) and (A2). It is simple to show that the solution $\vec{U}_h$ to the homogeneous problem

$$\nabla^2\vec{U}_h = 0, \qquad \nabla\cdot\vec{U}_h = 0 \tag{A5}$$

is

$$\vec{U}_h = \nabla\times(\vec{r}\chi) + \nabla\phi \tag{A5a}$$

Now

$$\nabla\cdot\vec{U}_h = \nabla\cdot\left[\nabla\times(\vec{r}\chi)\right] + \nabla^2\phi = 0 \tag{A6}$$

since ϕ is harmonic and the divergence of the curl of any vector is identically zero.

Furthermore

$$\nabla^2\vec{U}_h = \nabla(\nabla\cdot\vec{U}_h) - \nabla\times(\nabla\times\vec{U}_h) = -\nabla\times(\nabla\times\vec{U}_h) \tag{A7}$$

and

$$\begin{aligned} -\nabla\times(\nabla\times\vec{U}_h) &= -\nabla\times\left[\nabla\times\left[\nabla\times(\vec{r}\chi)\right]\right] - \nabla\times(\nabla\times\nabla\phi) \\ &= -\nabla\times\left[\nabla\times\left[\nabla\times(\vec{r}\chi)\right]\right] \end{aligned} \tag{A8}$$

since the curl of the gradient of any scalar is identically zero.

Now

$$-\nabla x\left[\nabla x\left[\nabla x(\vec{r}\chi)\right]\right] = -\nabla x\left[\nabla x(\nabla\chi\, x\vec{r})\right] - \nabla x\left[\nabla x\,\chi(\nabla x\vec{r})\right] \tag{A9}$$

but

$$\nabla x\vec{r} = 0 \tag{A10}$$

and

$$-\nabla x\left[\nabla x(\nabla\chi\, x\vec{r})\right] = -\nabla x(\nabla\cdot\vec{r})\nabla\chi + (\nabla^2\chi)\vec{r} = -\nabla x3\nabla\chi \tag{A11}$$

since

$$\nabla\cdot\vec{r} = 3. \tag{A12}$$

Finally

$$-\nabla x3\nabla\chi = -\nabla 3x\nabla\chi - 3(\nabla x\nabla\chi) = 0 \tag{A13}$$

since the gradient of a constant and the curl of the gradient of a scalar are both identically zero. We have therefore demonstrated that the representation (A5a) is the solution to the homogeneous problem (A5).

To show that the particular solution, $\vec{U}_p$, may be expressed as

$$\vec{U}_p = r^2 \nabla R - \vec{r}S \ , \tag{A14}$$

we begin by noting that the pressure, p, will be some harmonic function P, satisfying $\nabla^2 P = 0$. Now

$$\nabla \cdot \vec{U}_p = \nabla \cdot (r^2 \nabla R) - \nabla \cdot (\vec{r}S) \tag{A15}$$

but

$$\nabla \cdot (r^2 \nabla R) = \nabla r^2 \cdot \nabla R + r^2 (\nabla^2 R) = 2\vec{r} \cdot \nabla R \tag{A16}$$

since

$$\nabla r^2 = 2\vec{r} \ , \tag{A17}$$

and

$$-\nabla \cdot (\vec{r}S) = -\nabla S \cdot \vec{r} - S(\nabla \cdot \vec{r}) = -\nabla S \cdot \vec{r} - 3S \tag{A18}$$

so that

$$\nabla \cdot U_p = 2\vec{r} \cdot \nabla R - \vec{r} \cdot \nabla S - 3S = 0. \tag{A19}$$

Now the remaining equation to be satisfied requires that $\nabla^2 \vec{U}_p = \nabla P$, where P is some harmonic function. Since $\nabla \cdot \vec{U}_p = 0$,

$$\nabla^2 \vec{U}_p = -\nabla \times \left[\nabla \times (r^2 \nabla R) \right] + \nabla \times \left[\nabla \times (\vec{r}S) \right] \ . \tag{A20}$$

We may express

$$\nabla x(r^2 \nabla R) = (\nabla r^2 x \nabla R) + r^2(\nabla x \nabla R) = (2\vec{r} x \nabla R) \quad (A21)$$

since, as noted above,(A17), $\nabla r^2 = 2\vec{r}$ and the curl of the gradient of a scalar is zero, and

$$\nabla x(\vec{r}S) = \nabla S x \vec{r} - S(\nabla x \vec{r}) = \nabla S x \vec{r} \quad (A22)$$

by use of (A10). We then obtain

$$\nabla^2 \vec{U}_p = -\nabla x(2\vec{r} x \nabla R) + \nabla x(\nabla S x \vec{r}), \quad (A23)$$

but

$$-\nabla x(2\vec{r} x \nabla R) = -2\vec{r}(\nabla^2 R) + 2\nabla R(\nabla \cdot \vec{r})$$
$$= 6\nabla R = \nabla 6R \quad (A24)$$

since R is harmonic, and

$$\nabla x(\nabla S x \vec{r}) = \nabla S(\nabla \cdot \vec{r}) - \vec{r}(\nabla^2 S) = 3\nabla S = \nabla 3S \quad (A25)$$

since S is harmonic. We therefore find that

$$\nabla^2 \vec{U}_p = \nabla 6R + \nabla 3S = \nabla(6R + 3S) = \nabla P \quad (A26)$$

since if R and S are general harmonic functions, then 6R + 3S will also obviously be harmonic. For any arbitrary P, we may construct R and S, where Rand S are related by (A19).

We have then demonstrated that the general solution to the creeping motion equations (A1) and (A2) may be represented by

$$\vec{U} = \nabla x(\vec{r}\chi) + \nabla\phi + r^2\nabla R - \vec{r}S$$

when

$$2\vec{r}\cdot\nabla R - \vec{r}\cdot\nabla S - 3S = 0.$$

Another way of showing the result (A3) and (A4) is to consider the special case of spherical harmonics. Lamb (1932) has then shown that the general solution to the creeping motion equations (A1) and (A2) may be represented by the sums of the general spherical harmonic functions of degree n as;

$$p = \sum_n P_n^*$$

$$\vec{U} = \sum_n \left[\nabla x(\vec{r}\chi_n^*) + \nabla\phi_n^* + a_n r^2 \nabla P_n - b_n \vec{r} P_n \right]$$

where χ_n^*, ϕ_n^*, and P_n^* are the spherical harmonics of order n, that is the general harmonic functions χ, ϕ, and P may be represented by

$$\chi = \sum_n \chi_n^*$$

$$\phi = \sum_n \phi_n^*$$

$$P = \sum_n P_n^*$$

and $a_n = \dfrac{(n+3)}{2(n+1)(2n+3)}$; $b_n = \dfrac{n}{(n+1)(2n+3)}$ are not functions of position. We may then define two new spherical harmonic representations $R = \sum_n R_n^*$ and $S = \sum_n S_n^*$ are merely

$$R_n^* = a_n P_n^* \qquad S_n^* = b_n P_n^*$$

then

$$\vec{U} = \sum_n \left[\nabla x(\vec{r}\chi_n^*) + \nabla\phi_n^* + r^2 \nabla R_n^* - \vec{r} S_n^* \right]$$

but we may put the summation inside the operators and obtain,

$$\vec{U} = \left[\nabla x(\vec{r}\chi) + \nabla\phi + r^2 \nabla R - \vec{r} S \right].$$

2) The identity $c^3(\Psi^3 - \Psi) = 1$

In evaluation of the volume and area integrals of the bulk heat flux relation, use of the identity

$$c^3(\Psi^3 - \Psi) = 1$$

is very helpful. The identity follows readily from the definitions of

$$c = (a^2 - b^2)^{1/2} = \frac{(\Gamma_p^2 - 1)^{1/2}}{p^{1/3}}$$

and $$\Psi = \cosh(\mathrm{ctnh}^{-1}\Gamma_p) = \frac{\Gamma_p}{(\Gamma_p^2 - 1)^{1/2}}$$

Making the substitutions,

$$c^3(\Psi^3 - \Psi) = \frac{(\Gamma_p^2-1)^{3/2}}{\Gamma_p}\left\{\frac{\Gamma_p^3}{(\Gamma_p^2-1)^{3/2}} - \frac{\Gamma_p}{(\Gamma_p^2-1)^{1/2}}\right\}$$

and rearranging

$$c^3(\Psi^3-\Psi) = \frac{(\Gamma_p^2-1)^{3/2}}{\Gamma_p}\ \frac{\Gamma_p^3-\Gamma_p^3+\Gamma_p}{(\Gamma_p^2-1)^{3/2}}$$

$$= \frac{(\Gamma_p^2-1)^{3/2}}{\Gamma_p}\ \frac{\Gamma_p}{(\Gamma_p^2-1)^{3/2}} = 1.$$

Following is the listing of the Fortran program used to evaluate the coefficients α_{nm}^{ij} and β_{nm}^{ij} for the O(Pe) contribution to the effective conductivity for strong rotational Brownian motion. The coefficients are numerically evaluated for various values of the particle aspect ratio, from which the plots in figures 8-16 were calculated. The various shape factors arising from the calculation of the microscale velocity and temperature fields are evaluated in the program as intermediate steps in the calculation.

```
// SET TIME=1
// SET REGION=256K
// SET PUN=700
//        EXEC  FORTG
//FORT    DD    *
COMMENT  THE FOLLOWING PROGRAM CALCULATES THE VALUES OF THE ASSOCIATED
C        LEGENDRE FUNCTIONS  OF THE FIRST AND SECOND KINDS, PNM AND QNM,
C        THE VELOCITY FIELD SHAPE FUNCTIONS, S1 THROUGH S24, THE
C        TEMPERATURE DISTRIBUTION SHAPE FUNCTIONS, B0 THROUGH B24,
C        AND THE SHAPE FUNCTIONS ARISING FROM THE VOLUME INTEGRATION,
C        R1 THROUGH R11.  FROM THESE VALUES, THE COEFFICIENTS FOR THE
C        THREE ORDER PECLET EFFECTIVE CONDUCTIVITY COMPONENTS, K11,K22,
C        AND K32 MAY BE CALCULATED.  THE PURELY HYDRODYNAMIC CONTRIBUTIONS
C        ( THE ALPHAS ) ARE SIGNIFIED BY AL(1) THROUGH AL(15).  THE DIRECT
C        BROWNIAN CONTRIBUTIONS ( THE BETAS ) ARE SIGNIFIED BY BL(1)
C        TROUGH BL(15).  FOR THE SITUATION WHERE THE PARTICLE AXIS RATIO,
C        GAMMA=AG, IS OF THE ORDER OF ONE, SO THAT THE PARTICLES ARE NEARLY
C        SPHERICAL IN SHAPE, SOME OF THE LEGENDRE FUNCTIONS AND SHAPE
C        FACTORS ARE CALCULATED FROM A SERIES REPRESENTATION IN TERMS OF
C        1/S, WHERE S IS THE VALUE OF THE PARAMETER  PSI, WHICH IS A
C        FUNCTION OF THE PARTICLE AXIS RATIO AG THAT BECOMES INFINITE AS
C        AG APPROACHES ONE.
      IMPLICIT REAL*8(A-H,O-Z)
      DIMENSION AL1(100),AL2(100),AL3(100),AL4(100),AL5(100),AL6(100),
     1AL7(100),AL8(100),AL9(100),AL10(100),AL11(100),AL12(100),AL13(100)
     2,AL14(100),AL15(100),AD1(100),AD2(100)
      DIMENSION BL1(100),BL2(100),BL3(100),BL4(100),BL5(100),BL6(100),
     1BL7(100),BL8(100),BL9(100),BL10(100),BL11(100),BL12(100),BL13(100)
     2,BL14(100),BL15(100)
  100 FORMAT(5(2XD14.7))
  101 FORMAT(5X'ALPHA  1 IS')
  102 FORMAT(5X'ALPHA  2 IS')
  103 FORMAT(5X'ALPHA  3 IS')
  104 FORMAT(5X'ALPHA  4 IS')
  105 FORMAT(5X'ALPHA  5 IS')
  106 FORMAT(5X'ALPHA  6 IS')
  107 FORMAT(5X'ALPHA  7 IS')
  108 FORMAT(5X'ALPHA  8 IS')
  109 FORMAT(5X'ALPHA  9 IS')
  110 FORMAT(5X'ALPHA 10 IS')
  111 FORMAT(5X'ALPHA 11 IS')
  112 FORMAT(5X'ALPHA 12 IS')
  113 FORMAT(5X'ALPHA 13 IS')
  114 FORMAT(5X'ALPHA 14 IS')
  115 FORMAT(5X'ALPHA 15 IS')
  116 FORMAT(5X'AD1 IS')
  117 FORMAT(5X'AD2 IS')
  118 FORMAT(5X'PURE HYDRODYNAMIC CORRECTION')
  119 FORMAT(5X'DIRECT BROWNIAN MOTION CORRECTION')
  500 FORMAT(' PROGRAM IS AT 11',5XD14.7)
  501 FORMAT(' PROGRAM IS AT 70',5XD14.7)
C    THE FOLLOWING PART OF THE PROGRAM CALCULATES S AS A FUNCTION OF AG
C  AND ASSIGNS VALUES OF AG
      DO 20 I=2,100
      AI=I
      AG=AI
      AGSQ=AG*AG
      AGP=AGSQ+1.D0
      AGM=AGSQ-1.D0
      AGMR=DSQRT(AGM)
      S=AG/AGMR
      S1=S*S-1.D0
```

```
      SR=DSQRT(S1)
      ABA=(S+1.DO)/(S-1.DO)
      S2=S*S                                                          9
      S3=S2*S                                                         10
      S4=S3*S                                                         11
      S5=S4*S                                                         12
      S6=S5*S                                                         13
C  FINISHED CALCULATING S AND AB
C  THE FOLLOWING PART OF THE PROGRAM CALCULATES THE ASSOCIATED LEGENDRE
C  FUNCTIONS  PMN AND QMN AS A FUNCTION OF S
C   RATHER THAN CALCULATING THE FUNCTIONS FROM THEIR EXPLICIT ALGEBRAIC
C   EXPRESSIONS AS A FUNCTION OF S, THE FUNCTIONS ARE CALCULATED BY THEIR
C   RECURSION RELATIONS, AS THIS WAS FOUND TO GIVE BETTER NUMERICAL RESULTS.
      P00=1.DO
      P01=S
      P02=((3.DO*S*P01)-(P00))/2.DO
      P03=((5.DO*S*P02)-(2.DO*P01))/3.DO
      P04=((7.DO*S*P03)-(3.DO*P02))/4.DO
      P05=((9.DO*S*P04)-(4.DO*P03))/5.DO
      P06=((1.1D1*S*P05)-(5.DO*P04))/6.DO
      Q00=5.D-1*(DLOG(ABA))
      Q01=S*Q00-1.DO
      P11=-SR
      P12=-3.DO*S*SR
      P13=((5.DO*S*P12)-(3.DO*P11))/2.DO
      P14=((7.DO*S*P13)-(4.DO*P12))/3.DO
      P15=((9.DO*S*P14)-(5.DO*P13))/4.DO
      P16=((1.1D1*S*P15)-(6.DO*P14))/5.DO
      Q1M1=S/SR
      Q10=1.DO/SR
      Q11=(P11*Q00)+Q1M1
      P22=-3.DO*S1
      P23=5.DO*S*P22
      P24=((7.DO*S*P23)-(5.DO*P22))/2.DO
      P25=((9.DO*S*P24)-(6.DO*P23))/3.DO
      Q21=-2.DO/S1
C   IF S IS LARGER THAN 1.50 Q07 AND Q06 ARE CALCULATED BY SERIES
C  AND THE REMAINING  2ND FUNCTIONS BY RECURSION
      IF(S.GT.1.5) GO TO 5
      QC2=((3.DO*S*QC1)-(Q00))/2.DO
      QC3=((5.DO*S*QC2)-(2.DO*QC1))/3.DO
      QC4=((7.DO*S*QC3)-(3.DO*QC2))/4.DO
      QC5=((9.DO*S*QC4)-(4.DO*QC3))/5.DO
      QC6=((1.1D1*S*QC5)-(5.DO*QC4))/6.DO
      Q12=((3.DO*S*Q11)-(2.DO*Q10))/1.DO
      Q13=((5.DO*S*Q12)-(3.DO*Q11))/2.DO
      Q14=((7.DO*S*Q13)-(4.DO*Q12))/3.DO
      Q15=((9.DO*S*Q14)-(5.DO*Q13))/4.DO
      Q16=((1.1D1*S*Q15)-(6.DO*Q14))/5.DO
      Q22=((S*Q12)-(3.DO*Q11))/SR
      Q23=((5.DO*S*Q22)-(4.DO*Q21))
      Q24=((7.DO*S*Q23)-(5.DO*Q22))/2.DO
      Q25=((9.DO*S*Q24)-(6.DO*Q23))/3.DO
      GO TO 11
    5 II=3
      J=1
      A1=2.31D2
      A2=3.15D2
      A3=1.05D2
      A4=5.DO
      GO TO 7
    6 II=4
```

```
      J=C
      A1=4.29D2
      A2=6.93D2
      A3=3.15D2
      A4=3.5D1
      GC TC 7
    7 SUM=C.DC
      DC 8 M=II,100
      X1=(2*M+5)*(2*M+3)*(2*M+1)
      X2=(2*M+7)*(2*M+3)*(2*M+1)
      X3=(2*M+7)*(2*M+5)*(2*M+1)
      X4=(2*M+7)*(2*M+5)*(2*M+3)
      X5=(2*M+7)*(2*M+5)*(2*M+3)*(2*M+1)
      SU=(A1*X1-A2*X2+A3*X3-A4*X4)/(1.6D1*X5)/(S**(2*M+J))
      SUM=SUM+SU
      SUL=SU/SUM
      SUX=SUU-1.D-14
      IF(SUX.LT.C) GC TC 9
    8 CONTINUE
    9 IF(II.EQ.4) GC TO 10
      QC6=SUM
      GC TC 6
   10 QC7=SUM
      QC5=(S*QC6-(7.DC*QC7/1.3D1))*1.3D1/6.DC
      Q04=(S*Q05-(6.D0*QC6/1.3D1))*1.1D1/5.DC
      Q03=(S*QC4-(5.DC*QC5/9.D0))*9.DC/4.DC
      Q02=(S*Q03-(4.DC*QC4/7.D0))*7.DC/3.D0
      C16=(Q05-Q07)*6.DC*7.DC/1.3D1/SR
      C15=(QC4-Q06)*5.DC*6.DC/1.1D1/SR
      C14=(C03-Q05)*4.DC*5.DC/9.DC/SR
      C13=(C02-Q04)*3.DC*4.DC/7.DC/SR
      C12=(CC1-Q03)*2.DC*3.DC/5.DC/SR
      Q25=(5.D0*4.D0*C16/1.1D1-(7.DC*6.DC*Q14/1.1D1))/SR
      Q24=(4.DC*3.DC*C15/9.DC-(6.DC*5.DC*C13/9.DC))/SR
      Q23=(3.D0*2.DC*Q14/7.D0-(5.D0*4.DC*Q12/7.D0))/SR
   11 C22=(2.DC*1.DC*C13/5.DC-(4.DC*3.DC*C11/5.DC))/SR
C  FINISHED CALCULATING THE LEGENDRE FUNCTIONS
C  THE FOLLOWING PART OF THE PROGRAM CALCULATES THE B SHAPE FACTORS FROM
C  THE TEMPERATURE FIELD
      A=(QC2-QOC)/QC1                                                    2C1
      B0=-2.DC*P03*A/3.DC/S1                                             2C2
      B1=-1.2D1*(PC4-P02)/7.DC/S1                                        2C3
      B2=-2.DC*A/3.DC/S1                                                 2C4
      B3=-2.DC*(Q05*A-(4.5D1*(QC6-QC4)/1.1D1))/3.DC/S1                   2C5
      B4=-2.DC*(Q04*A-(1.D1*(Q05-Q03)/3.DC))/3.DC/S1                     2C6
      B5=-2.DC*(C03*A-(1.8D1*(QC4-Q02)/7.DC))/3.DC/S1                    2C7
      B6=-2.DC*(C02*A-(9.DC*(C03-Q01)/5.DC))/3.DC/S1                     2C8
      B7=-2.DC*(COC*A+1.5DC)/3.DC/S1                                     2C9
C       THERE ARE TWC CARES NUMBERED 210
      B8=-2.DC*(CC5*QOC*A-(4.5D1*C06*QOC/1.1D1)+(4.5D1*C04*QOC/1.1D1)+(1 2C0
     A.5DC*CC5))/3.DC/S1                                                 210
      B9=-2.DC*(C03*QOC*A-(1.8D1*C04*QOC/7.DC)+(1.8D1*CC2*CCC/7.DC)+(1.5 211
     ADC*CC3))/3.DC/S1                                                   212
      B1C=-1.DC/S1                                                       213
      B11=-2.DC*(-S*A/S1-(1.5DC*(S2+1.DC)/S1))/3.DC/S1                   214
      A=(4.DC*Q1C-Q12)/3.DC/Q11                                          215
      AA=1.DC/S/SR                                                       216
      B12=P13*A*AA                                                       217
      B13=(9.DC*P14-(1.6D1*P12))*AA/7.DC                                 218
      B14=(C1M1*A-Q1C)*AA                                                219
      B15=(C15*A+((2.5D1*C16-(3.6D1*Q14))/1.1D1))*AA                     22C
      B16=(Q14*A+((1.6D1*C15-(2.5D1*C13))/9.DC))*AA                      221
```

```
      B17=(Q13*A+((9.D0*Q14-(1.6D1*Q12))/7.D0))*AA                          222
      B18=(Q12*A+((4.D0*Q13-(9.D0*Q11))/5.D0))*AA                           223
      B19=(Q10*A-Q11)*AA                                                   224
      B20=(Q15*QCC*A+((2.5D1*Q16-(2.6D1*Q14))*QCC/1.1D1)-Q15)*AA           225
      B21=(Q13*QCC*A+((9.D0*Q14-(1.6D1*Q12)))*QCC/7.D0-Q13)*AA             226
      B22=-Q11*AA                                                          227
      B23=(Q1M1*QCC*A+(Q1C*QCC)+(Q1M1))*AA                                 228
      B24=(A-(3.D0*S))*AA                                                  229
C  FINISHED CALCULATING THE B SHAPE FACTORS
C  THE FOLLOWING PART OF THE PROGRAM CALCULATES THE A AND R SHAPE FACTORS
      A=1.DC/(QCC-(1.DC/S))                                                3C1
      AA=1.DC/(QCC-(S/S1))                                                 3C2
      R1=(-QCC/2.DC/S+(1.DC/2.DC/S1))*A                                    3C3
      R4=((-1.DC/2.DC/S-(1.DC/S/S1))*QCC+(5.D-1/S1))*AA                    3C9
      IF(S.GT.1.25) GC TC 30
      R2=(-S2*QCC*QCC/2.DC+((S-(1.DC/1.2D1/S))*QCC)-5.D-1+(1.DC/1.2D1/S1   3C4
     A))*A                                                                 3C5
      R3=((-9.DC*S4/8.DC+(5.DC*S2/8.DC))*QCC*QCC+(((9.DC*S3/4.DC)-(3.7D1   3C6
     A*S/3.2D1)+(2.3D1/4.8D2/S))*QCC)+(-9.DC*S2/8.DC)+(1.7D1/3.2D1)+(1.1   3C7
     BD1/2.4D2/S1))*A                                                      3C8
      R5=((1.5DC*S2-1.5DC)*QCC*QCC+((-3.DC*S-(5.D-1/S)-(1.DC/S/S1))*QCC)   3C9
     A+1.5DC+(2.DC/S1))*AA                                                 311
      R6=((4.5D1*S4/8.DC-(7.5DC*S2)+(1.5D1/8.DC))*QCC*QCC+((-4.5D1*S3/4.   312
     ADC+(7.5D1*S/1.6D1)-(2.3D1/1.6D1/S)-(1.DC/S/S1)))*QCC)+(4.5D1*S2/8.D  313
     BC)+(4.9D1/1.6C1)+(1.9D1/8.DC/S1))*AA                                 314
      GC TC 7C
C   IF S IS GREATER THAN 1.25 , R2,R3,R5,R6 ARE CALCULATED BY SERIES
C  IN THE FOLLOWING PART OF THE PROGRAM
   30 SUMR2=C.DC
      SUMR5=0.DO
      DC 39 M=1,1CC
      AM=M
      M1=M+1
      M2=M+2
      M3=M+3
      ACA=1.DO/(2.DO*AM+1.DO)
      ACB=1.DC/(2.DC*AM+3.DC)
      ACC=1.DO/(2.DO*AM+1.DO)
      SUMBA=C.DO
      DC 31 J=1,M
      K=J-1
      SBA=2*M-2*K-1
      SUMBA=SUMBA+1.DC/SBA
   31 CCNTINUE
      BAA=SUMBA
      SUMCA=C.DO
      DC 32 J=1,M1
      K=J-1
      SCA=(2*K+1)*(2*M-2*K+1)
      SUMCA=SUMCA+1.DC/SCA
   32 CCNTINUE
      CCA=SUMCA
      SUMCB=C.DO
      DC 33 J=1,M2
      K=J-1
      SCB=(2*K+1)*(2*M-2*K+3)
      SUMCB=SUMCB+1.DO/SCB
   33 CCNTINUE
      CCB=SUMCB
      SUMCC=0.DO
      SS=S**(-2-2*M)
      SR2=(-CCB/2.DC+ACB-ACA/1.2D1+1.DC/1.2D1)*SS
```

```
      SR5=(3.D0*CCB/2.D0-3.D0*CCA/2.D0-3.D0*ACB-ACA/2.D0-BAA+2.D0)*SS
      IF(M.EQ.1)GO TO 35
      IF(M.EQ.2) GO TO 36
      GO TO 37
   35 SR2=0.D0
   36 SR5=0.D0
   37 SUMR2=SUMR2+SR2
      SUMR5=SUMR5+SR5
      IF(M.LT.5) GO TO 39
      SUA2=DABS(SR2/SUMR2)
      SUA5=DABS(SR5/SUMR5)
      SUX2=SUA2-1.D-14
      SUX5=SUA5-1.D-14
      IF(SUX2.GT.0.D0) GO TO 39
      IF(SUX5.GT.0.D0) GO TO 39
      GO TO 40
   39 CONTINUE
   40 R2=SUMR2*A
      R5=SUMR5*AA
      SUMR3=0.D0
      SUMR6=0.D0
      DO 80 MC=1,100
      ABSUM=0.D0
      BBSUM=0.D0
      M=MC-1
      AM=M
      DO 79 KC=1,MC
      AASUM=0.D0
      BASUM=0.D0
      K=KC-1
      AK=K
      DO 78 JC=1,KC
      J=JC-1
      AJ=J
      AAS=(6.3D1/8.D0/(2.D0*(AK-AJ)+1.1D1)-(7.D1/8.D0/(2.DC*(AK-AJ)+9.DC
     A))+(1.5D1/8.DC/(2.DC*(AK-AJ+7.D0)))/(2.D0*AJ+3.DC)
      BAS=AAS*(2.D0*AJ+3.D0)*(2.D0*(AK-AJ)+6.DC)*(1.DC/(2.DC*AJ+1.D0)-1.
     ADC/(2.D0*AJ+3.D0))
      AASUM=AASUM+AAS
      BASUM=BASUM+BAS
   78 CONTINUE
      ABS=AASUM/(2.D0*AK+7.DC)
      BBS=BASUM/(2.D0*AK+7.DC)
      ABSUM=ABSUM+ABS
      BBSUM=BBSUM+BBS
   79 CONTINUE
      ASR3=ABSUM/(S**(2*M+10))
      ASR6=BBSUM/(S**(2*M+10))
      SUMR3=SUMR3+ASR3
      SUMR6=SUMR6+ASR6
      SU1=DABS(ASR3/SUMR3)-1.D-14
      SU2=DABS(ASR6/SUMR6)-1.D-14
      IF(SU1.GT.0.DC) GO TO 80
      IF(SU2.GT.0.DC) GO TO 80
      GO TO 75
   80 CONTINUE
   75 R3=A*SUMR3
      R6=-AA*SUMR6
   70 R7=(AGSQ-1.D0)/(AGSQ+1.D0)                                        315
      R8=.5DC/(AGSQ+1.DC)                                               316
      R9=A                                                              317
      R10=AA                                                            318
```

```
      R11=(AGSQ-1.DO)/(AO**(2.DO/3.DO))                                  319
      A1=A/AA                                                            320
      A2=(QOO*((2.DO-S2)/(S*S1)))*AA                                     321
C FINISHED CALCULATING THE A AND B SHAPE FACTORS
C  THE FOLLOWING PART OF THE PROGRAM CALCULATES THE S SHAPE FACTORS
C  FROM THE VELOCITY FIELDS AND MUST BE CALCULATED AFTER B AND B FUNCTIONS
C  HAVE BEEN CALCULATED
      S1T=-5.DO/6.DO                                                     4O1
      S1B=(2.D2*QO2*QO5/1.89D2)-(2.D2*QO2*QO3/1.89D2)-(4.D1*QO4*QO3/2.1O  4O2
     A1)+(4.D1*QO4*QO1/2.1D1)                                            4O3
      S1=S1T/S1B                                                         4O4
      S2=-(4.D1*QO4*S1/6.3D1/QO2)-(PO2/QO2/3.DO)                         4O5
      S3=-(S1*(5.DO*PO2+PO)/(QO4-QO2))*4.9D1/1.O8D2                      4O6
      S4=((1.O24D3*Q14*Q14*Q13*Q12*Q12/7.35D2)+(2.355ED4*Q14*Q14*Q13*Q12  4O7
     A*Q1O/5.145D3)-(7.68D2*Q14*Q14*Q12*Q12*Q11/2.45D2)-(1.766ED4*Q14*Q1  4O8
     B4*Q12*Q11*Q1O/1.715D3)+(4.O96D3*Q14*Q13*Q12*Q12*Q1O/1.715D3)-(9.21  4O9
     C6D3*Q14*Q12*Q12*Q11*Q1O/1.715D3)+(6.912D3*Q14*Q14*Q13/1.2OO5D4)-(1  41O
     O.555ED4*Q14*Q14*Q11/1.2OO5D4)-(5.424D3*Q14*Q13*Q12/1.2OO5D4)+(2.45  411
     E52D4*Q14*Q12*Q11/1.2OO5D4)-(9.6D1*Q14*Q13*Q1O/2.45D2)+(2.16D2*Q14*  412
     FQ11*Q1O/2.45D2)-(9.625E48D6*Q13*Q12*Q12/8.751E45D6)+(9.O7O4D4*Q13*  413
     GQ12*Q1O/1.78605D5)-(3.2D1*Q13*Q1O*Q1O/7.29D2)+(2.745D3*Q12*Q12*Q11  414
     H/1.2OO5D4)-(3.84D2*Q12*Q11*Q1O/2.45D2))*4.DO*Q14*Q12/3.DO         415
      S5=((-4.DO*Q12*P13/9.DO)+(Q12*P11)-(4.DO*Q13*P12/9.DO)+(Q11*P12))*  416
     A8.DO*Q14*Q12*Q1O/2.5D1                                             417
      S6=((Q14*Q12*P11)-(1.28D2*Q15*Q12*P12/1.89D2)+(4.DO*Q14*Q13*P12/7.  418
     ADO)-(Q14*Q11*P12)+(2.D2*Q13*Q12*P12/1.89D2))*8.DO*Q12*Q1O/1.5D1    419
      S7=S5/S4                                                           42O
      S8=S6/S4                                                           421
      S9=-1.8D1*Q14/7.DO/Q1O                                             422
      S1O=((-1.D1*Q14*Q12/2.1D1)-(2.D1*Q14*Q1O/2.1D1)+(6.4D2*Q14*Q14*Q12  423
     A*Q12/4.1D1)+(1.472D4*Q14*Q14*Q12*Q1O/3.O87D3)+(2.56D3*Q14*Q12*Q12*  424
     BQ1O/1.029D3))/ Q12/Q1O                                             425
      S11=4.DO*P12/2.7D1/Q12-(S1O*S7)                                    426
      S12=(2.D1*P12/6.3D1/Q12+(S1O*S8))                                  427
      S13=((4.8D1*Q14*Q12*Q12/3.5D1)+(1.1O4D3*Q14*Q12*Q1O/2.45D2)+(1.152  428
     AD3*Q12*Q12*Q1O/2.45D2))/Q1O                                        429
      S14=-S13*S7                                                        43O
      S15=2.DO*P12/5.DO/Q14+(S13*S8)                                     431
      S16=((8.DO*Q14*Q12*P11/7.5D1)+(1.6D1*Q14*Q12*P13/2.55D2)-(5.18D2*Q  432
     A15*Q12*P12/2.835D3)+(3.52D2*Q14*Q13*P12/1.575D3)-(8.8D1*Q14*Q11*P1  433
     B2/1.75D2)+(1.6D2*Q12*Q12*P12/5.67D2))*Q12*Q1O                      434
      S17=S16/S4                                                         435
      S18=S1O*S17+(1.1D1*P12/6.3D1/Q12)                                  436
      S19=S13*S17-(P12/5.DO/Q14)                                         437
      S2O=-4.D2*Q25*Q22/7.DO+(1.D3*Q23*Q22/7.DO)+(1.2D2*Q24*Q23/7.DO)-(7  438
     A.2D2*Q24*Q21/7.DO)                                                 439
      S21=P23*Q22-(Q23*P22)+(6.DO*Q21*P22)                               440
      S22=1.D2*P22*Q25*Q22/6.3D2-(2.5D2*P22*Q23*Q22/6.3D1)-(1.D1*P22*Q24  441
     A*Q23/2.1D1)+(2.D1*P22*Q24*Q21/7.DO)-(1.D1*P23*Q24*Q22/2.1D1)+(1.D1  442
     B*P22*Q24*Q23/2.1D1)-(2.D1*P22*Q24*Q21/7.)                          443
      S23=S21/S2O                                                        444
      S24=S22/S2O                                                        445
C  FINISHED CALCULATING THE 24 S SHAPE FACTORS
C  THE FOLLOWING PART OF THE PROGRAM CALCULATES THE ALPHAS FOR THE PURE
C  HYDRODYNAMIC PART OF THE CORRECTION (ALA(I) )
      SA2=S*S                                                            5O1
      SA1=SA2-1.DO                                                       5O2
      SA3=SA2*S                                                          5O3
      SA4=SA3*S                                                          5O4
      SA5=SA4*S                                                          5O5
      SA6=SA5*S                                                          5O6
      AO1(I)=A1                                                          5O7
```

```
      AD2(I)=A2                                                          5C8
      AA1=1.DO-A1                                                        5C9
      AA2=1.DO-A2                                                        51C
C        THE FOLLOWING CALCULATES THE ALPHAS AND BETAS FOR THE K11 CONTRIBUTION
      AL1(I)=R7*R7*AA1/5.25D3
      AL2(I)=-R7*R7*AA2*((5.DO*SA2)-7.DO)/2.1D4
      AL3(I)=-R7*R7*BO*AA1/5.25D3
      AL4(I)=-(R7*R7*B12*AA1/1.575D4)-(R7*R7*BO*AA2/3.5D3)
      AL5(I)=-(R7*R7*B12*AA2/1.575D4)
      AL6(I)=-R7*R7*B11*SA2/1.05D3
      AL7(I)=-R7*R7*B11*SA1/1.05D3
      AL8(I)=-R7*R7*B1*AA1/5.25D3
      AL9(I)=-(R7*R7*B13*AA1/1.575D4)-(R7*R7*B1*AA2/3.5D3)
      AL10(I)=-R7*R7*B13*AA2/1.575D4
      B2A=-(R7*S7*S9+(R7*R7*S8*S9))/6.3D2
      B3A=-8.DO*(S14+(R7*S15))*R7/2.7783D4
      B4A=2.DO*R7*S1/1.9845D4
      B5A=R7*(8.DO*S1/9.9225D4+(S2/1.75D3)-(1.2D1*S7/6.125D3)-(S7*S9/5.2
     A5D3)-(1.2D1*R7*S8/6.125D3)-(R7*S8*S9/5.25D3)-(S11/5.25D2)-(R7*S12/
     B5.25D2)-(4.DO*S14/3.969D3)-(4.DO*R7*S15/3.969D3))
      X=B2*B2A+(B3*B3A)+(B4*B4A)+(B5*B5A)
      R1A=(S7*S9+(R7*S8*S9))*2.DO*R7*R11/3.15D2
      B2A=((1.6D1*S1/1.9845D4)+(S2/3.5D1)-(2.4D1*S7/1.225D3)-(S7*S9/5.25
     AD2)-(2.4D1*R7*S8/1.225D3)-(R7*S8*S9/5.25D2)-(1.2D1*S11/1.225D3)+(1
     B.2D1*R7*S12/1.225D3)+(1.6D1*S14/1.323D3)-(1.6D1*R7*S15/1.323D3))*R
     C11*R7
      B3A=((8.DO*S1/2.835D3)-(1.6D1*S14/5.67D2)+(1.6D1*R7*S15/5.67D2))*R
     A11*R7
      Y=R1*R1A+(R2*B2A)+(B3*B3A)
      AL11(I)=X+Y
      B14A=(S7+(R7*S8))*R7*S9/6.3D2
      B15A=(2.DO*S1/3.307SD4+(4.DO*S14/1.9845D4)-(4.DO*R7*S15/1.9845D4)+
     A(8.DO*S23/7.35D2))*R7
      B17A=(-2.DO*S1/3.307SD4+(S2/1.75D3)+(S7/1.575D4)+(R7*S8/6.125D3)+(
     AR7*S8*S9/1.575D4)+(S11/2.45D3)-(R7*S12/2.45D3)+(S14/3.969D3)-(R7*S
     B15/3.969)-(4.DO*S23/1.47D2)+(6.DO*S24/8.75D2))*R7
      X=B14*B14A+(B15*B15A)+(B17*B17A)
      R4A=-(S7*S9+(R7*S8*S9))*R11*R7/3.25D2
      B5A=(-4.DO*S1/6.615D3+(S2/1.75D2)+(2.DO*S7/1.225D3)-(S7*S9/1.575D3
     A)+(2.DO*R7*S8/1.225D3)-(R7*S8*S9/1.575D3)+(S11/1.75D2)-(R7*S12/1.7
     B5D2)+(1.D1*S14/3.969D3)-(1.D1*R7*S15/3.969D3)-(4.D1*S23/1.47D2)+(1
     C.2D1*S24/1.75D2))*R11*R7
      R6A=(8.DO*S1/4.725D3+(1.6D1*S14/2.835D3)-(1.6D1*R7*S15/2.835D3)+(3
     A.2D1*S23/1.05D2))*R11*R7
      Y=R4*R4A+(R5*R5A)+(R6*R6A)
      AL12(I)=X+Y
      B2A=-1.DO/6.3D2
      B4A=3.8D2*S1/9.9225D4
      B5A=(-1.DO+R7)/5.25D3
      B6A=2.DO*S1/2.205D3+(2.DO*S2/5.25D2)
      B7A=S1/7.35D3-(S2/5.25D2)
      B8A=2.DO*S1/1.9845D4
      B9A=8.DO*S1/9.9225D4+(S2/1.75D3)
      B10A=4.DO*S1/1.9845D4+(S2/2.625D3)
      X=(B2A*B2+(B4A*B4)+(B5A*B5)+(B6A*B6)+(B7A*B7)+(B8A*B8)+(B9A*B9)+(B
     A10A*B10))*R9*R7
      AL13(I)=X
      B2A=-R10*R7/3.15D3
      B4A=(S14+(R7*S15))*1.6D1*R10*R7/9.261D3
      B6A=(1.6D1*S7/1.225D3-(1.6D1*R7*SP/1.225D3)+(2.DO*S7*S9/1.575D3)-(
     A2.DO*R7*S8*S9/1.575D3)-(S11/8.4D1)-(R7*S12/8.4D1)+(2.DO*S14/3.43D2
     B)+(2.DO*R7*S15/3.43D2))*R10*R7
```

```
      B7A=(1.3D1*S7/1.225D3-(1.3D1*R7*S8/1.225D3)+(3.1D1*S7*S9/6.3D3)-(3
     A.1D1*R7*S8*S9/6.3D3)-(S11/7.D2)-(R7*S12/7.D2)+(2.D0*S14/2.205D3)+(
     B2.D0*R7*S15/2.205D3))*R1C*R7
      B8A=-(S14+(R7*S15))*8.D0*R1C*R7/2.778D4
      B9A=(1.2D1*S7/6.125D3-(1.2D1*R7*S8/6.125D3)+(S7*S9/5.25D3)-(R7*S9*
     AS9/5.25D3)-(S11/5.25D2)-(R7*S12/5.25D2)-(4.D0*S14/3.969D3)-(4.D0*R
     B7*S15/3.969D3))*R1C*R7
      B1CA=(1.2D1*S7/6.125D3-(1.2D1*R7*S8/6.125D3)+(1.1D1*S7*S9/7.875D3)
     A-(1.1D1*R7*S8*S9/7.875D3)+(S11/5.25D2)+(R7*S12/5.25D2)-(1.52D2*S14
     B/1.3891505)-(1.52D2*R7*S15/1.3891505))*R1C*R7
      B11A=(S7/1.225D3-(R7*S8/1.225D3)+(S7*S9/9.D2)-(R7*S8*S9/9.D2)+(S11
     A/7.D2)+(R7*S12/7.D2)+(S14/2.205D3)+(R7*S15/2.205D3))*R1C*R7
      X=B2*B2A+(B4*B4A)+(B6A*B6)+(B7A*B7)+(B8A*B8)+(B9A*B9)+(B10A*B10)+(
     AB11A*B11)
      B14A=B9*R7/2.1D3
      B16A=(1.3D1*S14/1.5845D4-(1.3D1*R7*S15/1.9845D4))*R9*R7
      B17A=-B9*R7/1.575D4
      B18A=(S7*S9/1.89D4+(R7*S8*S9/1.89D4)+(3.D0*S11/9.8D2)-(3.D0*R7*S12
     A/9.8D2)+(1.1D1*S14/5.67D3)-(1.1D1*R7*S15/5.67D3))*B9*R7
      B19A=(-S7/7.D2-(R7*S8/7.D2)+(1.7D1*S7*S9/7.35D3)+(1.7D1*R7*S8*S9/7
     A.35D3)-(S11/9.8D2)+(R7*S12/9.8D2)-(5.83D2*S14/7.938D4)+(5.83D2*R7*
     BS15/7.938D4))*R9*R7
      B2CA=((4.D0*S14/1.5845D4)-(4.D0*R7*S15/1.5845D4))*R9*R7
      B21A=(2.D0*S7/6.125D3+(2.D0*R7*S8/6.125D3)-(S7*S9/7.875D3)-(R7*S8*
     AS9/7.875D3)+(S11/1.225D3)-(R7*S12/1.225D3)+(2.D0*S14/2.835D3)-(2.D
     B0*R7*S15/2.835D3))*B9*R7
      B22A=(4.D0*S7/6.125D3+(4.D0*R7*S8/6.125D3)-(2.D0*S7*S9/7.875D3)-(2
     A.D0*R7*S8*S9/7.875D3)-(S11/7.D2)+(R7*S12/7.D2))*B9*R7
      B23A=(-3.D0*S7/1.225D3-(3.D0*R7*S8/1.225D3)+(S7*S9/9.D2)+(R7*S8*S9
     A/9.D2)-(S14/2.205D3)+(R7*S15/2.205D3))*B9*R7
      Y=B14*B14A+(B16*B16A)+(B17*B17A)+(B18*B18A)+(B19*B19A)+(B20*B20A)+
     A(B21*B21A)+(B22*B22A)+(B23*B23A)
      AL14(I)=X+Y
      B14A=-1.D0/4.5D2
      B16A=1.3D1*S1/5.67D4+(1.3D1*S23/3.15D2)
      B17A=-7.D0/2.25D4-(1.D0*R7/1.575D4)
      B18A=3.1D1*S1/5.67D4-(2.9D1*S23/3.15D2)+(1.2D1*S24/1.75D2)
      B19A=2.D0*S1/1.4175D4-(S2/8.D1)+(S23/6.23D2)-(1.7D1*S24/7.D2)
      B2CA=S1/1.4175D4+(4.D0*S23/3.15D2)
      B21A=-S1/1.4175D4+(S2/7.5D2)-(1.6D1*S23/3.15D2)+(2.D0*S24/1.25D2)
      B22A=S1/2.835D4+(7.D0*S2/5.D2)+(1.39D2*S23/6.3D2)-(1.3D1*S24/3.75D
     A2)
      B23A=S1/5.25D2-(S2/1.D2)+(3.D0*S24/1.75D2)
      B24A=-2.D0*S23/1.05D2
      Y=(B14A*B14+(B16A*B16)+(B17A*B17)+(B18A*B18)+(B19A*B19)+(B2CA*B2C)
     A+(B21A*B21)+(B22A*B22)+(B23A*B23)+(B24A*B24))*R10*R7
      AL15(I)=Y
C  FINISHED CALCULATING THE PURE HYDRODYNAMIC ALPHAS
      BL1(I)=-AA1*R7*R7/5.25D3
      BL2(I)=AA2*((5.D0*SA2)-7.D0)*R7*R7/2.1D4
      BL3(I)=AA1*BC*R7*R7/5.25D3
      BL4(I)=AA1*B12*R7*R7/1.575D4+(AA2*BC*R7*R7/3.5D2)
      BL5(I)=AA2*B12*R7*R7/1.575D4
      BL6(I)=SA2*B11*R7*R7/1.05D3
      BL7(I)=SA1*B11*R7*R7/1.05D3
      BL8(I)=AA1*B1*R7*R7/5.25D3
      BL9(I)=AA1*B13*R7*R7/1.575D4+(AA2*B1*R7*R7/3.5D2)
      BL10(I)=AA2*B13*R7*R7/1.575D4
      B2A=S8*S9/6.3D2
      B3A=8.D0*S15/2.778D4
      B5A=1.2D1*S8/6.125D3+(S8*S9/5.25D3)-(S12/5.25D2)+(4.D0*S15/3.969D3
     A)
```

```
      X=((B2A*B2)+(B3A*B3)+(B5A*B5))*R7*R7
      B1A=-2.DO*S8*S9/3.15D2
      B2A=S7*S9/5.25D2+(2.4D1*S8/1.225D3)+(S8*S9/5.25D2)-(1.2D1*S12/1.22
     A5D3)+(1.6D1*S15/1.323D3)
      B3A=-1.6D1*S15/5.67D2
      Y=(B1A*B1+(B2A*B2)+(B3A*B3))*B11*R7*R7
      BL11(I)=X+Y
      B14A=-S8*S9/6.3D2
      B15A=4.DO*S15/1.9845D4
      B17A=-S8/6.125D3-(S8*S9/1.575D4)+(S15/3.969D3)
      X=(B14A*B14+(B15A*B15)+(B17A*B17))*R7*R7
      B4A=S8*S9/3.15D2
      B5A=-2.DO*S8/1.225D3+(S8*S9/1.575D3)+(S12/7.5D2)+(S15/3.969D2)
      B6A=1.6D1*S15/2.835D3
      Y=(B4A*B4+(B5A*B5)+(B6A*B6))*B11*R7*R7
      BL12(I)=X+Y
      BL13(I)=-R7*R7*R9/5.25D3
      B4A=-1.6D1*S15/9.261D3
      B6A=1.6D1*S8/1.225D3+(2.DO*S8*S9/1.575D3)+(S12/8.4D1)-2.DO*S15/3.4
     A3D2
      B7A=1.3D1*S8/1.225D3+(3.1D1*S8*S9/6.3D2)+(S12/7.D2)-(2.DO*S15/2.2O
     A5D3)
      B8A=8.DO*S15/2.7783D4
      B9A=1.2D1*S8/6.125D3+(S8*S9/5.25D3)+(S12/5.25D2)+(4.DO*S15/3.969D3
     A)
      B10A=1.2D1*S8/6.125D3+(1.1D1*S8*S9/7.875D3)-(S12/5.25D2)+(1.52D2*S
     A15/1.3891505)
      B11A=S8/1.225D3-(S8*S9/9.D2)+(S12/7.D2)-(S15/2.205D3)
      X=(B4A*B4+(B6A*B6)+(B7A*B7)+(B8A*B8)+(B9A*B9)+(B1CA*B10)+(B11A*B11
     A))*B1C*R7*R7
      B16A=1.3D1*S15/1.9845D4
      B18A=-S8*S9/1.89D4+(3.DO*S12/9.8D2)+(1.1D1*S15/5.67D3)
      B19A=S8/7.D2-(1.7D1*S8*S9/7.35D3)-(S12/9.8D2)-(5.83D2*S15/7.938D4)
      B20A=4.DO*S15/1.9845D4
      B21A=-2.DO*S8/6.125D3+(S8*S9/7.875D3)+(S12/1.225D3)+(2.DO*S15/2.83
     A5D3)
      B22A=-4.DO*S8/6.125D3+(2.DO*S8*S9/7.875D3)-(S12/7.D2)-(3.4D1*S15/1
     A.9845D4)
      B23A=3.DO*S8/1.225D3-(S8*S9/9.D2)-(S15/2.205D3)
      Y=(B16A*B16+(B18A*B18)+(B19A*B19)+(B20A*B20)+(B21A*B21)+(B22A*B22)
     A+(B23A*B23))*B9*R7*R7
      BL14(I)=X+Y
      BL15(I)=B1C*R7*R7*B17/1.575D4
C FINISHED CALCULATING THE DIRECT BROWNIAN MOTION ALPHAS
C         THE FOLLOWING CALCULATES THE ALPHAS AND BETAS FOR THE K22 CONTRIBUTION
      AL1(I)=(+R7/1.75D3+(R8/3.75D2))*AA1*R7                                  511
      AL2(I)=(-R7/7.D3-(R8/1.5D3))*AA2*R7*(5.DO*SA2-7.DO)                     512
      AL3(I)=(R7/1.75D3+(R8/3.75D2))*BO*AA1*R7*(-1.DO)                        513
      AL4(I)=((-3.DO*R7/3.5D3-(R8/2.5D2))*BC*AA2+((-R7/5.25D3-(R8/1.125D      514
     A3))*B12*AA1))*R7                                                        515
      AL5(I)=(-R7/5.25D3-(R8/1.125D3))*B12*AA2*R7                             516
      AL6(I)=(-SA2*R7/3.5D2-(SA2*R8/7.5D1))*B11*R7                            517
      AL7(I)=(+R7/3.5DD2+(R8/7.5D1))*B11*R7*SA1                               518
      AL8(I)=(R7/1.75D3+(R8/3.75D2))*B1*AA1*R7*(-1.DO)                        519
      AL9(I)=((-3.DO*R7/5.5D3-(R8/2.5D2))*B1*AA2+((-P7/5.25D3-(R8/1.125D      520
     A3))*B13*AA1))*R7                                                        521
      AL1C(I)=(-R7/5.25D3-(R8/1.125D3))*AA2*B13*R7                            522
      B2A=S7*S9/7.D1-(R7*S8*S9/2.1DD2)-(R8*S8*S9/5.DO)                        523
      B3A=-8.DO*S18/3.969D3+(3.2D1*S14/2.7783D4)+(3.2D1*R7*S15/9.261D3)-      524
     A(1.6D1*R8*S15/3.969D3)                                                  525
      B4A=2.DO*S1/6.615D3                                                     526
      B5A=8.DO*S1/3.3075D4+(3.DO*S2/1.75D3)+(1.32D2*S7/6.125D3)+(1.1D1*S      527
```

```
A7*S9/5.25D3)+(4.D0*S11/5.25D2)+(1.6D1*S14/3.969D3)-(S18/7.5D1)-(4.
BDC*S19/5.67D2)-(3.6D1*R7*S9/6.125D3)-(R7*S8*S9/1.75D3)-(1.D0*R7*S1
C2/1.75D2)-(4.D0*R7*S15/1.323D3)-(2.4D1*R8*S8/8.75D2)-(R8*S8*S9/3.7
D5D2)-(2.D0*R8*S12/7.5D1)-(8.D0*R8*S15/5.67D2)
 X=B2*B2A+(B3*B3A)+(B4*B4A)+(B5*B5A)
C      CARD 533 IS BLANK
 R1A=-2.D0*S7*S9/1.05D2-(S17*S9/4.5D1)+(1.D0*R7*S8*S9)+(2.D0*R8*S9*
AS9/4.5D1)
 B2A=-6.DC*S2/3.5D1+(1.44D2*S7/1.225D3)+(2.DC*S7*S9/1.75D2)+(7.2D1*
AS11/8.75D2)-(3.2D1*S14/4.41D2)+(2.4D1*S17/1.75D2)+(S17*S9/7.5D1)-(
B1.2D1*S18/1.25D2)+(1.6D1*S19/1.89D2)-(7.2DD1*R7*S8/1.225D3)-(1.D0*
CR7*S8*S9/1.75D2)+(3.6D1*R7*S12/8.75D2)-(1.6D1*R7*S15/4.41D2)-(4.8D
D1*R8*S8/1.75D2)-(2.D0*R8*S8*S9/7.5D1)+(2.4D1*R8*S12/1.25D2)-(3.2D1
E*R8*S15/1.89D2)
 B3A=-3.2D1*S1/9.45D2+(3.2D1*S14/1.89D2)-(1.6D1*S19/8.1D1))+(1.6D1*R
A7*S15/1.89D2)+(3.2D1*R8*S15/8.1D1)
 Y=(R1*R1A+(R2*R2A)+(R3*R3A))*R11
 AL11(I)=(X+Y)*R7
 B14A=-S17*S9/9.D1-(2.DC*S7*S9/3.15D2)+(S8*S9*R7/2.1DD2)+(R8*S8*S9/
A4.5D1)
 B15A=4.DC*S1/9.9225D4-(1.6D1*S14/1.5845D4)+(4.D0*S19/2.835D3)-(4.D
AO*S23/7.35D2)-(4.DC*R7*S15/6.615D3)-(8.DC*R8*S15/2.835D3)
 B17A=-4.DC*S1/9.9225D4+((S2/2.625D3)-(4.DC*S7/6.125D3)+(2.DC*S7*S9
A/7.875D3)-(2.D0*S11/1.225 D3)-(4.DC*S14/3.969D3)-(S17/8.75D3)+(S17
B*S9/2.25D3)+(S18/3.5D2)+(S19/5.67D2)+(2.DC*S23/1.47D2)-(3.DC*S24/8
C.75D2)+(3.D0*R7*S8/6.125D3)+(R7*S8*S9/5.25DD3)+(3.DC*R7*S12/2.45DD
D3)-(1.DC*R7*S15/1.323D3)+(2.DC*R8*S8/8.75D2)+(R8*S8*S9/1.125D3)-(R
E8*S12/1.75D2)-(2.DC*R8*S15/5.67D2))
 X=B14*B14A+(B15*B15A)+(B17*B17A)
 R4A=(2.D0*S7*S9/1.05D2)+(S17*S9/4.5D1)-(1.D0*R7*S8*S9/1.05D2)-(2.D
AO*R8*S8*S9/4.5D1)
 B5A=-4.DC*S1/6.615D3+(S2/1.75D2)-(1.2D1*S7/1.225D2)+(2.D0*S7*S9/5.
A25D2)-(6.D0*S11/1.75D2)-(2.D1*S14/1.323D3)-(2.D0*S17/1.75D2)+(S17*
BS9/2.225D2)+(S18/2.5D1)+(S19/2.67D1)+(2.8D2*S23/4.41D2)-(2.3D1*S24
C/1.75D2)+(0.6D1*R7*S9/1.225D3)-(1.D0*R7*S8*S9/5.25D2)-(3.D0*R7*S12
D/1.75D2)-(1.D2*R7*S15/1.323D2)+(4.DC*R8*S8/1.75D2)-(2.D0*R8*S8*S9/
E2.25D2)-(2.DC*R8*S12/2.5D1)-(2.D1*R8*S15/5.67D2)
 R6A=8.D0*S1/4.725D3-(3.2D1*S14/9.45D2)+(1.6D1*S19/4.05D2)-(1.84D2*
AS23/3.15D2)-(1.6D1*R7*S15/9.45D2)-(3.2D1*R8*S15/4.05D2)
 Y=(R4*R4A+(R5*R5A)+(R6*R6A))*R11
 AL12(I)=(X+Y)*R7
 B2A=-1.DC/2.1D3
 B4A=3.8D1*S1/3.3C75D4
 B5A=-1.D0/1.75D3+(R7/1.75D3)+(R8/3.75D2)
 B6A=2.DC*S1/7.35D2+(2.DC*S2/1.75D2)
 B7A=S1/2.45D3-(S2/1.225D3)
 B8A=2.DC*S1/6.615D3
 B9A=S1*8.DD/3.3C75D4+(3.DC*S2/1.75D3)
 B1CA=4.D0*S1/6.615D3+(S2/8.75D2)
 X=(B2*B2A+(B4*B4A)+(B5*B5A)+(B6*B6A)+(B7*B7A)+(B8*B8A)+(B9*B9A)+(B
A10A*B10))*R9
 AL13(I)=X*R7
 B2A=1.DC/1.75D2
 B4A=1.6D1*S19/3.087D3+(1.6D1*R7*S15/3.C87D3)+(3.2D1*R8*S15/1.323D5
A)
 B5A=1.DC/1.75D3
 B6A=6.4D1*S7/1.225D3-(8.DC*S7*S9/1.575D3)+(S11/2.1D1)-(8.DO*S14/3.
A43D2)+(1.6D1*S17/1.75D2)+(2.DC*S17*S9/2.25D2)-(S18/1.2D1)+(2.DC*S1
B9/4.9D1)-(4.8D1*R7*S9/1.225D3)-(2.DO*R7*S8*S9/5.25D2)-(R7*S12/0.7D
C1)+(0.6D1*R7*S15/3.43D2)-(3.2D1*R8*S8/1.75D2)-(4.DO*R8*S8*S9/2.25D
D2)-(R8*S12/6.DD)+(4.DD*R8*S15/4.9D1)
 B7A=-5.2D1*S7/1.225D3-(3.1D1*S7*S9/1.575D3)+(S11/1.75D2)-(8.DO*S14
```

```
A/2.2C5D3)+(1.3D1*S17/1.75D2)+(3.1D1*S17*S9/9.D2)-(S18/1.D2)+(2.DC*   590
BS19/3.15D2)-(3.9D1*R7*S8/1.225D3)-(3.1D1*R7*S8*S9/2.10D3)-(3.DO*R7   591
C*S12/7.0D2)+(2.DC*R7*S15/7.35D2)-(2.6D1*R8*S8/1.75D2)-(3.1D1*R8*S8   592
D*S9/4.5D2)-(R8*S12/5.D1)+(4.DC*R8*S15/3.15D2)                        593
 R8A=3.2D1*S14/2.776D4-(8.DO*S19/3.969D3)-(C.8D1*R7*S15/9.261D3)-(    594
A1.6D1*R8*S15/3.969D3)                                                595
 R9A=-4.8D1*S7/6.125D3-(2.DC*S7*S9/2.625D3)+(4.DO*S11/5.25D2)+(1.6D   596
A1*S14/3.969D3)+(1.2D1*S17/8.75D2)+(S17*S9/7.5D2)-(S18/7.5D1)-(4.DO   597
B*S19/5.67D2)-(R7*((2.6D1*S8/6.125D3)+(S8*S9/1.75D3)+(1.DO*S12/1.75   598
CD2)+(4.DO*S15/1.323D3)))+(R8*((-2.4D1*S9/8.75D2)-(S8*S9/3.75D2)-(2   599
C.DC*S12/7.5D1)-(8.DC*S15/5.67D2)))                                   600
 R10A=-4.8D1*S7/6.125D3-(4.4D1*S7*S9/7.875D3)-(4.DC*S11/5.25D2)+(6.   601
AC8D2*S14/1.389150S)+(1.2D1*S17/8.75D2)+(1.1D1*S17*S9/1.125D3)+(S18   602
B/7.5D1)-(1.52D2*S19/1.9845D4)-(3.6D1*S8/6.125D3-(1.DC*S12/1.75D2)+   603
C(1.52D2*S15/4.630SD4))*R7-(2.4D1*S8/8.75D2+(2.DC*S12/7.5D1)-(3.04D   604
D2*S19/1.9845D4))*R8                                                  605
 R11A=-4.DC*S7/1.225D3-(S7*S9/2.25D2)-(S11/1.75D2)-(4.DO*S14/2.205D   606
A3)+(S17/1.75D2)+(7.DO*S17*S9/9.D2)+(S18/1.D2)+(S19/3.15D2)-(3.DC*S   607
B8/1.225D3+(S8*S9/3.CD2)-(3.DC*S12/7.CD2)-(1.DC*S15/7.35D2))*R7+(-2   608
C.DC*S8/1.75D2-(7.DC*S8*S9/4.5D2)+(S12/5.D1)+(2.DO*S15/3.15D2))*R8    609
 X=(R2A*R2+(R4A*R4)+(R5A*R5)+(R6A*R6)+(R7A*R7)+(R8A*R8)+(R9A*R9)+(R   610
A1CA*R1C)+(R11A*R11))*R10                                             611
 R14A=1.DO/7.D2                                                       612
 R16A=-5.2D1*S14/1.9845D4+(1.3D1*S19/2.835D3)-(1.3D1*R7*S15/6.615D3   613
A)-(2.6D1*S9*S15/2.835D3)                                             614
 R17A=2.DO/7.875D3                                                    615
 R18A=-S7*S9/4.725D2-(3.DO*S11/2.45D2)-(2.2D1*S14/2.835D3)-(S17*S9/   616
A 2.7D3)+(3.DC*S18/1.4D2)+(1.1D1*S19/8.1D2)-(-S8*S9/6.30D3+(9.DO*S1   617
B2/9.8D2)+(1.1D1*S14/1.89D3))*R7+(S8*S9/1.35D3-(3.DO*S12/7.D1)-(1.1   618
CD1*S14/4.C5D2))*R8                                                   619
 R19A=(S7/1.75D2)-(3.4D1*S7*S9/3.675D3)+(S11/2.45D2)+(5.83D2*S14/1.   620
A9845D4)+(S17/1.D2)-(1.7D1*S17*S9/1.05D3)-(S18/1.4D2)-(5.83D2*S19/1   621
B.134D4)-(3.DC*S8/7.CD2-(1.7D1*S8*S9/2.45CD3)-(3.DO*S12/9.8D2)-(2.9   622
C3*S15/1.323D4))*R7+(-S8/5.D1+(1.7D1*S8*S9/5.25D2)+(S12/7.D1)+(5.83   623
CD2*S15/5.67D3))*R8                                                   624
 R20A=-1.6D1*S14/1.9845D4+(4.DO*S19/2.835D3)-(4.DO*S15/6.615D3)*R7-   625
A(8.DO*S15*R8/2.835D3)                                                626
 R21A=-8.DC*S7/6.125D3+(4.DC*S7*S9/7.875D3)-(4.DO*S11/1.225D3)-(8.D   627
AO*S14/2.835D3)-(2.DC*S17/8.75D2)+(S17*S9/1.125D3)+(S18/1.75D2)+(2.   628
BDO*S19/4.05D2)-(-0.6D1*S8/6.125D3-(1.DC*S8*S9/2.625D3)+(3.DC*S12/1   629
C.225D3))*R7+(4.DC*S8/8.75D2+(2.DO*S8*S9/1.125D3)-(2.DO*S12/1.75D2)   630
D-(4.DO*S15/4.C5D2))*R8                                               631
 R22A=-1.6D1*S7/6.125D3+(8.DO*S7*S9/7.875D3)+(2.DO*S11/1.75D2)+(1.3   632
A6D2*S14/1.9845D4)-(4.DC*S17/8.75D2)+(2.DC*S17*S9/1.125D3)-(S18/1.D   633
B2)-(3.4D1*S19/2.835D3)-(1.24D2*S8/6.125D3+(2.DC*S8*S9/2.625D3)-(3.   634
CDC*S12/7.CD2)-(3.4D1*S15/6.615D3))*R7+(8.DC*S8/8.75D2-(4.DC*S8*S9/   635
D1.125D3)+(S12/5.D1)+(6.8D1*S15/2.835D3))*R8                          636
 R23A=1.2D1*S7/1.225D3-(S7*S9/5.25D2)+(4.DC*S14/2.205D3)+(3.DO*S17/   637
A1.75D2)-(7.DC*S17*S9/9.D2)-(S19/3.15D2)-(C.9D1*S8/1.225D3-(S8*S9/3   638
B.0D2)-(1.DO*S15/7.35D2))*R7+(-(.DC*S8/1.75D2+(7.DC*S8*S9/4.5D2)+(2   639
C.DO*S15/3.15D2))*R8                                                  640
 Y=(R14*R14A+(R16*R16A)+(R17*R17A)+(R18*R18A)+(R19*R19A)+(R2C*R20A)   641
A+(R21*R21A)+(R22*R22A)+(R23*R23A))*R9                                642
 AL14(I)=(X+Y)*R7                                                     643
 R14A=-2.DO/1.575D3                                                   644
 R16A=1.3D1*S1/9.922SD4-(1.3D1*S23/7.5D2)                             645
 R17A=-2.99D2/1.26D4+(R7/5.25CD3)+(R8/1.125D3)                        646
 R18A=3.1D1*S1/9.922SD4+(2.9D1*S23/7.35D2)-(3.6D1*S24/1.225D3)        647
 R19A=8.DO*S1/9.922SD4-(S2/1.4D2)-(S23/1.47D3)+(5.1D2*S24/4.9D2)      648
 R20A=4.DC*S1/9.922SD4-(4.DO*S23/7.25D2)                              649
 R21A=-4.DO*S1/9.922SD4+(2.DC*S2/2.625D3)+(1.6D1*S23/7.35D2)-(6.DC*   650
AS24/8.75D2)                                                          651
```

```
      B22A=2.D0*S1/9.9225D4+(S2/1.25D2)-(1.39D2*S23/1.4D3)+(1.3D1*S24/1.
     A875D3)
      B23A=4.D0*S1/3.675D3-(S2/1.75D2)-(9.D0*S24/1.225D3)
      B24A=2.D0*S23/2.45D2
      X=(B14A*B14 +(B16A*B16)+(B17A*B17)+(B18A*B18)+(B19A*B19)+(B20A*B20
     A)+(B21A*B21)+(B22A*B22)+(B23A*B23)+(B24A*B24))*B10
      AL15(I)=X*R7
C  FINISHED CALCULATING THE PURE HYDRODYNAMIC ALPHAS
C  THE FOLLOWING PART OF THE PROGRAM CALCULATES THE DIRECT BROWNIAN MOTION
C ALPHAS ( BLA(I) )
      BL1(I)=R7*R7*AA1/1.05D3/4.D1
      BL2(I)=-R7*R7*(5.D0*S2-7.D0)*AA2/4.2D3/4.D1
      BL3(I)=-R7*R7*BC*AA1/1.05D3/4.D1
      BL4(I)=(R7*R7*BC*AA2/7.D2+(R7*R7*B12*AA1/3.15D3))/(-4.D1)
      BL5(I)=-R7*R7*B12*AA2/3.15D3/4.D1
      BL6(I)=-R7*R7*B11*SA2/2.1D2/4.D1
      BL7(I)=R7*R7*B11*SA1/2.1D2 /4.D1
      BL8(I)=-R7*R7*B1*AA1/1.05D3/4.D1
      BL9(I)=(-B1*AA2/7.D2-(B13*AA1/3.15D3))*R7*R7/4.D1
      BL10(I)=-R7*R7*B13*AA2/3.15D3/4.D1
      B2A=-S8*S9/1.26D2
      B3A=-4.D1*S15/6.3D1
      B5A=-1.2D1*S8/1.225D3-(S8*S9/1.05D2)-(S12/1.05D2)-(2.D1*S15/3.969D
     A3)
      X=E2A*P2+(B3A*B3)+(B5A*B5)
      R1A=S8*S9/6.3D1
      R2A=-2.4D1*S8/2.45D2-(2.D0*S8*S9/1.05D2)+(1.2D1*S12/1.75D2)-(8.D0*
     AS15/1.323D3)
      R3A=8.D1*S15/5.67D2
      Y=(R1*R1A+(R2A*R2)+(R3A*R3))*R11
      BL11(I)=(X+Y)*R7*R7/4.D1
      B14A=S8*S9/1.26D2
      B17A=S8*S9/3.15D3+(S8/1.225D3)-(S12/7.35D2)-(9.D0*S15/3.969D3)
      B15A=-4.D0*S15/3.969D3
      X=B14A*B14+(B15A*B15)+(B17A*B17)
      R4A=-S8*S9/6.3D1
      R4A=-S8*S9/6.3D1
      R5A=2.D0*S8/2.45D2-(S8*S9/3.15D2)-(S12/3.5D1)-(5.D1*S15/3.969D3)
      R6A=-1.6D1*S15/5.67D2
      Y=(R4A*R4+(R5A*R5)+(R6A*R6))*R11
      BL12(I)=(X+Y)*R7*R7/4.D1
      B2A=-1.D0/1.26D3
      B4A=3.8D1*S1/1.9845D4
      B5A=-1.D0/1.05D3
      B6A=2.D0*S1/4.41D2+(2.D0*S2/1.05D2)
      B7A=S1/1.47D3-(S2/1.05D3)
      B8A=2.D0*S1/3.969D3
      B9A=8.D0*S1/1.9845D4+(S2/3.5D2)
      B10A=4.D0*S1/3.969D3+(S2/5.25D2)
      X=(P2*B2+(B4A*B4)+(B5A*B5)+(B6A*B6)+(B7A*B7)+(B8A*B8)+(B9A*B9)+(B
     A10A*B10))*B9
      BL13(I)=X*R7*R7 /4.D1
      B6A=- 1.6D1*S9/2.45D2-(2.D0*S8*S9/3.15D2)-(5.D0*S12/8.4D1)+(1.D1*S
     A15/3.4D2)
      B7A=-1.3D1*S8/2.45D2-(3.1D1*S8*S9/1.26D3)-(S12/1.4D2)+(2.D0*S15/4.
     A41D2)
      B8A=-4.D1*S15/2.7783D4
      B9A=-1.2D1*S8/1.225D3-(S8*S9/1.05D3)-(S12/1.05D2)-(2.D1*S15/3.969D
     A3)
      B10A=-1.2D1*S9/1.225D3+(S12/1.05D2)-(1.52D2*S15/2.7783D4)
      B11A=-S8/2.45D2-(S8*S9/1.8D2)+(S12/1.4D2)+(S15/4.41D2)
      X=(B6A*B6+(B7A*B7)+(B8A*B8)+(B9A*B9)+(B10A*B10)+(B11A*B11))*B10
```

```
      B16A=-1.3D1*S15/3.969D3                                                753
      B18A=S8*S9/3.78D3-(3.D0*S12/1.96D2)-(1.1D1*S14/1.134D3)                754
      B19A=-S8/1.4D2+(1.7D1*S8*S9/1.47D3)+(S12/1.96D2)+(5.83D2*S15/1.597     755
     A6D4)                                                                   756
      B20A=2.D0*S8/1.225D3+(S8*S9/1.575D3)-(S12/2.45D2)-(2.D0*S15/5.67D2     757
     A)                                                                      758
      B22A=4.D0*S8/1.225D3-(2.D0*S8*S9/1.575D2)+(S12/2.1D2)+(3.4D2*S15/3     759
     A.969D3)                                                                760
      B23A=-3.D0*S8/2.45D2+(S8*S9/1.8D2)+(S13/4.41D2)                        761
      Y=(B16A*B16+(B18*B18A)+(B19*B19A)+(B20A*B20)+(B21A*B21)+(B22*B22A)     762
     A+(B23A*B23))*R9                                                        763
      BL14(I)=(X+Y)*R7*R7/4.D1                                               764
      BL15(I)=R7*R7*R10*B17/3.15D3 /4.D1                                     765
C FINISHED CALCULATING THE DIRECT BROWNIAN MOTION ALPHAS
C         THE FOLLOWING CALCULATES THE ALPHAS AND BETAS FOR THE K32 CONTRIBUTION
      AL1(I) =(SA2*R7/3.D1-(1.3D1*R7/7.5D2)-(R8*SA2/1.5D1)+(2.D0*R8/7.5D
     A1))*AA1
       AL2(I)=(-4.D0*R7/1.5D3-(R8/3.D2))*AA2*((5.D0*SA2)-7.D0)-(AA2*((5.
     AD0*SA2)-1.D0)/3.D2)
      AL3(I)=(4.D0*R7/3.75D2-(R8/7.5D1))*BC*AA1
      AL4(I)=(-     R7/1.125D3+(R8/2.25D2))*AA1*B12+((R7/2.5D2-(R8/5.D1))
     A*BC*AA2)
      AL5(I)=(-     R7/1.125D3+(R8/2.25D2)+(1.D0/4.5D2))*B12*AA2
      AL6(I)=(4.D0*R7/7.5D1-((R8+1.D0)/1.5D1))*SA2*B11
      AL7(I)=(4.D0*R7/7.5D1-(R8/1.5D1)+(1.D-1))*B11*SA1
      AL8(I)=(4.D0*R7/3.75D2-(R8/7.5D1))*B1*AA1
      AL9(I)=(-     R7/1.125D3+(R8/2.25D2))*B13*AA1+((4.D0*R7/2.5D2-(R8/5
     A.D1))*B1*AA2)
      AL10(I)=(-     R7/1.125D3+(R8/2.25D2)+(1.D0/4.5D2))*B13*AA2
      B2A=(4.D0*S7/4.5D1+(S17/9.D0)+(4.D0*R7*S8/4.5D1)-(R8*S8/9.D0))*S9
      B3A=(6.4D1*S14-(8.D0*S19)+(6.4D1*R7*S15)-(8.D0*R8*S15))/3.969D3
      B4A=(4.D0*S1/2.835D3)
      B5A=1.6D1*S1/1.4175E4+(S2/1.25D2)+(9.6D1*S7/8.75D2)+(4.D0*S7*S9/3.
     A75D2)+(8.D0*S11/7.5D1)+(3.2D1*S14/5.67D2)+(2.4D1*S17/1.75D2)+(S17*
     BS9/7.5D1)-(2.D0*S18/1.5D1)-(4.D1*S19/5.67D2)+(9.6D1*R7*S8/8.75D2)+
     C(4.D0*R7*S8*S9/3.75D2)+(8.D0*R7*S12/7.5D1)+(3.2D1*R7*S15/5.67D2)-(
     D2.4D1*R8*S8/1.75D2)-(R8*S8*S9/7.5D1)-(2.D0*R8*S12/1.5D1)-(4.D1*R8*
     ES15/5.67D2)
      X=B2A*B2+(B3A*B3)+(B4A*B4)+(B5A*B5)
      R1A=(2.D0*S7/4.5D1+(2.D0*S17/9.D0)+(2.D0*R7*S8/4.5D1)-(2.D0*R8*S8/
     A9.D0))*S9
      R2A=3.2D1*S1/2.835D3+(2.D0*S2/5.D0)-(4.8D1*S7/1.75D2)-(2.D0*S7*S9/
     A7.5D1)-(2.4D1*S11/1.75D2)+(3.2D1*S14/1.89D2)-(4.8D1*S17/3.5D1)-(2.
     BD0*S17*S9/1.5D1)+(2.4D1*S18/3.5D1)-(1.6D2*S19/1.89D2)-(4.8D1 *R7*S
     C8/1.75D2)-(2.D0*R7*S8*S9/7.5D1)+(2.4D1*R7*S12/1.75D2)-(3.2 D1*R7*S
     D15/1.89D2)+(4.8D1*R8*S8/3.5D1)+(2.D0*R8*S8*S9/1.5D1)-(2.4D1*R8*S12
     E/3.5D1)+(1.6D2*R8*S15/1.89D2)
      R3A=1.6D1*S1/4.05D2-(3.2D1*S14/8.1D1)+(1.6D2*S19/8.1D1)+(3.2 D1*R7
     A*S15/8.1D1)-(1.6D2*R8*S15/8.1D1)
      Y=(R1A*R1+(R2A*R2)+(R3A*R3))*R11
      AL11(I)=X+Y
      B14A=(S7/4.5D1+(S17/9.D0)+(1.D0*R7*S8/4.5D1)-(R8*S8/9.D1))*S9
      B15A=-2.D0*S1/1.4175D4+(8.D0*S14/2.835D3)-(8.D0*S19/5.67D2)-(3.2D1
     A*S23/3.15D2)-(8. D0*R7*S15/2.835D3)+(8.D0*R8*S15/5.67D2)
      B17A=2.D0*S1/1.4175D4-(S2/7.5D2)-(S3/3.5D2)+(2.D0*S7/8.75D2)-(S7*S
     A9/1.125D3)+(S11/1.75D2)+(2.D0*S14/5.67D2)+(2.D0*S17/1.75D2)-(S17*S
     B9/2.25D2)-(S18/3.5D1)-(S19/5.67D1)+(4.D0*S23/6.3D1)-(2.D0*S24/1.25
     CD2)+(2.D0*R7*S8/8.75D2)+(1.D0*R7*S8*S9/1.125D3)-(1.D0*R7*S12/1.75D
     D2)-(2.D0*R7*S15/5.67D2)-(R8*S8*S9/2.25D2)-(2.D0*R8*S8/1.75D2)+(R8*
     ES12/3.5D1)+(R8*S15/5.67D1)
      X=B14A*B14+(B15A*B15)+(B17A*B17)
      R4A=(8.D0*S7/4.5D1+(2.D0*S17/9.D0)+(8.D0*R7*S8/4.5D1)-(2.D0*R8*S8/
```

```
A5.DC))*S9*R11
 R5A=(4.DO*S1/2.835D3-(S2/7.5D1)+(S3/3.5D1)-(1.6D1*S7/1.75D2)+(8.DO
A*S7*S9/2.25D2)-(8.DO*S11/2.5D1)-(8.DO*S14/5.67D2)-(4.DO*S17/3.5D1)
B+(S17*S9/2.25D1)+(2.DO*S18/5.DO)+(S19/5.67DO)+(2.D1*S23/2.1D1)-
C(6.DO*S24/2.5D1)-(1.6D1*R7*S8/1.75D2)+(8.DO*R7*S8*S9/2.25D2)+(8.DO
D*R7*S12/2.5D1)+(8.D1*R7*S15/5.67D2)+(4.DO*R8*S8/3.5D1)-(2.DO*R8*S8
E*S9/4.5D1)-(2.DO*R8*S12/5.DO)-(R8*S15/5.67DO))*R11
 R6A=(-8.DO*S1/2.025D3-(1.28D2*S14/4.05D2)+(3.2D1*S19/8.1D1)-(1.6D1
A*S23/1.5D1)+(1.28D2*R7*S15/4.05D2)-(3.2D1*R8*S15/8.1D1))*R11
 Y=(R4A*R4+(R5A*R5)+(R6A*R6))
 AL12(I)=X+Y
 B2A=-1.DO/4.5D2
 B4A=7.6D1*S1/1.4175D4
 B5A=-1.DO/3.75D2-(4.DO*R7/3.75D2)+(R8/7.5D1)
 B6A=4.DO*S1/3.15D2+(4.DO*S2/7.5D1)
 B7A=S1/5.25D2-(S2/7.5D1)
 B8A=4.DO*S1/2.835D3
 B9A=1.6D1*S1/1.4175D4+(S2/1.25D2)
 B10A=8.DO*S1/2.835D3+(2.DO*S2/3.75D2)
 AL13(I)=(B2A*B2+(B4A*B4)+(B5A*B5)+(B6A*B6)+(B7A*B7)+(B8A*B8)+(B9A*
AB9)+(B10A*B10))*R9
 B2A=1.4D1/2.25D2
 B4A=-1.28D2*S14/1.323D3+(1.6D2*S19/1.323D3)-(1.28D2*R7*S15/1.323D3
A)+(1.6D2*R8*S15/1.323D3)
 B5A=1.DO/3.75D2
 B6A=-1.2D2*S7/1.75D2-(1.6D2*S7*S9/2.25D2)+(2.DO*S11/3.DO)-(1.6D1*S
A14/4.9D1)+(3.2D1*S17/3.5D1)+(4.DO*S17*S9/4.5D1)-(5.DO*S18/6.DO)+(2
B.DO*S19/4.9D1)+(1.28D2*R7*S8/1.75D2)+(1.6D1*R7*S8*S9/2.25D2)+(2.DO
C*R7*S12/3.DO)-(1.6D1*R7*S15/4.9D1)-(3.2D1*R8*S8/3.5D1)-(4.DO*R8*S8
D*S9/4.5D1)-(5.DO*R8*S12/6.DO)+(2.D1*R8*S15/4.9D1)
 B7A=-1.04D2*S7/1.75D2-(6.2D1*S7*S9/2.25D2)+(2.DO*S11/2.5D1)-(1.6D1
A*S14/3.15D2)+(2.6D1*S17/3.5D1)+(3.1D1*S17*S9/9.D1)-(S18/1.D1)+(4.D
BO*S19/6.3D1)+(1.04D2*R7*S8/1.75D2)+(6.2D1*R7*S8*S9/2.25D2)+(2.DO*R
C7*S12/2.5D1)-(1.6D1*R7*S15/3.15D2)-(2.6D1*R8*S8/3.5D1)-(3.1D1*R8*S
D8*S8*S9/9.D1)-(R8*S12/1.DO)+(4.DO*R8*S15/6.3D1)
 B8A=6.4D1*S14/3.969D3-(8.D1*S19/3.969D3)+(6.4D1*R7*S15/3.969D3)-(8
A.D1*R8*S15/3.969D3)
 B9A=-9.6D1*S7/8.75D2-(4.DO*S7*S9/3.75D2)+(8.DO*S11/7.5D1)+(3.2D1*S
A14/5.67D2)+(2.4D1*S17/1.75D2)+(S17*S9/7.5D1)-(2.DO*S18/1.5D1)-(4.D
B1*S19/5.67D2)+(9.6D1*R7*S8/8.75D2)+(4.DO*R7*S8*S9/3.75D2)+(8.DO*R7
C*S12/7.5D1)+(3.2D1*R7*S15/5.67D2)-(2.4D1*R8*S8/1.75D2)-(R8*S8*S9/7
D.5D1)-(2.DO*R8*S12/1.5D1)-(4.DO*R8*S15/5.67D2)
 B10A=-9.6D1*S7/8.75D2-(8.8D1*S7*S9/1.125D3)-(8.DO*S11/7.5D1)+(1.21
A6D3*S14/1.9845D4)+(2.4D1*S17/1.75D2)+(2.2D1*S17*S9/2.25D2)+(2.DO*S
B18/1.5D1)-(3.04D2*S19/3.969D3)+(9.6D1*R7*S8/8.75D2)+(8.8D1*R7*S8*S
C9/1.125D3)-(8.DO*R7*S12/7.5D1)+(1.216D3*R7*S15/1.9845D4)-(2.4D1*R8
D*S8/1.75D2)-(2.2D1*R8*S8*S9/2.25D2)+(2.DO*R8*S12/1.5D1)-(3.04D2*S1
E5*R8/3.969D3)
 B11A=-8.DO*S7/1.75D2-(1.4D1*S7*S9/2.25D2)-(2.DO*S11/2.5D1)-(2.DO*S
A14/3.15D2)+(2.DO*S17/3.5D1)+(7.DO*S17*S9/9.D1)+(S18/1.D1)+(2.DO*S1
B9/6.3D1)+(8.DO*R7*S8/1.75D2)+(1.4D1*R7*S8*S9/2.25D2)-(2.DO*R7*S12/
C2.5D1)-(2.DO*R7*S15/3.15D2)-(2.DO*R8*S8/3.5D1)-(7.DO*R8*S9*S9/9.D1
D)+(R8*S12/1.D1)+(2.DO*R8*S15/6.3D1)
 X=(B2A*B2+(B4A*B4)+(B5A*B5)+(B6A*B6)+(B7A*B7)+(B8A*B8)+(B9A*B9)+(B
A10A*B10)+(B11A*B11))*B10
 B14A=-2.DO/7.5D1
 B16A=2.6D1*S14/2.835D3-(2.6D1*S19/5.67D2)-(2.6 D1)*R7*S15/2.835D3)+
A(2.6D1*R8*S15/5.67D2)
 B17A=-1.DO/1.125D3
 B18A=S7*S9/1.35D3+(3.DO*S11/7.D1)+(1.1D1*S14/4.05D2)+(S17*S9/2.7D2
A)-(3.DO*S18/1.4D1)-(1.1D1*S19/8.1D1)+(R7*S8*S9/1.35D3)-(3.DO*
BR7*S12/7.0D1)-(1.1D1*R7*S15/4.05D2)+(R8*S8*S9/2.7D2)+(3.DO*R8*S12/
```

```
     C1.4D1)+(1.1D1*R8*S15/8.1D1)
      B19A=-S7/5.D1+(1.7D1*S7*S9/5.25D2)-(S11/7.D1)-(5.83D2*S14/5.67D3)-
     A(S17/1.D1)+(1.7D1*S17*S9/1.05D2)+(S18/1.4D1)+(5.83D2*S19/1.134D3)-
     B(1.DO*R7*S8/5.0D1)+(1.7D1*R7*S8*S9/5.25D2)+(1.DO*R7*S12/7.0D1)+(1.
     C166D3*R7*S15/1.134D4)-(R8*S8/1.D1)+(1.7D1*R8*S8*S9/1.05D2)-(R8*S12
     D /1.4D1)-(5.83D2*R8*S15/1.134D3)
      B20A=8.DO*S14/2.835D3-(8.DO*S19/5.67D2)-(8.DDC*R7*S15/2.835D3)+(8.
     ADC*R8*S15/5.67D2)
      B21A=4.DC*S7/8.75D2-(2.DC*S7*S9/1.125D3)+(2.DC*S11/1.75D2)+(4.DC*S
     A14/4.05D2)+(4.DO*S17/1.75D2)-(2.DC*S17*S9/2.25D2)-(2.DO*S18/3.5D1)
     B-(4.DC*S19/8.1D1)+(4.0DC*R7*S8/8.75D2)-(2.DC*R7*S8*S9/1.125D3)-(2.
     CDC*R7*S12/1.75D2)-(4.0D0*R7*S15/4.05D2)+(4.DC*R8*S8/1.75D2)-(2.DO*
     DR8*S8*S9/2.25D2)+(2.DO*R8*S12/3.5D1)+(4.DC*R8*S15/8.1D1)
      B22A=-4.DO*S7*S9/1.125D3+(8.DC*S7/8.75D2)-(S11/5.D1)-(6.8D1*S14/2.
     A835D3)+(8.DO*S17/1.75D2)-(4.DC*S17*S9/2.25D2)+(S18/1.D1)+(6.8D1*S1
     B9/5.67D2)+(8.CDO*R7*S8/8.75D2)-(4.0DC*R7*S8*S9/1.125D3)+(1.DC*R7*S
     C12/5.0D1)+(6.8D1 *R7*S15/2.835D3)+(8.DC*R8*S8/1.75D2)-(4.DO*R8*S8*
     DS9/2.25D2)-(R8*S12/1.D1)-(6.8D1*R8*S15/5.67D2)
      B23A=-6.DC*S17/3.5D1+(7.DC*S17*S9/9.D1)+(2.DO*S19/6.3D1)-(6.DC*S7/
     A1.75D2)+(7.DO*S7*S9/4.5D2)-(2.DO*S14/3.15D2)-(6.CDO*R7*S8/1.75D2)+
     B(1.4D1*R7*S8*S9/9.CDD2)+(2.DC*R7*S15/3.15D2)-(6.DC*R8*S8/3.5D1)+(7
     C.DO*R8*S8*S9/9.D1)-(2.DO*R8*S15/6.3D1)
      Y=(B14A*B14 +(B16A*B16)+(B17A*B17)+(B18A*B18)+(B19A*B19)+(B20A*B20
     A)+(B21A*B21)+(B22A*B22)+(B23A*B23))*R9
      AL14(I)=X+Y
      B14A=1.D-2
      B16A=-1.3D1*S1/2.835D4-(2.6D1*S23/3.15D2)
      B17A=1.DO/4.5D2+(4.DO*R7/1.125D3)-(R8/2.25D2)
      B18A=3.1D1*S1/2.835D4+(5.8D1*S23/3.15D2)-(2.4D1*S24/1.75D2)
      B19A=-4.DC*S1/1.4175D4+(S2/4.D1)-(S23/3.15D2)+(1.7D1*S24/3.5D2)
      B20A=-2.DO*S1/1.4175D4-(8.DC*S23/3.15D2)
      B21A=2.DO*S1/1.4175D4-(S2/3.75D2)+(3.2D1*S23/3.15D2)-(4.DO*S24/1.2
     A5D2)
      B22A=-S1/1.4175D4-(7.DO*S2/2.5D2)-(1.39D2*S23/3.15D2)+(2.6D1*S24/3
     A.75D2)
      B23A=-2.DC*S1/5.25D2+(S2/5.D1)-(6.DC*S24/1.75D2)
      B24A=4.DO*S23/1.05D2
      Y=(B14A*B14+(B16A*B16)+(B17A*B17)+(B18A*B18)+(B19A*B19)+(B20A*B20)
     A+(B21A*B21)+(B22A*B22)+(B23A*B23)+(B24A*B24))*R10
      AL15(I)=Y
C  FINISHED CALCULATING THE PURE HYDRODYNAMIC ALPHAS
      BL1(I)=-(5.DC*SA2-2.DO)*AA1*R7/2.5D2
      BL2(I)=-(5.DC*SA2-7.DO)*AA2*R7/1.D3
      BL3(I)=-8C*R7*AA1/2.5D2
      BL4(I)=-(3.DO*BC*R7*AA2/5. D2)-(B12*R7*AA1/7.5D2)
      BL5(I)=-B12*R7*AA2/7.5D2
      BL6(I)=-R7*R11*SA2/5.D1
      BL7(I)=-R7*R11*SA1/5.D1
      BL8(I)=-B1*R7*AA1/2.5D2
      BL9(I)=-(3.DO*B1*R7*AA2/5.D2)-(B13*R7*AA1/7.5D2)
      BL10(I)=-B13*R7*AA2/7.5D2
      B2A=-S8*S9/3.D1
      B3A=-8.DO*S15/1.323D3
      B5A=-3.6D1*S8/8.75D2-(S8*S9/2.5D2)-(S12/2.5D1)-(4.DC*S15/1.89D2)
      X=(B2*B2A+(B3A*B3)+(B5A*B5))*R7
      R1A=S8*S9/1.5D1
      R2A=-S8*S9/2.5D1-(7.2D1*S8/1.75D2)+(3.6D1*S12/1.75D2)-(1.6D1*S15/6
     A.3D1)
      R3A=1.6D1*S15/2.7D1
      Y=(R1A*R1+(R2A*R2)+(R3A*R3))*R11*R7
      BL11(I)=X+Y
      B14A=S8*S9/3.D1
```

```
      B15A=-4.D0*S15/9.45D2
      B17A=S8*S9/7.5D2+(3.D0*S8/8.75D2)-(3.D0*S12/3.5D2)-(S15/1.85D2)
      X=(B14A*B14+(B15A*B15)+(B17A*B17))*B7
      B4A=-S8*S9/1.5D1
      B5A=-S8*S9/7.5D1+(6.D0*S8/1.75D2)-(3.D0*S12/2.5D1)-(S15/1.85D1)
      B6A=-1.6D1*S15/1.25D2
      Y=(B4A*B4+(B5A*B5)+(B6A*B6))*B11*B7
      BL12(I)=X+Y
      BL13(I)=B5*B7*B9/2.5D2
      B4A=1.6D1*S15/4.41D2
      B6A=-4.8D1*S8/1.75D2-(2.D0*S8*S9/7.5D1)-(S12/4.D0)+(6.D0*S15/4.9D1
     A)
      B7A=-3.9D1*S8/1.75D2-(3.1D1*S8*S9/3.D2)-(3.D0*S12)+(2.D0*S15/1.C5D
     A2)
      B8A=-8.D0*S15/1.323D3
      B9A=-3.6D1*S8/8.75D2-(S8*S9/2.5D2)-(S12/2.5D1)-(4.D0*S15/1.89D2)
      B10A=-3.6D1*S8/8.75D2+(S12/2.5D1)-(1.5D2*S15/6.615D3)
      B11A=-3.D0*S8/1.75D2-(7.D0*S8*S9/3.D2)+(3.D0*S12/1.D2)+(S15/1.C5D2
     A)
      X=(B4A*B4+(B6A*B6)+(B7A*B7)+(B8A*B8)+(B9A*B9)+(B10A*B10)+(B11A*B11
     A))*B10
      B16A=-1.3D1*S15/9.45D2
      B18A=S8*S9/9.D2-(9.D0*S12/1.4D2)-(1.1D1*S15/2.7D2)
      B19A=-3.D0*S8/1.D2+(1.7D1*S8*S9/3.5D2)+(3.D0*S12/1.4D2)+(5.83D2*S1
     A5/3.78D3)
      B20A=-4.D0*S15/9.45D2
      B21A=6.D0*S8/8.75D2+(S8*S9/3.75D2)-(3.D0*S12/1.75D2)-(2.D0*S15/1.3
     A5D2)
      B22A=1.2D1*S8/8.75D2-(2.D0*S8*S9/3.75D2)+(3.D0*S12/1.D2)+(3.4D1*S1
     A5/9.45D2)
      B23A=-9.D0*S8/1.75D2+(7.D0*S8*S9/3.D2)+(S15/1.05D2)
      Y=(B16A*B16+(B18A*B18)+(B19A*B19)+(B20A*B20)+(B21A*B21)+(B22A*B22)
     A+(B23A*B23))*B9
      BL14(I)=(X+Y)*B7
      BL15(I)=-B10*B17/7.5D2
C FINISHED CALCULATING THE DIRECT BROWNIAN MOTION ALPHAS
C  THE FOLLOWING PART OF THE PROGRAM WRITES AND/OR PUNCHS THE ALPHAS
C        THE PUNCHED OUTPUT IS THEN UTILIZED IN ANOTHER PROGRAM TO
C        EVALUATE THE CONTRIBUTIONS FOR DIFFERENT VALUES OF THE HEAT
C        CAPACITY RATIO AND THE THERMAL CONDUCTIVITY RATIO.
   20 CONTINUE
//
```

CHAPTER V

EXPERIMENTAL CONSIDERATIONS

1) Introduction

Although a number of experimental investigations have considered the rheo-optical and rheological properties of complex, suspension-like fluids, practically no experimental observations of their thermal constitutive behavior exist. The dearth of experimental work is due, in part, to the difficulties associated with designing an experiment that precisely isolates the conductive mechanism of heat transfer from the often more dominant mechanisms of forced and natural convection. The following work will consider the design of an experimental apparatus to produce the simple flow and temperature fields necessary for an experimental determination of the heat transfer properties of a flowing suspension, and presents the results of some preliminary experiments dealing with the measurement of the effective transverse conductivity of a suspension of rigid spheroids.

A number of different, highly accurate techniques exist for the determination of the thermal properties of solids. Techniques for the determination of the conductivity of a fluid are not so well developed, the added difficulties being mainly due to the establishment of natural convection cells in the fluid upon heating, which enhance the transport of heat, and may in fact become the dominant mode of heat transfer. For a fluid suspension, theoretical evidence

1) Introduction

Although a number of experimental investigations have considered the rheo-optical and rheological properties of complex, suspension-like fluids, practically no experimental observations of their thermal constitutive behavior exist. The dearth of experimental work is due, in part, to the difficulties associated with designing an experiment that precisely isolates the conductive mechanism of heat transfer from the often more dominant mechanisms of forced and natural convection. The following work will consider the design of an experimental apparatus to produce the simple flow and temperature fields necessary for an experimental determination of the heat transfer properties of a flowing suspension, and presents the results of some preliminary experiments dealing with the measurement of the effective transverse conductivity of a suspension of rigid spheroids.

A number of different, highly accurate techniques exist for the determination of the thermal properties of solids. Techniques for the determination of the conductivity of a fluid are not so well developed, the added difficulties being mainly due to the establishment of natural convection cells in the fluid upon heating, which enhance the transport of heat, and may in fact become the dominant mode of heat transfer. For a fluid suspension, theoretical evidence

suggests that the transport processes will be a complicated function of the flow, in fact this flow dependence of the constitutive behavior of the suspension is the primary feature of interest here. An experimental elucidation of the flow dependence hence adds the further constraint on the experimental technique that it be capable of producing flow patterns that can be accurately predicted. Since much of the available theory deals with the behavior of neutrally buoyant suspensions undergoing steady simple shearing motion in the presence of a linear temperature field it seems of primary practical significance to develop an experimental apparatus capable of producing these simple conditions.

The work of Singh (1968) appears to be the first and only detailed experimental investigation of the effective thermal properties of stationary and flowing suspensions. In the investigation, the effective thermal conductivity of neutrally and non-neutrally buoyant suspensions of polystyrene spheres suspended in aqueous sodium chloride solutions were measured. The stationary measurements were performed by means of a hot wire, transient technique, obtaining the response of a suddenly heated probe immersed in the fluid before natural convection cells have a chance to develop. The results obtained showed the approximate validity of the Maxwell result for dilute suspensions up to concentrations of 45%. The technique used for measurement of the flowing

suspension effective conductivity involved measuring the temperature rise of the suspension flowing through a tube of diameter d and length L, jacketted by a constant temperature bath. The temperature rise of the fluid flowing in the tube is functionally related to the Nusselt number, which may be correlated to the flow situation by the Graetz relation (in the absence of natural convection)

$$Nu_d = 3.65 + \frac{.0668\frac{d}{L}Re_d \cdot Pr}{1 + .04\cdot(\frac{d}{L}\ Re_d \cdot Pr)^{2/3}}$$

Unfortunately, the measurements were obtained in tubes of diameter only about ten particle diameters, and at particle Reynolds numbers >10. The suspension is therefore not homogeneous on the macroscopic scale, and wall effects as well as particle migrations play an important role in the results obtained. In this case it would not be expected that the suspension could be described by a simple scalar 'effective conductivity'.

To avoid these difficulties in the measurement of the thermal constitutive behavior of the flowing suspension, as well as to investigate other possible methods of determination, the design of an additional apparatus for the determination of the transverse conductivity of a flowing neutrally

buoyant suspension was undertaken. We shall first outline the exact nature of the apparatus, and attempt to model as many of its relevant flow and heat transfer features as possible. Then the results of the experimental determination of the conductivity of a flowing suspension of polystyrene spheres will be presented, as well as suggestions regarding some modifications of the system.

2) The Apparatus

Our goal is the development of an experimental technique for the measurement of the thermal constitutive behavior of a flowing suspension. The relation of the bulk heat flux in the flowing suspension to imposed temperature fields will not be a unique material property of the suspension itself. Even for a suspension of spheres, in which particle orientation is irrelevant, the distribution of relative position of the suspended particles will crucially depend on the type of flow and the strength of the hydrodynamic forces resulting from the flow in relation to other forces (e.g. translational Brownian motion) affecting the microstructural configuration of the suspension. Further the local convective transport resulting from the disturbance velocity and temperature fields near the particles will depend on the exact nature of the flow as well. Any local anisotropy of the microstructural configuration of the will be reflected in anisotropic constitutive behavior of the suspension. Despite these complexities, a few theoretical predictions in the idealized case of simple bulk shearing flows and linear bulk temperature fields exist for infinitely dilute suspensions. Due to the small length scale of the suspended particles in comparison to the length scales over which variations in the bulk variables occur in

many practical situations, these theoretical predictions have significant practical importance and it would appear useful to devise a suitable experimental technique capable of creating these idealized conditions. Under these conditions, the transport of heat in the direction orthogonal to the direction of flow is often of primary interest. In this case, we may associate a scalar effective transverse conductivity, k, with the bulk heat flux component resulting from the gradient of temperature, which will be a complicated function of the physical properties of the physical properties of the suspending fluid and suspended particles, the flow, and any other parameters describing the physical processes determining the microstructural configuration. An experimental apparatus devised to measure this transverse flux of heat should therefore satisfy the following constraints:

1) It should be capable of producing simple shear flow in a direction orthogonal to a linear temperature gradient.

2) Secondary heat transfer effects such as natural convection or viscous dissipation should be negligible, or at least predictable.

3) The experiments should be relatively simple to perform, and involve measurements that do not dis-

turb the flow and temperature fields.

4) The geometry of the apparatus should conform to the notion that the suspension may be viewed as an equivalent homogeneous material.

A number of techniques exist which reputedly give accurate data for stationary fluids. Numerous investigators have utilized an experimental situation involving concentric cylinders, the inner of which is heated and the outer cooled. An additional (or guard) heater may be affixed to the ends of the inner cylinder to compensate for axial losses of heat, and the gap width and temperature drop between the cylinders kept small enough to minimize natural convection. This geometry corresponds to a well known viscometric method of developing simple shearing, or Couette, flow between the cylinders when one or both is allowed to rotate steadily. Consequently, such a geometry was considered an appealing possibility.

Figure 1 illustrates the resulting device. The inner, rotating cylinder was prepared from a hollow tube of aluminum, machined to an outside diameter of $3.892 \pm .0005$ inches. A continuous groove was cut in the surface of the cylinder so that the wire heater lay slightly below the machined surface. The test and guard heater sections, which consisted of .020 inch diameter, high purity Nickel-A wire, insulated with a

.001 inch coating of H-ml enamel, were tightly wrapped around the cylinder, care being taken so that the wire lay flat in the groove with no exposed kinks, but that at the same time the insulation was not damaged. The resulting heater coils were tested for electrical shorts, as it was difficult to avoid scratching the enamel insulation during the winding operation. Upon successful completion of the winding process, the ends of the wire hearters, which entered the aluminum cylinder by means of small holes drilled in the tube walls, were affixed to 14 guage copper leads. Flat ends were threaded to the hollow tube, and hollow aluminum shafts press-fitted to the ends, the copper leads travelling through the center of the shaft. The wire heaters were finally coated with a high thermal conductivity epoxy resin, Helix Potting Compound X-476, and the epoxy machined to the final cylinder diameter. Figure 2 illustrates the exact dimensions of the inner cylinder and wire heater segments. The high purity Nickel-A wire was chosen for its relatively high resistance-temperature coefficient. The heater then not only served as the source of heat, but as a resistance thermometer for the inner surface temperature, the temperature being related to the measured resistance of the heater by the assumed linear expression

$$T = T_0 + \alpha R. \qquad (1)$$

The parameters T_0 and α were experimentally determined for

the heater, and will be given in the discussion of the experimental results.

The bottom shaft bearing and seal is illustrated in figure 3. The rotary ball-bearing was rigidly held in place to assure proper alignment of the shaft. The rotary seal between the spinning shaft and fixed bottom plate being affected by means of a Buna-N o-ring located above the rotary bearing to prevent seepage of particles into the bearing surface, which would result in damage to the machined surface, and the eventual failure of the bearing. The entire seal and bearing mechanism was removable, for the convenience of replacing the seal or bearing should failure occur.

The outer, stationary cylinder was fashioned from a precision bore glass tube of inside diameter $4.680 \pm .003$ inches. The ends were cut and ground by hand to a length of 11.932 inches, at which length the axis of the tube was perpendicular to the ends. The glass tube was of standard wall, with thickness of 3 mm. External to the precision bore glass tube was another glass cylinder with approximately 200 mm. internal diameter. The outer glass tube was similarly ground by hand to the length of 11.932 inches, it only being required that the ends be parallel. Cooling water was circulated from a constant temperature bath into the region between the two glass cylinders, stainless steel

baffles insuring turbulence and a high heat transfer coefficient on the external surface of the precision bore glass tube.

Some difficulty was encountered in the sealing of this water jacket. It was necessary that the apparatus be easily disassembled for periodic cleaning, requiring that the joints between the glass tubing and the bottom and top plates be non-permanent. Since alignment of the inner glass cylinder was critical, carefully machined alignment rings were permanently affixed to the plates, the glass tube fitting closely over the ring so that alignment could be affected on each reassembly. A thin neoprene gasket covered the plates in the cooling water jacket, the gasket being held in place by means of stopcock grease. The seal between the glass ends and the gasket was effected by means of a suitable grease, which further served the purpose of lubricating the glass cylinder when closely fitted over the alignment ring. The grease had to provide a suitable seal between the water and oil, yet provide for disassembly without damage to the fragile precision bore tube. Although considerable care was taken during the assembly process, involving pressing firmly on the glass tube to sufficiently compress the grease over the end surfaces of the tubes, and final uniform compression of the grease and gasket by means of spring loading the rods holding the plates in place,

failure of the seal resulted after a few weeks of continuous water pressure. Conventional stopcock greases, as well as high vacuum silicon greases were used to attempt to seal the apparatus, without much success. Finally a long lasting seal was obtained by means of High Vacuum Formula Lubriseal, a product of the Arthur H. Thomas Company. The grease is very thick and glue-like, causing the seal to be of a slightly more permanent nature than is actually desired, but with care the apparatus may be disassembled without damage.

Electrical connections between the rotating electrical heaters and the external circuitry were provided by means of mercury cups attached to the rotating shafts. Some problems were encountered with the connections which have not been completely resolved. Originally copper probes were immersed in the mercury to effect the connection. The heavy gauge copper leads coming from the heaters were fed through the shaft and connected to brass screws which entered the shaft through threaded plastic liners, to insulate the connection. Attached to the screw externally was a heavy gauge probe which fit into a copper ring laying on the bottom of the cup, rotating with it. External copper probes, to which the wires leading to the voltage supplies and measuring devices were attached, were attached to the frame of the apparatus and immersed in the spinning mercury. A light non-volatile oil was floated on top of the mercury cup to prevent the

escape of mercury vapor into the laboratory. Upon the introduction of current to the circuit, an amalgam of mercury was deposited on the copper probes, insuring good connections. Over a long period of time, of the order of a month, a thick, scum-like material, apparently a byproduct of the amalgamation reaction, formed on the surface of the mercury, eventually fouling the connections. This fouling problem was resolved in part, by fashioning silver probes, the external probes being in the form of a circular loop of wire that was immersed in the mercury. These probes provided a greater surface area in contact with the mercury, resulting in better connections, however, these silver leads would eventually disintegrate or break due to the motion of the mercury flowing past, and had to be replaced after about six months of operation. The mercury cups still became contaminated and required periodic cleaning and changing of the mercury. As this is an extremely inconvenient and somewhat hazardous chore, involving considerable (about 6 pounds) quantities of mercury, an improved system of contacts is highly desirable.

Rotation of the inner cylinder and shaft assembly was driven by means of a Minarik variable speed motor and motor control device, equipped with a ten-turn potentiometer. The rotational speed of the apparatus was highly reproducible and linear over the range utilized in the experiments and resulted in an expression for the rotational speed

Ω (rad/sec) in terms of the motor control setting (M.C.S.), of the form

$$\Omega = \beta(\text{M.C.S.}) + \Omega_o \qquad (2)$$

The parameters β and Ω_o were obtained by calibration experiments and will be presented later.

The required electrical circuits for the test and guard heaters are illustrated in figure 4, along with a tabulation of the particular instruments used. Power to the circuits were provided by regulated, constant voltage, DC power supplies. The resulting voltage applied to the test and guard heaters were measured at the mercury cups. The current flowing through the test heater was evaluated by measuring the voltage drop across a 1 ohm standard resistor placed in the circuit.

A Union Carbide lubricant, UCON Oil HB-280-XY-23, was utilized for the suspending fluid. The oil is a mixture of various polyethylene and polypropylene glycols, is of fairly high viscosity, has a density equivalent to the polystyrene latex spheres used as the suspended particles, and has a very low coefficient of thermal expansion, $\beta_f \sim 8 \times 10^{-4}$ $(^oC)^{-1}$. Its thermal conductivity is of the order of 6×10^{-4} cal/sec·cm·^oC, and heat capacity about .5 cal/gram.

3) The Idealized Operating Equations

We may now generate equations governing the operation of the apparatus. The description of the velocity and temperature distributions in the apparatus will be complicated, even in this rather simple geometry, by a number of effects. First, the equations describing the velocity and temperature distributions are coupled. Density and viscosity variations resulting from the non-uniform temperature distribution will result in flows different from the idealized situation of simple shearing motion. These flows will affect the temperature distribution, by the establishment of natural convection cells and by the action of viscous dissipation of energy to heat in the fluid. Second, the suspension will only be Newtonian as long as the concentration of spherical inclusions is not too large and the particle Reynolds number describing the disturbance flow near the particle is very small. For the idealized case of simple shearing motion with shear rate $G(sec^{-1})$, the appropriate Reynolds number is, $Re_p = \frac{\rho a^2 G}{\mu_f}$, where a is the particle radius, ρ the density of the particles and suspending fluid, and μ_f the fluid viscosity. Even if the suspension is Newtonian, inhomogeneities in the particle concentration in

the fluid will result in radial variations of the viscosity of the suspension. Radial migration of the particles is unavoidable at any non-zero shear rate in a device of finite dimensions. Finally, the flow situation utilized, with the inner cylinder rotating and the outer stationary, is inherently unstable. Centrifugal forces generated by the rotation of the inner cylinder act to destabilize the idealized simple unidirectional shearing motion. The complete problem of describing the velocity, temperature, and concentration profiles in the apparatus is thus seen to be overwhelmingly complicated. For this reason, we will first consider the idealized behavior of the apparatus, as follows, and then specifically consider the effects mentioned above.

We first consider the flow of a Newtonian fluid of constant density and viscosity in the central region of the apparatus, far from the ends. In terms of a cylindrical coordinate system coincident with the axes of the inner and outer cylinders, the velocity of the fluid will have only a tangential (U_Θ) component, governed by the ordinary differential equation

$$\frac{d}{dr}\left\{\frac{1}{r}\frac{d}{dr}(rU_\Theta)\right\} = 0, \qquad (3)$$

with boundary conditions,

$$\begin{aligned} &\text{at} \quad r = R_1 \qquad U_\theta = \Omega R_1 \quad , \\ &\text{at} \quad r = R_2 = \gamma R_1 \qquad U_\theta = 0 \ . \end{aligned} \tag{4}$$

Here, R_1 is the radius of the inner cylinder and $\gamma = R_2/R_1$ is the ratio of the outer to inner cylinder radii. The solution to this simple boundary value problem is well known, and is found to be,

$$U_\theta = \frac{\Omega}{(\gamma^2-1)} \left\{ \frac{\gamma^2 R_1^2}{r} - r \right\} . \tag{5}$$

An important parameter of the flow is the local shear rate, G(r), experienced by the suspended particles, since from theoretical considerations we expect the bulk heat flux of the suspension to be functionally dependent on the Peclet number relevant to the particle radius,

$$Pe = \frac{\rho C_p G a^2}{k_f} .$$

Here, ρ is the fluid density, C_p its heat capacity, a the particle radius, and k_f the thermal conductivity of the suspending fluid. Because of the cylindrical geometry, the shearing rate will not be constant in the apparatus, but is

rather found from (5) to be a function of radial position,

$$G(r) = -\frac{\Omega}{(\gamma^2-1)}\left[1 + \frac{2\gamma^2 R_1^2}{r^2}\right] \qquad (6)$$

To evaluate the average Peclet or Reynolds number relevant to the particles in the apparatus we will therefore utilize the radially-averaged shear rate

$$\bar{G} = \frac{\int_{R_1}^{\gamma R_1} G(r)\, r\, dr}{\int_{R_1}^{\gamma R_1} r\, dr} = -4.94\,\Omega\ (\text{sec}^{-1}) \qquad (7)$$

Having obtained the idealized velocity distribution in the test section of the apparatus, we may turn to the development of the description of the temperature profiles, and the relation of the transverse thermal conductivity of the test fluid to the imposed experimental conditions. The voltage E, and current I, applied to the test heater are measured experimentally. By relation (1) we therefore know its temperature. Further, this measurement determines the flux of heat into the fluid at the surface of the cylinder, assuming that all the heat dissipated in the heater goes into the fluid. The experiments are operated such that the inner Aluminum cylinder surface is approximately at ambient room

temperature, thereby minimizing any heat losses to the inside of the cylinder. The flux of heat, q, per unit area of the test heater (which occupies the center L cm. of the cylinder) is then given by

$$q = \frac{EI}{2\pi R_1 L f} \tag{8}$$

where f is the conversion factor

$$1 \text{ cal/cm}^2\text{sec} = f \text{ watts/cm}^2 = 4.184 \text{ watts/cm}^2$$

The temperature of the cooling water circulating in the water jacket external to the outer cylinder is measured as it exits the apparatus. The water is circulated at a high enough rate, and kept well stirred by the baffles, so that we shall assume that the outer cylinder external wall is of a temperature equal to that of the cooling water. We shall show later that stability requirements will necessitate the use of a fairly viscous ($\mu_f \sim 1.5$ poise) suspending fluid, so that the shearing of the fluid over the small gap width of the apparatus might be expected to cause non-negligible viscous dissipation of energy into heat. Assuming that the suspension may be treated as an equivalent homogeneous material, with transverse thermal conductivity k_f and viscosity

μ_f, the steady state temperature distribution, $T_f(r)$, in the fluid region far from the ends is governed by

$$k_f\left[\frac{1}{r}\frac{d}{dr}\left(r\frac{dT_f}{dr}\right)\right] + \mu_f\left[r\frac{d}{dr}\left(\frac{U_\theta}{r}\right)\right]^2 = 0 . \quad (9)$$

Substituting the expression (5) for the velocity field $U_\theta(r)$ into (9) results in

$$\frac{d^2T_f}{dr^2} + \frac{1}{r}\frac{dT_f}{dr} = \frac{-4\mu_f\Omega^2\gamma^4R_1^4}{k_f(\gamma^2-1)^2r^4}. \quad (10)$$

The solution to this equation is found to be of the form

$$T_f = A \ln r + B - \frac{\mu_f\Omega^2\gamma^4R_1^4}{k_f(\gamma^2-1)^2}\frac{1}{r^2} . \quad (11)$$

At the inner surface of the precision bore glass tube the temperature and radial heat flux must be continous. The distribution of temperature, T_g, in the glass region of conductivity k_g, will be governed by the conduction equation

$$k_g\frac{1}{r}\frac{d}{dr}\left(r\frac{dT_g}{dr}\right) = 0 , \quad (12)$$

the general solution of which has the simple form

$$T_g = C \ln r + D \,. \tag{13}$$

The four unknown constants A, B, C, and D are related to the conductivities k_f and k_g, and to the state of the heater by the boundary conditions

$$\text{at } r = R_1 \qquad T_f = T_{heater} = 14.24 \frac{E}{I} - 227.68 \tag{14}$$

$$-k_f \left.\frac{dT}{dr}\right)_{r = R_1} = q = \frac{EI}{2\pi R_1 Lf}$$

$$\text{at } r = \gamma R_1 \qquad T_f = T_g \tag{15}$$

$$k_f \left.\frac{dT_f}{dr}\right)_{r = \gamma R_1} = k_g \left.\frac{dT_g}{dr}\right)_{r = \gamma R_1}$$

and at $r = \sigma R_1$ (the external wall of the glass cylinder) we have

$$T_g = T_{water} \tag{16}$$

Evaluation of the temperature distributions (11) and (13)

in the light of the boundary conditions (14) - (16) results in an expression for the unknown conductivity of the fluid in terms of the experimentally measured voltage and current of the heater, rotation of the cylinder, and cooling water temperature,

$$k_f = \frac{\frac{EI\ln\gamma}{2\pi L f} + \frac{2\Omega^2\mu_f\gamma^2R_1^2}{(\gamma^2-1)}\left[\frac{\gamma^2\ln\gamma}{(\gamma^2-1)} - \frac{1}{2}\right]}{14.24\,\frac{E}{I} - 227.68 - T_w - \frac{EI\ln\sigma/\gamma}{2\pi L f k_g} - \frac{2\Omega^2\mu_f\gamma^2R_1^2\ln\sigma/\gamma}{(\gamma^2-1)\,k_g}} \qquad (17)$$

Equation (17) is the desired relation for the transverse conductivity k_f of the test fluid in terms of the experimentally measured quantities and the geometrical properties of the apparatus. For the apparatus used in the experiments, the expression becomes

$$k_f = \frac{.000701\ EI + .0000000439\ \mu_f\Omega^2}{14.24\,\frac{E}{I} - 227.68 - T_w - .03731\ EI - .0000440\,\mu_f\Omega^2} \qquad (18)$$

where k_f is the conductivity in cal/sec cm^2 $^\circ$C, T_w is the cooling water temperature in $^\circ$C, and μ_f is the fluid viscosity in poise. For the relatively high viscosity suspending fluid used here, viscous dissipation effects at the largest rotation rates utilized (Ω = 10 rad/sec) accounted

for about 2% of the measured value, therefore necessitating the inclusion of these effects.

4) Secondary Effects

Having obtained the relation (18) between the experimentally measured parameters E, I, , and T_w and the conductivity of the test fluid, we shall now consider in more detail the assumptions inherent in its derivation. First, the effects of natural convection have been neglected. By neglecting the effects of curvature in the gap, we may use the results of Batchelor (1954), who studied the natural convection in a fluid contained in a long, narrow vertical cavity with walls of different temperature. Although unable to analytically solve the general problem, Batchelor was able to estimate the effects in some limiting situations. We are specifically concerned, here, with the temperature and velocity profiles in the central, or test, region of the apparatus, i.e. about seven centimeters from the ends. Batchelor has shown that in the fluid region a distance $X > d^*Ra/1000$ from the ends, the temperature distribution is simply the linear distribution resulting from the purely conductive transfer of heat. Here, d is the gap width of the cavity, and Ra is the Rayleigh number, defined by

$$Ra = \frac{d^3 g \beta_f C_p \rho_f \Delta T}{\nu_f k_f} .$$

$\beta_f = -\frac{1}{\rho}\left[\frac{\partial \rho}{\partial T}\right]_p$ is the coefficient of volume expansion of the fluid, g the gravitational constant, and ΔT the temperature difference between the walls of the gap. For the oil used as a suspending fluid in the experiments, and at temperature drops of about $6^{\circ}C$, the Rayleigh numbers for the experiments were about 2×10^3. Thus at distances further from the ends than about 2 cm., the purely conductive, linear temperature field will be established. The fluid in the test section is then clearly in the region of linear temperature profile.

The fluid motion resulting from buoyancy effects due to the temperature distributions in this central core is the purely vertical velocity distribution

$$U_z = \frac{K^{*}Ra}{12d}\left(2y^3 - 3y^2 + y\right) \text{ (cm/sec)} \qquad (19a)$$

where $K = k_f/\rho C_p$ is the thermal diffusivity of the fluid and y is the distance in centimeters measured from the inner wall. For the Ucon oil used here, $K \sim 1.2 \times 10^{-3}$ cm^2/sec so that for $Ra \sim 2 \times 10^3$

$$U_z \sim .2\left(2y^3 - 3y^2 + y\right) \text{ (cm/sec)} \qquad (19b)$$

This motion is orthogonal to the temperature gradient, and will contribute an additional component of the local vorticity (or rotation rate of the suspended particles). The disturbance velocity and temperature fields associated with this flow will lead to enhancement of the radial heat flux, since disturbance flows near the spinning particle will act locally as a convective mechanism of heat. Differentiating (19b) we find, for the Ucon oil with Ra $\sim$ 2 x 10^3,

$$G_{NC} \sim 1.2 \left(y^2 - y + .167 \right) \text{ sec}^{-1} \qquad (20)$$

which has a maximum value of .2 sec^{-1} at the walls, a mimimum value of -.1 sec^{-1} at the midpoint y=½, and vanishes at the points y = .2114 and y = 1 - .2114. The average value of the magnitude of the shear rate can be found by integration of the absolute value of the shear rate across the gap, which yields

$$G_{NC,avg} = .08 \text{ sec}^{-1} ,$$

and results in negligibly small particle Peclet numbers corresponding to the motion (Pe$\sim 5 \times 10^{-4}$). For the conditions of the experiments, we thus expect that we may neglect the effects of natural convection.

We consider, secondly, the effects of the suspended

particles on the fluid motions. Infinitely dilute suspensions of spheres are Newtonian at low particle Reynolds numbers. The rheology of the suspension is then simply characterized by the effective viscosity $\mu(\phi)$. A theoretical prediction for this effective viscosity was derived by Einstein (1906) who obtained the well known relation

$$\mu_s = \mu_0(1 + \frac{5}{2}\phi). \qquad (21)$$

Here, μ_s is the effective viscosity of the suspension, μ_0 the viscosity of the suspending fluid, and ϕ the volume fraction of suspended particles. A considerable number of experimenters have investigated the effective viscosity of more concentrated suspensions, the work being reviewed by Rutgers (1962) and more recently by Acrivos and Jeffrey (1976). Theoretical considerations reveal that non-infinitely dilute suspensions are non-Newtonian. The Einstein correction (21) is merely the first $O(\phi)$ contribution in an integer power series representation for the shear viscosity

$$\mu_s = \mu_0 (1 + A\phi + B\phi^2 + C\phi^3 + \ldots\ldots) \qquad (22)$$

in which the first term $\frac{5}{2}\phi$, is due to the effects of the

non-interacting particles. The next $O(\phi^2)$ correction involves two particle hydrodynamic interactions and requires knowledge of the statistical distribution of relative particle location (c.f. Batchelor and Green (1972)). This statistical distribution is strongly flow dependent, as well as dependent upon any other forces, such as translational Brownian motion, inertial effects, or higher order particle interactions, acting on the particles; in fact the purely viscous problem is indeterminate for simple shearing flow. As a result, the effective viscosity will not be a unique material property of the suspension and will not in general be Newtonian, a necessary conclusion that has not always been appreciated in the literature. For this reason, the viscosity of the suspensions used in the experiments was measured in a Stormer Viscosimeter, a rotating cup device creating rotational shearing flows similar to those of the conductivity apparatus, at particle Reynolds numbers and temperatures encountered in the experimental conditions. At the low particle Reynolds numbers involved here, of the order of 10^{-4}, no discernible dependence on shear rate was found at any of the concentrations. Viscosity data for the suspensions are presented in figure 5. The deviations from the Einstein result are seen to be fairly substantial, the curve drawn through the points representing a coefficient of the ϕ^2 term of B = 20. Experimentally measured values of

the suspension viscosity were used in equation (18) to evaluate the experimental conductivity data.

Another effect of the suspended particles is the lateral inertial migration of the particles in the simple shearing motion. This migration has been observed in Poiseuille flow in tubes (Segre and Silberberg (1962)) and in Couette flow (Hallow (1968)). Recently, Ho (1974), has theoretically considered the problem, and obtained results which correlated extremely well with the observation of Hallow. In a rotating cylindrical device, as a result of the fluid inertia and the presence of the bounding walls, particles migrate to a preferred equilibrium position $\frac{r_{eq} - R_1}{\gamma R_1 - R_1} = .53$, creating a non-uniform concentration distribution of particles in the suspension. This distribution will be resisted by translational Brownian motions of the particles, however with the relatively large (50 micron) particles used here, the effect is negligible. From the work of Ho, we are able to estimate the time for considerable migration to occur, obtaining the result that the time for radial migration at the largest rotation rates used is of the order of several days, and at the average rates of the order of several weeks. Suspensions were only used in the apparatus for a little over a week, therefore, and only at the highest shear rates for about a day.

The flow field in the apparatus will further be complicated by the inherent instability of the simple shearing motion at high rotation rates. Taylor (1923) has considered the stability of the flow to infinitessimal disturbances and obtained the result that the flow is stable as long as the characteristic Taylor number P, satisfies the condition

$$P = \frac{\Pi^2 \nu_f (\gamma + 1)}{2\Omega^2 R_1^4 (\gamma - 1)^3} \geq .0535 \qquad (23)$$

Evaluating the critical rotation rate from this expression. using the viscosity of the Ucon oil at the average temperature in the device, results in a maximum rotational speed of about 10 rad/sec, a maximum speed that was never exceeded in practice due to the delicacy of the electrical connections in the mercury cups. We note that this prediction of the onset of instability is only valid for infinitessimal disturbances, and does not take into account the fact that, here, fluid motions induced by natural convection may alter the stability of the flow.

A number of investigators have considered the stability of concentric cylinder devices in the presence of radial temperature distributions, both theoretically and experimentally. Similarly, several studies have been reported in the literature concerned with the heat transfer characteristics

of such systems, especially the effect of natural convection and forced convection due to the Taylor vortices established in the annular region at rotations above the critical speed of rotation. Becker and Kaye (1962) considered the effect of radial temperature variations on the predicted critical rotation speed for the case of an outer stationary cylinder and an inner rotating cylinder and theoretically found that heating of the inner cylinder stabilizes the flow, while heating of the outer cylinder serves to destabilize the flow. in this analysis, however, gravitational accelleration of the fluid was neglected compared to centrifugal forces. For fairly small imposed temperature gradients, the stability criteria for the flow is very nearly equal to the isothermal stability criteria obtained by Taylor, evaluating the fluid properties at the mean temperature of the gap. This result is experimentally confirmed by several investigators (c.f. Haas and Nissan (1961)) who found for a horizontal arrangement of cylinders, virtually no effect of the imposed temperature gradient on the critical Taylor number observed for the flow.

Similarly, experimental data of Haas and Nissan (1961), Bjorklund and Kays (1959), and Ho, Nardicci, and Nissan(1964)

report that below the critical rotation speed, calculated for an isothermal system, heat transfer and temperature distributions are established by conduction alone. Above the critical rotation speed, considerable heat transfer due to convection by the Taylor vortices results.

in none of the theoretical investigations, however, has a complete analysis of all of the physical processes involved been accomplished; i. e. a complete analysis taking into account natural convection resulting from gravitational as well as centrifugal acellerations of the fluid in the gap, viscosity-temperature dependence as well as density-temperature effects. The experimental evidence, however, apparently supports the conclusions that the stability is little affected by the temperature field, and that conduction is the dominant mode of heat transfer at rotation speeds below the critical speed predicted by Taylor's analysis.

Finally, although the Ucon oil was chosen for its high viscosity, and its low temperature-coefficient of expansion, it was found that the viscosity was an extremely sensitive function of temperature. Viscosity data for the

pure Ucon oil were obtained in the Stormer viscosimeter, and a Connon-Fenske tube-type viscometer as well, both of which were calibrated with Dow silicon oil of viscosity 1 poise. The results are presented in figure 6, in the form suggested by Bird, Stewart, and Lightfoot (1966) from which we obtained the correlation

$$\mu = (6.241 \times 10^{-7}) \exp\left[\frac{4311}{T}\right] . \qquad (24)$$

Here, μ is the viscosity in poise and T the absolute temperature in ^{o}Kelvin. The suspension viscosity reflected the same temperature variation. For the common experimental conditions here of inner wall temperature about 25 ^{o}C and outer wall temperature about 19 ^{o}C, we find a viscosity variation between inner and outer walls of about 35%. To investigate the effect of this variation on the flow field we consider equation (3) in the light of a variation in space of the viscosity. From the predicted temperature distribution (11), neglecting the viscous dissipation term which at maximum rotation speeds only causes about a 2% change in the temperature, and from the conditions that the wall temperatures are $T_{inner} = 298\ ^{o}K$ and $T_{outer} = 292\ ^{o}K$, we obtain the temperature field in terms of the dimensionless radial coordinate $r = r/R_1$,

$$T = -32.6 \ln r + 298 .$$

Substituting this into the viscosity-temperature correlation (24) we obtain

$$\mu(r) = (6.24 \times 10^{-7}) \exp\left[\frac{14.47}{1 - .1094 \ln r}\right] .$$

Recognizing that .1094 ln r will only vary between 0 and .02, we may approximate

$$\begin{aligned} \mu(r) &\sim (6.24 \times 10^{-7}) \exp\left[14.47 + 1.583 \ln r\right] \\ &= 1.20\, r^{1.583} = \mu_0 f(r) \end{aligned} \tag{25}$$

The governing equation for the tangential velocity distribution $U_\Theta(r)$, nondimensionalized with respect to the characteristic velocity ΩR_1, is then

$$r^\beta \frac{d^2U_\Theta}{dr^2} + \left[(\beta + 1)r^{\beta - 1}\right]\frac{dU_\Theta}{dr} - \left[(\beta + 1)r^{\beta - 2}\right] U_\Theta = 0 ,$$

where, $\beta = 1.583$.

This may be rearranged to the form (since r is non-zero)

$$\frac{d^2U_\Theta}{dr^2} + \frac{(\beta + 1)}{r}\frac{dU_\Theta}{dr} - \frac{(\beta + 1)}{r^2} U_\Theta = 0 \tag{26a}$$

which must satisfy the boundary conditions

$$\begin{aligned} r &= 1 & U_\theta &= 1 \\ r &= \gamma & U_\theta &= 0. \end{aligned} \tag{26b}$$

The solution is simply

$$U_\theta = -\frac{1}{(\gamma^{\beta+2}-1)}\left\{ r - \frac{\gamma^{\beta+2}}{r^{\beta+1}} \right\}$$

from which the dimensional, average shear rate may be calculated

$$\begin{aligned} \overline{G} &= -\frac{\Omega}{(\gamma^{\beta+2}-1)}\left[1 + \frac{2(\beta+1)\gamma^2(\gamma^\beta-1)}{(\gamma^2-1)\beta}\right] \\ &= -4.93\Omega \text{ sec}^{-1} \end{aligned} \tag{27}$$

Comparing this with the result (7) for the uniform viscosity idealization, we see that the stratification of viscosity causes a negligible difference in the average shear rate in the apparatus.

5) The Experimental Results

Having obtained the expression (18) relating the transverse conductivity of the test fluid to the experimentally measured quantities, and obtained estimates for the limits on rotation rate and temperature drop, we may proceed to our program of experimental investigation.

Initial experimentation involved calibration of the resistance-temperature characteristics of the heater and rotational speed of the apparatus. Figure 7 presents the data obtained for the resistance of the heater for different temperatures, along with the linear relation obtained from a least squares analysis of the data,

$$T = 14.24\ R - 227.68 \qquad (28)$$

Here, T is the surface temperature in ^{o}C, and R is the test heater resistance, R = E/I, in ohms. Figure 8 presents the data obtained for the rotational speed Ω(rad/sec) of the apparatus for a number of different motor control settings, as well as the linear relation from the least squares analysis of the data,

$$\Omega = 2.456\ (MCS) - 2.567 \qquad (29)$$

We next considered the thermal conductivity of the pure Ucon oil. The response of the system to the rotation of the cylinder, temperature drop and amount of guard heating being effectively held constant, was first considered. Figure 9 presents the data obtained for a temperature drop of about six degrees, as well as data obtained for a drop in temperature between the walls of about thirteen degrees centigrade. The amount of guard heating is given here as the ratio of guard heater voltage drop to test heater voltage drop, expressed as a percentage

$$\%GH = \frac{E_{GH}}{E_{TH}} \times 100 .$$

It was found that the system required a long time (about a day) to come to steady state, after which minor fluctuations of the water bath temperature induced a slowly varying nature to the resulting voltage measurements. Data were therefore taken, after the initial start-up period, over several hours and then averaged to obtain the average values plotted here. For the lower temperature drop ($\Delta T \sim 6^{\circ}C$) the measured conductivity of the fluid was found to be relatively constant for rotational speeds up to about 10 rad/sec. At speeds above this rate, the measured value became greater. This is about the rotational speed corresponding to the predicted

onset of Taylor instability. The resulting laminar roll cells, predicted by Taylor's theory and observed by numerous investigators, would be expected to create considerable convection, enhancing the transport of heat and causing an apparently higher measurement of the conductivity. If the rotational speed was increased to higher rates, the mercury in the cups became quite agitated, mixing with the oil that was floating on the surface. The end result of the agitation was a poor electrical connection, as could be seen by some rapid fluctuation of the measured voltage and current.

The data for the higher temperature drop are seen to give a higher value of the conductivity, and to be considerably more dependent on the rotation rate. The increase in the magnitude of the conductivity is apparently due to the higher average temperature in the fluid (glycols have an increase in conductivity with increasing temperature, c.f. Handbook of Chemistry and Physics (1969)) although the increase in magnitude is larger than would be expected. At this larger temperature drop the Rayleigh number is considerably larger, due both to the increased temperature difference and the corresponding decrease in the average viscosity of the fluid. The Rayleigh number for this case is about 8000 as opposed to about 2500 for the smaller ($6^{\circ}C$) temperature drop. The end regions predicted by Batchelor's theory are therefore about 8 centimeters in length, and intrude into

the test region. At this higher Rayleigh number, then, natural convection evidently may be responsible for an enhancement of heat transfer, resulting in an apparently higher value of the conductivity. The increased dependence of the measured value on the rotational speed may also be qualitatively explained. First, the region of fluid near the heated inner wall has a much lower viscosity in this higher temperature drop case. This reduction of viscosity near the wall would be expected to result in reduced stability of the flow, since in this region the 'local' Taylor number P which is a measure of the stabilizing influence of viscous forces to the destabilizing centrifugal forces is considerably reduced. Further, the natural convection velocity fields in this case are over three times as strong in comparison to the smaller temperature drop case, which may contribute to destabilization of the flow, although as we previously stated, no theoretical predictions for stability of the modified flow exists. In this case, one would have to consider stability of the coupled velocity and temperature distributions, including spatial variations of density and viscosity due to the temperature distribution, and the fully three dimensional velocity fields resulting from the rotation of the inner cylinder superposed on the vertical, natural convection velocity distribution.

Figure 10 presents data obtained for variation of the

amount of guard heating. Considerable variation in these data was found, as indicated by the solid lines surrounding the plotted average values. This scatter is believed to be due to problems with the guard heater power supply. The original supply used for some of the data failed, and a replacement had to be substituted. This replacement was found not to supply a highly constant voltage, and had to be continuously adjusted. The data do indicate a general pattern of decreasing measured conductivity with increased amounts of guard heat. This may be due to the net axial input of heat to the test fluid and heater with increased levels of guard heating. This net addition of heat raises the steady state temperature of the fluid and test heater. Since the outer cylinder wall temperature is fixed by the cooling water temperature, the overall temperature drop, ΔT, radially across the fluid increases. The measured conductivity is associated with the measured test heater heat flux and ΔT by $k \sim \frac{Q_{test}}{\Delta T}$, but Q_{test} is <u>fixed</u> by the power supply output, so that the increased ΔT results in a lower measured value of the conductivity. As a result of this dependence on guard heating, the comparison of the suspension conductivity to pure suspending fluid conductivity was obtained by performing experiments holding the amount of guard heating and the temperature drop effectively constant.

The conductivity of a flowing suspension of spherical particles was determined for several concentrations, ranging from .5% by volume to 5% by volume. It was desired that the particles have a size distribution that was fairly monodisperse, so that analysis of the results would not be complicated by a broad distribution of particle sizes. Availability and cost severely limited the size and type of particles that could be used. Monodisperse spherical particles of diameter the order of a few microns (μ) were only available at the time of the beginning of these experiments at a cost of several hundred dollars per gram. Polystyrene latex spheres of nominal diameter $50\mu \pm 5\mu$ were obtained at considerably less expense from the Diamond Shamrock Chemical Company in Redwood City, California. Figure 11 presents typical photographs of the particles taken under microscopic magnification. The size distribution of the particles was obtained from the photographs by comparison to a photograph, taken under identical magnification, of a thin wire of known uniform diameter. The particle sizes were found to be normally distributed with a mean value diameter of 53.4μ and a standard deviation of 3.8μ.

Each suspension was prepared by a carefully weighed sample of particles to a known volume of pure Ucon oil. The suspension was vigorously stirred by hand for a short time, to break up the large agglomerations of particles that

initially resulted. When the suspension appeared visually homogeneous (the addition of particles causing the normally brownish-red oil to appear a lighter, milky color) it was placed on a magnetic stirring plate and continuously agitated for several days, until needed.

Figure 12 presents data obtained for the effective conductivity, $k_{suspension}/k_{fluid}$, as a function of volume fraction of particles. The data are seen to have a considerable amount of scatter, making it difficult to verify the theoretical prediction for the stationary case, which is also shown in the figure. A number of suggestions for reducing this scatter are given in the appendix. We merely state here that other investigators (Singh,1968) have reported confirmation of the Maxwell prediction for neutrally buoyant suspensions of spheres up to concentrations of over 30%. Jeffrey (1973) has obtained the theoretical prediction for the effective conductivity of a 'well stirred' suspension, in which all possible particle pair configurations are equally probable, up to $O(\phi^2)$. The ϕ^2 correction to Maxwell's result is found to always be positive, except for the case where the particle conductivity is equal to the suspending medium conductivity, where it identically vanishes. For the case here, and of Singh's experiments, where the ratio $k_{particles}/k_{fluid} \sim \frac{1}{2}$, this $O(\phi^2)$ correction is always small compared to Maxwell's result, the expression being

$$\frac{k_{susp}}{k_{fluid}} = 1 - .6\phi + .11\phi^2 + \ldots\ldots \text{ when } m=\tfrac{1}{2} \quad (30)$$

At concentrations $\phi = .3$, the $0(\phi^2)$ correction is therefore less than 1% of the total conductivity, explaining the validity of Maxwell's infinitely dilute result at this high concentration.

The data for flowing suspensions weretaken over a range of Peclet numbers, $Pe = \rho C_{pf} a^2 G/k_f$, varying from .04 to about 0.3. Leal (1973) has obtained the theoretical prediction for a dilute suspension of spheres in simple shear flow at low Reynolds and Peclet number. The expression relevant to the situation here of rigid particles with conductivity ratio $k_p/k_f \sim \tfrac{1}{2}$ is found to be

$$k_s = k_f \left(1 - .6\phi + 3\, Pe^{3/2}\phi + \ldots\ldots \right) . \quad (31)$$

To this order, the flow dependence of the effective conductivity is therefore seen to be proportional to the volume fraction, and to increase with the Peclet number to the 3/2 power. Figures 13-17 present the experimentally measured relative flow enhancement of the effective conductivity, $\frac{k_s - k_f (1 - .6\phi)}{k_f \phi}$ as a function of the Peclet number for the various concentrations of suspensions investigated,

along with the prediction (31). The flow enhancement is seen to always be larger than the prediction, although the data apparently increase at about the rate ($Pe^{3/2}$) predicted by Leal. All the data are presented in figure 18. The results again show considerable scatter, although the rate of increased enhancement with increasing Peclet number is fairly consistent. The line representing the best fit of the data to a form $\frac{k_s - k_f (1 - .6\phi)}{k_f \phi} = A\ Pe^n$ is also shown in the figure. The result from the statistical analysis is A = 20, n = 1.3, giving about the right power dependence on Peclet number, but a coefficient that is about seven times as large as the theoretical prediction. We note first that the next term in the expansion (31) for a dilute suspension would be of order Pe^2, which for Peclet number greater than .1 is approaching the same order of magnitude as $Pe^{3/2}$. These Pe^2 terms may then cause enhancements of approximately the same order of magnitude as the $Pe^{3/2}$ terms for Pe >.1, however this would not be expected to produce the level of enhancement indicated by the data. A more likely reason for the disagreement between the data and the theory may be the formation of particle doublets, and perhaps higher agglomerates, in the flowing suspension. Goldsmith and Mason (1967) have observed the formation of so-called 'collision doublets"

in simple shear flow. This doublet formation is a result of regions of closed streamlines surrounding single spheres in simple shear flow (c.f. Frankel and Acrivos (1968)). Particles that are initially close to one another tend to remain permanently so, and are observed to behave essentially like single dumb-bell shaped bodies in that they undergo apparent rigid-body rotation about an axis passing through the midpoint of their lines of centers. The photographs in figure 19 illustrate the appearance of these doublets, and of higher agglomerations, in the suspension, although it is only illustrative, as it pertains to the condition of particles on a microscope slide, not under the conditions of shearing motion. It is indicative, however, of the fact that particles tend to exist in configurations of close proximity to one another, and will then rotate in the manner described above upon the onset of shearing motion. In this case the particles might be expected to behave somewhat like rigid prolate spheroids. Theoretical predictions (McMillen (1976)) indicate that any O(Pe) contributions would identically vanish so long as the particles traversed closed Jeffrey orbits. No theoretical predictions exist for the $O(Pe^{3/2})$ corrections for spheroids. However, if the correction is of the same order as that for spherical particles, i. e. $3Pe^{3/2}$, a considerable enhancement will occur simply due to the fact that the particles are about twice as large.

In this case the particle Peclet number will be about 4 times as large, resulting in $Pe^{3/2}$ being 8 times as large. Thus, if a large fraction of the particles exist as agglomerations of two particles or more, considerable enhancement of the bulk heat flux may be expected to occur.

APPENDIX

Suggestions for Future Work and Modifications in the Apparatus

Based on the experience gained from this experimental investigation, several suggestions may be made regarding to upgrading the system to allow more accurate data to be obtained.

Much of the scatter in the data is believed to be due to problems related with some of the electronic equipment used, and can possibly be corrected. In the following a few specific suggestions concerned with the obtaining of different instruments will be given, which it is believed, will allow more accurate data to be measured.

The data of figure 10 indicate a fairly strong dependence of the measured value of conductivity on the level of guard heating, a fifteen percent increase in guard heating voltage apparently resulting in about a fifteen percent decrease in the measurement. Unfortunately, the power supply presently used for the guard circuit is not highly regulated, supplying a voltage to the circuit that sometimes varied by more than one percent. This resulted in an inability to measure exactly the effect of variation in guard heating levels, as well as difficulties in holding

the level of guard heating constant for a set of measurements on a particular suspension. A power supply equivalent to the supply used for the test circuit (which produced constant test voltages very accurately) should be obtained.

One constant source of error was the differential voltmeter utilized for measuring the voltage drop in the test heater. It was originally planned that the voltage and current of the test section would be constantly recorded from the output of the differential voltmeters. This idea had to be abandoned, however, when it was found that the voltmeter used for measuring the voltage drop in the heater had considerable zero drift, requiring resetting prior to each measurement. Further, the calibration of the instrument was apparently not constant. The instrument would have to be periodically checked with a reference source, and the entire instrument recalibrated when the measurement was found to be in appreciable error. The measurement of the conductivity of the fluid is extremely sensitive to errors in measurement of the voltage and current of the heater, since the measurement not only is used to evaluate the heat flux at the inner surface, but also the temperature as well. We may analyze the error in measurement of the conductivity by considering the expression (18) used in analysis of the data, without the small

and complicating effects of viscous dissipation. The expression becomes

$$k_f = \frac{.000701\ EI}{14.24\frac{E}{I} - 227.68 - T_w - .03731\ EI} \cdot \qquad (32)$$

We consider the error δk_f in the measured value of k_f caused by errors δE, δI, and δT_w in the measurements of the voltage, current, and cooling water temperature respectively. Retaining only terms to first order we have

$$\delta k_f = \left.\frac{\partial k_f}{\partial E}\right]_{I,T_w} \delta E + \left.\frac{\partial k_f}{\partial I}\right]_{E,T_w} \delta I + \left.\frac{\partial k_f}{\partial T_w}\right]_{E,I} \delta T_w \qquad (33)$$

The partial differentials in (33) may be obtained from (32) and evaluated at the typical conditions of the experiments, $T_w \sim 18.00\ ^\circ C$, $E \sim 10.00$ volts, and $I \sim .566$ amps. The result is

$$\delta k_f = -.00279\ \delta E + .0244\ \delta I + .000114 \delta T_w \qquad (34)$$

First considering the error δE in the voltage, we see that an error of .1 volts, or a 1% error in the total voltage measurement, corresponds to a 43% error in the

measurement of the conductivity of the fluid (k_f = .000279 cal/sec cm ^{o}C). Analogous considerations for the error in the current, δI, yield the result that a 1% error in the current measurement corresponds to an error in k_f of 20%. The measurement of the cooling water temperature is not as critical, an error of .02^{o}C yielding an error of .3% in the measured conductivity. It is therefore imperative that accurate measurements of the voltage and current be obtained. The John Fluke model 887 AB differential voltmeter utilized for the measurement of the current is highly accurate and does not require constant zeroing. Obtaining another (or comparable instrument) for inclusion in the system would not only insure better measurements of the voltage, but also allow the original notion of recording continuously the measurements to be used. With these modifications, it is believed, highly accurate heat transfer data may be obtained for the flowing fluids.

It would be useful to perform the experiments on suspensions of spherical particles of different sizes, in order to test the assumption that the material may be considered statistically homogeneous on the scale of the apparatus, and further to investigate the effects of particle migration which is extremely sensitive to the particle size. Experiments should also be performed using some suitable dispersing agent, to see if any significant differences in the

formation of multi-particle assemblies or conductivity results are obtained. Based on the suggestions of Singh, no dispersing agents were utilized here. However the rather large discrepancy between the theoretical prediction and the experimental results, and the microscopic inspection of the suspension suggest that considerable particle agglomeration may be occurring. Finally, it is suggested that experiments be performed on real, complex fluids, for example, solutions of large macromolecules, which might be expected to behave in an ideal limit like suspensions of dispersed particles in a suspending fluid, in order to see if significant flow dependence of the thermal constitutive behavior is discernible.

REFERENCES

Acrivos, A. and Jeffrey, D. J., 1976 "The Rheological Properties of Suspensions of Rigid Particles," AIChE Journal, 22, pp. 417-432.

Batchelor, G. K., 1954 "Heat Transfer by Free Convection Across a Closed Cavity Between Vertical Boundaries at Different Temperatures," Quart. of Applied Math., 12, pp. 209-233.

Batchelor, G. K., and Green, J. T., 1972 "The Determination of the Bulk Stress in a Suspension of Spherical Particles to Order c^2," JFM, 56, pp. 401-427.

Bird, R. B., Stewart, W. E., and Lightfoot, E. N., 1966 Transport Phenomena, New York: John Wiley & Sons, Inc., pp. 26-29.

Einstein, A., 1906 "A New Determination of Molecular Dimensions," contained in Investigations on the Theory of Brownian Movement, R. Furth (Ed.) 1956 New York: Dover Publications, Inc., pp. 36-62.

Goldsmith, H. L., and Mason, S. G., 1967 The Microrheology of Dispersions, Pointe-Claire, P.Q., Canada: Pulp and Paper Research Institute of Canada.

Hallow, 1968 Ph.D. thesis, Virginia Polytechnic Institute.

Ho, B. P., 1974 "Inertial Migration of Rigid Spheres in Two-Dimensional Unidirectional Flows," JFM, 65, pp.365-400.

Ho, C. Y., and Taylor, R. E. (Ed) 1969 Thermal Conductivity Proceedings of the Eighth Conference, New York: Plenum Press.

Jeffrey, D. J., 1973 "Conduction Through a Random Suspension of Spheres," Proc. Roy. Soc. Lond., A335, pp.355-367.

Kirk, R. E., and Othmer, D. F. (Ed) 1951 Encyclopedia of Chemical Technology,Vol. 7, New York: The Interscience Encyclopedia, Inc., pp 238-262.

Leal, L. G., 1973 "On the Effective Conductivity of a Dilute Suspension of Spherical Drops in the Limit of Low Particle Peclet Number," Chem. Eng. Comun., 1, pp. 21-31.

Rutgers, I. R., 1962 "Relative Viscosity and Concentration," Rheologica Acta, Band 2, Heft 4, p.305.

Singh, A., 1968 Ph.D. thesis, University of Minnesota.

Taylor, G. I., 1923 "Stability of a Viscous Liquid Contained Between Two Rotating Cylinders," Phil. Trans. A223, pp. 289-343.

Weast,R.C. (Ed) 1969 Handbook of Chemistry and Physics, Cleveland: The Chemical Rubber Co.

Segre, G. and Silberberg, A. 1962 "Behavior of Macroscopic Rigid Spheres in Poiseuille Flow," JFM 14 p 115.

Frankel, N. A. and Acrivos, A. 1970 "The Constitutive Equation for a Dilute Emulsion" JFM 44 pp. 65-78.

Becker, K. M., and Kaye, J. 1962 "The influence of a Radial Temperature Gradient on the Instability of Fluid Flow in an Annulus..." J. of Heat Transfer 84 pp.106-110.

Bjorklund, I., and Kays, W., 1959 "Heat Transfer between Concentric Rotating Cylinders" J. of Heat Transfer 81 pp. 175-186.

Haas, F. C. and Nissan, A. H. 1961 "Experimental heat transfer characteristics of a liquid in Couette motion with Taylor vortices" Proc. Roy. Soc. Lond. A261 pp. 215-226.

Ho, C. Y., Nardicci, J. L., and Nissan, A. H. 1964 "Heat Transfer Characteristics of Fluids Moving in a Taylor System of Vortices" A.I.Ch.E. Journal 10 pp. 194-202.

Yih, C. S. 1961 "Dual Role of Viscosity in the Instability of Revolving Fluids of Variable Density" Physics of Fluids 4 pp. 806-811.

FIGURE CAPTIONS

Figure 1: The Experimental Apparatus

Figure 2: The Inner Cylinder

Figure 3: The Bottom Shaft Bearing and Seal

Figure 4: The Electrical Circuit and Instruments Used

Figure 5: The Effective Viscosity of the Suspensions o - Experimental Data; — — — Einstein Result; ——— $\mu_s/\mu_0 = 1 + \frac{5}{2}\phi + 20\phi^2$.

Figure 6: The Viscosity of Pure Ucon Oil as a Function of Temperature o - Data Obtained in Stormer Viscosimeter; ▲ Data Obtained in Cannon-Fenske Tube-type Viscometer; ——— $= (6.241 \times 10^{-7}) \exp\left[\frac{4311}{T}\right]$.

Figure 7: Resistance-Temperature Characteristics of Test Heater o - Experimental Data; ——— Best Fit $T = 14.24\ R - 227.68$.

Figure 8: Rotational Speed of Inner Cylinder for Various Motor Control Settings o - Experimental Data; ——— Best Fit $\Omega = 2.456(MCS) - 2.567$.

Figure 9: Measured Conductivity of Ucon Oil for Various Rotation Rates o - $\Delta T \sim 6^{\circ}C$; □ - $\Delta T \sim 13^{\circ}C$.

Figure 10: Measured Conductivity of Ucon Oil for Various Guard Heating Levels.

Figure 11: The Unsuspended Particles a: 100x Magnification b: 200x Magnification

Figure 12: The Effective Conductivity, k_s/k_f, of Stationary Suspensions at Various Volume Concentrations o - Experimental Data; ——— Maxwell Result, $k_s/k_f = 1 - .6\phi$.

Figure 13: The Relative Flow Enhancement of the Effective Conductivity for Various Values of the Particle Peclet Number ϕ = .005, GH = 115%; o - Experimental Data; ——— Leal Result ($3Pe^{3/2}$) .

Figure 14: The Relative Flow Enhancement of the Effective Conductivity for Various Values of the Particle Peclet number ϕ = .01, GH = 110%; □ - Experimental Data; ——— Leal Result ($3Pe^{3/2}$) .

Figure 15: The Relative Flow Enhancement of the Effective Conductivity for Various Values of the Particle Peclet Number ϕ = .03, GH = 105%; ▽ - Experimental Data; ———Leal Result ($3Pe^{3/2}$) .

Figure 16: The Relative Flow Enhancement of the Effective Conductivity for Various Values of the Particle Peclet Number ϕ = .035, GH = 105%; Δ - Experimental Data; ———— Leal Result ($3Pe^{3/2}$) .

Figure 17: The Relative Flow Enhancement of the Effective Conductivity for Various Values of the Particle Peclet Number ϕ = .05, GH = 105%; ● - Experimental Data; ———— Leal Result ($3Pe^{3/2}$) .

Figure 18: The Relative Flow Enhancement of the Effective Conductivity for Various Values of the Particle Peclet Number and All Volume Fractions Investigated ———— Leal Result ($3Pe^{3/2}$); — — — — Best Fit of Data ($20Pe^{1.3}$) .

Figure 19: The Polystyrene Particles Suspended in Ucon Oil

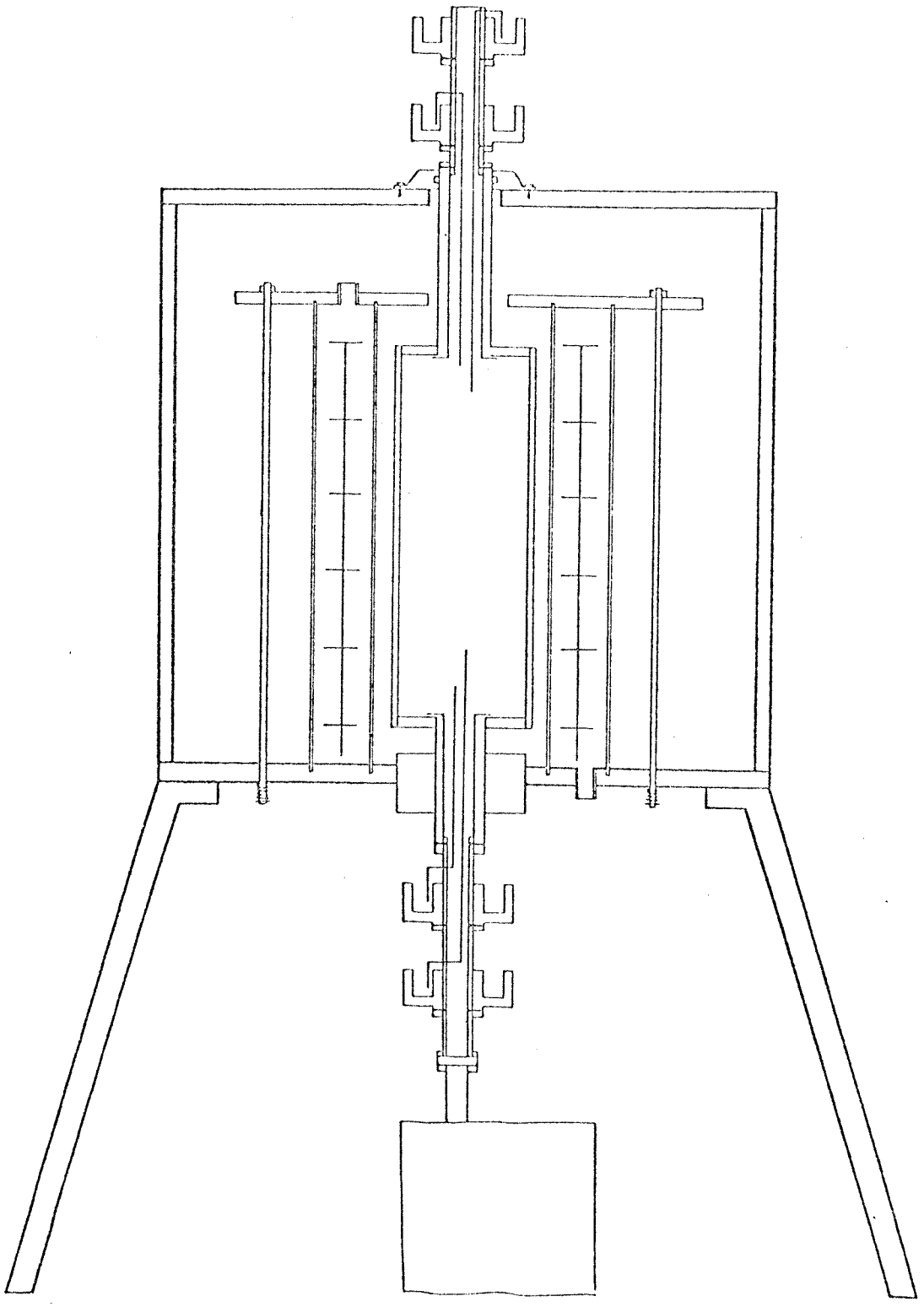

Figure 1: The Experimental Apparatus

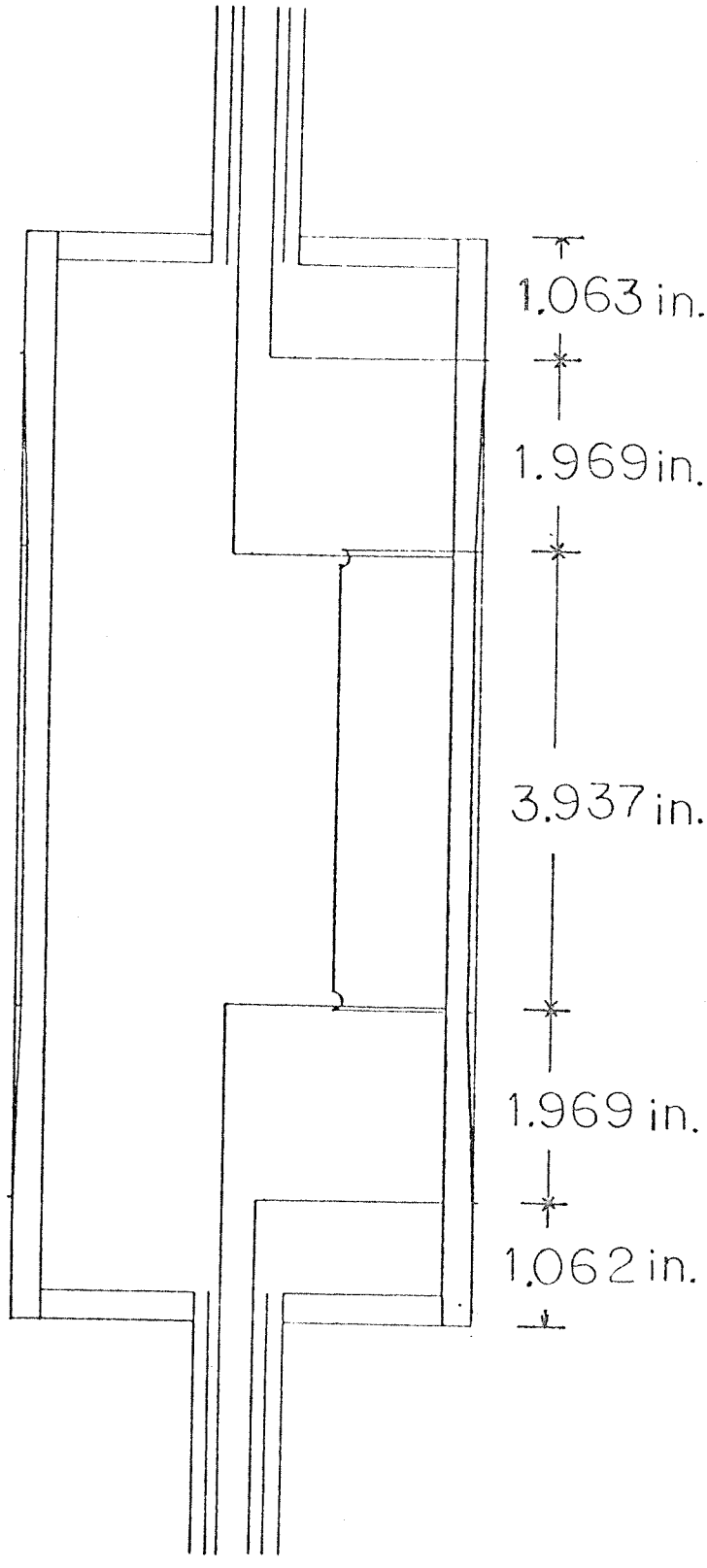

Figure 2: The Inner Cylinder

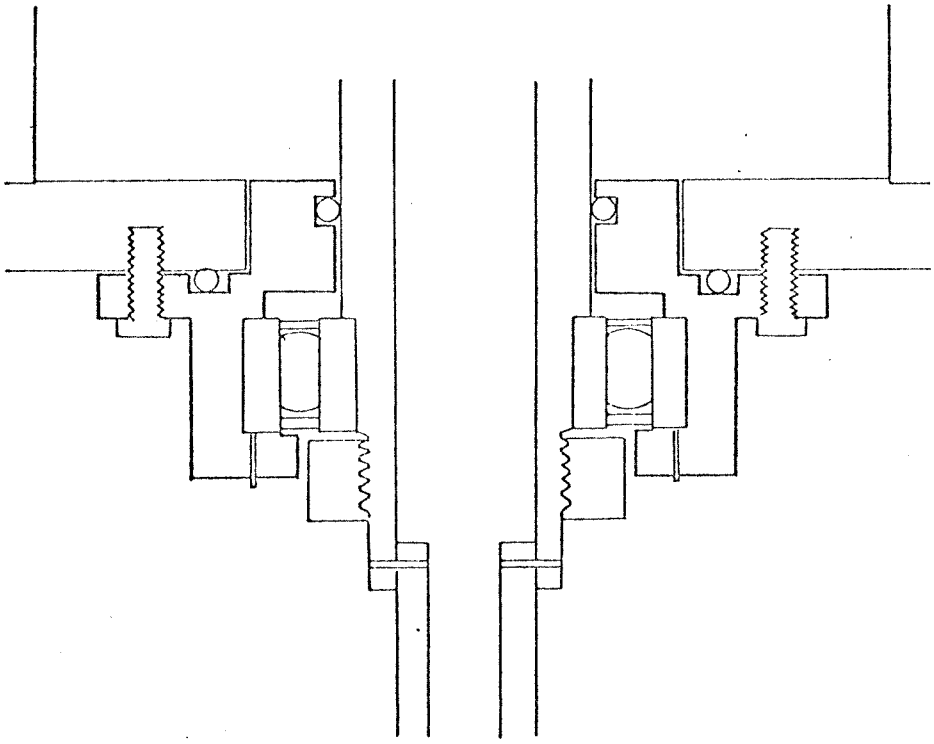

Figure 3: The Bottom Shaft Bearing and Seal

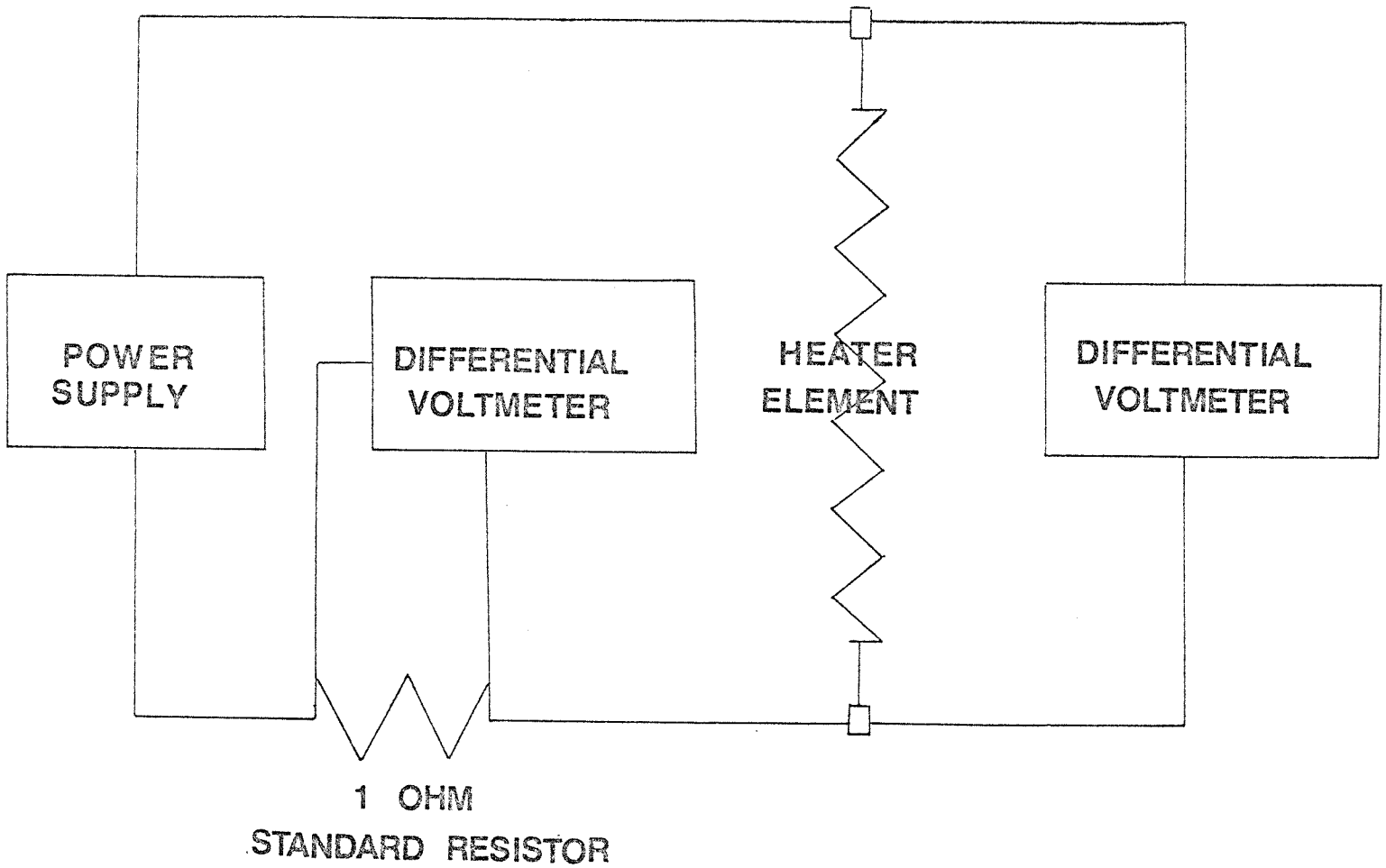

Figure 4: The Electrical Circuit

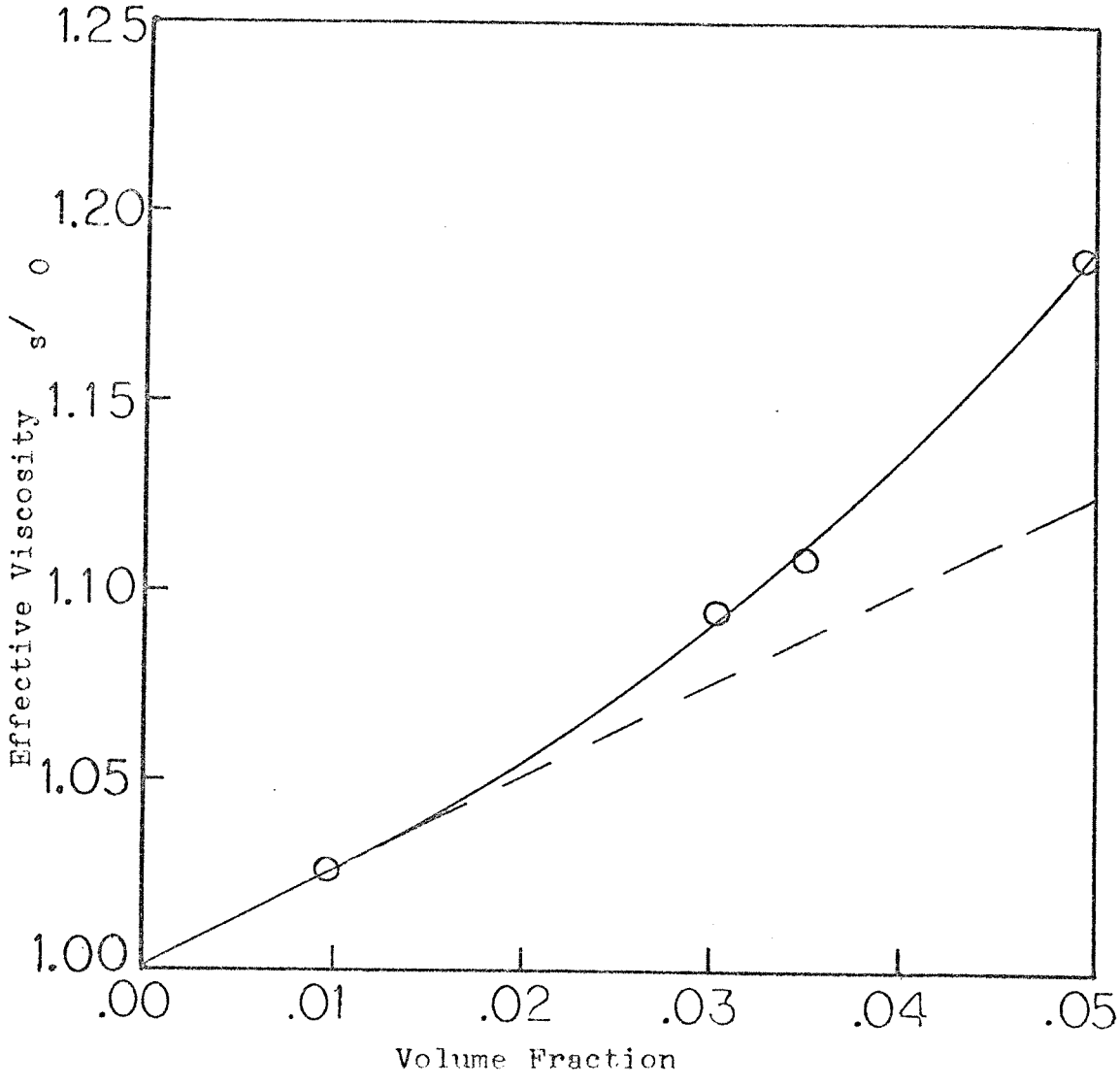

Figure 5: The Effective Viscosity

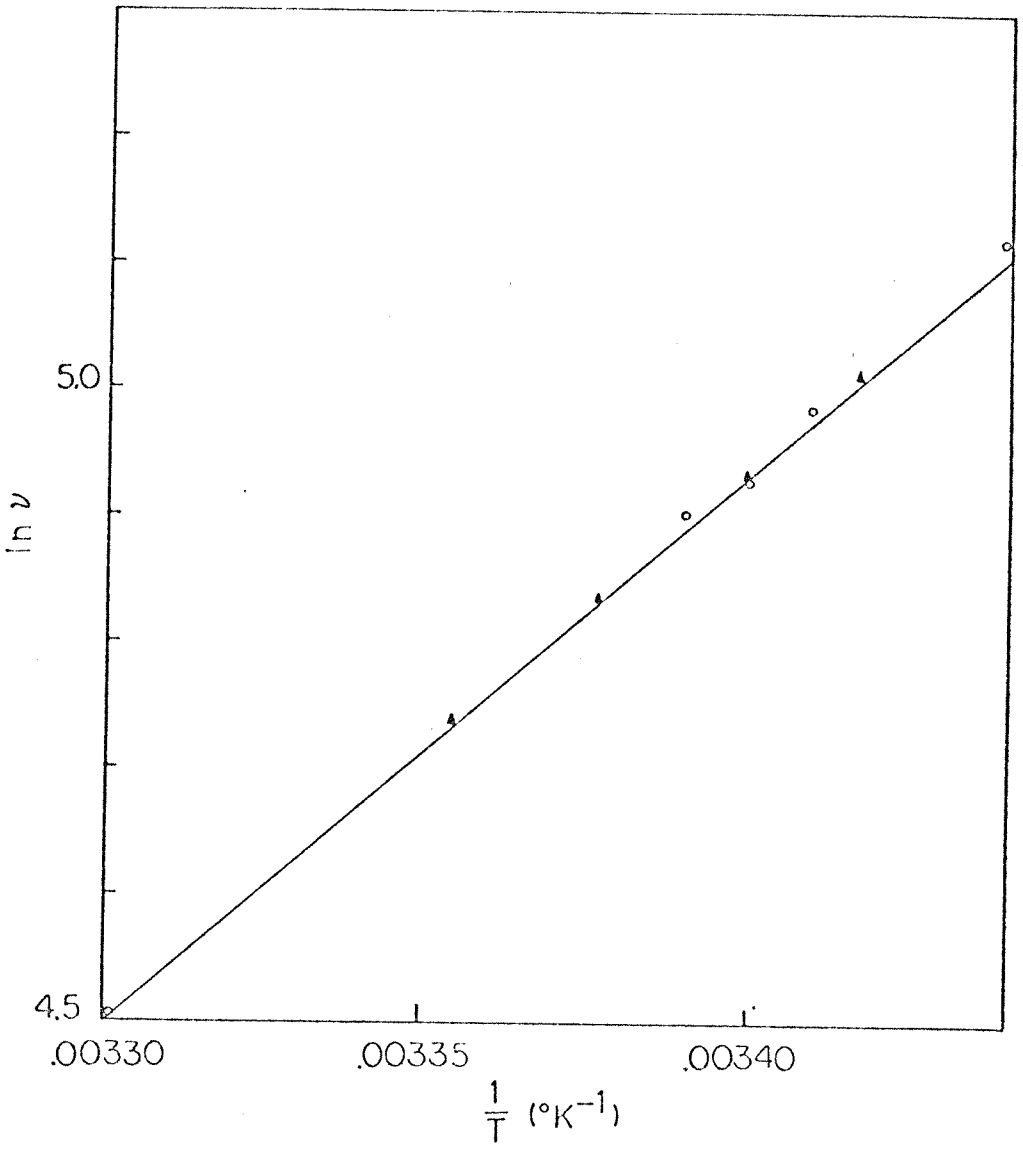

Figure 6: The Viscosity of Pure Ucon Oil as a Function of Temperature

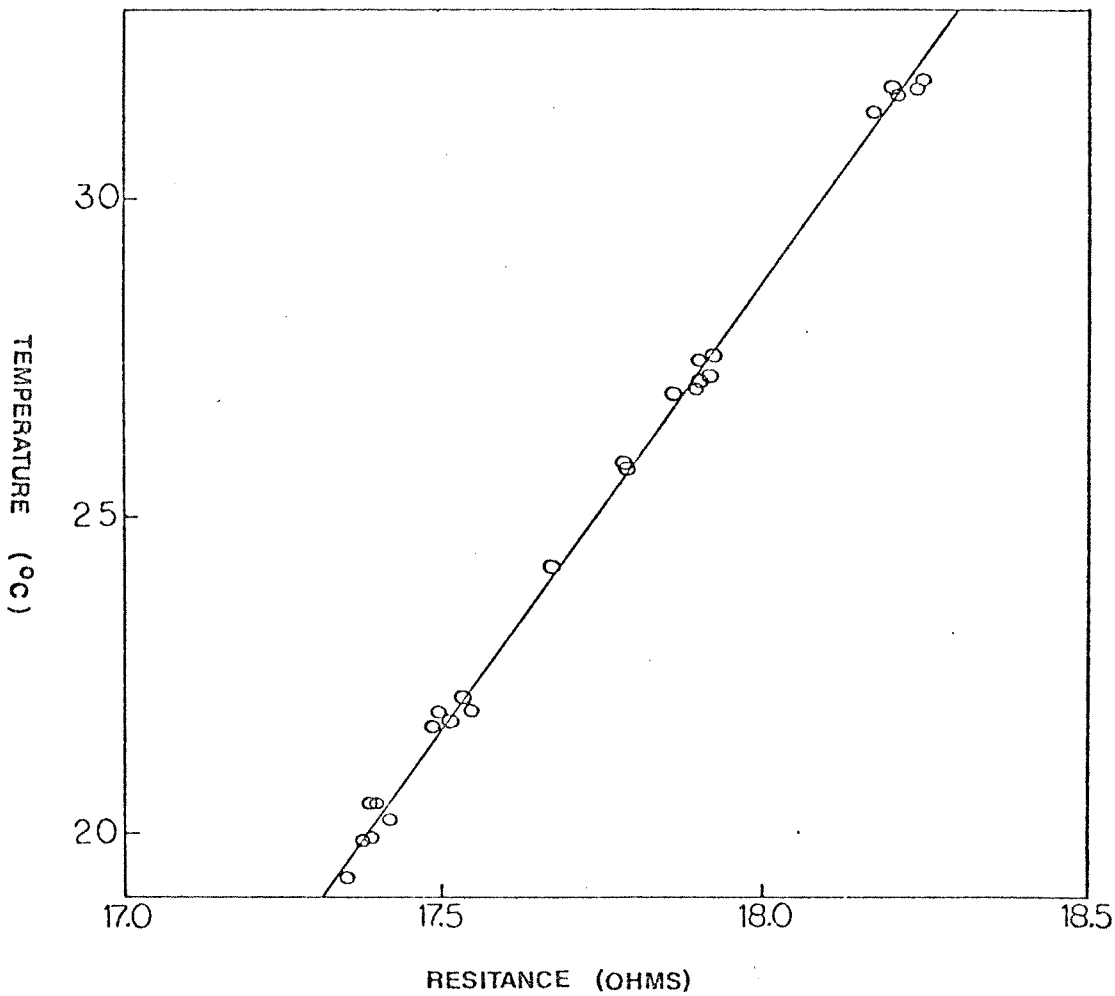

Figure 7: Resistance-Temperature Characteristics of the Test Heater

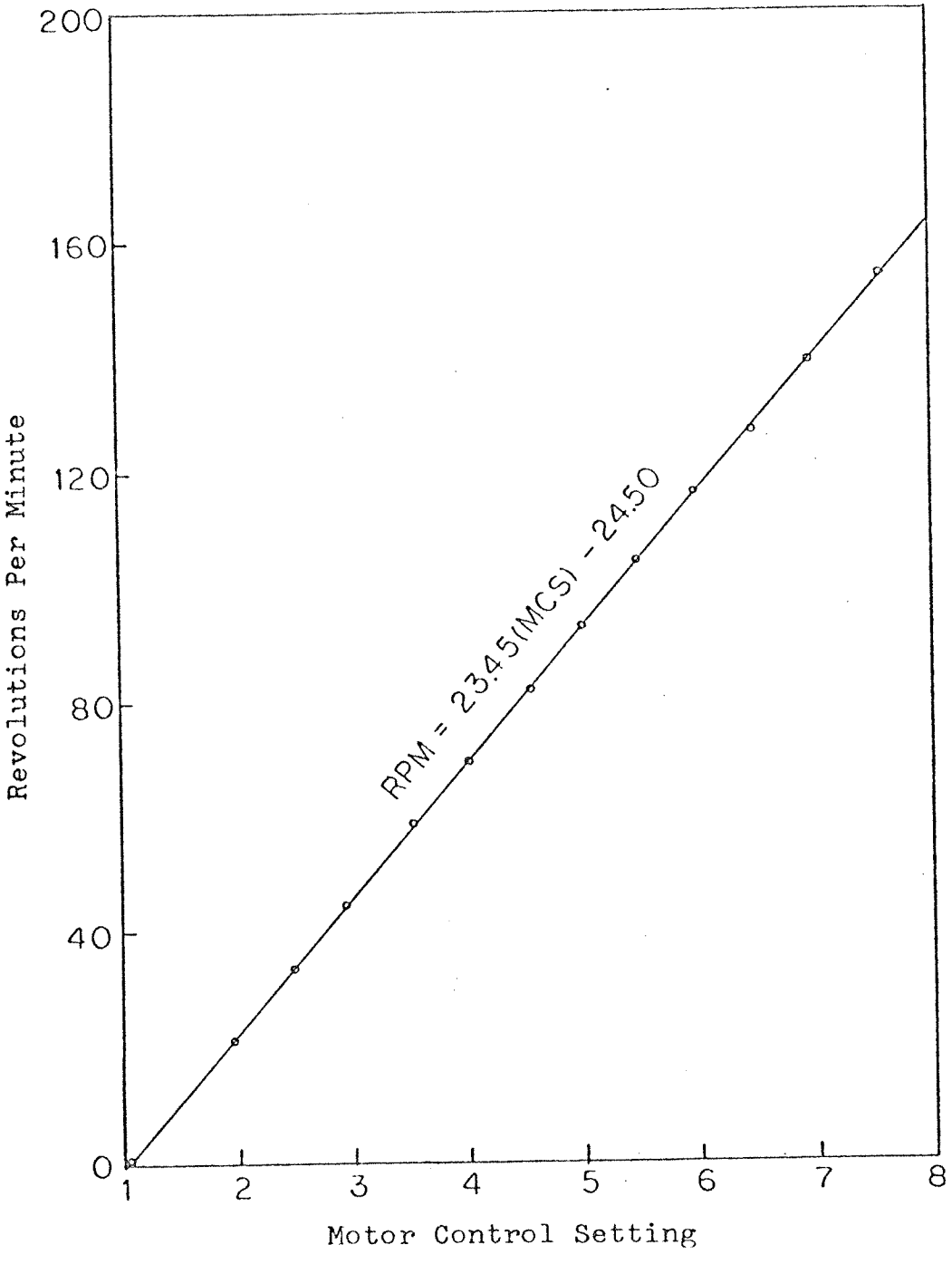

Figure 8: Rotational Speed of Inner Cylinder

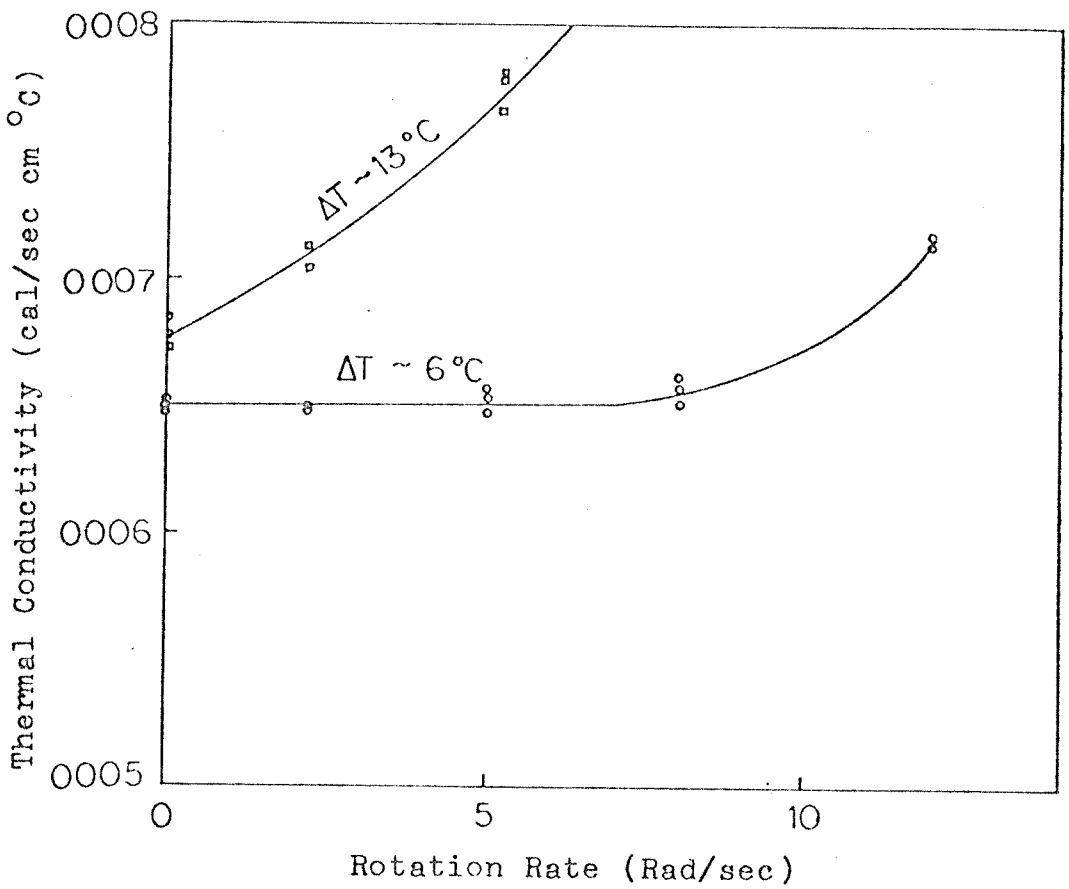

Figure 9: Measured Conductivity of Ucon Oil

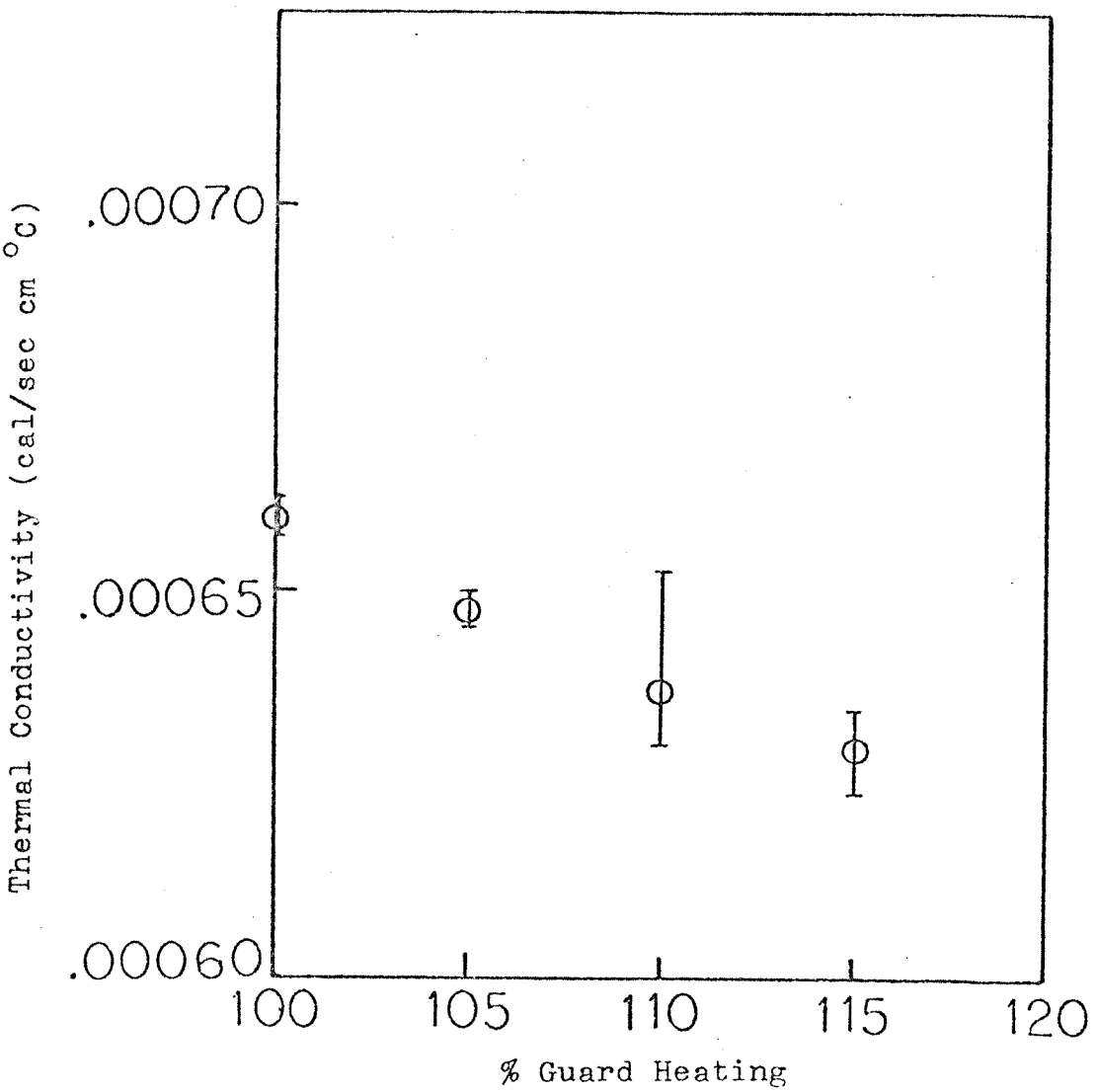

Figure 10: Measured Conductivity of Ucon Oil for Various Levels of Guard Heating

a

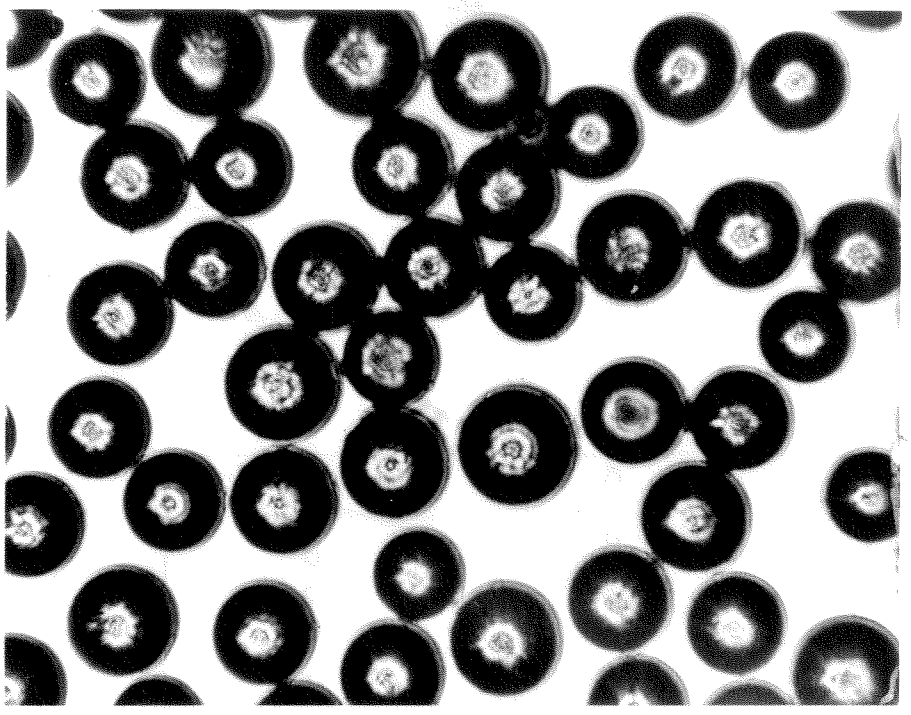

b

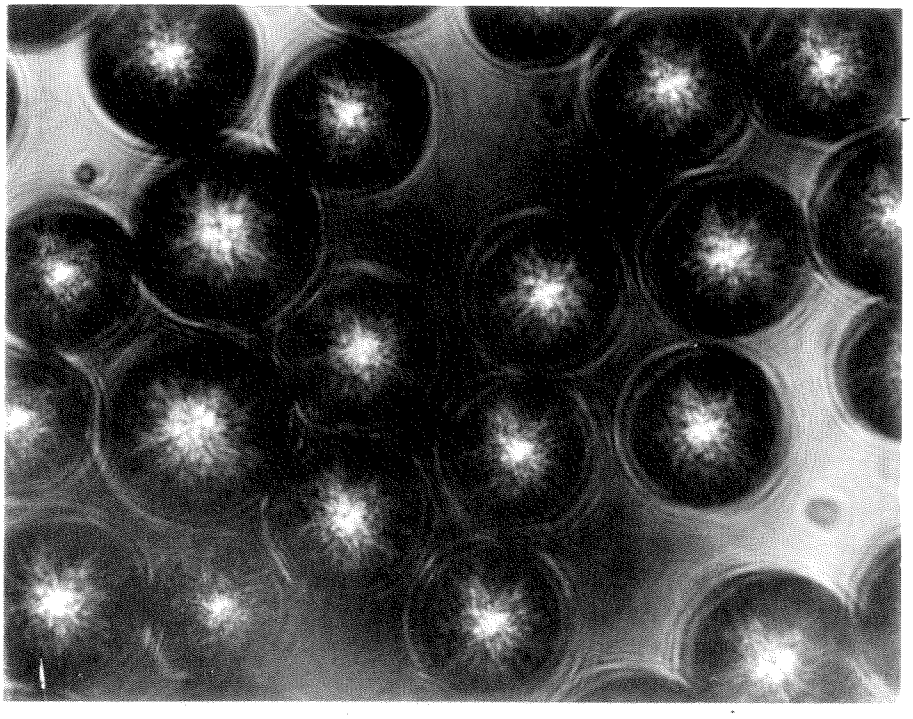

Figure 11: The Unsuspended Particles

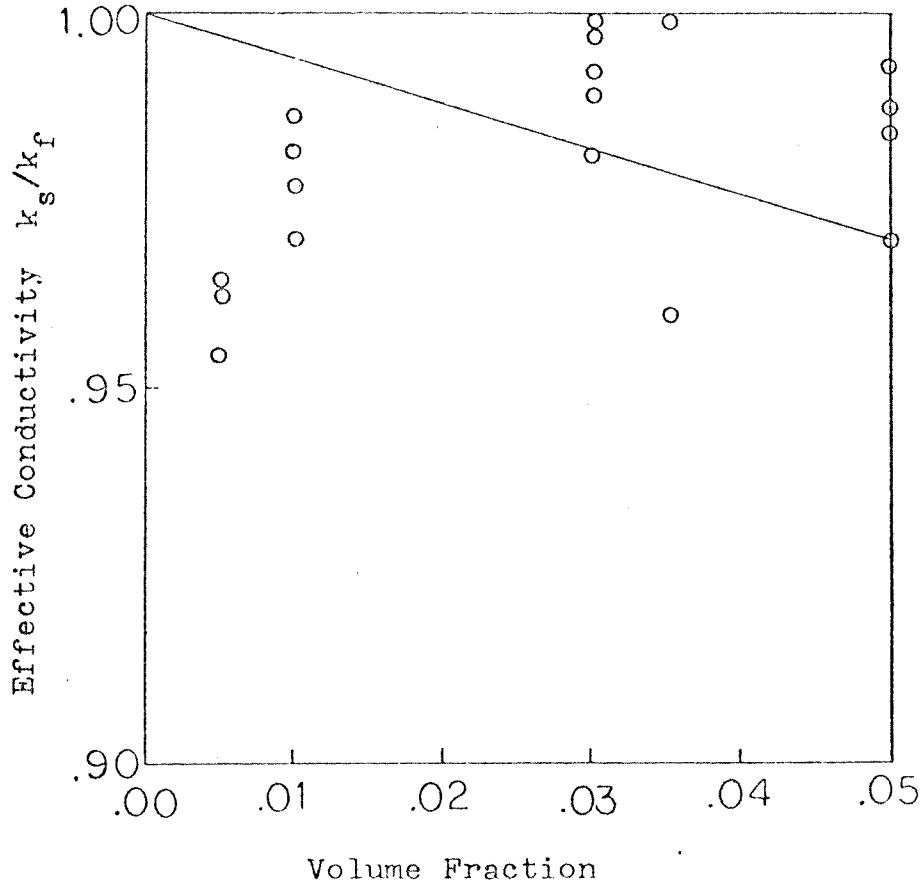

Figure 12: The Effective Conductivity k_s/k_f of Stationary Suspensions

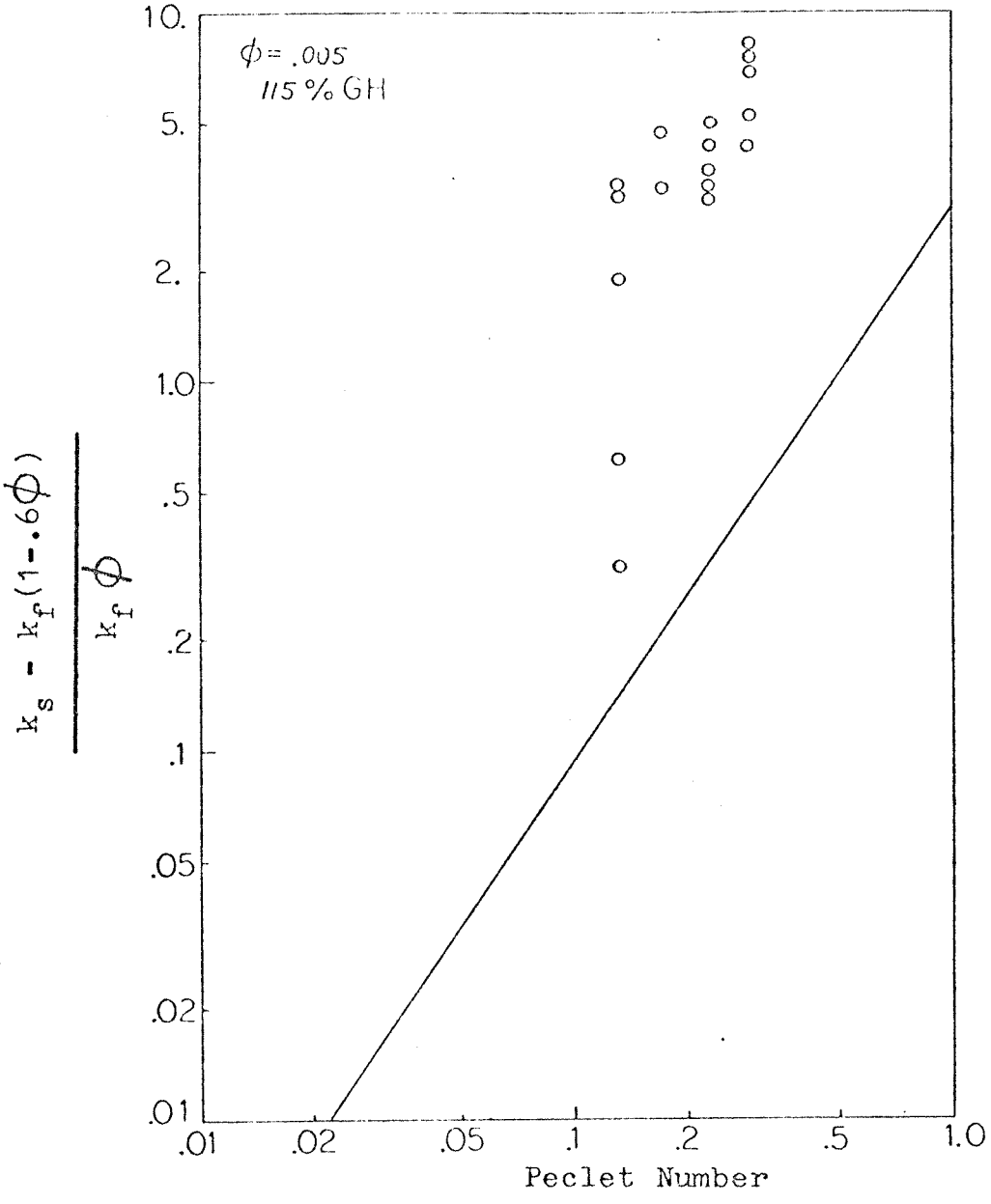

Figure 13: The Relative Flow Enhancement of the Effective Conductivity

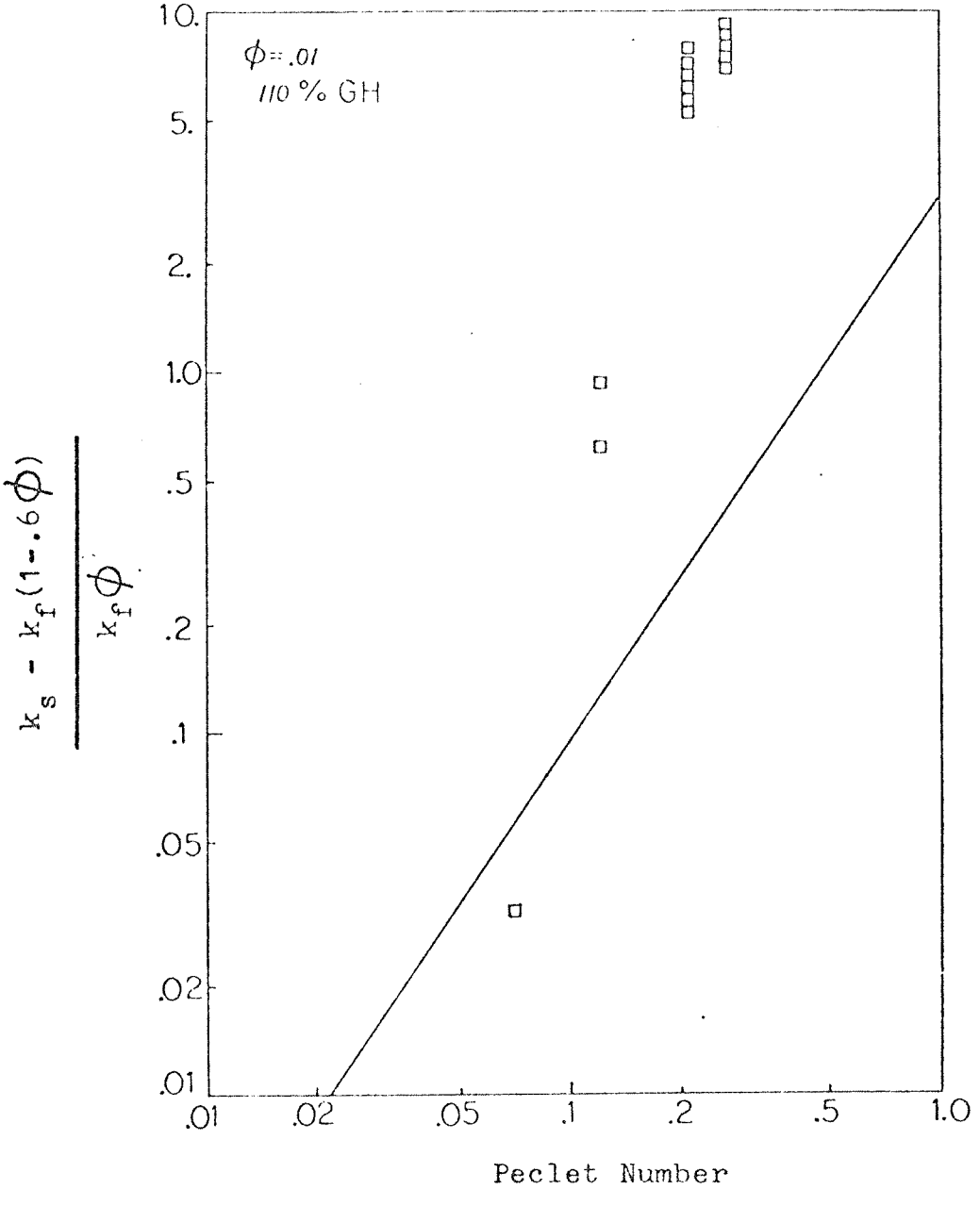

Figure 14: The Relative Flow Enhancement of the Effective Conductivity

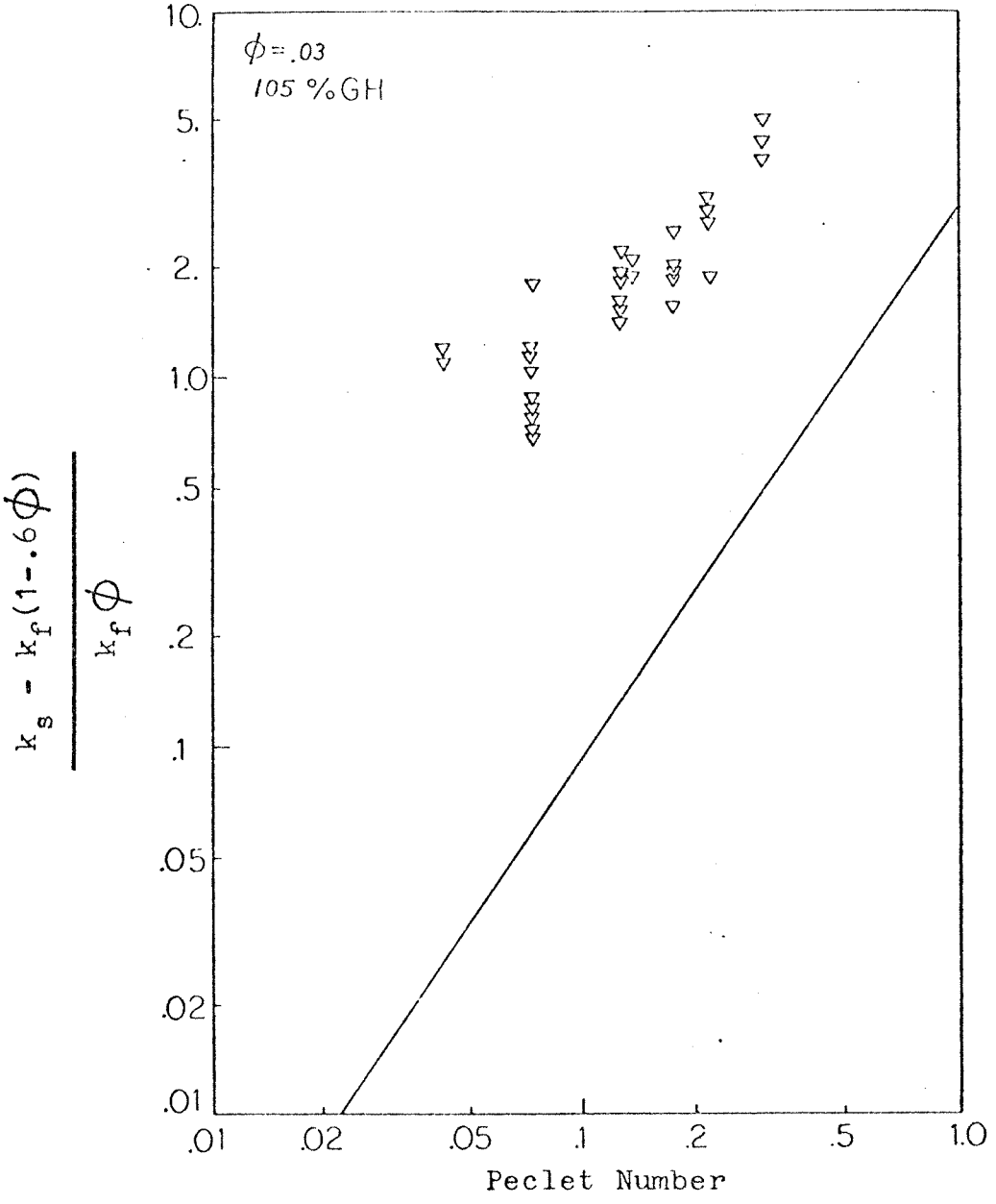

Figure 15: The Relative Flow Enhancement of the Effective Conductivity

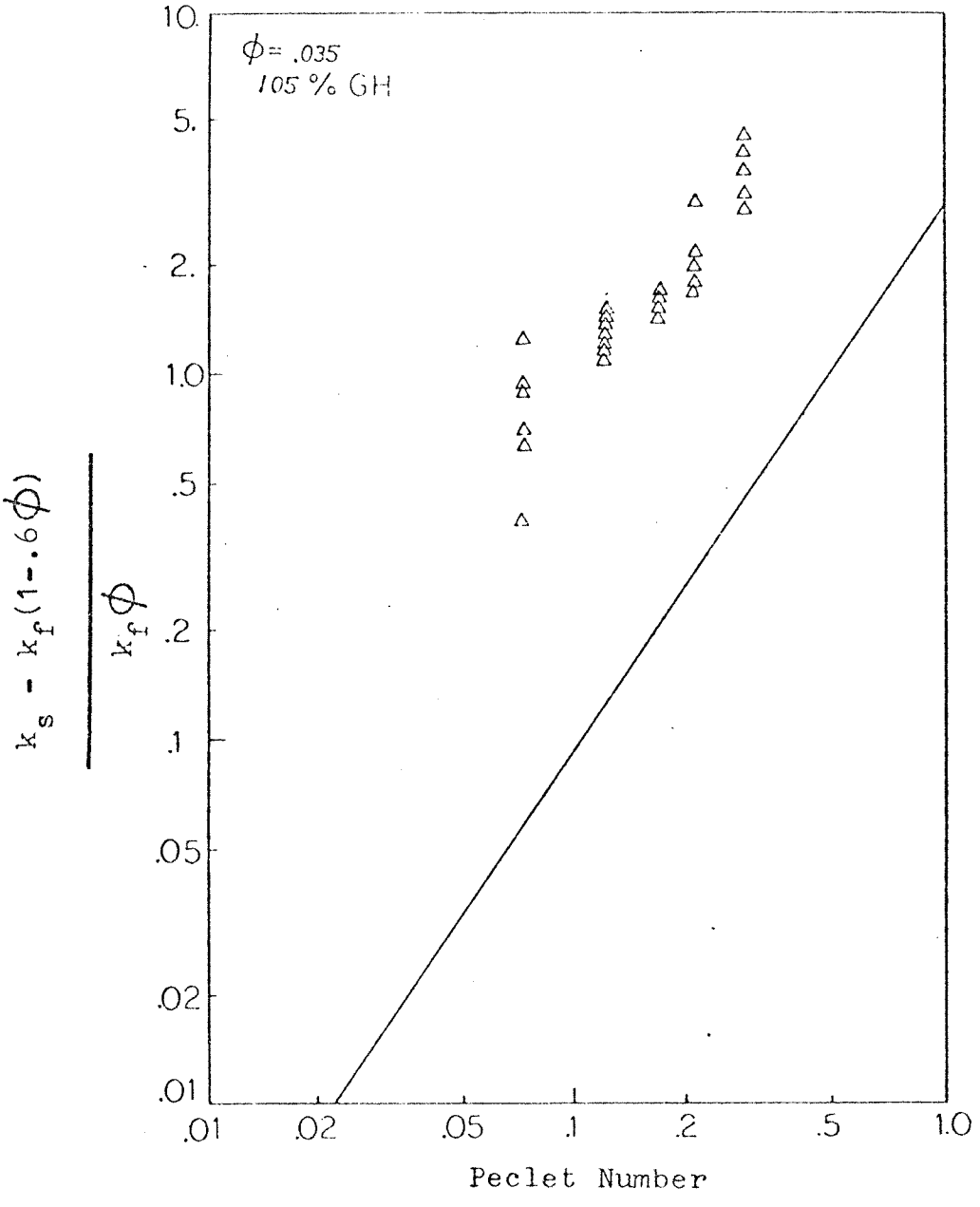

Figure 16: The Relative Flow Enhancement of the Effective Conductivity

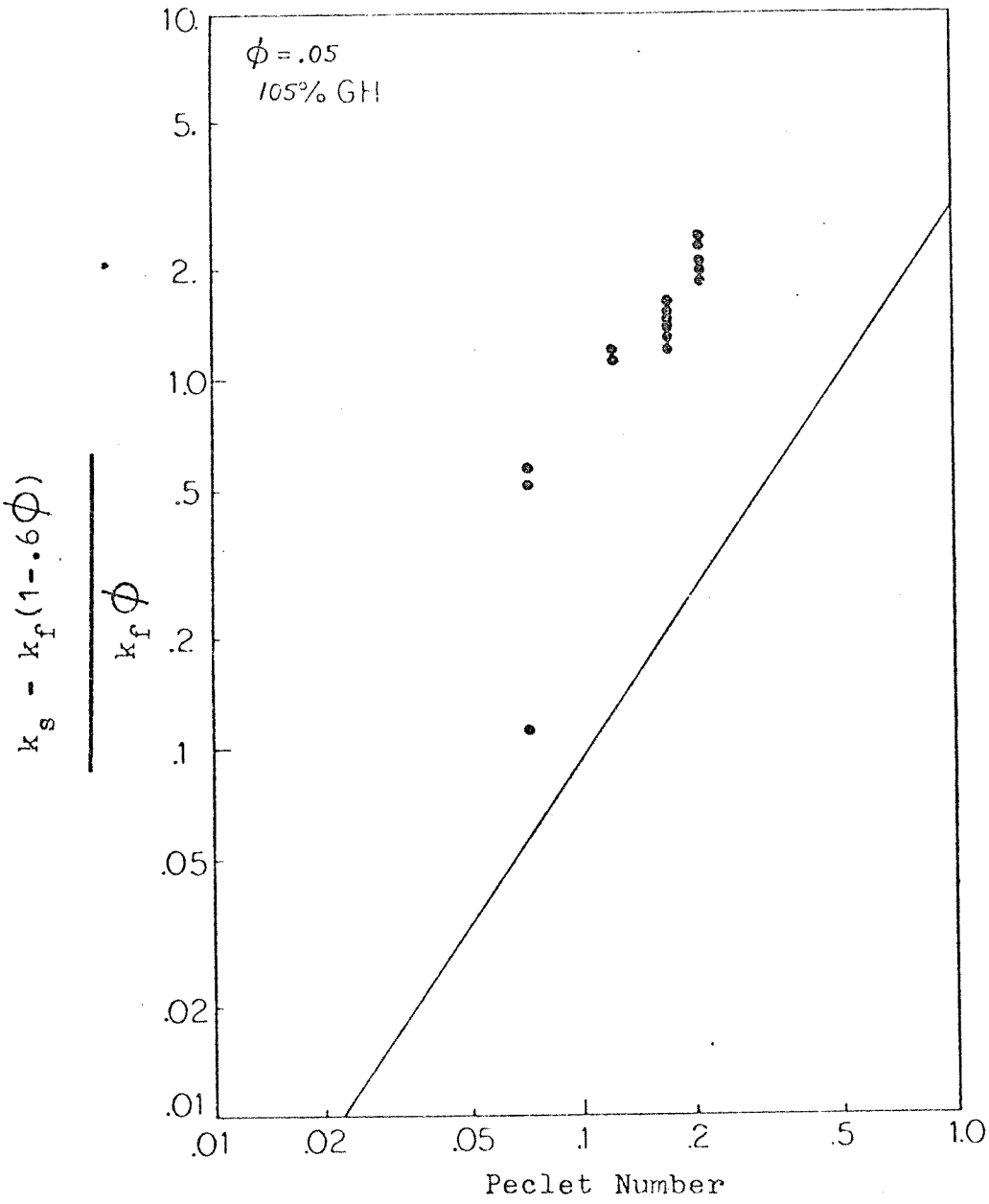

Figure 17: The Relative Flow Enhancement of the Effective Conductivity

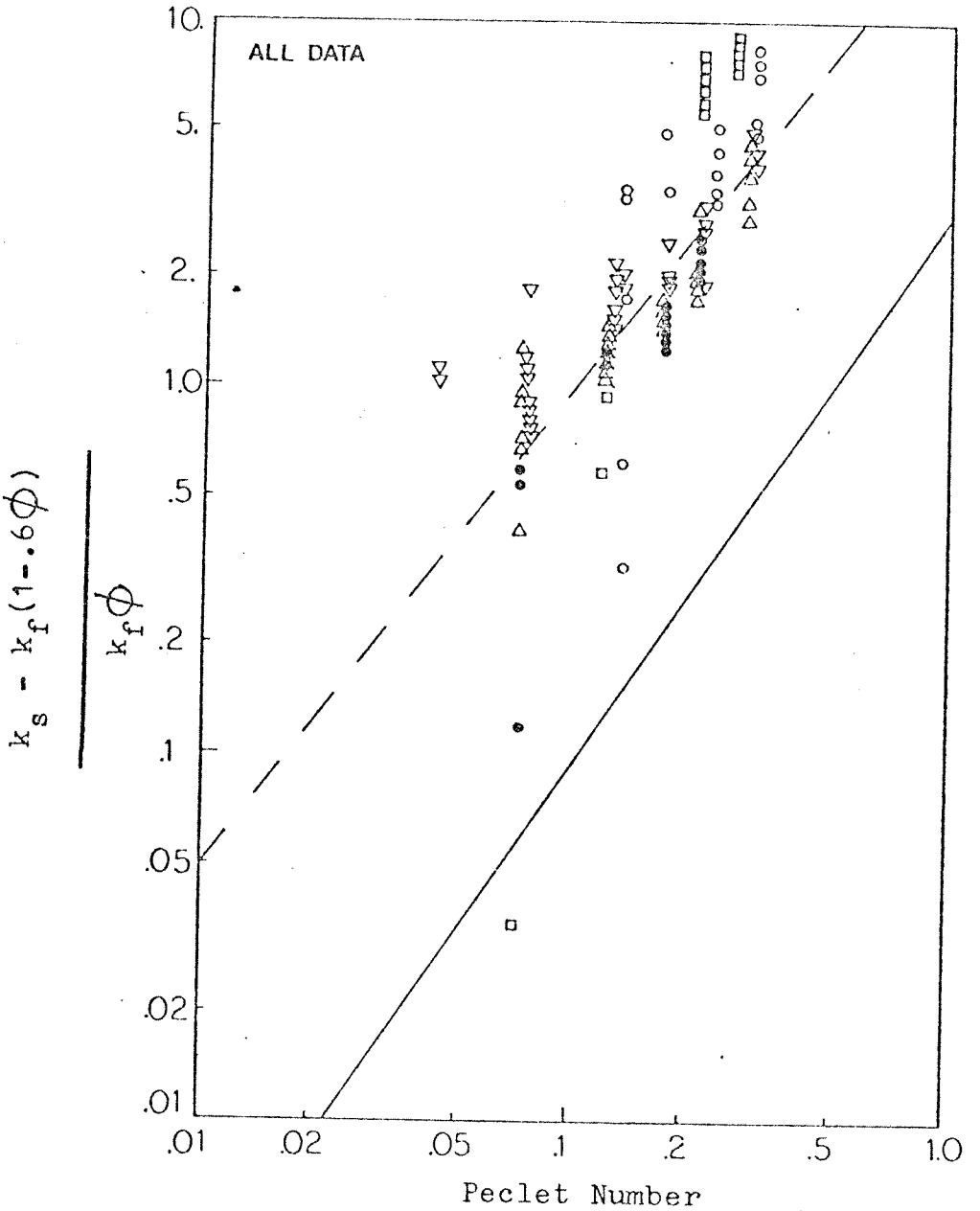

Figure 18: The Relative Flow Enhancement of the Effective Conductivity; All Concentrations

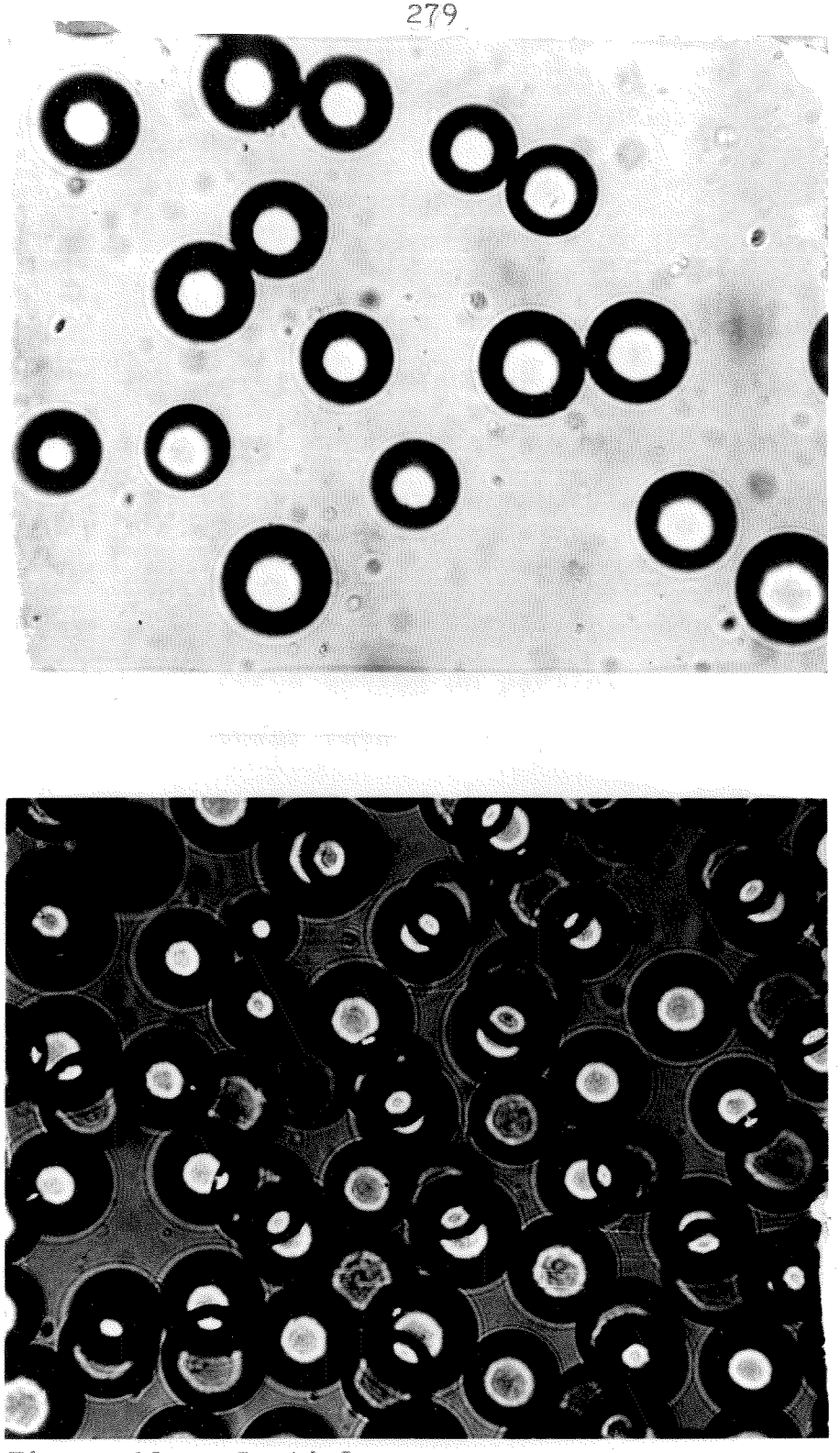

Figure 19: Particles suspended in Ucon Oil

NOMENCLATURE

A_0	surface area of a single particle
C	orbit constant for Jeffrey orbits
C_p	heat capacity of suspending fluid
D_r	Stokes-Einstein rotational diffusivity
E_{GH}	voltage drop across guard heater
E_{TH}	voltage drop across test heater
$\bar{F}_p(t)$	force acting on particle
G	shear rate
$G_{NC,AVE}$	average natural convection-induced shear rate in gap
%GH	percent of guard heat
I	convective-deformation contribution to effective transverse conductivity of a suspension of deformed droplets
I	current in test heater
$\underline{J}_p$	moment of inertia tensor of particle
K_{ij}	"effective conductivity" of suspension

L	length scale descriptive of bulk flow or temperature field
L	length of heated section in experimental apparatus
$\bar{M}_p(t)$	torque acting on particle
Nu_d	Nusselt number for tube flow
P	deterministic pressure field
P_n	spherical harmonic of order n
P_n^m	associated Legendre function of the first kind
Pr	Prandtl number
Q_i	bulk conductive heat flux of suspension
Q_i^*	particle contribution to bulk heat flux
Q_i^*	average single particle contribution to bulk heat flux
Q_n^m	associated Legendre function of the second kind
Ra	Rayleigh number
Re	Reynolds number

R_n	spherical harmonic of order n
R_1	outer radius of inner cylinder of experimental apparatus
R_2	inner radius of glass cylinder
R_3	outer radius of glass cylinder
S_0	surface area of single particle
S_n	spherical harmonic of order n
T	local temperature
T'	random component of local temperatur
T_c	temperature in continuous phase
T_d	temperature in dispersed phase
T_p	temperature in particle
$T_p^{\pm}$	fluctuating temperature in particle
T_{bulk}	bulk average temperature in suspension
T_f	temperature in fluid region of apparatus
T_g	temperature in glass region of apparatus
T_w	cooling water temperature
$\bar{U}$	deterministic velocity field associated with motion of suspension as a whole

V	averaging volume in suspension
V_0	volume of individual particle
V_c	veloctiy scale characteristic of bulk motion
V_p	translational velocity of center of mass of particle
a	radius of spherical particle
a	major semi-axis length of prolate spheroid
b	minor semi-axis length of prolate spheroid
d	tube diameter
d	gap width of apparatus
f	conversion factor
$\overline{g}$	spontaneous local heat flux in fluid
$\overline{g}_p$	spontaneous local heat flux in particle
g	gravitational constant
h	local enthalpy
h'	random component of local enthalpy

k	thermal conductivity of suspending fluid
m	ratio of particle thermal conductivity to fluid thermal conductivity
m	mass of particle
n	number of particles in averaging volume
p	Brownian pressure field
$p^{\pm}$	local spontaneous pressure field
q_i	local heat flux
q_i'	random component of local heat flux
q	heat flux across fluid in gap
r_s	surface of droplet
r	radial coordinate of spherical coordinate system
r_{eq}	migration equilibrium position of particle
$\underline{\underline{s}}$	spontaneous local stress
t	time
u_i	local velocity field
u_i'	random component of local velocity field
$\underline{u}^{\pm}$	fluctuating velocity field

$\bar{u}_{bulk}$	bulk average velocity field
u	x component of velocity field
$\bar{u}^{*}$	disturbance velocity field
$\bar{v}$	Brownian velocity field
v	y component of velocity field
w	z component of velocity field
x_i	Cartesian coordinate system
x_i^{*}	fixed-in-particle Cartesian coordinates
ℓ	length scale descriptive of suspended particles
ℓ_{ij}	direction cosines of particle axes
α	intermolecular length scale of suspending fluid
α_j	temperature gradient in x_j direction
β	parameter in description of motor control device

β_f	temperature coefficient of expansion of fluid
Γ_p	particle axis ratio
γ	shear rate
γ	ratio of radii R_1/R_2
δ_{ij}	Kroenecker delta
ϵ	deformation parameter
ξ	coordinate in prolate coordinate system
η	coordinate in prolate coordinate system
θ	bulk average temperature
θ	coordinate in spherical coordinate system
θ_1	orientation angle
κ	thermal diffusivity
λ	ratio of viscosity of inner and outer fluid
μ	viscosity of suspending fluid
ν	kinematic viscosity of suspending fluid
ρ	density
ρ	stretched radial coordinate

$\underline{\underline{\Sigma}}$ deterministic stress field

$\underline{\underline{\sigma}}$ Brownian stress field

$\underline{\underline{\sigma}}^{\pm}$ fluctuating stress field resulting from fluctuating velocity fields

σ interfacial tension

σ ratio of radii R_3/R_1

τ heat capacity ratio

ϕ volume fraction of particles

ϕ coordinate in spherical coordinate system

ϕ_n spherical harmonic of order n

ϕ_1 orientation angle of particle axes

χ_n spherical harmonic of order n

Ω rotation rate of experimental apparatus

Ω_0 parameter in description of motor control device

$\bar{\omega}_p$ angular rotation of particle about center of inertia